The Role of EROS in T Cell Biology

Paige Marie Mortimer

A Thesis Submitted in Requirement for the Degree of

Doctor of Philosophy (PhD)

Supervisor: Dr David Thomas

January 2023

Department of Immunology and Inflammation,

Imperial College London

Declaration of Originality

I declare that the work in this thesis is my own work. Work of others is acknowledged in text, where included.

Copyright Declaration

Acknowledgements

Firstly, I'd like to give my biggest thanks to my supervisor, Dr David Thomas, for his endless support and infectious enthusiasm. You have been the best supervisor I could have wished for (even after numerous late night/weekend work texts/calls/emails..). Thank you for keeping us in good supply of chocolate biscuits and fizzy cola bottles.

Next, I'd like to thank my fellow PhD students Stacey Mc Intyre and Isabella Cinti. I could not have got through these 3 years without you both! Stacey, for help keeping me sane in the lab and answering all of my weird questions - I'm so glad of that day when you arrived with no forewarning in classic Thomas lab style. Isabella, for helping me with all my animal work and literally being a shoulder to cry on. I will miss our lunch times!

I'd also like to thank my best friend Esme Nichols. Still can't believe I managed to bag the Thomas lab the best RA in the world! Thank you for forever listening to my worries and bringing me back down to Earth with your sound words of advice. And thank you for coating my plates and various other annoying tasks I asked of you at the last minute. I'm sorry for leaving you in London - who'd have thought!

Another thank you goes to Dr Lyra Randzavola, for answering all my questions and pointing me in the right direction. Thank you to all current and past members of the CID!

Finally, I'd like to thank my fiancé Jack. Thank you for your infinite support and encouragement, especially these past 3 years. Thank you for making weekend lab work so much more bearable. Thank you for helping me re-word sentences, even when you don't really know what they mean. Thank you for always keeping me on track and following me around the country so I can achieve my goals. I could not have done any of this without you.

Abstract

EROS (Essential for Reactive Oxygen Species) regulates the protein expression of gp91*phox* in macrophages and neutrophils. gp91*phox* is an essential membrane-bound component of the phagocyte NADPH oxidase. If EROS or gp91*phox* are absent, the primary immunodeficiency Chronic Granulomatous Disease (CGD) develops. CGD in EROS deficient patients has additional autoimmune features compared to gp91*phox* deficient patients, suggesting further functions of EROS besides gp91*phox* regulation. EROS also regulates the expression of the ATP-gated purinergic receptor P2X7. gp91*phox* and P2X7 are both involved in various signalling processes in CD4+ T cells, therefore I hypothesised that EROS may too have an effect on CD4+ T cell biology.

This thesis demonstrates that EROS is expressed in CD4+ T cells, and regulates gp91*phox* and P2X7 expression in these cells. Losing EROS reduces the ATP-driven shedding of CD27, CD62L and IL-6R from the cell surface, and the induction of cell death in CD4+ T cells. EROS deficiency drives Th2 skewing of CD4+ T cells, highlighted by 4-10x fold excess secretion of IL-4, IL-5 and IL-13, and upregulated *Rbpj*, *Plexin d1* and *Gata3* expression. P2X7 deficiency or inhibition recapitulates EROS deficiency, but gp91*phox* deficiency does not, demonstrating that the Th2 phenotype is a P2X7-dependent process. There are more T resident memory (TRM) and Type 2 Innate Lymphoid Cells (ILC2) in EROS deficient mice, however this does not contribute to a more effective Th2-orchestrated immune response. Less IgG1 is secreted in EROS deficient mice, dampening any Th2-driven protection against Helminth parasitic infections. CRISPR-mediated deletion of EROS in human CD4+ T cells demonstrates conservation of function, with decreased P2X7 levels, augmented IL-4 production and impaired surface marker shedding.

Overall, this thesis shows that EROS negatively regulates Th2 immune responses in mouse and human CD4+ T cells by upregulating the expression of P2X7.

Contents

Table of figures

Table of tables

Abbreviations

ATP	Adenosine Triphosphate
BMDM	Bone Marrow Derived Macrophage
BSA	Bovine Serum Albumin
CGD	Chronic Granulomatous Disease
CNS	Central Nervous System
CYBC1	Cytochrome B Chaperone 1
DHR	Dihydrorhodamine
DMSO	Dimethyl Sulfoxide
DN	Double Negative
DNA	Deoxyribonucleic Acid
DP	Double Positive
DPI	Diphenyleneiodonium
DUOX	Dual Oxidase
EAE	Experimental autoimmune encephalomyelitis
EC50	Half maximal effective concentration
ER	Endoplasmic Reticulum
EROS	Essential for Reactive Oxygen Species
FAD	Flavin Adenine Dinucleotide
FBS	Fetal Bovine Serum
GFP	Green Fluorescent Protein
GSEA	Gene Set Enrichment Analysis
GTP	Guanidine Triphosphate
HES	H. polygyrus Excretory/Secretory products
IFN	Interferon
IL-	Interleukin-
ILC	Innate Lymphoid Cells
iLN	Inguinal Lymph Node
IRG	Interferon Response Genes
KO	Knock out
KOMP	Knockout Mouse Project

LPS	Lipopolysaccharide
MFI	Median Fluorescence Intensity
MPO	Myeloperoxidase
N.S	Non-specific
NAD	Nicotinamide adenine dinucleotide
NF-kB	Nuclear factor kappa B
NLRP3	NLR family pyrin domain containing 3
NOD	Non-obese Diabetic
NOX2	NADPH oxidase 2
NP-CGG	4-hydroxy-3-nitrophenyl acetyl Chicken Gamma Globulin
OST	Oligosaccharyltransferase
RNA	Ribonucleic acid
RNP	Ribonucleoprotein
ROS	Reactive Oxygen Species
RT	Room temperature
SEM	Standard Error of the Mean
sgRNA	single guide RNA
SLE	Systemic Lupus Erythematosus
SOD	Superoxide Dismutase
STAT-	Signal transducer and activator of transcription-
TCM	T Central Memory
TCR	T Cell Receptor
TEM	T Effector Memory
Tfh	T follicular helper
Th-	T helper-
TLR4	Toll-like Receptor 4
TMT MS	Tandem Mass Tagging Mass Spectrometry
TNF	Tumour Necrosis Factor
Treg	T regulatory
TRM	T Resident Memory
WT	Wild type

Chapter 1: Introduction

1.1. Reactive Oxygen Species

Reactive Oxygen Species (ROS) are highly reactive molecules formed from oxygen, and can be produced by the mitochondria, endoplasmic reticulum, cytoplasm and the plasma membrane. ROS can be present as a singlet oxygen, or oxygen can accept free electrons to form superoxide (O_2-). Superoxide dismutase (SOD) can convert these molecules into the non-radical hydrogen peroxide (H_2O_2), which can act as a signalling molecule within cells. H_2O_2 can then be converted into hydroxyl radicals (OH-), hypochlorous acid (HOCl) by myeloperoxidase (MPO) or H_2O by the action of catalase or glutathione peroxidase (figure 1). ROS signalling can be involved in both normal physiological and pathological processes, therefore it is essential that ROS production must be tightly controlled. There is a fine balance between ROS signalling and the development of oxidative stress driven tissue damage (reviewed in [1,2]). ROS can be neutralised by small molecule antioxidants, such as vitamin A, C and E, or by enzymes such as superoxide dismutase (SOD), catalase, perioxiredoxins and glutathione peroxidase [3].

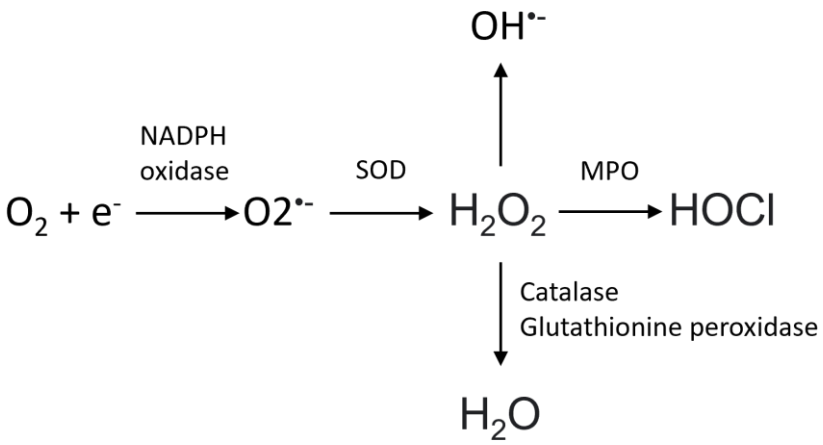

Figure 1.1: The generation of ROS from oxygen. Superoxide forms when O_2 accepts an electron, and this can be dismutated into hydrogen peroxide (H_2O_2) by superoxide dismutase (SOD). H_2O_2 can be further dismutated into hydroxyl radicals (OH-), HOCl by myeloperoxidase (MPO) or H_2O by catalase or glutathione peroxidase.

It was historically thought that ROS were a toxic by-product of cellular respiration, however both mitochondrial and NADPH oxidase derived ROS can be harnessed as important signalling molecules.

1.1.1. Mitochondrial ROS

During oxidative phosphorylation in the mitochondria, electrons can escape the electron transport chain, resulting in the generation of ROS [4]. Mitochondrial ROS (mtROS) can be involved in a range of processes depending on the levels at which they are present. Low levels of mtROS are important for inducing metabolic adaptive states such as hypoxia [5]. moderate mtROS levels are involved in regulating the inflammatory response, such as by inactivating MAP kinase phosphatases, thereby causing sustained MAP kinase signalling [6]. High mtROS levels can induce apoptosis and autophagy [7]. In summary, mtROS are involved in inducing and regulating numerous physiological processes within and between cells.

1.1.2. NADPH derived ROS

ROS can also be produced by a dedicated enzyme complex, called the phagocyte NADPH oxidase. ROS are generated by the phagocyte NADPH oxidase to fulfil specific cellular requirements, which will be discussed in section 1.2.

1.1.3. Other sources of ROS

Cellular ROS can also be generated by other enzymes such as xanthine oxidase and cytochrome P450. Xanthine oxidase is widely expressed in mammalian tissues [8]. It is primarily involved in purine catabolism and ROS is generated during the breakdown of hypoxanthine and xanthine into uric acid. Xanthine oxidase-derived ROS has been found to regulate NLPR3 inflammasome activation in macrophages [9], which is required to drive inflammation during malaria infections [10], demonstrating an integral role of this enzyme in immunity.

Cytochrome P450 is a superfamily of highly conserved metabolic enzymes that are expressed in many different tissues and cell types, including macrophages [11]. They can break down a variety of endogenous and exogenous compounds, during which ROS can be produced [12]. ROS was previously considered a toxic by-product of these metabolic reactions, however one study found that cytochrome P450-derived ROS is involved in the regulation of

corticosteroid production [13]. Additionally, the expression of cytochrome P450s can be regulated by proinflammatory cytokines [14], demonstrating a link with immunity.

In summary, ROS can be produced by a number of sources and can play important roles in a variety of physiological and immunological processes.

1.2. Phagocyte NADPH oxidase

The phagocyte NADPH oxidase, also known as NOX2, is predominantly expressed in the professional phagocytes of the innate immune system: macrophages and neutrophils [15,16]. It is also expressed by cells of the adaptive immune system including; CD4, CD8+ T cells, T regulatory cells (Tregs) and B cells [1].

1.2.1. Structure

The phagocyte NADPH oxidase is a multi-subunit protein complex that can form an active enzyme complex capable of producing superoxide. It has two integral membrane bound components; gp91*phox* and p22*phox*, which form the co-dependent heterodimer cytochrome b558. gp91*phox* and p22*phox* depend on each other for stable expression, if one is absent, so is the other. The phagocyte NADPH oxidase also has cytosolic components including p40*phox,* p47*phox,* p67*phox* and Rac1 in macrophages or Rac2 in neutrophils (figure 1.2).

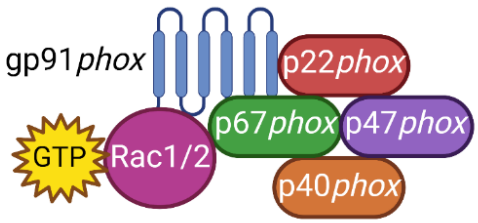

Figure 1.2: Structure of the activated phagocyte NADPH oxidase. The phagocyte NADPH oxidase contains the cytochrome b558; gp91*phox* and p22*phox*, which forms the membrane bound constituent of the enzyme complex. It also contains the subunits p40*phox*, p47*phox*, p67*phox* and GTP-bound Rac, which are located in the cytosol.

1.2.2. Activation

The spatial separation of the cytosolic and membrane-bound components of the NADPH oxidase at rest prevents aberrant activation of the complex [17]. The NADPH oxidase becomes activated upon phagocytosis of a pathogen, which causes the phosphorylation of p47*phox* [18]. This releases p47*phox* from its auto-inhibitory state, allowing the heterotrimeric cytoplasmic complex to translocate to the membrane [19]. Here, activated p67*phox* can directly interact with gp91*phox* of the cytochrome b558, and this is stabilised by p47*phox* that acts as an adaptor molecule by contacting p22*phox* of the cytochrome b558 [20]. GTP-bound Rac independently translocates to the membrane, where it can simultaneously act as a scaffold by interacting with both p67*phox* and cytochrome b558 and maximise electron transfer by driving electron transport across the membrane [21]. Two electrons are transferred from NADPH to FAD, reducing it to FADH2. These electrons are then transferred successively to a proximal then a distal heme located within cytochrome b558 [22], and finally to molecular oxygen, generating extracellular ROS and intracellular NADP+. This process is known as the respiratory burst, which is essential during the innate immune response [15,16].

1.2.3. Discovery

The discovery of the entire phagocyte NADPH oxidase paralleled the description of the disease in which it is disrupted, Chronic Granulomatous Disease (CGD), which will be discussed in the next section, section 1.2.4. It has taken over 100 years to elucidate the role of the phagocytic NADPH oxidase, and essential regulators are still being discovered today (figure 1.3).

The physiological production of ROS was first identified in 1908 where Warburg noted a large and rapid increase in O_2 consumption, followed by H_2O_2 production during the fertilisation of sea urchin eggs [23]. In 1933, Baldridge and Gerard observed an increase in oxygen consumption by leucocytes following phagocytosis, the first description of ROS in the immune system [24]. It wasn't until 1959 that Sbarra and Karnovsky found that the raised oxygen consumption during phagocytosis did not accompany an increase in mitochondrial function, but it remained unclear what the oxygen was being used for [25]. NADPH was identified as the substrate of this reaction in 1964 [26], leading to the discovery of neutrophils that were unable to use NADPH in 1967 [27]. These neutrophils had no bactericidal activity

and they had lost their ability to increase oxygen consumption. In a landmark study in 1978, Segal identified the cytochrome b558 in neutrophils and described their role in the production of ROS [28]. The development of a cell-free system to study the cytochrome b558 in isolated membranes in 1984 [29] quickly led to the discovery that the cytosolic factors p47*phox* and p67*phox* are necessary and critical members of the complex [30]. In 1991 the role of the GTPases Rac1 [31] and Rac2 [32] in the activation of the NADPH oxidase complex was described, following the discovery that GTP was involved in the process of ROS generation. The final member of the complex, p40*phox,* was identified in 1993 [33].

This project focuses on EROS (Essential for Reactive Oxygen Species), first described in 2017. EROS is essential for the protein expression of gp91*phox*, and subsequently p22*phox* [34]. EROS also regulates the expression of P2X7 (section 1.3). EROS will be discussed in greater detail in section 1.4.

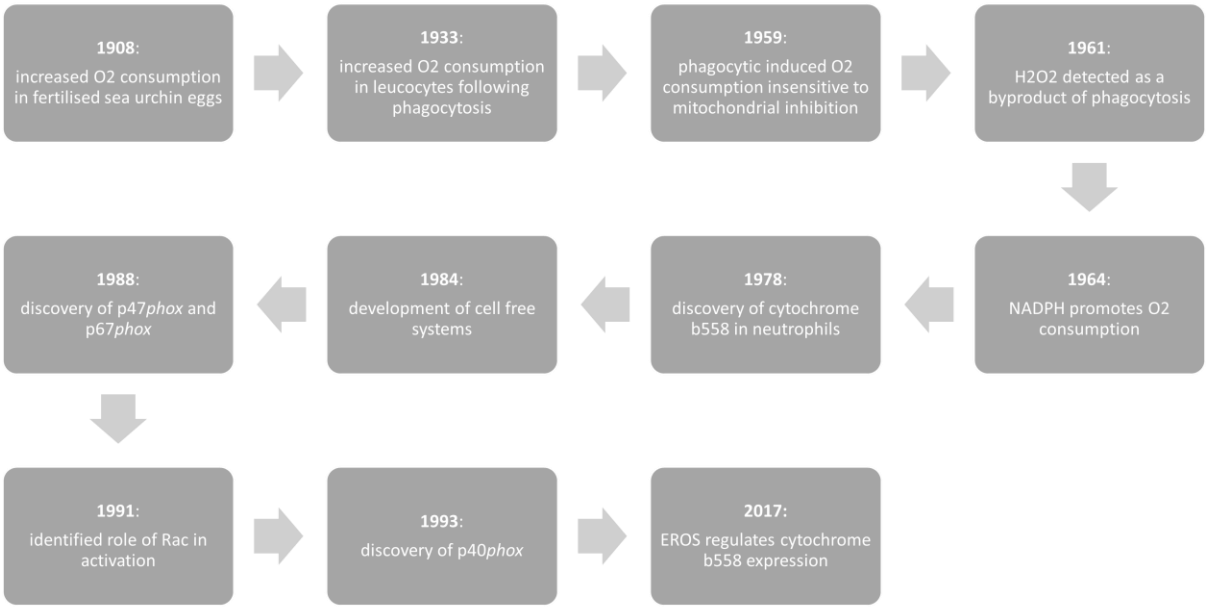

Figure 1.3: Timeline of the discovery of the phagocyte NADPH oxidase.

1.2.4. Chronic Granulomatous Disease

The complete discovery of the phagocyte NADPH oxidase was assisted by clinical observations of a rare and fatal disease in young boys in 1959 [35]. The unusual disease consisted of lymphadenitis, pulmonary infiltrations, and eczematoid dermatitis. It was discovered in 1967 that the phagocytes from these patients were unable to produce the respiratory burst [36]. It was later described that the causative mutation mapped to Xp21.1

was deleterious for cytochrome b558, which was found to be absent from the phagocytes of these patients [37]. Additionally, autosomal recessive forms of the same disease were identified [30,38,39], which were found to be deleterious for the cytosolic components of the phagocyte NADPH oxidase. This deficiency of the phagocyte NADPH oxidase in humans is called Chronic Granulomatous Disease (CGD).

CGD is a severe primary immunodeficiency characterised by recurrent bacterial and fungal infections. Deficiencies in any one of the subunits that form the phagocyte NADPH oxidase complex can cause CGD. Mutations in gp91*phox,* located on the X chromosome, is responsible for two-thirds of CGD cases (X-linked CGD). Autosomal recessive mutations in p22*phox*, p47*phox* or p67*phox* are responsible for approximately 30% of cases [40]. X-linked CGD typically manifests as a more clinically severe phenotype than autosomal recessive CGD, with greater mortality and morbidity [41]. Increased severity of disease has been associated with residual NADPH oxidase function and ROS production, patients with X-linked CGD have less residual ROS production than those with autosomal recessive mutations [42].

Owing to the absence of a functional phagocyte NADPH oxidase, CGD patients are unable to produce the ROS that are essential for inducing an effective immune response to clear opportunistic infections [43]. Ineffective elimination of pathogens results in the accumulation of phagocytes at the infection site resulting in the formation of granulomas. However, sterile granulomas can also form in the absence of an infectious pathogen, confirmed by absence of a pathogen inside the granuloma, a hallmark of CGD. These granulomas respond to immunomodulatory treatment, as they are the result of hyperinflammation [44].

CGD patients often present with hyperinflammatory and autoimmune phenomena; they typically develop a Crohn's-like inflammatory bowel disease [45], or autoimmune diseases such as cutaneous and systemic lupus erythematosus [43]. Interestingly, heterozygous mothers of males with X-linked CGD are also more likely to develop lupus-like symptoms, as half of their innate immune cells are deficient in gp91*phox* secondary to X-linked inactivation [46–48].

In a study on a French cohort of 98 CGD patients, 70% of patients experienced inflammatory manifestations typically involving the gut, lung or eye [49]. They also found that patients with X-linked gp91*phox* deficiency were twice as likely to experience inflammatory episodes compared to patients with autosomal recessive CGD [49]. Similarly, in another cohort of CGD patients it was found that 89% of patients who had inflammation of the gut were those with

X-linked CGD [50]. Altogether, the variety of symptoms shown by CGD patients indicate that the phagocyte NADPH oxidase has influences over both the innate and adaptive immune systems.

1.2.5. Function

Phagocyte NADPH oxidase derived ROS has two major roles within the immune system; to kill bacteria and to regulate immune responses.

1.2.5.1. Bactericidal activity

One major role for the phagocyte NADPH oxidase in the immune system is in antimicrobial host defence, either through direct or indirect mechanisms, via its ability to produce ROS. Vesicles containing the activated NADPH oxidase complex can bind to the phagosome, releasing antimicrobial ROS to directly kill the engulfed bacteria [15].

ROS produced by the NADPH oxidase can also indirectly kill bacteria by activating cellular signalling pathways. ROS can trigger the formation of neutrophil extracellular traps (NETs), which are comprised of decondensed chromatin and granular proteins [51]. Pro-inflammatory signals received by the neutrophil trigger the release of these NETs into the extracellular space, allowing the capture and killing of invading bacteria [51,52]. Neutrophils from CGD patients are unable to form NETs, demonstrating that the lack of ROS prevents the formation of an effective innate immune response [52]. Therefore, the microbicidal activity mediated by the phagocyte NADPH oxidase is critical during the innate immune response.

1.2.5.2. Modulation of immunity

The phagocyte NADPH oxidase is also involved in modulating the immune response. gp91*phox* deficient mice experience exaggerated inflammation in response to an intradermal injection of Aspergillus fumigatus, and this resulted in the formation of sterile granulomas. Wildtype control mice briefly experienced a mild inflammatory response and had no granuloma formation [53]. A later study by the same group found that retroviral-mediated gene transfer to reconstitute gp91*phox* expression prevents the exaggerated inflammatory response and granuloma formation in response to Aspergillus infection [54]. Similarly, Segal *et al*., (2010) found that both p47*phox* deficient mice and gp91*phox* deficient

mice develop persistent inflammation when treated with zymosan, a sterile component of fungal cell walls, whereas wildtype mice develop mild inflammation only. This paper went on to describe that these NADPH oxidase deficient mouse models have increased NF-κB activity and higher levels of pro-inflammatory cytokines TNFα and IL-17 when compared to wildtype controls [55]. Another group found that when p47*phox* expression was rescued in p47*phox* deficient mice, they experienced only mild inflammation similar to that of wildtype animals [56]. Additionally, p47*phox* deficient animals develop more severe arthritis than healthy controls when challenged with collagen-specific T cells, which can be reduced following treatment with NADPH oxidase activating drugs [57,58]. These studies indicate that the generation of ROS from the phagocyte NADPH oxidase is essential to prevent hyperinflammation and autoimmune responses from developing. This finding across two different mouse models reinforces the role of the entire phagocyte NADPH oxidase complex in regulating immune responses, rather than through individual *phox* proteins. In order to regulate immune responses, the NADPH oxidase complex has been implicated in the modulation of NF-κB signalling, type I interferon and the inflammasome.

1.2.5.2.1. NF-κB signalling

It has been known since 1991 that the activity of NF-κB can be regulated by its redox state [59]. It has since been discovered that the activity of the phagocyte NADPH oxidase can upregulate NF-κB activation, and NADPH oxidase inhibition prevents activation of NF-κB [6061]. Early studies identified the phagocyte NADPH oxidase in human airway smooth muscle cells. The flavoprotein inhibitor, diphenylene iodonium (DPI), inhibited the proliferation of human airway smooth muscle cells *in vitro* by preventing the activation of NF-κB [60]. This demonstrates that NADPH oxidase can regulate the proliferation of airway smooth muscle cells via its activation of NF-κB signalling. Another study found that NF-κB was activated in the human K562 cell line that expressed all components of the NADPH oxidase following stimulation, whereas NF-κB was not activated when any components of the NADPH oxidase were missing [61]. This is supported by Fan *et al.,* (2002) that found significantly reduced NF-κB activity in the lungs of p47*phox* deficient mice, when compared to wildtype controls [62]. These studies suggest that the phagocyte NADPH oxidase can positively regulate NF-κB signalling.

However, the phagocyte NADPH oxidase can also negatively regulate NF-κB activity. Trevelin *et al*., (2016) describe a novel p40*phox*/thioredoxin-1/NF-κB signalling pathway responsible for restraining inflammation. Activation of the phagocyte NADPH oxidase causes p40*phox* and thioredoxin-1 (TRX-1) to interact, resulting in the nuclear exclusion of TRX-1. TRX-1 regulates the redox state of NF-κB, therefore when it is unable to enter the nucleus, NF-κB remains inactivated and is unable to induce the transcription of TNFα and TLR4. Inversely, in CGD patients or following NADPH oxidase inhibition, this interaction is prohibited so TRX-1 accumulates in the nucleus, triggering NF-κB to induce enhanced transcription of inflammatory mediators [63]. Another study found that p47*phox* deficient mice have enhanced NF-κB activation and increased production of proinflammatory cytokines following LPS stimulation, compared to wildtype controls [64]. Addition of H_2O_2 prevents the exaggerated LPS-induced NF-κB activation in p47*phox* deficient mice to similar levels as wildtype controls, demonstrating that NADPH oxidase derived ROS can regulate the intracellular redox state to restrain LPS-induced NF-κB activation [64]. Similarly, Warnatsch *et al*., (2017) found that secretion of NADPH oxidase derived ROS dictates the appropriate immune response according to microbe size, acting to modulate NF-κB signalling. ROS are secreted into the phagosome following phagocytosis of small microbes, which oxidise p50 and triggers its degradation, thus suppressing NF-κB activity. This mechanism prevents excess cell recruitment and hyperinflammation in response to small microbes. The authors also suggest that when ROS is absent, such as in CGD, immune cells erroneously mount an excessive immune response via activation of the NF-κB pathway required for elimination of large pathogens, resulting in hyperinflammation [65]. These studies demonstrate the complex and differing roles of the phagocyte NADPH oxidase in the development of hyperinflammation.

Alternatively, some studies have found that NF-κB can regulate the expression of the phagocyte NADPH oxidase. Anrather *et al*., (2006) found reduced gp91*phox* expression in NF-κB deficient fibroblasts, which could be rescued by reconstituting NF-κB expression [66.] This is supported by another study that found TNFα-induced NF-κB activation upregulates the transcription and protein expression of gp91*phox,* p47*phox* and p67*phox.* Inhibitors of NF-κB signalling blocked TNFα induced upregulation of gp91*phox*, p47*phox* and p67*phox* at both message and protein level, and resulted in decreased ROS production [67]. These studies

suggest that NF-κB and NADPH oxidase may act in a positive feedback loop and propagate the activation of each other, which can result in sustained immune responses and the development of hyperinflammation.

Overall, it is clear there is crosstalk between NF-κB and the phagocyte NADPH oxidase, which together can act as a highly important but context dependent regulator of immunity.

1.2.5.2.2. Type I Interferon

There is evidence that the phagocyte NADPH oxidase can regulate the production of type I interferons; IFNα and IFNβ. Olofsson *et al*., (2003) identified that polymorphisms in the gene encoding p47*phox* can regulate arthritis severity in rats. Disease-associated mutations in p47*phox* resulted in reduced ROS production and increased activation of arthritogenic CD4+ T cells, suggesting p47*phox* deficiency is a driver of severe inflammatory arthritis in rats [68]. However, a criticism of this paper is that the rat model used is not completely deficient in functional phagocyte NADPH oxidase and ROS production. Thus, in a later study in which they utilised p47*phox* deficient mice, they found that 55% of differentially expressed genes were interferon-regulated genes (IRGs). They also found upregulated expression of STAT1, the transcription factor that regulates downstream IFN signalling. In comparative studies of CGD patients they found that 53% of upregulated genes were IRGs, and STAT1 was also upregulated [69]. In a later study, the authors restored p47*phox* expression in knock out mice. They found this conditional expression of p47*phox* normalised the exaggerated type I IFN signature, and subsequently ameliorated arthritis development [70]. Together, these results demonstrate a pronounced type I IFN signature in p47*phox* deficient mice and CGD patients that is responsible for driving inflammatory conditions such as arthritis.

In contrast to the arthritis model above, studies using the non-obese diabetic (NOD) mouse model of type 1 diabetes found that NOD mice are resistant to spontaneous diabetes development when p47*phox* is absent [71]. In a later study, the same authors found reduced STAT1 activation in p47*phox* deficient NOD mice [72], a marked contrast to the elevated STAT1 phosphorylation found in the arthritis studies. These conflicting data suggest that the influence of NADPH oxidase derived ROS on interferon signalling via STAT1 is complex and context dependent.

1.2.5.2.3. Inflammasome

The interaction between the phagocyte NADPH oxidase and the inflammasome is complex. One argument is that the activation of the inflammasome is phagocyte NADPH oxidase dependent. Macrophages that are stimulated with the classical activator of the inflammasome, ATP, results in the production of ROS, which is required for the activation of caspase-1 and secretion of IL-18 and IL-1β [73]. A later study found that ATP-driven production of ROS by the phagocyte NADPH oxidase was essential to activate Apoptosis Signal-Regulating Kinase 1 (ASK1) to trigger ATP-induced apoptosis in macrophages [74]. Additionally, stimulation of the NLRP3 inflammasome with asbestos or silica, requires the activation of the phagocyte NADPH oxidase. When p22*phox* was silenced or antioxidants were used, the secretion of IL-1β was reduced in response to asbestos or silica treatment [75]. Similarly, NLRP3 inflammasome component expression, caspase-1 activation and IL-1β secretion is increased in a model of traumatic brain injury, but reduced when the phagocyte NADPH oxidase is absent [76]. These studies demonstrate that the NADPH oxidase is essential for complete inflammasome activation in response to ATP, asbestos and silica.

However, one study found chronic inflammasome activation in the absence of the phagocyte NADPH oxidase. Monocytes from CGD patients with mutations in gp91*phox*, p22*phox* or p47*phox* had very high caspase-1 and IL-1β levels compared to healthy controls, even in the absence of stimulation [77]. Such unrestrained inflammasome activity may contribute to driving the development of autoimmunity in CGD patients.

Alternatively, it has also been noted that the inflammasome can potentiate ROS production. Pfeiffer *et al*., (2007) identified that stimulation of a murine macrophage cell line with ATP resulted in the production of ROS [78]. Cruz *et al* (2007) confirmed these findings in rat macrophages and found that production of ROS resulted in the activation of phosphatidylinositol 3-kinase (PI3K) pathways, Akt and ERK1/2 via the inactivation of PTEN [73]. It has also been found that the NLRP3 inflammasome can negatively regulate phagocyte NADPH oxidase activity. The NLRP3 inflammasome and caspase-1 can modulate the activity of the phagocyte NADPH oxidase by cleaving gp91*phox*. This prevents the generation of ROS and ultimately regulates the acidification of phagosomes containing phagocytosed Staphyloccus aureus. Therefore, when the NLRP3 inflammasome is absent, the activity of the phagocyte NADPH oxidase is unrestrained and excessive ROS is produced [79].

In summary, the production of ROS can assist in the activation of the inflammasome, and the activation of the inflammasome can modulate the production of ROS. These studies demonstrate a complex and dynamic relationship between the phagocyte NADPH oxidase and the inflammasome.

1.2.6. NOX family members

Following the discovery of the phagocyte NADPH oxidase, it was observed that similar complexes were present in other cell types, such as fibroblasts. The respiratory burst was normal in fibroblasts from CGD patients, suggesting the phagocyte NADPH oxidase was not the source of ROS in these cell types [80]. Once the human genome sequence was made available, the identity of the other NOX family members was quickly elucidated. NOX1 was first discovered, followed by NOX3, NOX4 and NOX5. In parallel, the large NOX homologs Dual Oxidase 1 (DUOX1) and Dual Oxidase 2 (DUOX2) were also discovered [81].

Table 1.1: Location, structure and function of the NADPH oxidase homologs.

Homolog	Location	Subunits	Function	Ref
NOX1	Colon epithelium Uterus Prostate	NOX1 p22*phox* NOXO1 NOXA1 Rac	Gut microbiota homeostasis	82 83
NOX3	Inner ear	NOX3 p22*phox* NOXO1 NOXA1 Rac	Balance and spatial orientation in mice	84
NOX4	Kidney Endothelial cells Osteoclasts	NOX4 p22*phox*	Involved in osteoclastogenesis and preventing atherosclerosis	85 86 87 88 89
NOX5	Lymph nodes Spleen Testes	NOX5 Ca^{2+} dependent	Unknown	90 91
DUOX1	Thyroid gland Airway epithelial cells	DUOX1 DUOXA1 Ca^{2+} dependent	Thyroid hormone biosynthesis	92 93
DUOX2	Thyroid gland Airway epithelial cells Salivary glands Colon epithelium	DUOX2 DUOXA2 Ca2+ dependent	Thyroid hormone biosynthesis Gut microbiota homeostasis	92 93 94 95

The NOX homologs have a variety of expression patterns and functions (table 1.1). NOX1-4 are similar in that they are comprised of a membrane-bound stabilising subunit and two

cytosolic subunits; an activating subunit and an organiser subunit. p22*phox* is present in NOX1-, NOX2-, NOX3- and NOX4- containing oxidases and has the same role of stabilising the NOX protein. NOXO1 present in NOX1 and NOX3 is homologous to p47*phox*, and acts as the organiser subunit. NOXA1 present in NOX1 and NOX3 is homologous to p67*phox* and acts as the activating subunit. NOX5 and the two DUOX complexes are similar in that their activation is dependent on Ca2+. DUOX1 and DUOX2 differ from NOX1-5 as they have seven transmembrane domains, rather than six [81].

1.2.6 Phagocyte NADPH oxidase in T cells

1.2.6.1 Differentiation

There are many conflicting studies regarding the influence of the phagocyte NADPH oxidase on the differentiation of T helper subsets, reviewed in [1]. Briefly, the first published study on T helper differentiation in NADPH oxidase deficiency describes a preferential Th1 response in gp91*phox* $^{-/-}$ and p47*phox* -/- CD4+ T cells [96]. IFNγ secretion is indicative of a Th1 response, IL-4, IL-5 and IL-13 of a Th2 response, and IL-17 and TGFβ of a Th17 response (figure 1.4). Jackson *et al*., (2004) found that stimulation with anti-CD3 causes an increase in IFNγ secretion and decrease in IL-4 and IL-5 secretion from CD4+ T cells. As this study preceded the discovery of Th17 cells, polarisation towards a Th17 response was not assessed [97]. However, Kwon *et al.,* (2016) later found IL-4 secretion was increased from gp91*phox* -/- CD4+ T cells following anti-CD3 and anti-CD28 stimulation, indicative of a Th2 response in NADPH oxidase deficiency [98]. Contradicting both, Tse *et al.,* (2010) found increased IL-17 and TGFβ secretion, but decreased IFNγ and IL-4 secretion from p47*phox* $^{-/-}$ CD4+ T cells. Therefore, the authors suggest that a Th17 response develops following anti-CD3 and anti-CD28 stimulation [99]. Although, this group used the NOD strain of mice whereas the previous mentioned studies used the C57BL/6 strain. NOD mice are renowned for their autoimmune phenotype, which may account for the difference in findings. Most studies find that NADPH oxidase deficiency results in the development of combined Th1/Th17 responses, with increased levels of IFNγ, IL-17 and their associated transcription factors T-bet and RORγt [100–102]. The importance of the phagocyte NADPH oxidase during CD4+ T helper differentiation remains to be clarified, but it appears that proinflammatory Th1/Th17 skewing is favoured.

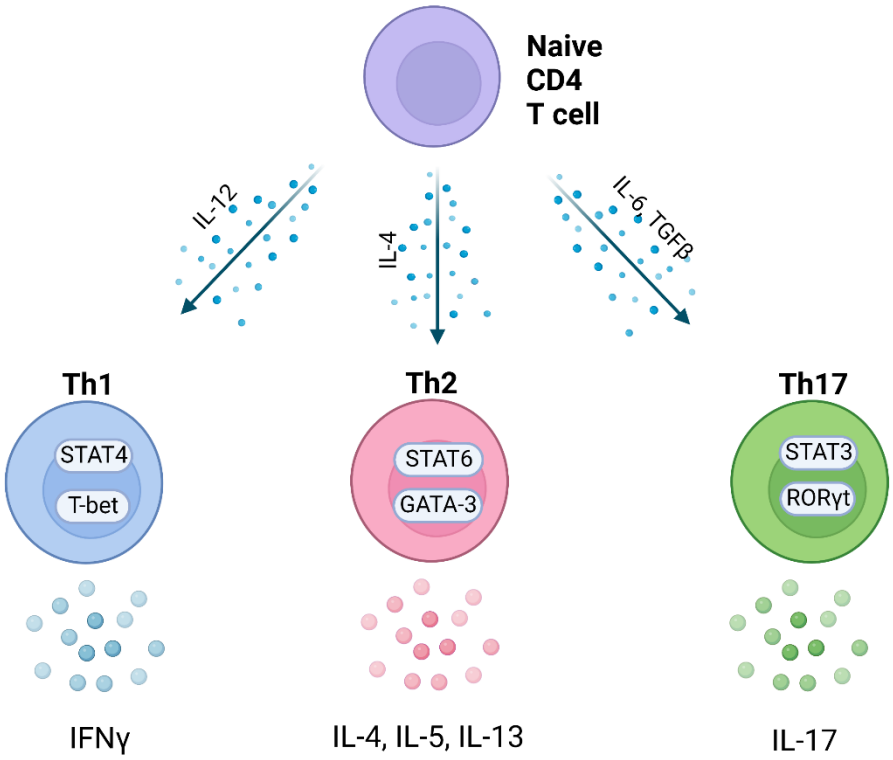

Figure 1.4: Naïve CD4+ T cells can polarise into Th1, Th2 or Th17 cells. Following TCR engagement and co-stimulation, the cytokine environment can direct different T helper skewing programmes. IL-12 induces the transcription of T-bet via STAT4 and produces IFNγ, indicative of a Th1 response. IL-4 induces the transcription of GATA-3 via STAT6 and produces IL-4, IL-5 and IL-13, indicative of a Th2 response. IL-6 and TGFβ induces the transcription of RORγt via STAT3 and produces IL-17, indicative of a Th17 response [103]. Naive cells can also differentiate into Th9, T regulatory and T follicular helper cells, to name a few.

NADPH oxidase derived ROS is also involved in the differentiation T regulatory cells (Tregs). gp91*phox* -/- mice have fewer circulating CD4+CD25+ Tregs and decreased FoxP3 expression, indicating that the NADPH oxidase has a role in controlling the development of Tregs [101]. However, a study of CGD patients did not find a decrease in Treg number or function, except in those with gp91*phox* deficiency [104]. The authors suggest this correlates with the fact that gp91*phox*$^{-/-}$ CGD patients have more inflammatory symptoms than those with mutations in other NADPH oxidase subunits [49,104].

1.2.6.2 Signalling

Stimulation of the T cell receptor (TCR) results in the production of ROS. First demonstrated in 2002, Devadas *et al*., showed that culturing a murine cell line with anti-CD3 resulted in the rapid production of ROS, and was inhibited by the flavoprotein inhibitor DPI [105]. These results were later confirmed by the same group, they showed that ROS production was absent in gp91*phox*-/- and p47*phox*-/- T cells following stimulation with anti-CD3 [96]. These data suggest that phagocyte NADPH oxidase derived ROS are important signalling molecules during the T cell signalling cascade.

Expression of the phagocyte NADPH oxidase is required for restraining the suppressive ability of Tregs. gp91*phox*$^{-/-}$ Tregs have significantly greater expression of the immunosuppressive molecules CTLA-4, GITR, CD39 and CD73. Additionally, gp91*phox*$^{-/-}$ Tregs have increased FOXP3 expression and greater NF-κB activation. Subsequently, Tregs deficient in gp91*phox* have greater suppressive activity than wildtype control Tregs [106]. Interestingly, p47*phox*$^{-/-}$ Tregs have poorer suppressive capabilities than their wildtype counterparts [107], which may relate to the functions of p47*phox* independent of phagocyte NADPH oxidase [108,109].

1.2.6.3 Apoptosis

The phagocyte NADPH oxidase is required for inducing apoptosis in activated T cells during the resolution of an immune response [110]. Clearance of excess T cells after antigen clearance is essential to prevent an over exuberant immune response when responding to new and repeated antigenic challenges. gp91*phox*$^{-/-}$ T cells display significantly improved survival *in vivo* following cytokine deprivation. Greater antigen-specific proliferative responses are also observed when compared to wildtype controls, due to the larger pool of T cells that remain after the initial antigen challenge [110]. This demonstrates that the phagocyte NADPH oxidase is required for both the activation and restraint of T cell responses.

1.3 P2X7

1.3.1 Structure

P2X7 is a member of the P2X family (P2X1-7) of non-selective ligand-gated ion channels that can bind ATP. Binding of ATP induces the formation of a homo- or heterotrimeric channel that is permeable to Na+, K+ and Ca2+. P2X receptors contain two transmembrane domains

that are linked by an extracellular ATP binding domain, and intracellular N- and C- termini that are not well conserved between family members. P2X7 is most structurally different from its family members as it has a long C-terminus of 240 amino acids, compared to less than 100 amino acids for most of the other P2X family members [111].

1.3.2 Function

Activation of P2X7 initiates opening of the ion channel and following prolonged stimulation a "macropore" forms, which allows the passage of larger molecules. Functionally, P2X7 has a lower affinity for ATP than its family members, with P2X1-6 having an EC50 of 1–10 μM, whereas its >100 μM for P2X7 [112]. This low sensitivity to ATP means P2X7 is able to detect high ATP concentrations released at sites of tissue damage, acting as a danger sensor [111].

P2X7 is expressed on a variety of immune cells including macrophages, dendritic cells (DCs) and T cells. It is well known that P2X7 is involved in the activation of the NLRP3 inflammasome in macrophages [113]. Priming signals such as LPS stimulation of TLR4 induces the expression of NLRP3 and pro-IL-1β. Activation of P2X7 by ATP initiates the assembly of the NLRP3 inflammasome, triggering caspase-1 to cleave pro-IL-1β and IL-18 into their mature pro-inflammatory states [113]. Recently, it has also been described that P2X7 signalling in non-classically activated M2 macrophages results in secretion of anti-inflammatory proteins, suggesting P2X7 signalling is involved in many immune pathways [114]. Activation of P2X7 in DCs also results in formation of the NLRP3 inflammasome that drives IL-1β secretion [115]. IL-1β secreted from the DC is necessary for the priming of IFNγ-producing CD8+ T cells, demonstrating that P2X7 signalling is also important in linking the innate and adaptive immune responses [115].

P2X7 signalling can be modulated in a number of ways [116]. Pannexin-1 channels on the cell membrane can release ATP into the extracellular space, which can act on P2X7 receptors in an autocrine or paracrine manner. The expression of pannexin-1 channels is highly dynamic, channels are able to translocate and accumulate in response to appropriate signals. Ectonucleotidases are also important in modulating P2X7 signalling. CD39 hydrolyses ATP to AMP, and CD73 further hydrolyses AMP into adenosine, preventing P2X7 signalling by removing its ligand. Differential expression of ectonucleotidases contributes to the pro- or anti-inflammatory mechanisms of certain cell types [116].

1.3.3 Splice variants

Splice variants have been identified for both the human and mouse P2X7 receptor. Nine splice variants of the human P2X7A receptor have been described so far, P2X7B – P2X7J. P2X7B is widely expressed, it has a truncated C-terminus and is able to respond to ATP but unable to induce apoptosis [117]. Additionally, multiple single nucleotide polymorphisms (SNPs) have been identified in the human P2X7 receptor, some of which have been associated with aberrant immune cell functions [118].

In mice, a P2X7 SNP variant P451L was discovered in the long C-terminal tail of the P2X7 receptor [119]. 451L is expressed in C57BL/6 mice whereas P451 is expressed in BALB/c mice. When expressed in the HEK293 cell line, it was found that 451L affects the function of the P2X7 receptor, when compared to the P451. Additionally, 451L showed impaired functional responses in T cells compared to the P451, demonstrating that the P451L SNP can affect P2X7 receptor induced T cell responses [119]. However it was later discovered that P2X7 is very lowly expressed on T cells from C57BL/6 mice, which may account for the impaired functional responses found in earlier studies [120].

Two splice variants were also identified in mice: P2X7a and P2X7k. P2X7k has 8-fold higher sensitivity to ATP agonists compared to the P2X7a variant [121]. P2X7a is predominantly expressed in macrophages, whereas P2X7k is predominantly expressed by T cells [122,123]. P2X7k can also be activated by NAD. Mouse T cells express an ADP-ribosyltransferase, ARTC2.2, which can catalyse the ADP-ribosylation of arginine residues on P2X7, thus making the mouse P2X7k receptor sensitive to extracellular NAD [124–126].

There are two strains of P2X7 knockout mice available, generated by GSK and Pfizer. The P2X7 deficient mouse generated by GSK is disrupted in exon 1, whereas the Pfizer generated mouse is disrupted in exon 13 [127,128]. It later emerged that P2X7a was knocked out in both strains, whereas P2X7k was also knocked out in the Pfizer strain [129]. Therefore, P2X7 was deleted in all immune cells in the Pfizer generated mouse, whereas the GSK generated mice expressed a functional P2X7 receptor on the T cells but lacked P2X7 in all other immune cells [121,130]. This finding was integral to interpret contradicting results, one group found that development of experimental autoimmune encephalomyelitis (EAE) was exacerbated in Pfizer generated P2X7 knock out mice, whereas another group found attenuated

development of EAE in the GSK generated mice [131,132]. Therefore, the different P2X7 mouse strains can be tactically used when designing experiments, but it is important to know and understand the different P2X7 variants when conducting mouse studies.

1.3.4 Relationship with P2X4

P2X4 and P2X7 are widely co-expressed in cells of the immune system. The gene encoding P2X7 is located in close proximity to P2X4; on chromosome 12 in humans where they are only 24kbp apart, and chromosome 5 in mice [133]. They also exhibit 41% sequence homology, and the highest amino acid sequence similarity [134] together suggesting a gene duplication event occurred [135].

Studies regarding the interaction between P2X4 and P2X7 are conflicted. Early co-immunoprecipitation studies suggested that P2X7 forms a homotrimeric channel only, whereas all other P2X family members can heterotrimerise [136]. A later study reported heteromerisation between P2X4 and P2X7 [137], however this has been disputed. Further studies suggest separate homotrimerisation of the P2X4 and P2X7 receptors, that are located in close proximity to each other [138,139].

Additionally, data suggests that P2X4 and P2X7 receptors can influence the expression of each other. Weinhold *et al*., (2010) found that P2X4 expression is upregulated when P2X7 is absent and vice versa [140]. This suggests that P2X4 and P2X7 may be able to compensate for the other when one is absent. Recent studies have also found that P2X4 and P2X7 can act cooperatively. Sakaki *et al*., (2013) found that P2X7-mediated secretion of IL-1β and IL-18 from mouse bone marrow derived DCs required the expression of P2X4 [141]. This suggests that P2X4 and P2X7 are independent homotrimers that can physically interact to contribute to functionally relevant processes.

1.3.5 In disease

Dysfunctional P2X7 signalling has been associated with a range of diseases, particularly of the central nervous system (CNS) where P2X7 is readily expressed on microglia [142,143]. In studies of Alzheimer's disease (AD), injection of Amyloid beta (Aβ) triggered IL-1β secretion via the P2X7 receptor in wild type mice, but not P2X7 receptor deficient mice, demonstrating that P2X7 signalling can be activated by Aβ. This suggests P2X7 signalling is

involved in a pathological feedback loop resulting in the development of AD [144]. Additionally, α-synuclein, which is involved in the pathogenesis of Parkinson's disease, can bind to P2X7 receptors expressed on microglial cells and subsequently activate the phagocyte NADPH oxidase, which can lead to the exacerbation of oxidative stress [145]. This demonstrates that the P2X7 receptor can bind multiple damaging pathogenic molecules and propagate CNS diseases.

1.3.6 P2X7 in T cells

1.3.6.1 Differentiation

P2X7 activation has been found to promote the polarisation or conversion of CD4+ T cells into proinflammatory Th1 or Th17 cells. In an *in vitro* mouse model of malaria infection, P2X7-/- CD4+ T cells stimulated with infected red blood cells secrete less IFNγ than wildtype CD4+ T cells. Moreover, the authors found less T-bet expression in P2X7-/- CD4+ T cells compared to wildtype [146]. This suggests stimulation of P2X7 induces Th1 skewing in naïve T cells.

P2X7 stimulation induces the conversion of T regulatory cells (Tregs) into Th17 cells [147]. Wildtype Tregs were stimulated with BzATP, which induced a gradual decrease in Foxp3 and increase in RORyt expression, but this was not seen in P2X7-/- Tregs. Pharmacological inhibition of the P2X7 receptor has also been found to result in reduced Th1/Th17 differentiation [148]. These studies demonstrate that the P2X7 signalling is involved in the development of Th1 and Th17 responses.

Additionally, P2X7 signalling combined with gamma-delta TCR expression contributes to the commitment of immature thymocytes to the gamma-delta T cell lineage [149].

1.3.6.2 TCR signalling

TCR stimulation results in the release of ATP from the cell via pannexin-1 channels, and the subsequent autocrine stimulation of P2X7 receptors of the cell membrane [150,151]. This autocrine signalling contributes to TCR-mediated Ca2+ influx, NFAT activation and IL-2 secretion necessary for T cell activation. Additionally, the presence of P2X7 in the immunological synapse has been suggested to provide tonic co-stimulatory signals during

activation of the T cell [152]. Therefore, P2X7 signalling contributes to generating successful TCR signalling responses.

1.3.6.3 Marker shedding

Stimulation of P2X7 receptors triggers the activation of the metalloproteinases ADAM10 and ADAM17 [126]. These metalloproteinases can induce the shedding of cell surface markers CD62L, CD27 and IL-6R [126,153,154]. P2X7 induced CD62L shedding promotes the migration of T cells from lymph nodes. P2X7 induced CD27 shedding prevents it binding with its ligand CD70, which is essential for shaping T cell responses [155]. P2X7 induced IL-6R shedding increases the availability of soluble IL-6R to bind IL-6 and influence proinflammatory IL-6 trans-signalling [154]. P2X7 driven shedding has a crucial role in many T cell functions.

1.3.6.4 Apoptosis

Activation of P2X7R in T cells triggers a novel cell death pathway that combines features of both apoptosis and necrosis [156]. Following P2X7 stimulation, cells rapidly undergo shrinkage and translocation of phosphatidylserine to the outer membrane. This is quickly followed by cell swelling and lysis [156]. P2X7 stimulation can trigger apoptosis in double positive (DP) thymocytes that fail to undergo positive selection. Positively selected DP thymocytes down regulate expression of P2X7 in order to protect from apoptosis during this developmental stage [157]. This demonstrates that P2X7 may utilise this novel cell death mechanism to modulate T cell development.

Signalling via P2X7 to induce cell death is an effective method to control T cell responses. ATP driven P2X7 activity is involved in controlling Tfh cell numbers in secondary lymphoid tissues [158]. P2X7 signalling restricts the proliferation of aberrant Tfh cells in experimental models of systemic lupus erythematosus (SLE), a condition in which patients have reduced P2X7 activity in Tfh cells [158,159]. Tfh cells that receive TCR stimulation downregulate P2X7 receptor expression in order to protect the antigen responding T cell from cell death [158]. Similarly, P2X7 is also downregulated in T resident memory (TRM) cells that experience TCR signalling [160]. This ensures the protection and amplification of rapid responding cells upon reinfection with antigen.

1.4 EROS

1.4.1 Discovery

EROS (Essential for Reactive Oxygen Species; gene symbol *CYBC1*) was first described in 2017 [34]. It was identified as part of the Knockout Mouse Project (KOMP), which utilised an unbiased hypothesis-free approach to uncover new genes involved in host defence [161]. EROS is encoded by the previously undescribed and uncharacterised open reading frame *bc017643* and is highly conserved with the human orthologue *C17ORF62*.

EROS deficient mice are highly susceptible to Salmonella Typhimurium infection and die within 5 days of infection [34]. The organs of these mice suffer overwhelmingly high bacterial loads, as their immune cells fail to generate the ROS required to control bacterial replication and eliminate such infections. It emerged that EROS deficient immune cells lacked gp91*phox* and p22*phox* protein expression, two crucial members of the phagocyte NADPH oxidase complex. The phenotype of the EROS deficient mouse was similar to that of the gp91*phox* deficient mouse. It transpired that EROS is an ER-resident transmembrane protein that co-immunoprecipitates with gp91*phox*, regulating the expression of gp91*phox* and subsequently the expression of its binding partner, p22*phox.* Mass spectrometry analysis showed that P2X7 receptor expression was also downregulated in EROS deficient cells [34]. This was later independently verified by another group [162], demonstrating that EROS mediates the expression of both gp91*phox* and P2X7.

1.4.2 Function

EROS acts as a highly selective placeholder chaperone. EROS is required very early during gp91*phox* biogenesis, where it interacts with the oligosaccharyltransferase (OST) complex. The OST complex is a component of the translocon, and is involved in glycosylation, assisting in the appropriate folding of proteins and insertion into the Endoplasmic Reticulum (ER) membrane [163]. EROS directly binds to an “unsatisfied surface” on the inherently unstable gp91*phox* precursor, stabilising and preventing the misfolding of gp91*phox* during the initial glycosylation steps [164]. This occurs prior to the incorporation of heme and stabilisation by p22*phox*. EROS remains associated with gp91*phox* following its heterodimerisation with p22*phox*, until the heterodimer is successfully exported from the ER [164] (figure 1.5).

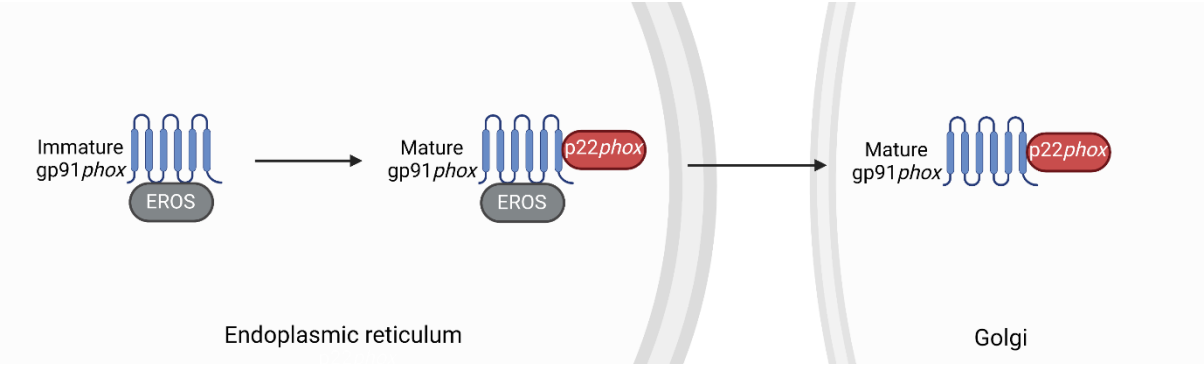

Figure 1.5: EROS regulates the protein expression of gp91*phox*. EROS binds to immature gp91*phox,* providing the necessary stabilisation for gp91*phox* maturation prior to its heterodimerisation with p22*phox*, where it is subsequently exported from the endoplasmic reticulum.

1.4.3 In disease

It was hypothesised that as EROS deficient mice lack ROS and phagocyte NADPH oxidase expression similar to that of gp91*phox* -/- mice, that mutations in the human EROS orthologue may also cause CGD. EROS deficiency in humans caused by homozygous mutations in the human orthologue *C17ORF62*, were identified as the 5th cause of CGD (CGD5; OMIM: 618334) [165,166].

The first described EROS patient, born of consanguineous marriage, initially presented with recurrent opportunistic bacterial infections [165]. He had a severely impaired dihydrorhodamine (DHR) test result, a diagnostic test that examines the oxidative burst by granulocytes, indicating CGD. It was later discovered that he had sterile granulomatous inflammation, typical of CGD. Intriguingly, he also developed autoimmune haemolytic anaemia, not typically characteristic of CGD.

There is a high incidence of EROS deficiency in Iceland, with 8 cases in the population of approximately 350,000. Interestingly, it has been noted that one of these patients has developed the autoimmune condition glomerulonephritis, not typically characteristic of CGD. Patients have also experienced unusual infections including *Legionella* and *Mycobacterium tuberculosis*. In Iceland, 1:70 people are heterozygous for a mutation in CYBC1, which encodes a premature stop codon [166]. The siblings of the first described CGD5 patient were heterozygous and expressed approximately 50% of EROS protein compared to

healthy controls, but had no apparent CGD5 symptoms [165]. This suggests that only a small amount of EROS is required to fulfil its major function in regulating gp91*phox* expression to enable NADPH oxidase-derived ROS generation, and perhaps EROS has additional functions not yet described.

1.5 Project rationale

EROS regulates the expression of two distinct proteins, gp91*phox* and P2X7, both of which have important functions within T cells, suggesting that EROS may too play a role in T cell biology. Additionally, as EROS deficient patients present with atypical autoimmune characteristics, suggests EROS may play a role in the development and regulation of T cell responses. Therefore, my project will focus on the role of EROS in T cell biology.

1.6 Overall project hypothesis

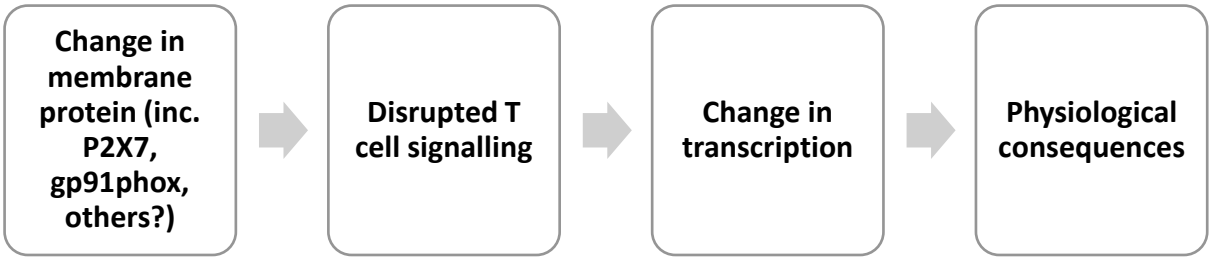

1.7 Overall project aims

To determine whether EROS affects membrane protein expression in CD4+ T cells

To examine T cell signalling pathways in EROS deficient CD4+ T cells

To identify the transcriptional changes that occur in EROS deficient CD4+ T cells

To describe the physiological consequences of EROS deficiency in CD4+ T cells

Chapter 2: Materials & Methods

2.1 Mice

All mice used in this thesis were on the C57BL/6 background and bred either in-house, in the WTSI or University of Manchester animal facilities. All mice were maintained in individually ventilated cages under specific pathogen free conditions. Age and sex matched mice were used for all experiments at 8-20 weeks of age. All studies complied with institutional guidelines and UK Home Office regulations.

2.1.1 EROS-/- mice

bc017643/EROS-/- mice were first described in [34]. Briefly, mice were generated as part of the Knock Out Mouse Project (KOMP) [167]. Knock out mice were generated using a tm1a (KOMP) knockout-first approach. Targeted embryonic stem cells were selected for neomycin resistance and β-galactosidase expression. bc017643tm1a(KOMP) allele structure was confirmed by long-range PCR and sequencing. A single-integration event was confirmed by neomycin-copy number analysis with quantitative RT-PCR. The bc017643tm1a/tm1a mouse line was derived from the EPD0079_5_A11 ES cell clone and maintained on a C57BL/6N genetic background. All genetically altered mice were genotyped using PCR to confirm the knockout status before use in experiments.

2.1.2 gp91*phox-/-* mice

B6.129S-Cybb^{tm1Din}/J (gp91*phox*) mice were obtained from JAX, strain 002365.

2.1.3 P2X7-/- mice

B6.129P2-P2rx7tm1Gab/J (P2X7) mice were kindly provided by Dr Nadja Kobold (Imperial College London), strain 005576.

2.1.4 Genotyping

EROS-/- mice were subjected to ear punching for identification purposes. Ear snips were suspended in 20µl digestion buffer (100mM Tris-HCl (Sigma), 200mM NaCl (Sigma) 0.2% SDS (Sigma), 5mM EDTA (Sigma), 100ug/ml Proteinase K (Thermofisher)) and incubated at 55°C overnight 300rpm. The following day the solution was centrifuged at 13000xg 5min RT, and

the homogenate was diluted 1:7 in 140µl autoclaved double distilled H_2O. It was then heated to 75°C for 15 mins before being put on ice or stored at -20°C.

Each mouse required 2 PCRs: one to confirm absence of the 458bp WT band and one to confirm presence of the 272bp knockout band (see table 2.1). PCR reaction mixtures were prepared on ice, according to table 2.2. PCR programme was as according to table 2.3. PCR was run on a 2% agarose (Thermofisher) gel with 1x Gel Red (Cambridge Bioscience), with a 100bp ladder (Thermofisher) at 150v for 30-60minutes. Bands were visualised on UVP BioDoc-IT imaging system.

Table 2.1: List of primers and their combinations used for genotyping

Primer	**Sequence**	**WT PCR?**	**KO PCR?**
BC017643_Fwd	TCCCTGGCTCAGACCTCTTC	Yes	Yes
BC017643_Rev	TCGCAACCTCATGCAACTTC	Yes	No
CAS_R1	TCGTGGTATCGTTATGCGCC	No	Yes

Table 2.2: Reagents used in genotyping PCR

Reagent	**Amount/ reaction**	**Manufacturer**
DNA	2ul	
2x OneTaq Master Mix	12.5ul	NEB
BC017643_Fwd primer	0.4uM	Sigma
BC017643_Rev / CAS_R1 primer	0.4uM	Sigma
DMSO	2%	Sigma
H_2O	To 25ul	

Table 2.3: PCR programme used in genotyping PCR

Stage	Temperature (°C)	Time	Repeat
Denature	94	5 min	
Denature	94	30 sec	X 34 cycles
Anneal	58	30 sec	
Extend	68	30 sec	
Extend	68	5 min	

2.2 Cell culture

2.2.1 Cell lines

HEK293/T cells were maintained in complete DMEM (Invitrogen), supplemented with 10% Fetal Bovine Serum (FBS; Biosera/PanBiotech), 1x Penicillin-Streptomycin-Glutamate (Invitrogen) and 10mM HEPES (Invitrogen). Cells were passaged at 90% confluency and used at 50% confluency in experiments.

PLB985 and EROS-/- PLB985 cells were maintained in complete RPMI (Invitrogen), supplemented with 10% Fetal Bovine Serum (FBS), 1x Penicillin-Streptomycin-Glutamate (Invitrogen), 1X Glutamax (Invitrogen), 1mM Sodium Pyruvate (Invitrogen) and 10mM HEPES (Invitrogen). Cells were passaged every 3-4 days.

Hut78 cells were maintained in complete IMDM (Invitrogen), supplemented with 20% Fetal Bovine Serum (FBS) and 1x Penicillin-Streptomycin-Glutamate (Invitrogen). Cells were passaged every 3-4 days.

2.2.2 Primary mouse cells

Spleens were harvested from mice, mascerated through a 70µM cell strainer and washed in 20mls MACS buffer (PBS + 0.5% Bovine Serum Albumin (BSA; Sigma)). Cells were subjected to magnetic bead isolation using the following cell isolation kits from Miltenyi Biosciences: Mouse CD4+ (L3T4) positive selection, Mouse naïve CD4+ negative selection, Mouse B cell negative selection, Mouse CD8a positive selection. Isolation performed according to manufacturer's protocol, briefly, cells were resuspended in appropriate volume of isolation beads according to cell number, incubated at 4°C for 10 minutes, washed if required, added

to primed LS column, falcon tube rinsed with 3ml MACS buffer and added to empty column (first wash), 3ml MACS buffer added to column once emptied (second wash). Negative selection = column eluate, positive selection = flushed from column. Purity checks were performed by flow cytometry to stain for CD4+ T cells; >95% purity for positive selection and >90% for negative selection was acceptable. Cells were cultured at densities of 1-2x10^6 cells/ml in complete IMDM (cIMDM; Invitrogen) supplemented with 10% Fetal Bovine Serum (FBS; Biosera/PanBiotech), 1x Penicillin-Streptomycin-Glutamate (Invitrogen), 1 mM Sodium Pyruvate (Invitrogen) and 10mM HEPES (Invitrogen).

2.3 PBMC isolation

Whole blood was collected in EDTA tubes (Greiner) from healthy donors. Blood was diluted 1:1 in PBS, layered on 15ml lymphoprep (StemCell), and spun at 800xg 20 mins without brake. Buffy coat layer was removed, washed twice in PBS, counted and frozen at 2x10^7 cells per vial in FBS + 10% DMSO (Sigma) and stored in liquid nitrogen until use.

2.4 Stimulations

2.4.1 ATP

In 96 well plates, 5mM ATP (2x; Invivogen) was prepared in 100µl cIMDM. Cells were resuspended at 2x10^6 cells/ml and 100µl cell suspension was added to ATP dilution, to produce a final 1x concentration of 2.5mM. Cells were incubated at 37°C, 5% CO_2 for 30 mins. Reaction was stopped by placing plate on ice and immediately harvesting cells for flow cytometric analysis.

2.4.2 Polyclonal anti-CD3/CD28

Tissue culture plates were coated with 10ug/ml anti-CD3 (BD) overnight at 4°C or at 37°C for a minimum of 2 hours. Plates were washed 2x with PBS prior to use. 2ug/ml anti-CD28 was added to cell solutions for the duration of the incubation. Cells were incubated at 37°C, 5% CO_2 for 48-72 hours. Stimulated cells were harvested, and spun at 2000rpm 5 mins. Supernatants were aliquoted to prevent freeze-thaw and stored at -80°C. Cell pellets were washed in PBS, flash frozen and stored at -80°C until use.

2.4.3 P2X7 inhibition

A438079 and A740003 were obtained from Sigma and prepared according to manufacturer's instructions. For titration experiments; inhibitors were serially diluted 1:10 in cIMDM from 400µM (4x), producing 1X concentrations ranging 100µM – 1pM. Inhibitors were present for the duration of the incubation. Cells were incubated at 37°C, 5% CO_2 for 48-72 hours. Stimulated cells were harvested, and spun at 2000rpm 5 mins. Supernatants were aliquoted to prevent freeze-thaw and stored at -80°C. Cell pellets were washed in PBS, flash frozen and stored at -80°C until use.

2.5 Transfections

HEK293T cells were seeded at a density of $2x10^5$ cells/well into 12 well plates and incubated at 37°C 5% CO_2 overnight. Cells were checked the following day to ensure attachment at approximately 50% confluence. cDNA and lipofectamine solutions were prepared in Opti-MEM (Gibco). RNAi Max lipofectamine (Thermofisher) was used for P2X7/P2X1/P2X4 co-transfections, see table 2.4 for cDNA concentrations. cDNA and lipofectamine were homogenised at RT for 15 mins. Media was gently aspirated from cells and replaced with DNA-lipofectamine mix, and incubated for 4-6hrs at 37°C. After this time, wells were topped up to 1ml with cDMEM and incubated for the remaining 42-44 hours. Cells were harvested by vigorous pipetting and washed in PBS prior to further analysis.

2.6 Lentiviral transduction

HEK293T cells were seeded in a T75cm^2 flask in antibiobiotic-free complete DMEM and incubated at 37°C 5% CO_2 overnight. Lentiviral mix was prepared at a ratio of 4 lentiviral plasmid: 3 psPAX2 packaging vector (Addgene): 1 pMD2.G envelope vector (Addgene), using 7µg of lentiviral plasmid/T75cm^2 flask, and transfected into cells using Lipofectamine 2000 (Thermofisher) (figure 2.1). Flasks were incubated at 37°C, 5% CO2 for 48hrs. The viral supernatant was harvested and filtered through a 0.45µm syringe to remove cell debris. 1 volume of LentiX concentrator (Takara) was added to 3 volumes of lentiviral supernatant, inverted 10 times and incubated at 4°C for 30mins. Samples were centrifuged at 1500xg for 45mins at 4°C. Supernatant was removed and the viral particle pellet resuspended in 125µl PBS. Viral particles were aliquoted and stored at -80°C until use.

1x10^5 PLB985 and EROS-/- PLB985 were seeded per well in a 96 well plate in complete RPMI. 8µg/ml polybrene (Merck) was added to all wells except untransduced. 20µl of viral supernatant or RPMI media was added to appropriate wells and incubated at 37°C, 5% CO2 for 4-6 hrs. The wells were topped up to 100µl with complete RPMI and incubated at 37°C, 5% CO2 for 72hrs.

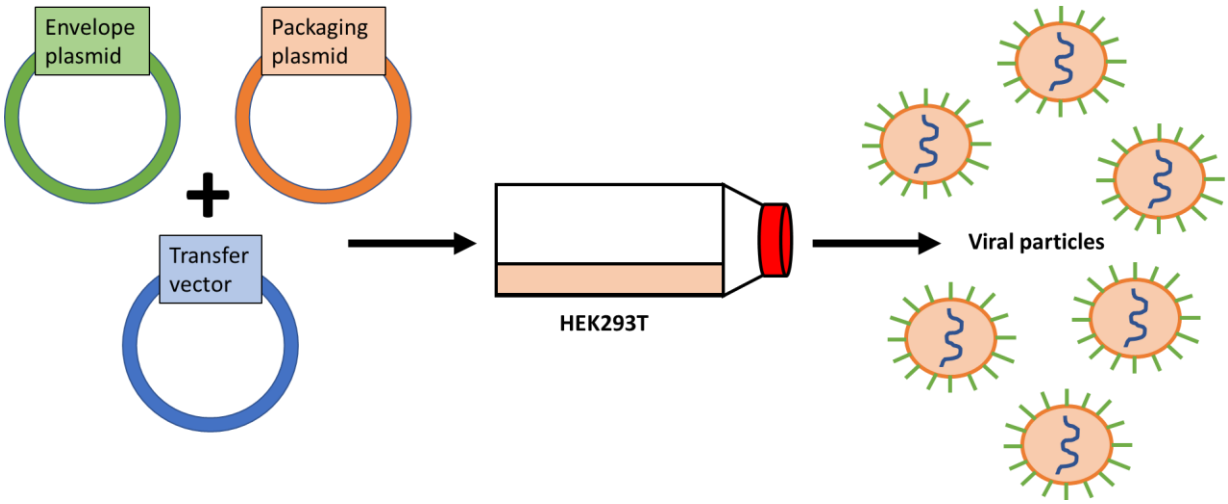

Figure 2.1: Overview of generating lentiviral particles for transduction.

Table 2.4: cDNA sequences and concentrations used in transfection experiments.

cDNA	Tag	Species	Accession #	Catalog #	Concentration (µg)
EROS	-	Mouse	NM_144832	MC201263	1.6
P2X7	GFP	Mouse	NM_011027	MG227216	1.6
P2X1	-	Human	NM_002558	SC118594	2
P2X4	-	Human	NM_002560	SC122124	2
Phactr4	GFP	Human	NM_001048183	RC20642514	1.6
gp91*phox*	-	Human	NM_001033046	SC122091	1.2
EROS	-	Human	NM_001033046	SC324452	1.2
EROS	GFP	Human	NM_001033046	RG200883	1.2
EROS-lenti	GFP	Human	NM_001033046	RC200883L4	7
Empty vector	GFP	Human	-	PS100093	7

2.7 Western blotting

$1x10^6$ cells were lysed in 40µl RIPA buffer (Thermofisher) + 1X Halt Protease Phosphatase Inhibitor (Thermofisher) on ice for 30 minutes. Benzonase was added to viscous lysates. Debris was pelleted following centrifugation at 14000xg for 30 minutes 4°C. Supernatant was subjected to BCA protein quantification assay (Pierce), following the manufacturers protocol. 20µg protein was mixed with 4x LDS (Thermofisher) + 10% reducing agent (Thermofisher) prior to denaturating at 72°C for 10 minutes. Samples were loaded on a NuPAGE 4-12% Bis-Tris pre-cast gel (Thermofisher). 1X MOPS running buffer was prepared from 20X running buffer (Formedium). Gel was run at 100v for 30 minutes, then 150v for 60-90 minutes. Proteins were transferred onto nitrocellulose membranes at 100v for 75 minutes, in transfer buffer (3.05g Tris-base (Sigma), 14.45g glycine (Sigma), 20% methanol (Sigma)). Ponceau staining was performed to ensure successful transfer. Membranes were blocked with 5% skim milk (Marvel) in Tris Buffered Saline + 0.1% Tween (TBST) for 1 hour at RT. Membranes were cut if required. Primary antibodies were diluted in blocking buffer and incubated at 4°C overnight (see table 2.5 for dilutions). The following day membranes were washed 3x for 10 minutes in TBST. Appropriate species secondary antibodies were diluted 1:10000 in blocking buffer and incubated at RT for 1 hour. Membranes were washed 3x for 10 minutes in TBST and Enhanced Chemiluminescence (ECL) reagents (Thermofisher) added immediately prior to imaging. Bands were visualised on Chemidoc (Biorad) and analysed on ImageLab (Biorad). Densitometry analysis was performed using ImageLab and shown as relative to the appropriate loading control.

Table 2.5: Details of antibodies used for western blotting experiments.

Antibody	Dilution	Species	Manufacturer
EROS (anti-C17ORF62)	1:1000	Rabbit	Atlas
P2X7	1:500	Rabbit	Alomone
P2X7	1:500	Rabbit	Atlas
P2X1	1:250-500	Rabbit	Alomone
P2X4	1:500	Rabbit	Alomone
gp91*phox*	1:1000	Mouse	Santa Cruz
ZAP70	1:1000	Rabbit	CST
pZAP70 (Tyr319)	1:500	Rabbit	CST
LCK	1:2000	Rabbit	CST
pLCK (Tyr505)	1:500	Rabbit	CST
LAT	1:1000	Rabbit	CST
Actin	1:2000	Rabbit	Abcam
Vinculin	1:1000	Rabbit	CST

2.8 Mass spectrometry (MS)

2.8.1 Preparation for Tandem Mass Tagging (TMT) MS

Whole CD4+ T cells were isolated from mouse splenocytes as described above. Eluted cells were washed 5x in cold PBS. Cell pellets were dried, flash frozen and transferred to Lu Yu and Jyoti Choudary at the Institute for Cancer Research for Mass spectrometry analysis.

2.8.2 TMT MS

Cell pellets were lysed in 1% Sodium deoxylate / 10% isopropanol / 50mM NaCl /100mM TEAB (tetraethylammonium bromide, Sigma) with Halt™ Protease and Phosphatase Inhibitor Cocktail (1x, Thermo Scientific). Lysates were sonicated and heated at 90°C for 5min. 100µg of proteins per sample were reduced with TCEP, alkylated with iodoacetamide, and digested with 3µg of trypsin (Pierce MS grade, Thermo) prior to labelling with TMT10plex according to the manufacturer's instructions. Samples were pooled, acidified, and then centrifuged to

remove precipitated deoxycholic acid. The supernatant was dried, resuspended in 0.1% NH4OH and fractionated on an XBridge BEH C18 column (2.1mm i.d. x 150mm, Waters) with an initial 5min loading then linear gradient from 5% CH3CN/0.1% NH4OH (pH 10) – 35% CH3CN /0.1% NH4OH for 30min, then to 80% CH3CN /0.1% NH4OH for 5min and stayed for another 5min. The flow rate was at 200µl/min. Fractions were collected at every 42s from 7.8min to 50min and then concatenated to 28 fractions and dried.

Peptides were reconstituted in 0.1% formic acid and a 25% aliquot injected for on-line LC-MS/MS analysis on the Orbitrap Fusion Lumos hybrid mass spectrometer coupled to an Ultimate 3000 RSLCnano UPLC system (Thermo Fisher). Samples were desalted on a PepMap C18 nano trap (100µm i.d. x 20mm, 100 Å, 5µ), then separated on a PepMap C18 column (75µm i.d. x 500mm, 2µm) over a linear gradient of 5.6 – 30.4% CH3CN/0.1% formic acid in 90min at a flow rate at 300nl/min. The MS acquisition used MS3 level quantification with Synchronous Precursor Selection (SPS5) with the Top Speed 3s cycle time. Briefly, the Orbitrap full MS survey scan was m/z 375 – 1500 with the resolution 120,000 at m/z 200, with AGC set at 4e5 and 50ms maximum injection time. Multiply charged ions (z = 2 – 5) with intensity threshold at 5000 were fragmented in ion trap at 35% collision energy, with AGC at 1e4 and 50ms maximum injection time, and isolation width at 0.7Da in quadrupole. The top 5 MS2 fragment ions were SPS selected with the isolation width at 0.7Da, fragmented in HCD at 65% NCE, and detected in the Orbitrap. The resolution was set at 50,000, and the AGC at 1e5 with maximum injection time at 86ms. The dynamic exclusion was set 40s with ± 10ppm exclusion window.

Raw files were processed with Proteome Discoverer 2.4 (Thermo Fisher) using Sequest HT. Spectra were searched against Uniprot mouse database (April 2020) and cRAP contaminant database. Search parameters were: trypsin with 2 maximum miss-cleavage sites, mass tolerances at 20ppm for precursors and 0.5Da for fragment ions, dynamic modifications of Deamidated (N, Q), Oxidation (M) and Acetyl (Protein N-terminus), static modifications of Carbamidomethyl (C) and TMT6plex (Peptide N-terminus and K). Peptides were validated by Percolator with q-value set at 0.01 (strict) and 0.05 (relaxed). The TMT10plex reporter ion quantifier included 20ppm integration tolerance on the most confident centroid peak at the MS3 level. The co-isolation threshold was set at 100%. Only unique peptides, with average

reported signal-to-noise ratio >3, were used for protein quantification, and the SPS mass matches threshold was set at 55%. Only master proteins were reported.

2.9 Tissue preparation

2.9.1 Lung digestion

EROS-/- and gp91*phox-/-* mouse lungs were perfused with PBS prior to removal from the cadaver. Lobes were dissected, manually minced with scissors, and digested in 1ml of digestion buffer (0.5mg/ml collagenase I (Sigma) and 0.1mg/ml DNase I (Sigma)) at 37°C, 45 minutes, 500rpm. Digested lung was forced through a 70µM cell strainer, washed and RBCs lysed for 1 min at RT (HybriMax, Sigma). $1/5^{th}$ of the resultant cells were used per flow panel.

2.9.2 Peyer's patch isolation

Intact intestines were removed from mouse cadavers. Peyers patches were identified in the intestinal wall, isolated with curved scissors and forcepts, and forced through 70µM cell strainers to make a single cell suspension.

2.9.3 Lymph node isolation

Inguinal lymph nodes were isolated from mouse cadavers, fat was removed with tweezers and lymph nodes were forced through a 70µM cell strainer to make a single cell suspension.

2.10 Flow cytometry

2.10.1 Tissue phenotyping

Approximately $1x10^6$ cells were stained per sample. Single cell suspensions were blocked for non-specific antibody binding using 50µl 1:200 anti-mouse FC block (Biolegend) for 10 mins at RT. Cell suspensions were stained with 50µl of 2x antibody staining mix (table 2.6) to produce 1x antibody dilutions and these were incubated in the dark at 4°C for 30 mins. Cells were washed and resuspended in FACS buffer (PBS + 2% FBS + 2mM EDTA (Thermofisher)) for analysis. Samples were acquired on a LSRFortessa X20 (BD) flow cytometer and analysed using FlowJo software (BD).

Table 2.6: List of antibodies used for tissue phenotyping experiments.

Antigen	Fluorochrome	Clone/Cat #	Manufacturer
Live/Dead	eFluor 780	65-0865-14	eBioscience
B220	FITC	RA3-6B2	Biolegend
CD11b	FITC	M1/70	Biolegend
CD11c	FITC	N418	Biolegend
CD19	FITC	ID3/CD19	Biolegend
CD25	PE	PC61	Biolegend
CD3	PE	17A2	Biolegend
CD3	FITC	17A2	Biolegend
CD4	BV421	GK1.5	Biolegend
CD44	BV605	IM7	Biolegend
CD45	BV421	30-F11	Biolegend
CD5	FITC	53-7.3	Biolegend
CD62L	APC	MEL-14	Biolegend
CD69	PerCp-Cy5.5	HI.2F3	Biolegend
CD8	BV785	53-6.7	Biolegend
CD8a	FITC	53-6.7	Biolegend
F4/80	FITC	BM8	Biolegend
CD45.2	FITC	104	Biolegend
Gr-1	FITC	RB6-8C5	Biolegend
IL-7Ra	PE	A7R34	Biolegend
NK1.1	FITC	PK136	Biolegend
TCRb	FITC	H57-597	Biolegend
Ter-119	FITC	TER-119	Biolegend

2.10.2 Cell surface staining

1-10x10^5 cells were stained with LiveDead (1:2000) and other cell surface antibodies (see table 2.7) at 4°C for 30 minutes, then washed and resuspended in FACS buffer for analysis.

Samples were acquired on a LSRFortessa X20 (BD) flow cytometer and analysed using FlowJo software (BD).

Table 2.7: List of antibodies used for cell surface flow cytometry experiments.

Antigen	Fluorochrome	Clone/Cat #	Manufacturer
Live/Dead	eFluor 780	65-0865-14	eBioscience
CD4	BV421	GK1.5	Biolegend
CD27	FITC	LG.3A10	Biolegend
CD62L	APC	MEL-14	Biolegend
IL-6R	PE	D7715A7	Biolegend
CD4	PE-Cy7	GK1.5	Biolegend
CD38	PerCP-Cy5.5	90	Biolegend
CD39	PE	Duha59	Biolegend
CD73	BV421	TY/11.8	Biolegend
IL-4Rα	APC	1015F8	Biolegend
CD25	Pacific blue	PC61	Biolegend

2.10.3 Phospho-flow cytometry

CD4+ T cells were stained with CD4 (1:100) and LiveDead (1:2000) at 4°C for 15 minutes, then washed. Cells were vortexed thoroughly, fixed in 4% PFA (EMS) for 10 mins at RT and washed. 100µl ice cold FACS buffer wash added to cells followed by ice cold methanol (Sigma) added dropwise to cell suspension and incubated at -20°C for 2 days. Permeabilised cells were washed and stained with 1:20 pSTAT6 (BD), 1:20 pSTAT4 (eBioscience) or 1:20 pSTAT5 (eBioscience) (table 2.8) in the dark for 90 minutes at 4°C. Cells were washed and resuspended in FACS buffer for analysis. Samples were acquired on a LSRFortessa X20 (BD) flow cytometer and analysed using FlowJo software (BD).

Table 2.8: List of antibodies used for phospho-flow cytometry experiments.

Antigen	Fluorochrome	Clone/Cat #	Manufacturer
Live/Dead	eFluor 780	65-0865-14	eBioscience
CD4	BV421	GK1.5	Biolegend
pSTAT4 (Tyr693)	APC	4LURPIE	eBioscience
pSTAT5 (Tyr694)	PerCP-eFluor710	SRBC2X	eBioscience
pSTAT6 (Tyr641)	PE	J71-773.58.11	BD

2.10.4 GFP transfection validation

Transfected HEK293T cells were harvested by vigorous pipetting, washed in PBS and resuspended in FACS buffer for analysis. Samples were acquired on a LSRFortessa X20 (BD) flow cytometer and analysed using FlowJo software (BD).

2.10.5 Apoptosis and cell death

Following ATP or NAD stimulation, cells were washed in PBS and apoptosis and cell death were measured using the Dead Cell Apoptosis Kit from Invitrogen (Cat # V13241). Briefly, cells were resuspended in 1x annexin-binding buffer. 5µL of Alexa Fluor™ 488 Annexin V and 1 µL 100 µg/mL PI working solution were added to each condition and incubated at RT for 15 minutes. Then 400µL 1X annexin-binding buffer was added and cells were immediately analysed on a LSRFortessa X20 (BD) flow cytometer and analysed using FlowJo software (BD).

2.10.6 gp91*phox* intracellular flow cytometry

Cells were harvested, stained with LiveDead (1:2000) at 4°C for 15 minutes, then washed. Then cells were Fixed/Permebilised using the Fixation/Permeabilisation solution kit by BD, following the manufacturer's instructions. 16µl of the anti-human gp91*phox* (Clone: 7D5) was directly added to the residual buffer in each condition and incubated in the dark at 4°C for 75 minutes. Cells were washed and analysed on the LSRFortessa X20 (BD) flow cytometer and analysed using FlowJo software (BD).

2.11 ELISA

Supernatants were harvested following cell incubations and stored at -80°C until use. Mouse IL-4, IL-5, IL-13, IFNγ and IL-2 and human IL-4 and IFNγ Duoset ELISA kits were purchased from R&D and manufacturer's instructions were followed. Briefly, capture antibody was bound to plates overnight, plates were washed and blocked for 1 hour. 100µl supplied standards and 100µl supernatant was added to the appropriate well for 2 hours. Supernatant was diluted 1:2-1:10 in reagent diluent for IFNγ ELISA. Detection antibody was added for 2 hours, followed by streptavidin-HRP, the substrate and the stop solution. All steps were performed at RT in the dark, with washing between. Plates were read at 450nm – 540nm on a SkanIt microplate reader (Thermofisher).

2.12 T: B cell cocultures

Naïve CD4+ T cells were isolated from mouse splenocytes (as described above 2.3.2), and activated with 10ug/ml immobilised anti-CD3 and 2ug/ml soluble anti-CD28 and 100IU/ml IL-2 (Peprotech) for 24 hours. Simultaneously B cells were isolated (as described above 2.3.2) and activated with 10ug/ml anti-IgM F'ab for 24 hours. Then T and B cells were co-cultured at a 1:1 ratio ($5x10^4$ cells each) in the presence of 150ng/ml Staphylococcal Enterotoxin B (SEB; Sigma) for 9 days at 37°C, 5% CO_2 (figure 2.2). Supernatants were harvested on day 10 for ELISA analysis using a murine isotyping kit (BD), as per manufacturer's instructions. Plates were read at 450nm.

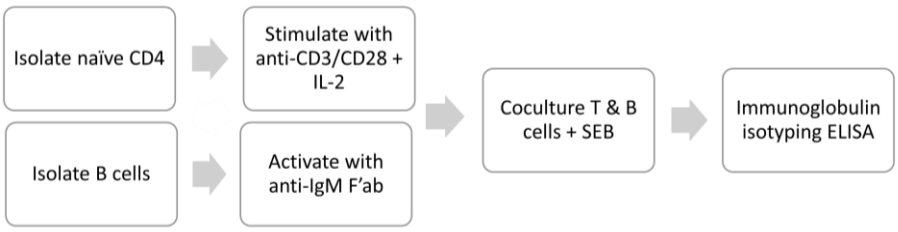

Figure 2.2: Overview of the T:B cell co-culture protocol.

2.13 NP-CGG immunisations

WT and EROS-/- mice were challenged via intraperitoneal injection with 150mg/kg NP-CGG (Biosearch Technologies) plus alum (Serva) in a 1:2 ratio. Mice were sacrificed on day 10 and peripheral blood was harvested for serum analysis. NP-specific immunoglobulins were

detected in serum and quantitated by using ELISAs with NP(23)-BSA (Biosearch Technologies) as a capture antigen. Plates were read at 450nm.

2.14 Helminth infection

Mice were orally gavaged with 150-200 L3-stage Heligmosomides polygyrus baki larvae in 200µl of distilled water. Larvae were maintained and counted as described previously [168]. H. polygyrus excretory secretory (HES) restimulations performed as described previously [168].

2.15 RNA sequencing

2.16 RNA isolation

RNA was isolated using a quick-RNA kit (Zymo), according to manufacturer's instructions.

2.16.1 RNA sequencing library preparation

cDNA libraries were prepared using Universal Plus Total RNA-Seq Library Preparation Kit (Tecan Genomics) where ribosomal RNA were depleted using AnyDeplete according to manufacturer's protocol. The final libraries were assessed using TapeStation 2200 System (Agilent) and sequenced using Illumina Hi-Seq 4000 instrument with PE100 reactions.

2.16.2 RNA sequencing data analysis

The quality of the sequencing fastq files was analysed using MultiQC and all samples passed quality QC, with mean Phred quality score >30 for all positions. Sequence reads were adapter- and quality- trimmed using Trimmomatic (v0.40) before aligning to the human genome (Ensembl GRCh38 build 88) using STAR aligner (v2.7.10). Gene expression was quantified using RSEM (v.1.2.29). Genes with <5 read counts in at least 50% of the samples were removed prior to differential gene expression analysis using DESeq2 (v3.15) with default parameters. DESeq2 uses a generalised linear model to estimate log2 fold change (log2FC) between comparison groups and the Benjamini-Hochberg false discovery rate was applied for multiple testing corrections, resulting in an adjusted *P*-value (padj) for each gene per comparison. Gene Set Enrichment Analysis (GSEA) was performed using Reactome database (v7.5.1) on the entire gene set to identify pathways that were positively or negatively enriched in each condition. All RNA-Seq datasets were deposited to Gene Expression Omnibus.

2.17 qPCR

RNA was isolated using the RNeasy Mini kit (Qiagen) according to manufacturer's instructions, including all optional steps and RNA was eluted with 30µl H_2O. RNA quantity and purity was measured using a Nanodrop (Thermofisher). 1µg of RNA was transcribed into cDNA using the SuperScript IV VILO kit (Thermofisher) according to manufacturer's instructions. Briefly, RNA was mixed with 4µl of Reverse Transcriptase/ No Reverse transcriptase and H_2O to 20µl. Thermofisher cycler programme was set as follows: 25°C 10 mins, 50°C 10 mins, 85°C 5 mins. Then, 50ng of cDNA was mixed with 5µl Taqman Fast Advanced MasterMix (Thermofisher), 0.5µl Taqman probe (Thermofisher; table 2.9) and H20 to 10µl per reaction. qPCR programme used is listed in table 2.10 and was performed using the Viia 7 Real-Time PCR system (Thermofisher).

Table 2.9: Probes used for qPCR experiments.

Target	**Species**	**Catalog #**
GATA3	Mouse	Mm00484683
TBX21	Mouse	Mm00450960
HPRT	Mouse	Mm01324427
HPRT	Human	Hs02800695
IL-4	Mouse	Mm00445259
EROS exon 2-3	Human	Hs00978805
EROS exon 3-4	Human	Hs00978806
EROS exon 5-6	Human	Hs00978808

Table 2.10: qPCR Thermofisher cycler programme.

Temperature (°C)	**Time**	
50	2 min	
95	2 min	
95	1 sec	X 40 cycles
60	20 sec	

2.18 EROS patient sequencing

DNA was extracted from the whole blood of the EROS patient and an unrelated healthy control using the Gentra Puregene blood kit (Qiagen), following the manufacturer's instructions. DNA was eluted into H_2O and subjected to PCR.

PCR was performed with reagents and concentrations detailed in table 2.2 using 200ng patient DNA plus the primers detailed in table 2.11. PCR programme detailed in table 2.12. PCR reactions were subjected to PCR clean up (Qiagen) and submitted for sequencing (Genewiz) using the forward primer. SnapGene 6.1 (Dotmatics) was used for sequence alignments.

Table 2.11: Primers used to PCR the causative mutation in the EROS patient.

Primer	Sequence
EROS patient mut fwd	AGTGCAGTGTAAAGATGG
EROS patient mut rev	GTCCACAAACTCATCTCC

Table 2.12: PCR programme for EROS patient PCR.

Stage	Temperature (°C)	Time	Repeat
Denature	94	5 min	
Denature	94	30 sec	x30 cycles
Anneal	50	30 sec	
Extend	68	45 sec	
Extend	68	5 min	

2.19 CRISPR-Cas9

2.19.1 T cell activation

Human CD4+ T cells were isolated from PBMC using a negative selection CD4+ kit (Miltenyi). Cells were resuspended at $1x10^6$ cells/ml in a 24 well plate in complete human IMDM (IMDM, Human AB Serum (Sigma), 1x Penicillin-Streptomycin-Glutamate). Cells were stimulated with 25µl washed anti-CD3/CD28 (Dynabeads) + 30IU recombinant human IL-2

(Peprotech), as per manufacturer's instructions. Cells were activated for 72hrs at 37°C, 5% CO_2.

2.19.2 sgRNA design

Single guide RNA (sgRNA) were kindly designed by Dr George Gentsch (CRUK), using the InDelphi software, which assesses off-target score, precision and frameshift to produce a combo score (table 2.13). sgRNA were purchased from Synthego and reconstituted to 61.7pmol/µl in H_2O.

Table 2.13: sgRNA targets and sequences used for CRISPR-Cas9 deletion of EROS.

sgRNA target	Sequence	Off-target *	Precision **	Frameshift ***	Combo score ****
Exon 2	GAGAGCCUUACCAACCAGCA	73.8	0.55	81.7	70.2
Exon 3	TTCATAGGAATCTTGTCGAT	90.6	0.49	81.5	73.7
Exon 4	CGTAGAAGAGCTTCCAGCCC	39.8	0.67	91.5	66.1

* Specificity score from Hsu *et al.* (2013). Score spans from 0 to 100. Higher is better [169].

** This score is based on experiments in K562. A high precision score (>0.4) implies that DNA repair outcomes are uniform and enriched for just a handful of unique genotypes.

*** This score is based on experiments in K562. A high (>80%) frameshift frequency will tend to knock a protein-coding gene out of frame. The typical genomic frameshift frequency is above 66% because 1-bp insertions and 1-2 bp deletions are particularly common repair outcomes.

**** Combined score = (Off-target score + Precision score*100 + Frameshift)/3

2.19.3 Nucleofection

After the 72hr stimulation, magnetic beads were removed and cells were washed in PBS and counted. HiFi Cas9 (IDT) was diluted 1:3.3. To make the ribonucleoprotein (RNP) complex the diluted Cas9 was complexed with sgRNA targeting exon 2 of EROS at a molar ratio of 1:3 for 10 mins at RT. The P3 kit from Lonza was used for nucleofection. $2x10^5$ cells were

resuspended in 20µl of the supplied P3 buffer (Lonza), mixed with the RNP complex, transferred to the nucleofector strip and immediately pulsed using EO-115 in the 4D nucleofector machine (Lonza). Cells were quickly transferred to pre-warmed cIMDM and rested for 48 hours at 37°C, 5% CO_2. After resting cells were fed fresh cIMDM + 100IU rhIL-2, replenished every 2 days, and expanded for 7-14 days.

2.19.4 Confirmation of gene deletion

DNA was extracted from cell pellets using the DNA extraction kit (Qiagen) as per manufacturer's instructions and eluted in 30µl H_2O. DNA was measured using a nanodrop (Thermofisher).

PCR primers used to confirm EROS deletion detailed in table 2.14. PCR reaction mixtures were prepared on ice, according to table 2.15. PCR programme was as according to table 2.16. PCR was run on a 2% agarose (Thermofisher) gel with 1x Gel Red (Cambridge Bioscience), with a 100bp ladder (Thermofisher) at 150v for 30-60minutes. Bands were visualised on UVP BioDoc-IT imaging system.

Table 2.14: PCR primers to confirm CRISPR-Cas9 deletion of EROS.

Primer	Sequence
EROS fwd	TGCAGGTGACTTAGTTGG
EROS rev	TGTGAGTCCTACGAAGAGG

Table 2.15: PCR reagents for CRISPR-Cas9 confirmatory PCR.

Reagent	Amount	Manufacturer
DNA	100ng	
2x OneTaq Master Mix	12.5ul	NEB
Forward primer	0.4uM	Sigma
Reverse primer	0.4uM	Sigma
H_2O	To 25ul	

Table 2.16: PCR conditions for CRISPR-Cas9 confirmatory PCR.

Stage	Temperature (°C)	Time	Repeat
Denature	94	5 min	
Denature	94	15 sec	X 10 cycles
Anneal	64 – 0.5 each cycle	15 sec	
Extend	68	15 sec	
Denature	94	15 sec	X 28 cycles
Anneal	58	15 sec	
Extend	68	15 sec	
Extend	68	5 min	
Hold	4	Forever	

PCR reactions were subjected to PCR clean up (Qiagen) and submitted for sequencing (Genewiz). Knockout efficiency was assessed using the Inference of CRISPR Edits (ICE) analysis software (Synthego).

2.20 Statistical analysis

The appropriate statistical test used is stated in figure legend. Statistics were performed with Prism 9 (GraphPad). A p value of less than 0.05 was considered statistically significant, where * $p<0.05$, ** $p<0.01$, *** $p<0.001$, **** $p<0.0001$. If not significant then no asterisk or p value is shown. Error bars represent standard error of the mean (SEM). n represents the number of biological or technical repeats, as stated in the figure legend.

Chapter 3: EROS mediated control of gp91*phox* and P2X7 in CD4+ T cells

Introduction

As discussed in section 1.4, EROS deficient mice exhibit 100% lethality in response to Salmonella infections. Reactive oxygen species (ROS) must be produced by the phagocyte NADPH oxidase complex to successfully eradicate Salmonella infections. Thomas *et al.,* (2017) found that EROS deficient macrophages and neutrophils have a severely impaired ROS burst in response to PMA and zymosan [34]. Label-free mass spectrometry was performed and identified that the essential phagocyte NADPH oxidase components gp91*phox* and p22*phox* were the most significantly downregulated proteins in EROS deficient macrophages and neutrophils. P2X7 was the 3rd most significantly downregulated protein in EROS deficient macrophages. Further experiments showed that EROS specifically and consistently immunoprecipitated with gp91*phox* and P2X7 from the RAW264.7 macrophage cell line [34,164]. These studies demonstrate that EROS regulates and stabilises the protein expression of gp91*phox* and P2X7 in macrophages and neutrophils.

However, Thomas *et al*., (2017) note that the EROS human ortholog *C17ORF62* (now CYBC1) is also highly expressed in CD4+ T cells by microarray. This is supported by Kim *et al.,* (2014) who found high expression of *C17ORF62* in CD4+ T cells during proteomic analysis of human tissues. It is unclear what the requirement of EROS may be in CD4+ T cells as these cells do not produce a ROS burst in response to pathogens. They do, however, utilise ROS produced by the NADPH oxidase during T cell differentiation, signalling and apoptosis. Similarly, CD4+ T cells also utilise P2X7 signalling during similar T cell processes. Therefore, EROS may have an important yet undefined role in CD4+ T cells via its regulation of gp91*phox* and P2X7 protein expression.

This chapter will investigate whether gp91*phox* and P2X7 are regulated by EROS in CD4+ T cells. It will also identify any additional proteins that may be regulated by EROS in CD4+ T cells. Furthermore, it will determine whether EROS-driven loss of protein expression causes any physiological consequences in CD4+ T cells.

Hypotheses

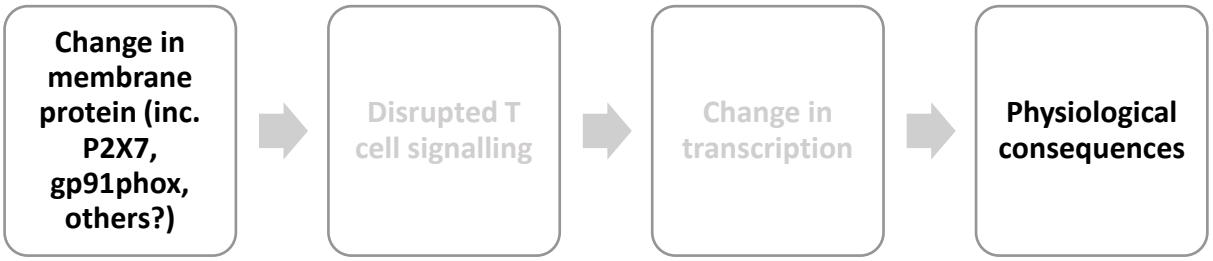

This chapter will address the following parts of my hypothesis:

EROS regulates the protein expression of gp91*phox* and P2X7 in CD4+ T cells

Loss of EROS disrupts P2X7-driven physiological processes in CD4+ T cells

Results

To assess whether EROS regulates gp91*phox* and P2X7 in CD4+ T cells and to determine whether EROS regulates any other membrane proteins in CD4+ T cells, mass spectrometry was performed. Whole CD4+ T cells were isolated from EROS-/- and wildtype (WT) mouse splenocytes and subjected to Tandem Mass Tagging (TMT) labelled mass spectrometric analysis at the Institute for Cancer Research. As expected, EROS was the most significant downregulated protein in EROS-/- CD4+ T cells (figure 3.1). gp91*phox*, p22*phox* and P2X7 were also significantly downregulated, similar to results gained in mass spectrometry analysis of neutrophils and macrophages [34]. On the whole, there were not many differentially regulated proteins, suggesting that EROS regulates only a small number of proteins. However, this analysis does highlight a previously undetected protein, Phactr4, which was also significantly downregulated in EROS-/- CD4+ T cells (figure 3.1).

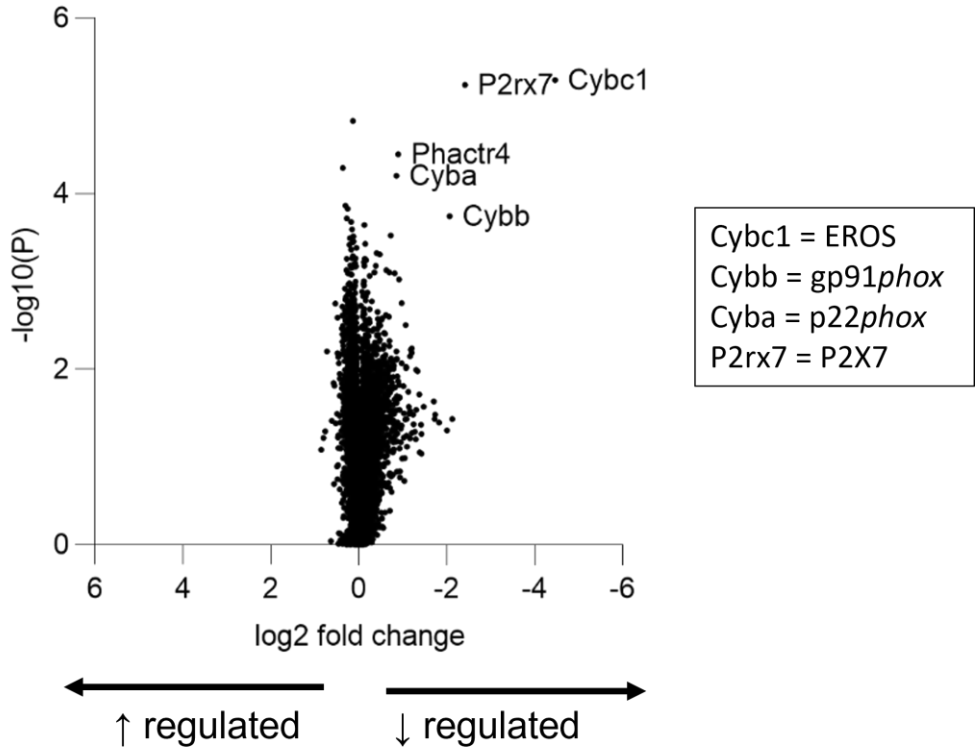

Figure 3.1: gp91*phox*, p22*phox* and P2X7 are downregulated in EROS-/- CD4+ T cells

Whole CD4+ T cells were isolated from EROS-/- and wildtype (WT) mouse splenocytes and subjected to Tandem Mass Tag (TMT) mass spectrometry. Gene names listed as follows: *cybc1*=EROS, *cybb*=gp91*phox*, *cyba*=p22*phox*, *p2rx7*=P2X7. n=5 mice per group.

Next, western blots were performed to confirm the mass spectrometry results gained in figure 3.1. CD4+ T cells from EROS-/- and WT mice were blotted for gp91*phox* and P2X7 protein expression. Additionally, P2X7 expression was evaluated in CD8+ T cells and B cells, as these lymphocytes are also integral to adaptive immunity. EROS-/- CD4+ T cells had reduced expression of P2X7 (figure 3.2A) and gp91*phox* (figure 3.2B) levels compared to WT controls, confirming the results of the mass spectrometry analysis. EROS-/- CD8+ T cells and B cells also had reduced P2X7 levels (figure 3.2 C-D). Overall, EROS regulates the protein expression of gp91*phox* and P2X7 in CD4+ T cells.

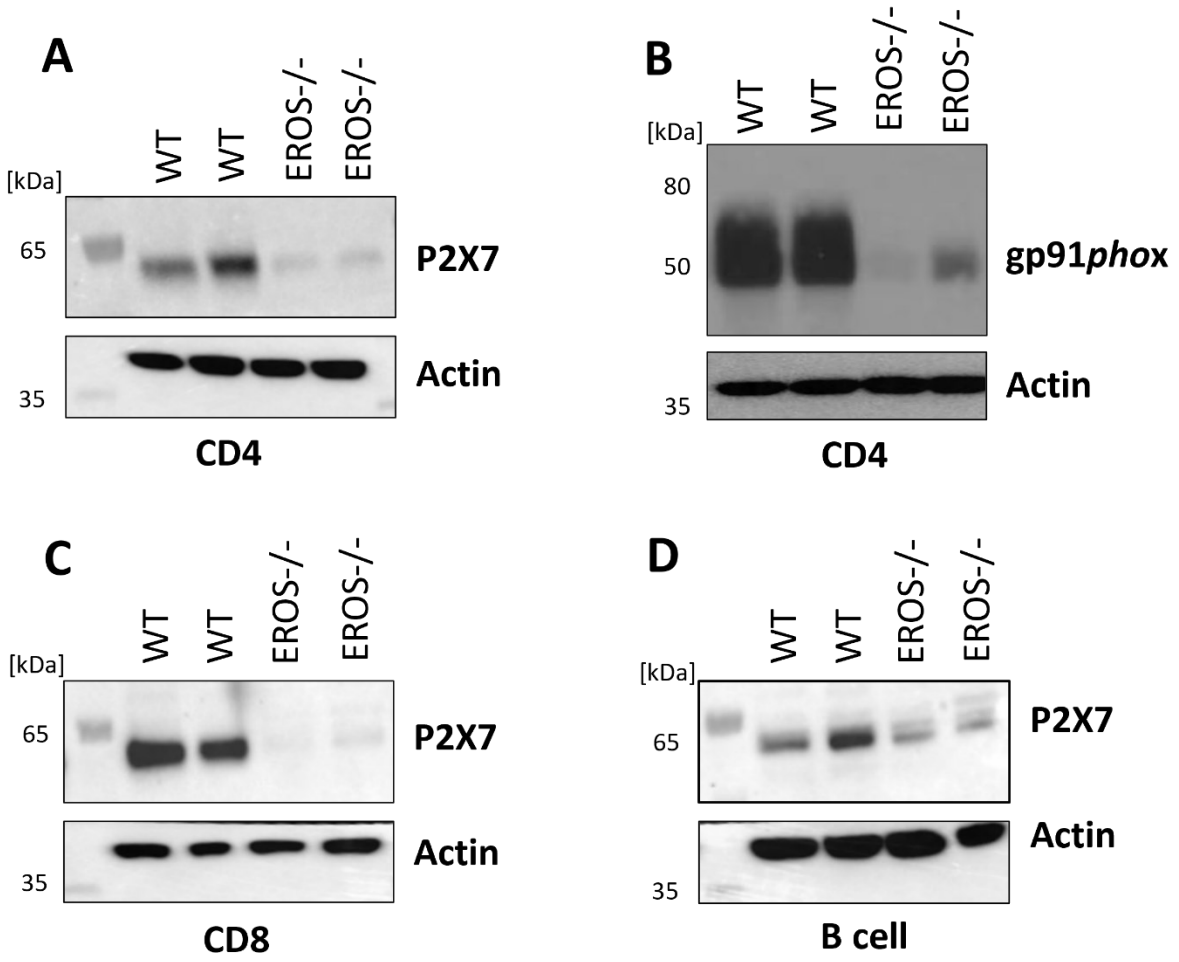

Figure 3.2: EROS regulates the expression of gp91*phox* and P2X7 in CD4+ T cells

CD4+ T cells from EROS-/- or wildtype (WT) mice were analysed by western blot for P2X7 (A) or gp91*phox* (B) expression. P2X7 expression was also blotted in CD8+ T cells (C) and B cells (D). Actin used as loading control. n=2 mice per group.

Randzavola, Mortimer *et al.,* (2021) have shown that EROS is required for the expression of the immature gp91*phox* precursor, prior to its binding with p22*phox*. As loss of EROS expression also results in loss of P2X7 expression, next it was investigated whether EROS is necessary for the expression of P2X7. Co-transfection experiments were performed using the HEK293 cell line as a reductionist system, as they do not express EROS or P2X7. P2X7 was transfected into HEK293 cells either alone or with EROS. The expression of P2X7 was greater when co-transfected with EROS, than when P2X7 was transfected alone, by both western blot (figure 3.3A) and flow cytometry (figure 3.3B). This suggests EROS is responsible for increasing the abundance of and stabilising P2X7, both *in vitro* systems and potentially physiologically too.

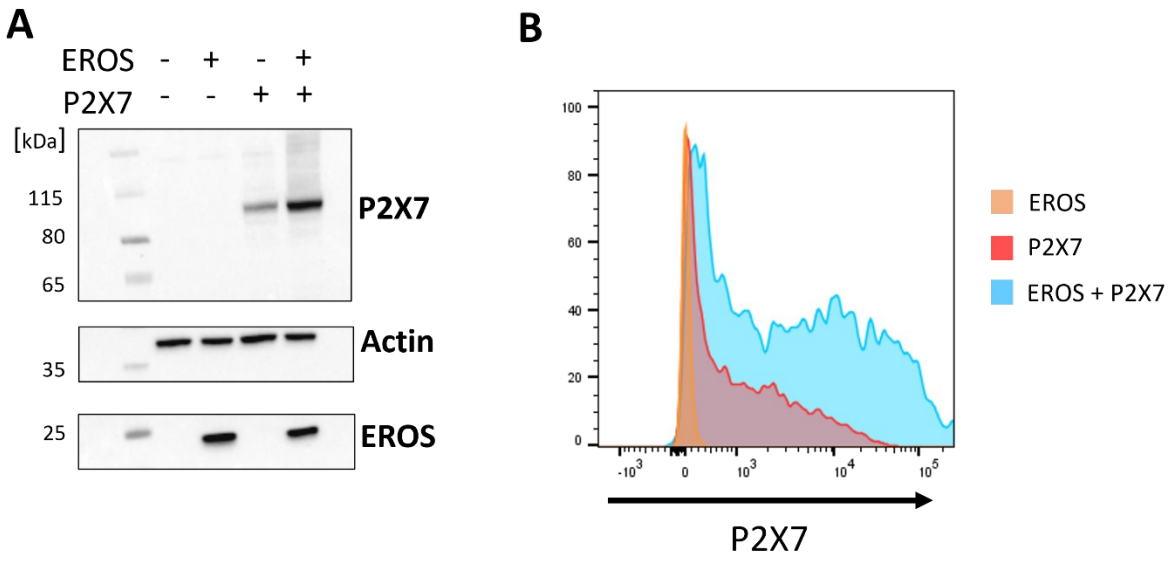

Figure 3.3: EROS increases the abundance of P2X7

HEK293 cells were transfected with P2X7 or EROS, or co-transfected with both EROS and P2X7. (A) Western blot analysis of P2X7-GFP and EROS expression. Actin used as loading control. (B) Flow cytometric analysis of P2X7-GFP expression levels. Mouse cDNA constructs used. Data representative of n=3.

Phactr4 was also downregulated in EROS deficient CD4+ T cells (figure 3.1) and macrophages [164] by mass spectrometry. Little is currently known about Phactr4; it has recently been associated with Lupus Nephritis [170] and has previously been implicated in embryogenesis [171,172]. Owing to the limited previous research on the role of Phactr4 there were few reagents available to measure it, especially with mouse reactivity. Western blots were performed on bone marrow derived macrophages (BMDM) from EROS-/- and WT mice, HEK293 and Hut78 human cell lines to validate the available antibodies for Phactr4 expression. The first antibody from Proteintech failed to produce a band at the expected 70 kDa in either human or mouse samples (figure 3.4A). There was a band at 80 kDa for the mouse BMDM, but with no difference in expression between WT and EROS-/-, suggesting it is not the correct band. There was a band at approximately 115 kDa in the human cell lines, but this was also the wrong size, suggesting the antibody from Proteintech was not specific (figure 3.4A). Next, an antibody from Abcam was tested, however this failed to produce any bands in the mouse samples and only had the non-specific 115 kDa band in the HEK293 samples (figure 3.4B). As the available western blot antibodies were non-specific and have poor mouse specificity, an alternative method was tested. Using a similar method to figure 3.3A, a GFP-tagged Phactr4 construct was transfected into HEK293 cells to avoid any issues with antibody specificity and to confirm whether EROS regulates the expression of Phactr4. The 30-50% Phactr4-GFP signal for each transfection demonstrates Phactr4 was successfully transfected into HEK293 cells (figure 3.4C). However, there was no consistent difference in GFP expression when EROS was co-transfected with Phactr4 (figure 3.4C), suggesting EROS may not regulate Phactr4 in the same manner as P2X7 (figure 3.3).

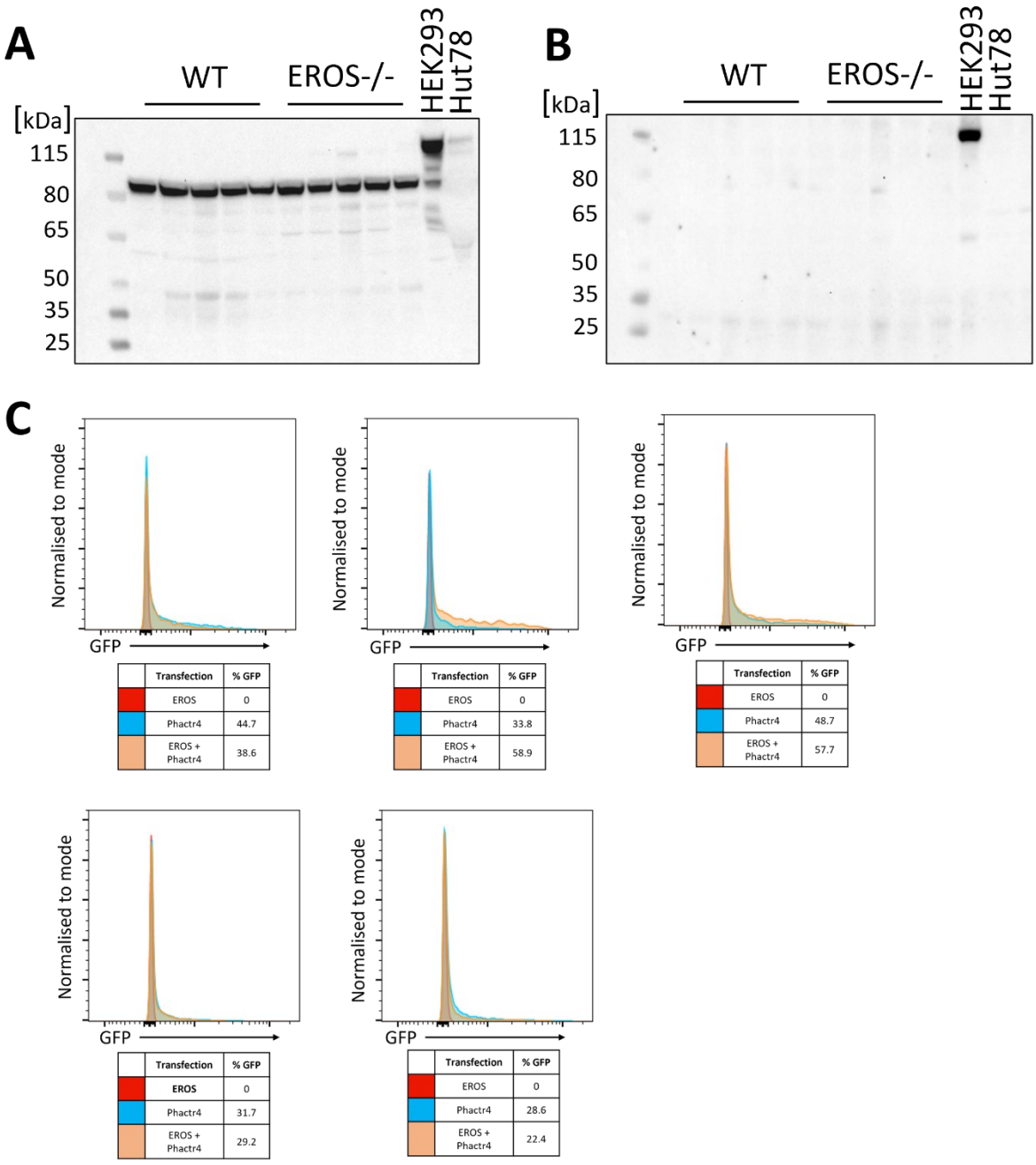

Figure 3.4: EROS does not increase the abundance of Phactr4

Bone marrow derived macrophages (BMDM) from wildtype (WT) control and EROS-/- mice, and the HEK293 and Hut78 human cell lines were subjected to western blot analysis. Western blot antibodies from (A) Proteintech and (B) Abcam were validated for Phactr4 specificity. HEK293 cells were transfected with Phactr4-GFP or EROS, or co-transfected with both EROS and Phactr4-GFP. (C) Flow cytometric analysis of Phactr4-GFP expression levels. Each graph represents an individual repeat.

It is known that the P2X7 family members P2X1 and P2X4 are also expressed on CD4+ T cells [152]. Additionally, it is accepted that there is in intricate relationship between P2X4 and P2X7 expression, as discussed in section 1.3.4. Therefore, as EROS can modulate the expression of P2X7, it may be expected that EROS can also modulate the expression of P2X1 and P2X4. The expression of P2X1 and P2X4 was measured in macrophages and CD4+ T cells from EROS-/- mice by western blot. P2X1 expression was reduced in EROS-/- macrophages and CD4+ T cells compared to WT (figure 3.5A-B, E-F). P2X4 expression was more variable between mice in both WT and EROS-/- conditions. Also, there was greater P2X4 expression in EROS-/- macrophages (figure 3.5C-D) but reduced P2X4 expression in EROS-/- CD4+ T cells compared to WT (figure 3.5G-H). This suggests that the regulatory effect of EROS on P2X1 is more consistent than with P2X4.

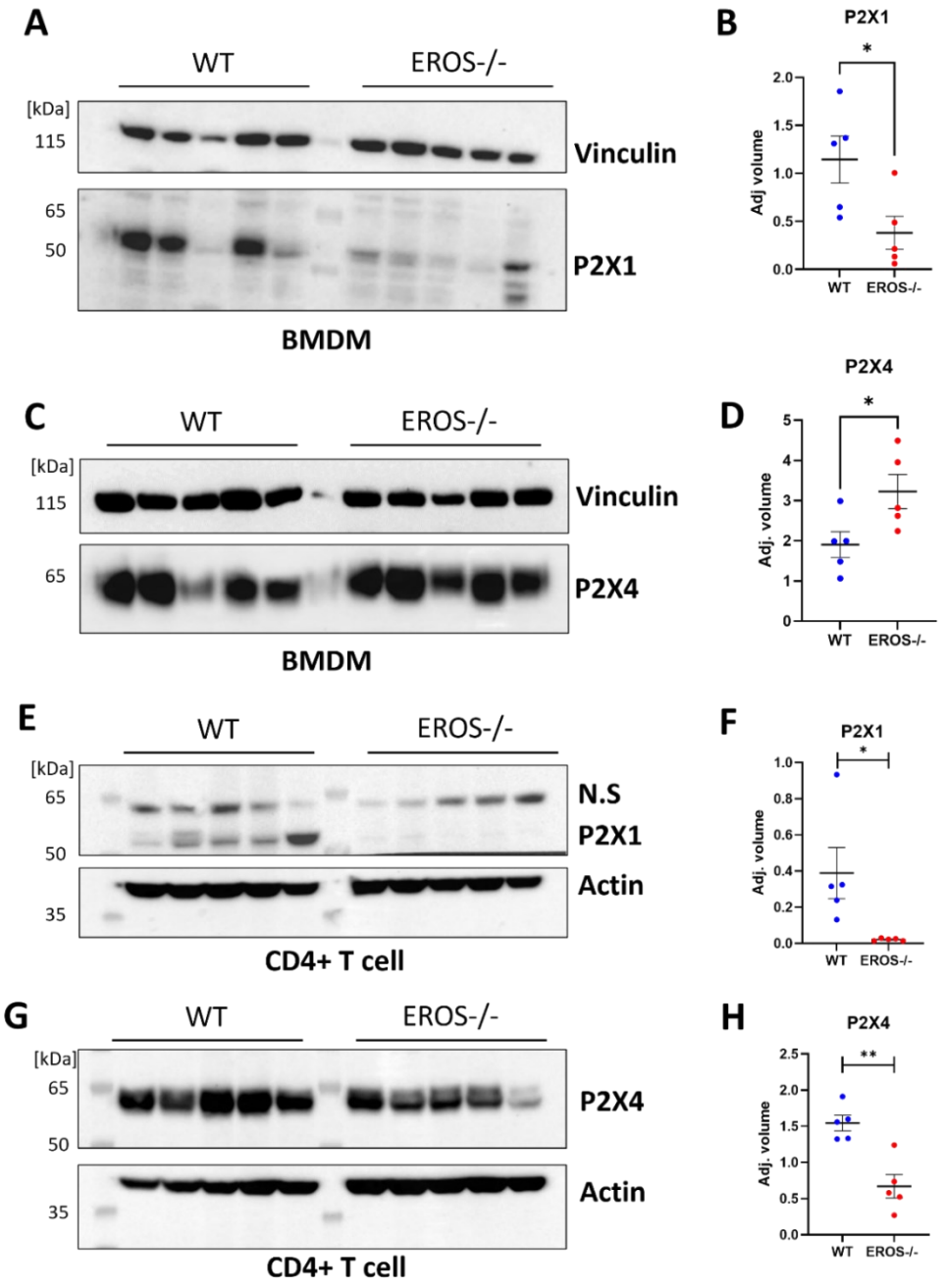

Figure 3.5: EROS can regulate multiple members of the P2X family

Macrophages were differentiated from the bone marrow (BMDM; A-D) and CD4+ T cells were isolated from splenocytes (E-H) of EROS-/- or wildtype (WT) control mice and subjected to western blot analysis. P2X1 (A-B, E-F) and P2X4 (C-D, G-H) expression were measured. Vinculin or actin used as loading controls. Quantification (B, D, F, H) performed on image lab software, relative to loading control. n=5 mice per group. Data represented as mean ± SEM. Statistical significance was calculated using an unpaired two-tailed Student's *t*-test. * $p<0.05$, ** $p<0.01$.

Next, co-transfection experiments were performed to determine whether EROS is required for the expression of P2X1 or P2X4. P2X1 or P2X4 were transfected into HEK293 cells either alone or with EROS, and western blotting was performed to assess protein expression. The expression of P2X1 was greater when co-transfected with EROS, than when P2X1 was transfected alone (figure 3.6A). In contrast, the expression of P2X4 was reduced when co-transfected with EROS, than when P2X4 was transfected alone (figure 3.6B). This suggests that EROS acts to upregulate P2X1 expression, whereas it acts to downregulate P2X4 expression. Overall, this demonstrates that EROS has a family wide effect on P2X expression levels.

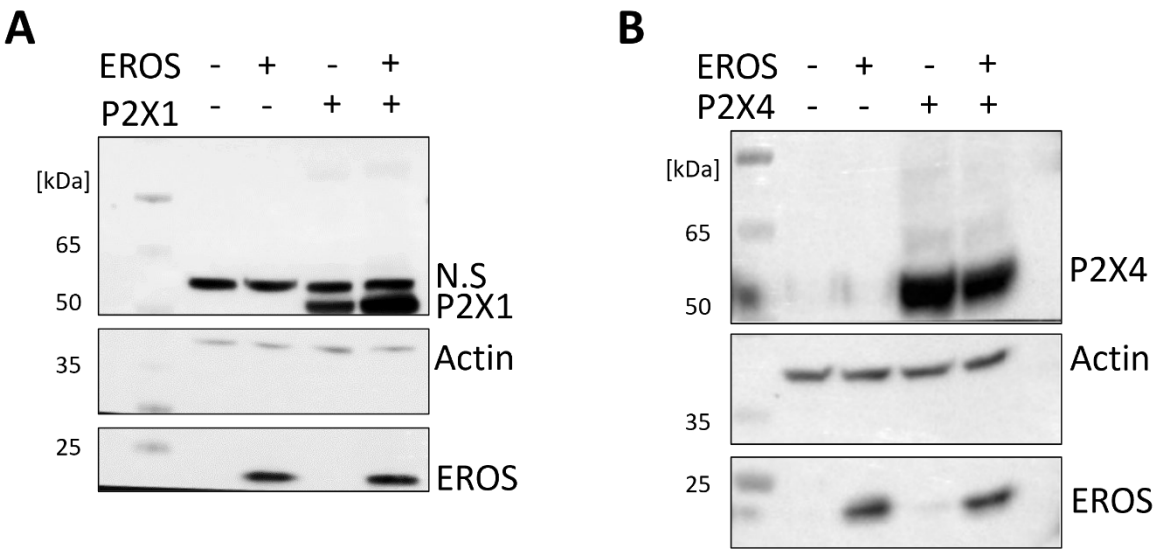

Figure 3.6: EROS positively regulates P2X1 expression, but negatively regulates P2X4 expression

HEK293 cells were transfected with P2X1, P2X4 or EROS, or co-transfected with both EROS and P2X1 or P2X4. (A) Western blot analysis of P2X1 and EROS expression. Actin used as loading control. N.S = non-specific band. Data representative of n=3. (B) Western blot analysis of P2X4 and EROS expression. Actin used as loading control. Data representative of n=3.

As EROS can regulate the expression of P2X7 and its related family members P2X1 and P2X4, functional experiments were carried out to examine the effects of loss of EROS expression on P2X7 signalling. Activation of P2X7 signalling by its ligand ATP triggers the shedding of key surface molecules CD62L, CD27 and IL-6R [126,153,154].

Whole CD4+ T cells from EROS-/- and WT mice were stimulated with ATP or NAD and CD62L, CD27 and IL-6R levels were measured by flow cytometry. In WT CD4+ T cells, treatment with ATP caused the rapid shedding of CD62L, CD27 and IL-6R, to levels <10% for CD62L and CD27 (figure 3.7 B & D) and <1% for IL-6R (figure 3.7F). Whereas in EROS-/- CD4+ T cells significantly less marker shedding occurred, approximately 40% of cells remained positive for CD62L and CD27, and 4% remained positive for IL-6R following ATP treatment (figure 3.7 B, D, F).

Treatment with NAD induced shedding but to a lesser degree, approximately 40% of WT CD4+ T cells remained positive for CD62L and CD27, and 6% of cells remained positive for IL-6R post-treatment (figure 3.7 C, E, G). However, significantly less shedding occurred in EROS-/- CD4+ T cells, as approximately 60% of cells remained positive for CD62L and CD27, and 12% of cells remained positive for IL-6R following NAD treatment (figure 3.7 C, E, G). Interestingly, CD27 expression levels were significantly higher at baseline in EROS-/- CD4+ T cells compared to WT (figure 3.7 D-E). Overall, these data demonstrate that loss of EROS abrogates P2X7 induced surface marker shedding in CD4+ T cells.

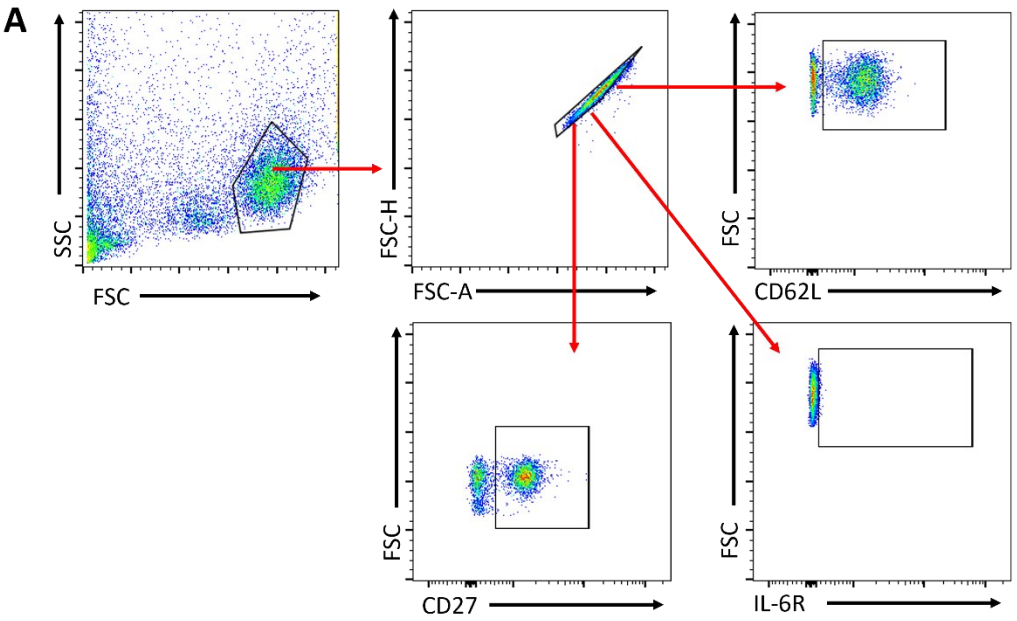
A
SSC
FSC
FSC-H
FSC-A
FSC
CD62L
FSC
CD27
FSC
IL-6R

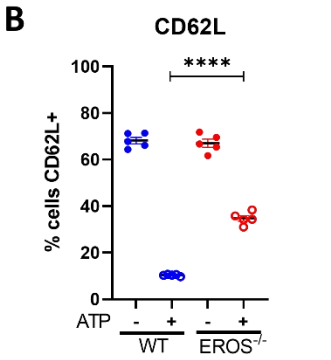
B
CD62L
% cells CD62L+
****
ATP
WT
EROS-/-

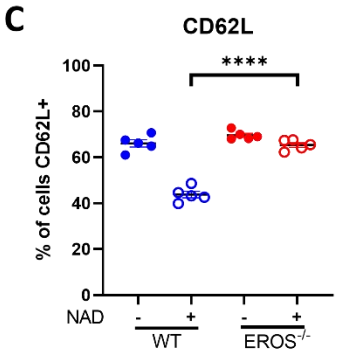
C
CD62L
% of cells CD62L+
****
NAD
WT
EROS-/-

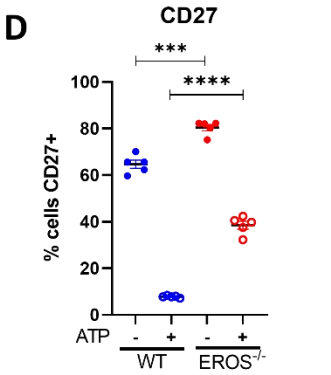
D
CD27
% cells CD27+
***
****
ATP
WT
EROS-/-

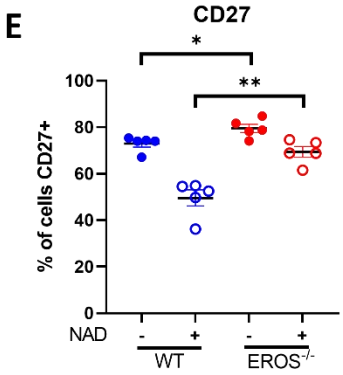
E
CD27
% of cells CD27+
*
**
NAD
WT
EROS-/-

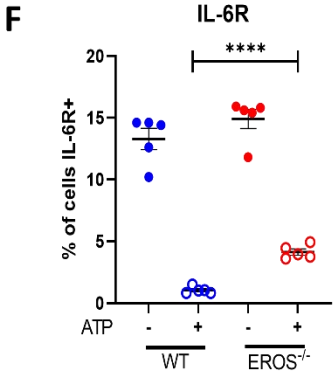
F
IL-6R
% of cells IL-6R+
****
ATP
WT
EROS-/-

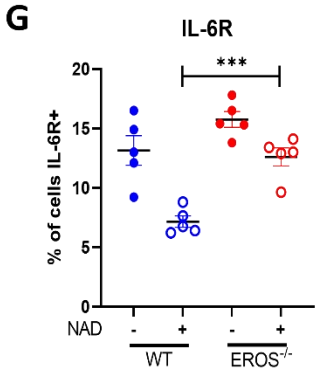
G
IL-6R
% of cells IL-6R+
***
NAD
WT
EROS-/-

Figure 3.7: Loss of EROS reduces P2X7-driven surface marker shedding

CD4+ T cells were isolated from wildtype (WT) or EROS-/- splenocytes, treated with ATP or NAD for 30 minutes and cell surface marker expression was measured by flow cytometry. (A) gating strategy and representative plots. CD62L (B-C), CD27 (D-E) and IL-6R (F-G) expression was measured following ATP treatment (B, D, F) or NAD treatment (C, E, G). n=5 mice per group. Data represented as mean ± SEM. Statistical significance was calculated using an unpaired two-tailed Student's *t*-test. * $p<0.05$, ** $p<0.01$, *** $p<0.001$, **** $p<0.0001$.

Another important functional effect of P2X7 signalling in CD4+ T cells is to induce cell death [156–158,160]. Again, CD4+ T cells from WT or EROS-/- mice were stimulated with ATP or NAD and cell death and apoptosis were measured by flow cytometry. ATP treatment caused WT CD4+ T cells to rapidly undergo cell death, as approximately 80% of cells expressed the apoptotic marker Annexin V post-ATP treatment (figure 3.8 B). Whereas in EROS-/- CD4+ T cells, significantly fewer cells underwent cell death, as only approximately 30% of cells expressed Annexin V following ATP treatment (figure 3.8 B). Similarly, NAD induced apoptosis in WT CD4+ T cells, but the number of EROS-/- CD4+ T cells that underwent cell death was significantly reduced (figure 3.8 C). Intriguingly, at baseline there was significantly less EROS-/- CD4+ T cells undergoing cell death than WT CD4+ T cells (figure 3.8 B-C). This demonstrates that loss of EROS abrogates P2X7 induced cell death CD4+ T cells.

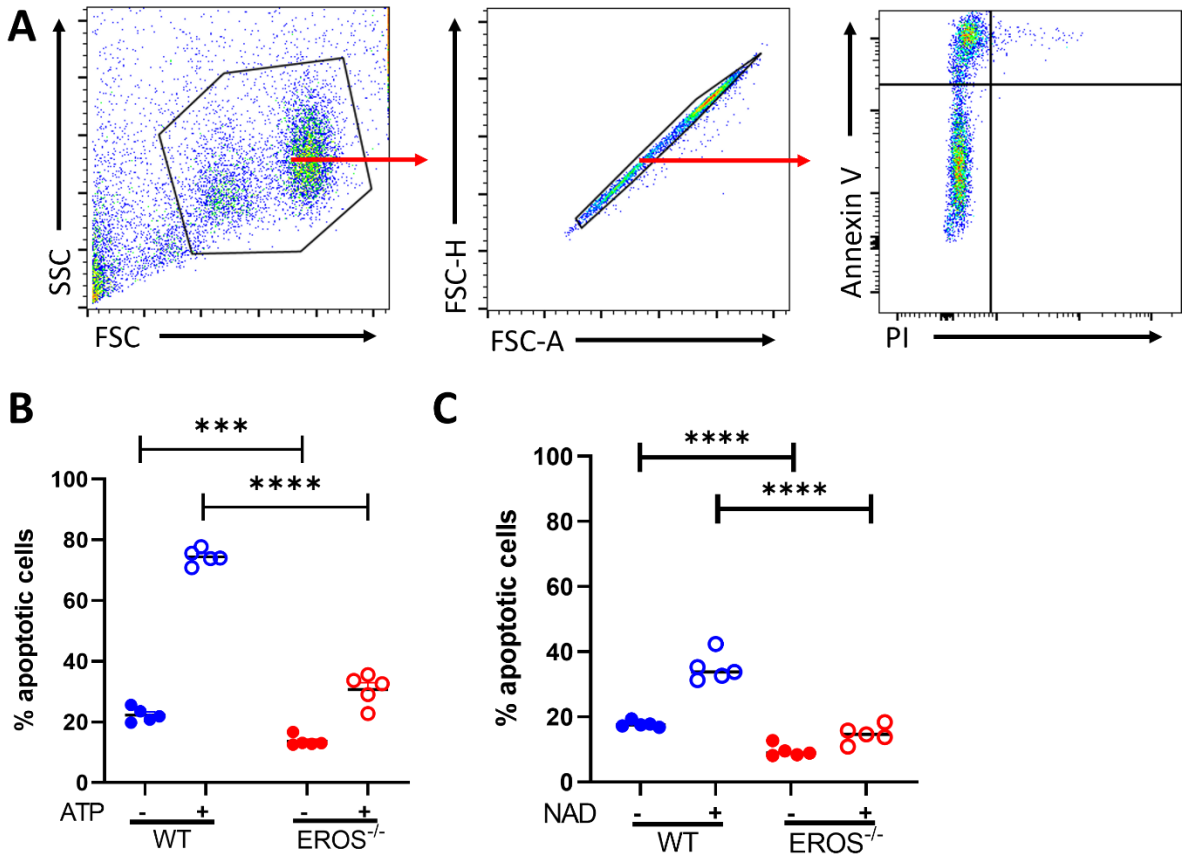

Figure 3.8: Loss of EROS reduces ATP-driven cell death

CD4+ T cells were isolated from wildtype (WT) or EROS-/- splenocytes and were treated with ATP or NAD for 30 minutes. Flow cytometry was used to measure Annexin V expression and Propidium Iodide uptake. (A) gating strategy and representative plots. Levels of apoptosis were measured following ATP (B) or NAD (C) treatment. n=5 mice per group. Data represented as mean ± SEM. Statistical significance was calculated using an unpaired two-tailed Student's *t*-test. *** $p<0.001$, **** $p<0.0001$.

As the baseline expression of CD27 was greater in EROS-/- CD4+ T cells than WT CD4+ T cells (figure 3.7 D-E), but CD27 surface expression is controlled P2X7 signalling (figure 3.7 & [153]), next it was investigated whether EROS can directly or indirectly regulate CD27 expression via P2X7 expression. Whole CD4+ T cells from P2X7-/- and WT mice were stained for CD27 and measured by flow cytometry. The MFI of CD27 was significantly greater in P2X7-/- CD4+ T cells (figure 3.9B), indicating that P2X7 regulates CD27 expression levels both at baseline and following ATP/NAD stimulation (figure 3.7D-E). Therefore, this could suggest that EROS may act to indirectly regulate CD27 expression via the regulation of P2X7 expression.

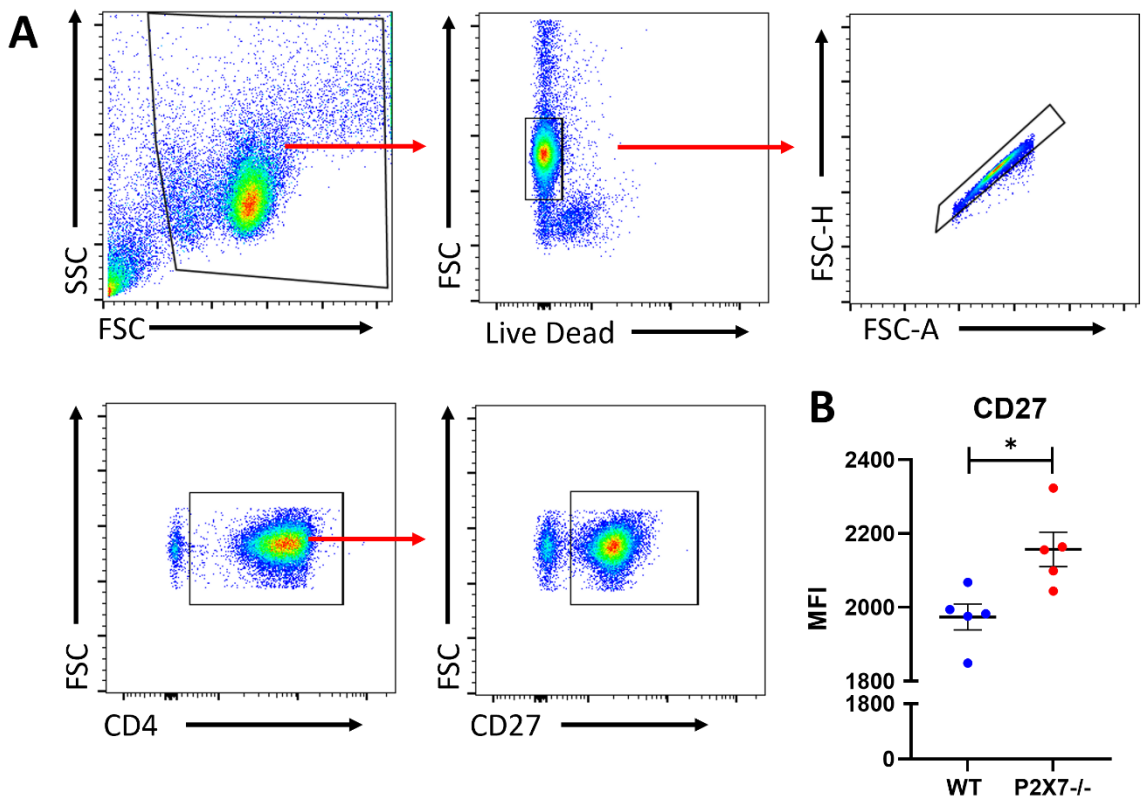

Figure 3.9: CD27 expression is upregulated on P2X7-/- CD4+ T cells

CD4+ T cells were isolated from wildtype (WT) or P2X7-/- splenocytes and stained to measure CD27 expression by flow cytometry. (A) gating strategy and representative plots. (B) Mean Fluorescence Intensity (MFI) of CD27. n=5 mice per group. Data represented as mean ± SEM. Statistical significance was calculated using an unpaired two-tailed Student's *t*-test. * $p<0.05$.

Discussion

EROS regulates gp91*phox* and P2X7 in CD4+ T cells

EROS has previously been described to regulate the protein expression of gp91*phox* and P2X7 in macrophages and neutrophils [34]. Here, gp91*phox* and P2X7 are downregulated in EROS deficient CD4+ T cells, by both mass spectrometry (figure 3.1) and western blot (figure 3.2), demonstrating that EROS can regulate the expression of gp91*phox* and P2X7 in CD4+ T cells. Additionally, P2X7 expression is reduced in B cells and CD8+ T cells (figure 3.2) demonstrating that EROS has a consistent role across multiple adaptive immune cells, to regulate the expression of P2X7.

P2X7 abundance is increased by EROS expression

EROS increases the abundance of P2X7 protein expression (figure 3.3), similar to its role of increasing gp91*phox* precursor abundance [164]. EROS expression is necessary to stabilise the inherently unstable gp91*phox* precursor, allowing glycosylation and maturation to occur, thus stabilising the gp91*phox* protein. It could be speculated that EROS has a similar role for the P2X7 protein, as the enlarged P2X7 band following EROS co-transfection is accompanied by lane 'smearing' (figure 3.3), suggesting that increased glycosylation may have occurred. However, this would need to be confirmed with specific experiments to measure the glycosylation of P2X7 in the presence and absence of EROS.

It is also important to consider whether there would be any difference when transfecting human P2X7 and EROS constructs, as these co-transfections were performed with mouse constructs (figure 3.3). However, it is unlikely there would be much difference with human constructs as the role of EROS is highly conserved between human and mouse [165], and EROS regulates mouse gp91*phox* in the same manner as it regulates human gp91*phox* [164], so it's likely the same for P2X7 but this would need to be experimentally confirmed.

EROS has a complex relationship with Phactr4

The mass spectrometric analysis highlighted that Phactr4 is highly downregulated in EROS deficient CD4+ T cells (figure 3.1). Phactr4 is also downregulated in EROS deficient macrophages [164]. Phosphatase and actin regulator 4 (Phactr4) is the 4th member of the Phactr1-4 family, with Protein Phosphatase 1 (PP1) and actin-interacting regulatory domains

[173]. Phactr4 deficient mice have severe birth defects, as Phactr4 controls cell proliferation and Retinoblastoma (Rb) phosphorylation via PP1, implicating it in embryogenesis [171]. Additionally, Phactr4 has been implicated in cellular migration during embryogenesis, by regulating actin cytoskeleton dynamics via PP1 [172]. Phactr4 has also been identified as a tumour suppressor. Solimini *et al.,* (2013) found that Phactr4 is severely mutated or downregulated in several cancers. Reconstituting Phactr4 expression in cancer cell lines reduces proliferation and tumour formation [174,175].

EROS cannot increase the abundance of Phactr4 (figure 3.4C), in the same manner that it can increase the abundance of P2X7 (figure 3.3). Therefore, this may suggest that EROS does not directly regulate Phactr4, but its expression may be regulated by a protein that EROS regulates, such as P2X7 or gp91*phox.* However, this would need to be confirmed and Phactr4 is an ongoing interest in the Thomas lab.

Little is known about the role of Phactr4 in the immune system. Recently, Tang *et al.,* (2022) identified that Phactr4-containing immune complexes were significantly elevated in Lupus Nephritis patients compared to healthy controls. The authors suggest that aberrant expression of Phactr4 in the kidney and its ability to form immune complexes may contribute to the pathogenesis of Lupus Nephritis [170]. As CGD patients often develop lupus it would be interesting to know whether Phactr4 is negatively regulated by ROS signalling, and whether this affects the pathogenesis of autoimmunity in CGD patients.

EROS controls the expression of P2X1 and P2X4

EROS can positively regulate the expression of P2X1 in macrophages and CD4+ T cells and negatively regulate the expression of P2X4 in macrophages. P2X1 expression is decreased in EROS deficient macrophages (figure 3.5A-B) and CD4+ T cells (figure 3.5E-F), which is corroborated by further data showing that co-transfection of EROS increases the abundance of P2X1 protein (figure 3.6A). Additionally, these data are also supported by findings from Human Binary Protein Interactions database, in which P2X1 was found to interact with EROS [176].

In contrast, P2X4 expression is increased in EROS deficient macrophages (figure 3.5C-D), which is supported by co-transfection experiments that show EROS decreases the abundance of P2X4 (figure 3.6B). However, P2X4 expression decreased in EROS deficient

CD4+ T cells (figure 3.5G-H). A possible explanation for this contentious result is that, unlike in the macrophage experiments, the wildtype controls were not perfectly age and sex matched. Therefore, it could be argued that this result is an experimental artefact due to lack of proper experimental controls. Additionally, current literature that states that there is an inverse relationship between P2X4 and P2X7 expression [140], further contradicting the CD4+ result. This experiment highlights the absolute importance of proper age and sex matched experimental controls.

It remains to be determined whether EROS is directly regulating P2X4 expression, or whether it may be indirectly regulating P2X4 expression via its effect on P2X7. To answer this, a NanoBIT assay used by Randzavola, Mortimer *et al.,* (2021) could be performed to assess whether EROS directly binds to P2X4.

Ultimately, these data suggest that EROS has a similar, but more modest, effect on P2X1 expression than it does on P2X7 expression, but a likely opposite effect on P2X4 expression when compared to both.

Loss of EROS is detrimental to cell surface marker shedding

EROS deficiency reduces P2X7-driven cell surface marker shedding, meaning CD62L, CD27 and IL-6R remain on the cell surface after ATP treatment in EROS deficient CD4+ T cells (figure 3.7 B-G). This may impact cellular functions involving CD26L, CD27 and IL-6R, such as recirculation during immune surveillance [177], generation of immunological memory [178] or soluble IL-6 trans-signalling during inflammation [179] respectively. However, although the levels of marker shedding are significantly reduced compared to wildtype, some shedding still occurs. As P2X4 can somewhat compensate for P2X7 [140], it may be responsible for the low levels of shedding that still occurs when P2X7 is absent in EROS deficient T cells. However, one critique of this flow cytometry experiment is that a live/dead stain was not used. As ATP triggers cell death, it would have been useful to use a discriminatory stain instead of purely using size exclusion.

CD27 expression is indirectly regulated by EROS via P2X7

CD27 expression is higher on EROS deficient CD4+ T cells at baseline (figure 3.7 D-E), due to the loss of P2X7 expression (figure 3.9B). CD27 is a member of the tumour necrosis factor

(TNF) receptor superfamily and acts as a costimulatory molecule on CD4+ T cells, following binding of its ligand CD70 [178]. It is upregulated upon antigen stimulation, and then irreversibly downregulated [180].

CD27 signalling has been implicated in the development of Th1 responses. Stimulation of naïve CD4+ T cells with anti-CD3 and IL-12 in the presence of CD70-expressing fibroblasts induced the secretion of the Th1 defining cytokine IFNγ, and blocking CD27-CD70 ligation reduced this IFNγ secretion [181]. Further experiments found that Tbet was upregulated following anti-CD3 and CD27-CD70 ligation. Cultures in which IL-12 was replaced with IL-4 did not lead to the secretion of the Th2 defining cytokine IL-4 [181], suggesting CD27 signalling is important for the polarisation of Th1, but not Th2 effector cells. However, a later *in vivo* study that found that CD70 transgenic mice on the Th1-prone C57Bl/6J background develop more Th1 cells, but this is lost when the CD70 transgenic mice are backcrossed onto the Th2-prone Balb/c background [182]. This suggests that CD27 signalling is an important factor in T helper cell differentiation, but it depends on the inflammatory context, and/or the genetic background of the mice. As EROS-/- mice have elevated CD27 expression, it would be interesting to examine whether this influences T helper skewing.

EROS expression affects apoptosis

Less P2X7-driven apoptosis occurs following ATP treatment in EROS deficient cells (figure 3.8 B). However, despite the absence of P2X7 signalling, some apoptosis is still triggered in EROS deficient CD4+ T cells. A likely candidate for inducing apoptosis in response to ATP treatment would be P2X4, which is known to control apoptosis in microglia [183,184]. He *et al.,* (2022) and Vázquez-Villoldo *et al.,* (2013) both found that less microglial cell death occurred following LPS treatment or traumatic brain injury when a P2X4 antagonist was used. This demonstrates that P2X4 signalling can contribute to inducing apoptosis in microglia. This suggests P2X4 may be responsible for inducing apoptosis in the absence of P2X7 in EROS deficient CD4+ T cells, however this would need to be investigated further using P2X4 deficient mice or P2X4 antagonists.

Interestingly, even at baseline apoptosis is reduced in EROS deficient CD4+ T cells, suggesting more cells are alive prior to the addition of ATP. This may be due to the loss of P2X7 signalling affecting basal cell turnover. Additionally, the forceful maceration of mouse

spleens during tissue preparation likely caused the release of ATP and NAD, meaning that wildtype CD4+ T cells with functional P2X7 receptors are more susceptible to cell death prior to the start of the experiment. Rissiek *et al*., (2018) developed a protocol to block ARTC2.2 from inducing ADP-ribosylation in response to released NAD during tissue preparations. However, this protocol would not protect cells from any ATP released during the process, still leaving them vulnerable to apoptosis prior to the experiment. Measuring apoptosis *in vivo* in EROS deficient mice may be worthwhile to eliminate any effects of the tissue preparation process.

Overall, EROS can regulate the expression of gp91*phox,* P2X7, P2X1 and P2X4. EROS-mediated loss of P2X7 expression affects ATP-driven surface marker shedding and apoptosis in CD4+ T cells.

Chapter 4: EROS deficiency causes Th2 skewing

Introduction

EROS can regulate the expression of gp91*phox* and P2X7 in CD4+ T cells, as discussed in chapter 3. ROS signalling via the phagocyte NADPH oxidase and P2X7 signalling are more typically associated with innate immunity as they were first described here. However, both systems have important signalling roles in CD4+ T cells, and therefore EROS may influence CD4+ T cell biology.

ROS signalling and P2X7 signalling are involved in T cell differentiation. Multiple studies have found that Th1/Th17 skewing occurs in gp91*phox* deficient CD4+ T cells following polyclonal stimulation [96,100,101]. Additionally, studies have found that P2X7 signalling is required for Th1 skewing and Th17 conversion [146–148]. These skewing differences are identified by increases in IFNγ or IL-17 cytokine secretion and changes in gene expression of Tbet and RORγt. This suggests that loss of either ROS signalling via the phagocyte NADPH oxidase or P2X7 signalling in EROS deficiency may affect T cell differentiation.

ROS and P2X7 signalling are triggered following engagement of the TCR during T cell signalling. Stimulation of the TCR results in the rapid production of ROS, which is inhibited in gp91*phox* deficient CD4+ T cells [105]. Additionally, stimulation of the TCR results in rapid ATP release from the T cell, which can bind its own or adjacent P2X7 receptors, triggering a cascade of intracellular calcium signalling and IL-2 secretion [147,150]. These rapid responses to TCR engagement suggest that both ROS and P2X7 signalling are important during the T cell response, and loss of either signalling mechanism in EROS deficiency may impact T cell signalling. However, none of these studies focus directly on downstream T cell signalling pathways such as TCR proximal signalling or JAK/STAT phosphorylation, both of which are integral T cell signalling pathways.

The importance of coordinated ROS and P2X7 signalling are also exemplified by EROS deficient CGD5 patients. Patients with defective EROS expression have additional symptoms of autoimmunity, including autoimmune haemolytic anaemia and glomerulonephritis [165,166]. Both of these autoimmune mediated diseases are not typically seen in CGD1-4 patients, where the disease is caused solely by loss of phagocyte NADPH oxidase derived ROS signalling. This suggests that sufficient EROS expression may play a role in the development

of T cell responses and ultimately protection against autoimmunity, however this will be discussed in greater detail in chapter 6.

This chapter will investigate whether EROS deficiency affects CD4+ T cell differentiation, both by examining cytokine secretion and changes in gene expression. It will explore any altered signalling pathways in EROS deficient CD4+ T cells. This chapter will also determine whether any changes in T cell responses are due to loss of gp91*phox* and P2X7 expression.

Hypotheses

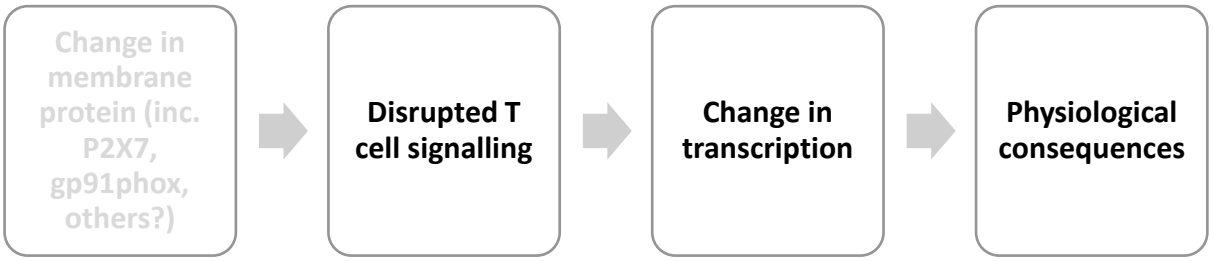

This chapter will address the following parts of my hypothesis:

Loss of EROS disrupts physiological processes in CD4+ T cells

Abnormal physiological consequences in EROS deficient cells are due to transcriptional changes

Loss of gp91*phox* and P2X7 in EROS deficiency affects T cell signalling pathways

Results

As cytokine secretion is a major function of CD4+ T cells during an immune response, cytokine secretion by EROS deficient CD4+ T cells was assessed. Whole CD4+ T cells were positively selected from EROS-/- and WT splenocytes and subjected to polyclonal anti-CD3/anti-CD28 stimulation for 48-72 hours. There was approximately 10-fold greater secretion of IL-4, 4-fold greater secretion of IL-5 and 9-fold greater secretion of IL-13 from EROS deficient CD4+ T cells, compared to WT CD4+ T cells (figure 4.1A-C). Whereas, there was only a 2-fold greater secretion of IFNγ from EROS deficient CD4+ T cells, compared to WT CD4+ T cells (figure 4.1D), suggesting greater skewing towards a Th2 differentiation profile. IL-2 secretion was not statistically significant between EROS deficient and WT CD4+ T cells (figure 4.1E), demonstrating the cells in the different conditions have been activated to the same degree. There was, however, slightly less IL-2 secretion from the EROS deficient CD4+ T cells, but this may be due to EROS deficient CD4+ T cells being more resistant to apoptosis (chapter 3), and therefore requiring more IL-2. Similarly, it is worth considering that as EROS deficiency increases cell survival (chapter 3), this may mean that the increased cytokine secretion is due to the higher number of surviving cells, rather than greater secretion of cytokines.

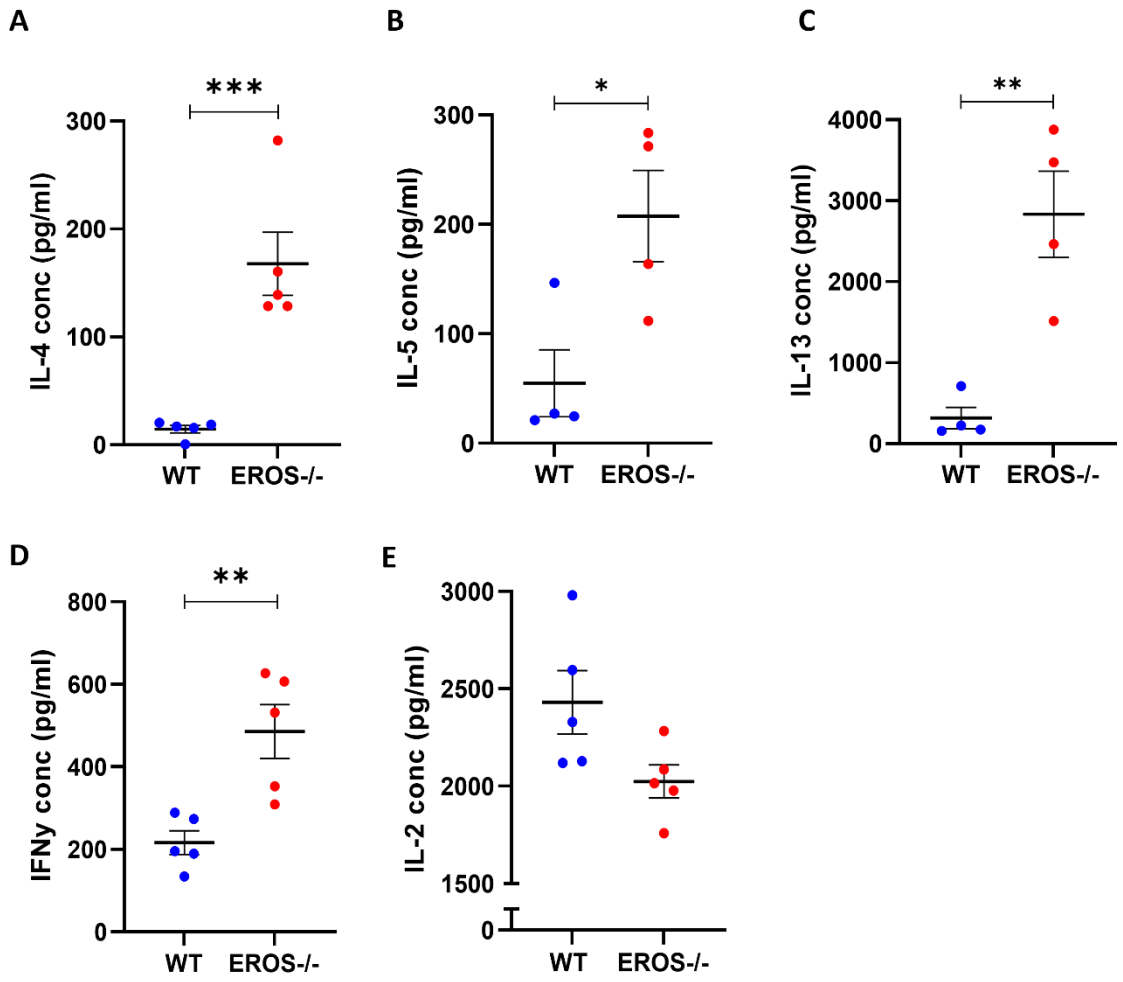

Figure 4.1: Excess IL-4, IL-5 and IL-13 is secreted from EROS-/- CD4+ T cells

Whole CD4+ T cells from WT and EROS-/- mice were polyclonally stimulated with 10ug/ml immobilised anti-CD3 and 2ug/ml soluble anti-CD28 for 48-72 hours and supernatants harvested for (A) IL-4, (B) IL-5 (C) IL-13, (D) IFNγ and (E) IL-2 ELISA analysis. Each dot represents an individual mouse. n=5 mice per group. Data represented as mean ± SEM. Statistical significance was calculated using an unpaired two-tailed Student's *t*-test. * $p<0.05$, ** $p<0.01$, *** $p<0.001$.

Next the transcriptome of these cells was examined for changes in gene expression, as EROS deficient CD4+ T cells secrete cytokines in excess. Naïve CD4+ T cells were negatively selected from the splenocytes of WT and EROS deficient mice and subject to polyclonal anti-CD3/anti-CD28 stimulation for 24-48 hours. Following RNA extraction, the RNA was submitted for RNAseq by Dr Rachel Lai. As expected, the most significant downregulated gene was EROS/*CYBC1* (figure 4.2A). The 5th most significantly upregulated gene was *Gata3*, the Th2 defining transcription factor [185]. Also *Rbpj* and *Plexin d1* were upregulated, both of which have been implicated with Th2 skewing [186,187]. The 2nd most significantly downregulated gene was *Mid1* (figure 4.2A).

Gene Set Enrichment Analysis (GSEA) was performed on the RNAseq dataset. This analysis revealed that 2 pathways involved in the cell cycle, "E2F targets" and "G2M checkpoint", were enriched in the EROS deficient CD4+ T cells (figure 4.2B). Also "IL-2 STAT5 signalling" pathway was enriched in the EROS deficient CD4+ T cells (figure 4.2B).

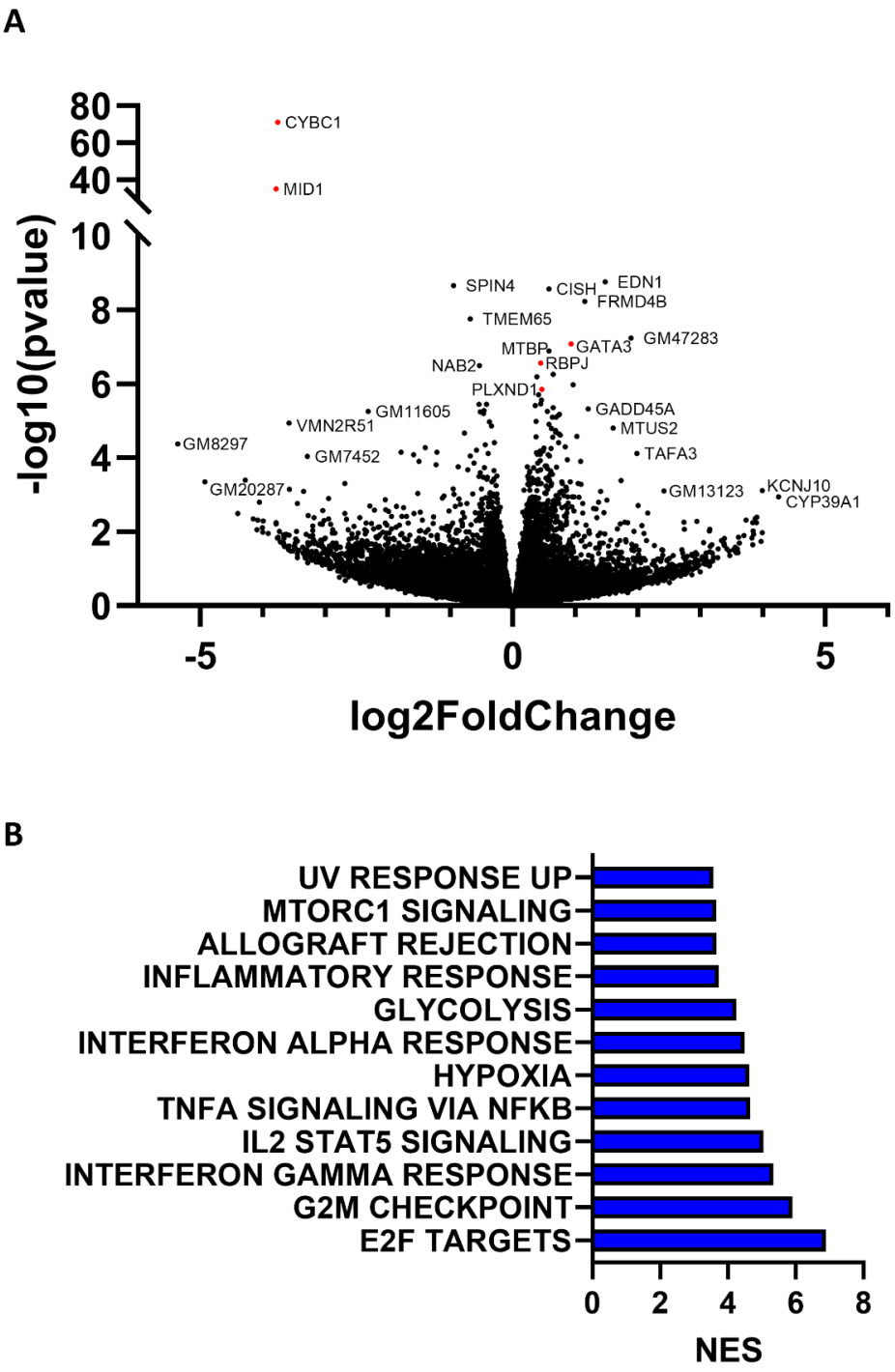

Figure 4.2: GATA3 is upregulated in EROS-/- CD4+ T cells

Naïve CD4+ T cells from WT and EROS-/- mice were polyclonally stimulated with 10ug/ml immobilised anti-CD3 and 2ug/ml soluble anti-CD28 for 24-48 hours and RNA was isolated for RNAseq analysis. (A) Volcano plot showing differentially expressed genes at 48 hours. Genes of interest shown as red dots. (B) Gene Set Enrichment Analysis of the RNAseq dataset. RNAseq and analysis performed by Dr Rachel Lai.

RNAseq analysis of T effector memory cells from EROS deficient and WT mice was performed in parallel to RNAseq of the naïve T cells in figure 4.2. These cells were separated by FACS from splenocytes of WT and EROS deficient mice and subjected to RNA isolation, prior to RNAseq analysis performed by Dr Rachel Lai. Similar to the naïve EROS deficient CD4+ T cells, *Mid1* is the most significantly downregulated gene (figure 4.3). Also worthy of note, *Sell*/CD62L and *Lrrc32*/GARP were the 2nd and 3rd most significantly downregulated genes in EROS deficient CD4+ T effector memory cells (figure 4.3). *Il2ra* was the 6th most downregulated gene, which was surprising as the IL-2 signalling pathway was enriched in the naïve transcriptome (figure 4.2B). Unfortunately the data failed to meet the minimum threshold requirement for GSEA, so no significant pathways could be identified.

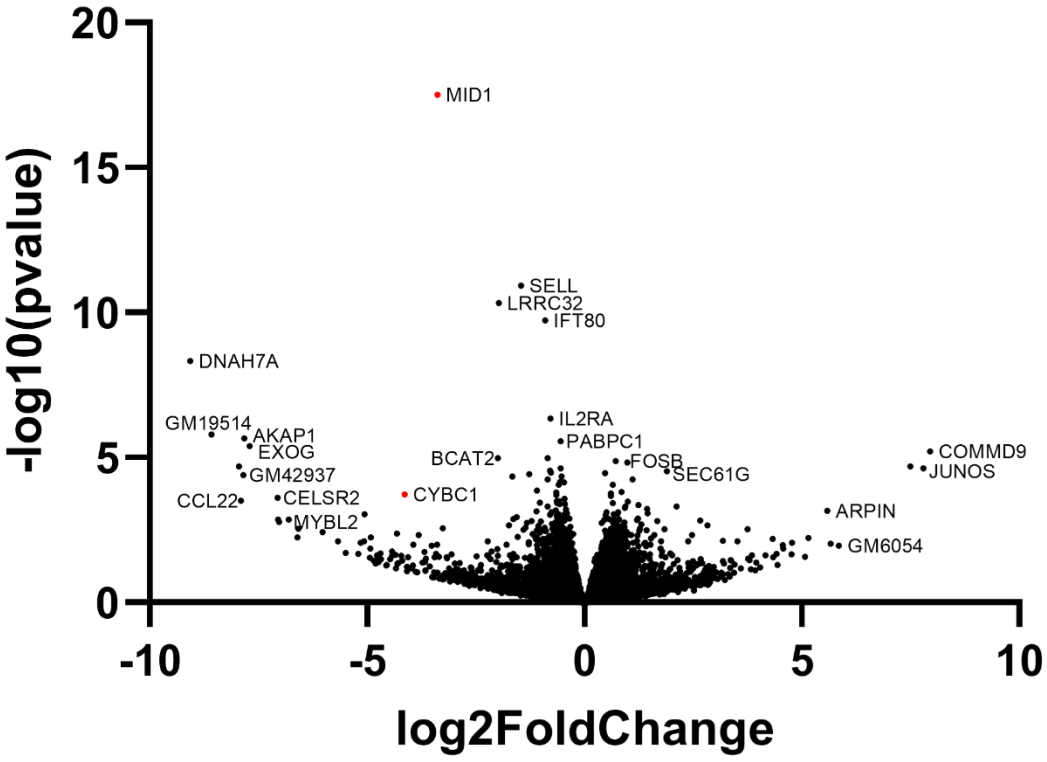

Figure 4.3: MID1 is significantly downregulated in EROS-/- T effector memory cells

T effector memory CD4+ T cells (CD44hi CD62Llo) from WT and EROS-/- mice were separated by FACS and RNA was isolated for RNAseq analysis. Volcano plot shows differentially expressed genes. Genes of interest shown as red dots. RNAseq and analysis performed by Dr Rachel Lai.

As EROS deficient CD4+ T cells secrete excess amounts of the Th2 defining transcription factor IL-4 and upregulate GATA-3 and other Th2 related genes, next the phosphorylation of STAT6 was investigated. It is well known that during Th2 differentiation, the binding of IL-4 to its receptor causes the phosphorylation of STAT6, which induces the expression of GATA3 (figure 4.16) [188]. Therefore, it could be hypothesised that there would also be an increase in phosphorylation of STAT6 in EROS deficient CD4+ T cells.

To optimise the experiment, whole CD4+ T cells from WT mice were polyclonally stimulated with anti-CD3/anti-CD28 for a range of timepoints and phosphorylated STAT6 measured by intracellular flow cytometry. There was no detectable change in pSTAT6 signal between 0 and 60 minutes (figure 4.4B), or between 0 and 48 hours, but there was a readily detectable pSTAT6 signal at 72 hours (figure 4.4C), so this timepoint was used in further experiments. Surprisingly there was no consistent increase in STAT6 phosphorylation in EROS deficient CD4+ T cells; in n=1 phosphorylated STAT6 was significantly increased (figure 4.4D), whereas there was no statistical difference in n=2 (figure 4.4F).

Alternatively, phosphorylation of STAT4 is required for Th1 differentiation [189,190], therefore it would be reasonable to think that levels of STAT4 phosphorylation may be decreased in EROS deficient CD4+ T cells. However, again, there was no consistent decrease in STAT4 phosphorylation in EROS deficient CD4+ T cells (figure 4E, G).

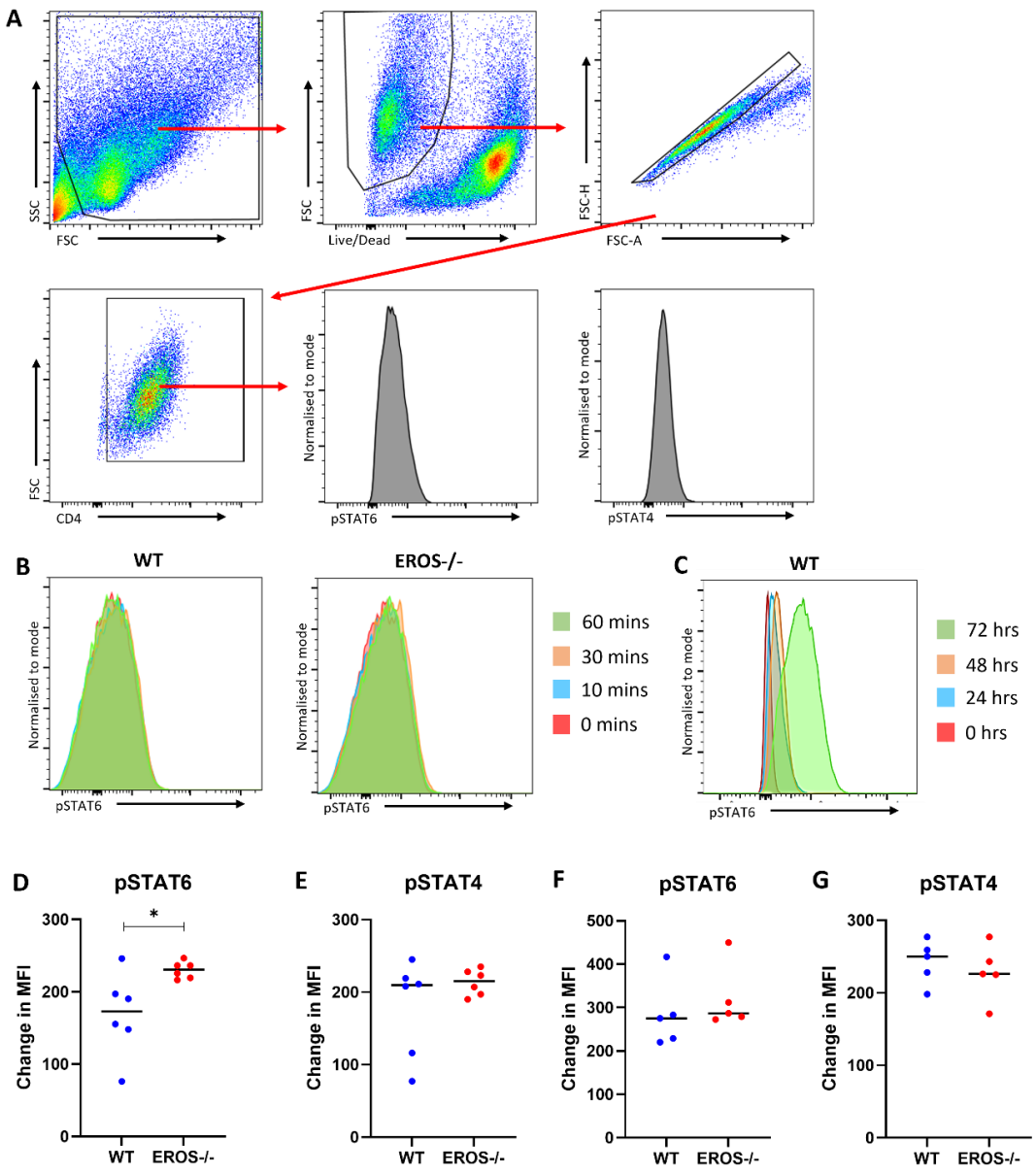

Figure 4.4: No difference in STAT4 or STAT6 phosphorylation in EROS-/- CD4+ T cells

Whole CD4+ T cells from WT and EROS-/- mice were polyclonally stimulated with 10ug/ml immobilised anti-CD3 and 2ug/ml soluble anti-CD28 for time points indicated and cells were harvested for intracellular flow cytometry. (A) Representative gating strategy (B) Comparison of phosphorylated STAT6 at 60, 30, 10 and 0 minutes. (C) Comparison of phosphorylated STAT6 at 72, 48, 24 and 0 hours. (D&F) Phosphorylated STAT6 is measured, (E&G) Phosphorylated STAT4 is measured. Each dot represents an individual mouse. n=5 mice per group. Data shown are 2 technical repeats (D-G). Data represented as mean ± SEM. Statistical significance was calculated using an unpaired two-tailed Student's *t*-test. * $p<0.05$.

Alongside the phosphorylation of STAT6, IL-2 and subsequent STAT5 signalling is also important for the differentiation towards a Th2 phenotype. Additionally, IL-2 STAT5 signalling was a key enriched pathway in the GSEA (figure 4.2B). Previous studies have found that STAT5 deficiency impairs Th2 differentiation and IL-4 secretion *in vitro* [191,192]. *In vivo* studies have found that binding of phosphorylated STAT5 improves the accessibility to the *Il4* gene during Th2 polarisation [192]. Owing to this important role of IL-2 and STAT5 signalling in the development of a Th2 response, expression of the IL-2 receptor CD25 and STAT5 phosphorylation were measured in EROS deficient CD4+ T cells at baseline and following stimulation. Whole CD4+ T cells from WT and EROS deficient mice were either unstimulated or polyclonally stimulated with anti-CD3/anti-CD28 for 72 hours. CD25 was measured by surface staining and phosphorylated STAT5 measured by intracellular flow cytometry. There was no difference in CD25 expression between WT and EROS-/- CD4+ T cells either pre or post polyclonal stimulation (figure 4.5A). However, surprisingly there was less phosphorylation of STAT5 post stimulation in EROS-/- CD4+ T cells (figure 4.5B).

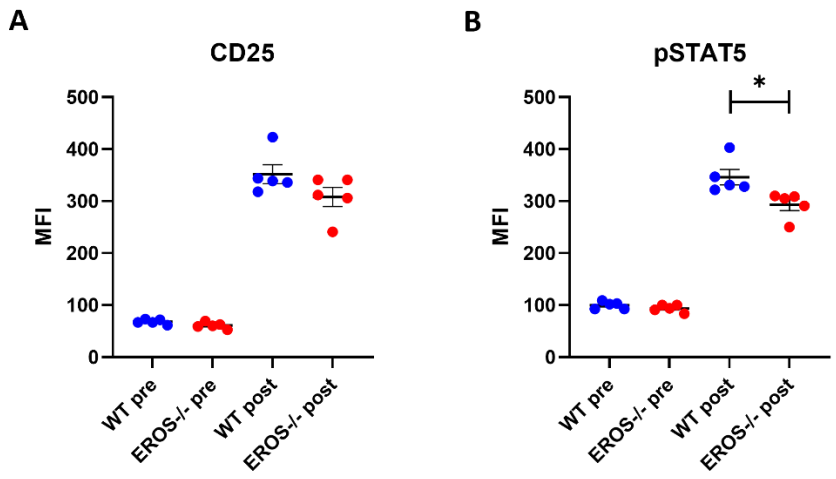

Figure 4.5: Less STAT5 is phosphorylated in EROS-/- CD4+ T cells

Whole CD4+ T cells from WT and EROS-/- mice were either unstimulated or polyclonally stimulated with 10ug/ml immobilised anti-CD3 and 2ug/ml soluble anti-CD28 for 72 hours and harvested for flow cytometry. Cells were stained for (A) CD25 and (B) phosphorylated STAT5. Each dot represents an individual mouse. n=5 mice per group. Data representative of n=1. Data represented as mean ± SEM. Statistical significance was calculated using an unpaired two-tailed Student's *t*-test. * $p<0.05$.

Next, as there were no significant differences in STAT6 or STAT4 phosphorylation in EROS deficient CD4+ T cells, alternative signalling pathways were examined. T cell receptor (TCR) proximal signalling was investigated for a number of reasons; firstly the GSEA indicated that early signalling pathways are enriched in EROS deficiency (figure 4.2B). Additionally, it is arguably one of the most important signalling pathways in T cells following receptor ligation. Briefly, TCR engagement and co-stimulation triggers the activation of LCK, which phosphorylates the immunoreceptor tyrosine-based activation motifs (ITAMs) on the CD3 complex. This recruits ZAP70, where it becomes phosphorylated, and can activate and phosphorylate LAT in turn, which is responsible for further downstream activation and signal amplification [193]. Furthermore, all experiments thus far have utilised stimulation of the TCR complex to activate the CD4+ T cell, rather than alternative methods that bypass the TCR/CD3 complex such as PMA stimulation.

Whole CD4+ T cells from WT and EROS deficient mice were polyclonally stimulated with anti-CD3/anti-CD28 for 60, 45, 30, 15, 10 or 5 minutes, or left unstimulated. Cell lysates were blotted for ZAP70, LCK and LAT, and their phosphorylated counterparts. There was no difference in the total protein or phosphorylated protein at any timepoint between WT and EROS-/- CD4+ T cells (figure 4.6).

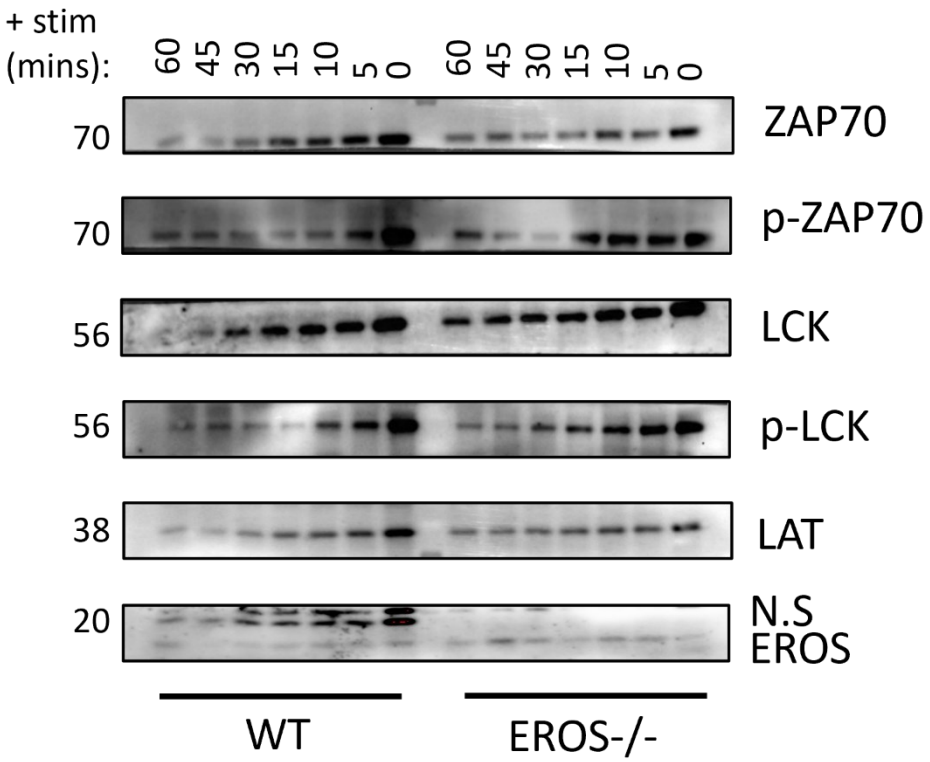

Figure 4.6: No difference in TCR proximal signalling in EROS-/- CD4+ T cells

Whole CD4+ T cells from WT and EROS-/- mice were stimulated with 10ug/ml immobilised anti-CD3 and 2ug/ml soluble anti-CD28 for indicated times, and blotted for ZAP70, phospho-ZAP70 (Y319), LCK, phospho-LCK (Y505), LAT and EROS. Data representative of n=4.

As signalling cascades are triggered from receptors on the cell surface membrane, next the expression of some cell surface receptors was examined. IL-4Rα was examined for 2 reasons; firstly the Th2 response is triggered and propagated by IL-4 signals received by the cell [194], secondly EROS strongly interacts with DOCK2 protein [164], which has previously been found to regulate the cell surface expression of the IL-4Rα [195]. Dock2-/- cells were unable to traffic IL-4Rα from the membrane, meaning IL-4 signals were amplified and a Th2 response formed [195]. IL-4Rα expression was measured by flow cytometry in WT and EROS-/- CD4+ T cells following polyclonal anti-CD3/anti-CD28 stimulation for 2-4 hours. Unexpectedly, EROS-/- CD4+ T cells had less IL-4Rα expression than WT cells at both time points (figure 4.7A-B). However, EROS-/- CD4+ T cells had less of an overall reduction in IL-4Rα expression after 4 hours compared to WT CD4+ T cells (figure 4.7C), suggesting IL-4Rα is removed from the membrane at a slower rate in the EROS deficient cells.

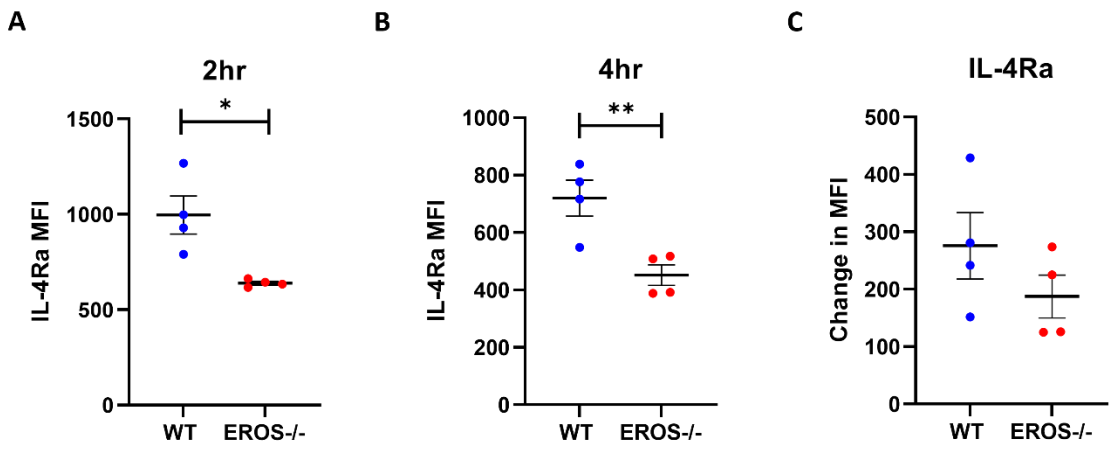

Figure 4.7: Less IL-4Rα is removed from the cell surface of EROS-/- CD4+ T cells after 4 hours

Whole CD4+ T cells from WT and EROS-/- mice were polyclonally stimulated with 10ug/ml immobilised anti-CD3 and 2ug/ml soluble anti-CD28 for (A) 2 and (B) 4 hours. IL-4Rα expression was measured by flow cytometry. (C) Change in IL-4Rα expression between 4 and 2 hours. Each dot represents an individual mouse. n=4 mice per group. Data representative of n=1. Data represented as mean ± SEM. Statistical significance was calculated using an unpaired two-tailed Student's *t*-test. * $p<0.05$, ** $p<0.01$.

Another signalling pathway of interest is the degradation of ATP by the ectoenzymes CD38, CD39 and CD73. ATP is the ligand of the P2X7 receptor, and EROS regulates the expression of the P2X7 receptor in CD4+ T cells (chapter 3). CD39 hydrolyses ATP to AMP, CD73 further hydrolyses AMP into adenosine, and CD38 degrades NAD+ into nicotinamide, preventing P2X7 signalling by degrading its ligands [116,196]. Emmerson *et al.,* (2018) found that gp91*phox* deficient Tregs express greater amounts of CD39 and CD73. Therefore, whole CD4+ T cells were positively selected from WT and EROS deficient mice and stained for CD38, CD39 and CD73 ectonucleotidase expression by flow cytometry. EROS-/- CD4+ T cells had significantly greater expression of CD38 and CD73 than WT CD4+ T cells (figure 4.8A, C), likely controlled by the loss of gp91*phox*. This demonstrates that EROS has a dual role in regulating P2X7 signalling; by regulating both the expression of P2X7 and the degradation of its ligands.

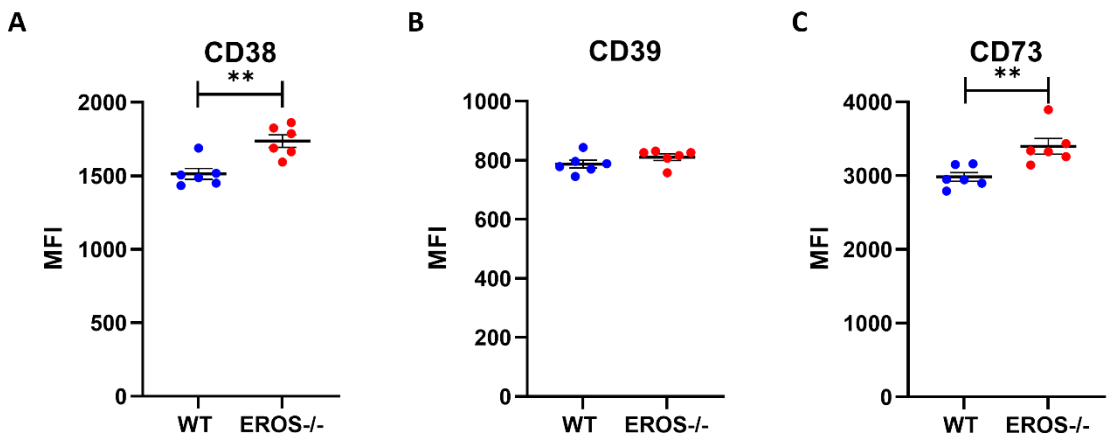

Figure 4.8: EROS CD4+ T cells downregulate CD38 and CD73

Whole CD4+ T cells from WT and EROS-/- mice were stained for (A) CD38 (B) CD39 and (c) CD73 and examined by flow cytometry. Each dot represents an individual mouse. n=6 mice per group. Data representative of n=2 experiments. Data represented as mean ± SEM. Statistical significance was calculated using an unpaired two-tailed Student's *t*-test. ** $p<0.01$.

As EROS regulates the expression of gp91*phox* and P2X7 in CD4+ T cells (chapter 3), next it was examined whether loss of either of these were responsible for the Th2 skewing seen in EROS deficiency.

First, whole CD4+ T cells were positively selected from gp91*phox*-/- and WT splenocytes and stimulated with polyclonal anti-CD3/anti-CD28 for 48-72 hours. Unlike the EROS-/- CD4+ T cells, there was no significant difference in IL-4 or IFNγ secretion between WT and gp91*phox*-/- CD4+ T cells (figure 4.9A-B).

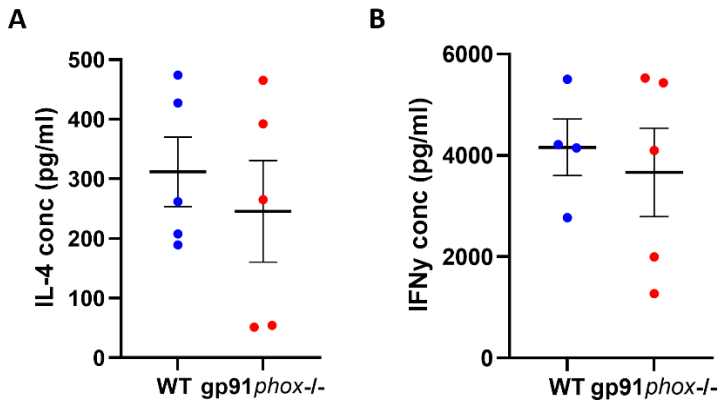

Figure 4.9: No excess cytokine secretion from gp91*phox-/-* CD4+ T cells

Whole CD4+ T cells from WT and gp91*phox*-/- mice were polyclonally stimulated with 10ug/ml immobilised anti-CD3 and 2ug/ml soluble anti-CD28 for 48-72 hours and supernatants harvested for (A) IL-4 and (B) IFNγ ELISA analysis. Each dot represents an individual mouse. n=5 mice per group. Data represented as mean ± SEM.

Despite no differences in cytokine secretion, gp91*phox* deficiency has effects on important signalling molecules like CD38 and CD73 (figure 4.8A,C) [106] so it is expected that lack of gp91*phox* has some contribution to the overall EROS phenotype, even if it is not driving the cytokine skewing. The transcriptome of gp91*phox*-/- CD4+ T cells was examined to determine what proportion of the EROS genotype is due to loss of gp91*phox,* as bulk RNAseq of these cells has never previously been undertaken.

Naïve CD4+ T cells were negatively selected from the splenocytes of WT and gp91*phox* deficient mice and underwent polyclonal anti-CD3/anti-CD28 stimulation for 24-48 hours. Following RNA extraction, the RNA was submitted for RNAseq by Dr Rachel Lai. *Cybb*/gp91*phox* was identified as the 3rd most significant upregulated gene in gp91*phox*-/- CD4+ T cells (figure 4.10A) however this is a well-known artefact of the analysis [197]. *Tbx21*/Tbet, the Th1 defining transcription factor, was the 14th most significantly upregulated gene in gp91*phox*-/- CD4+ T cells (figure 4.10A), a direct contrast with the upregulation of *Gata3* in the EROS-/- CD4+ T cell transcriptome (figure 4.2A). However, a similarity with the EROS-/- transcriptomes, both naïve and memory, is that *Mid1* is the most significant downregulated gene in gp91*phox*-/- CD4+ T cells (figure 4.10A).

The GSEA of gp91*phox*-/- CD4+ T cells was in stark contrast to that of the EROS-/- CD4+ T cells. All identified enriched pathways in the gp91*phox*-/- CD4+ T cells was completely different to those identified by the EROS-/- GSEA, with the exception of "Inflammatory Response" which was identified in both (figure 4.10B, 4.2B). Genes both upregulated and downregulated by KRAS activation were also enriched in gp91*phox-/-* CD4+ T cells (figure 4.10B).

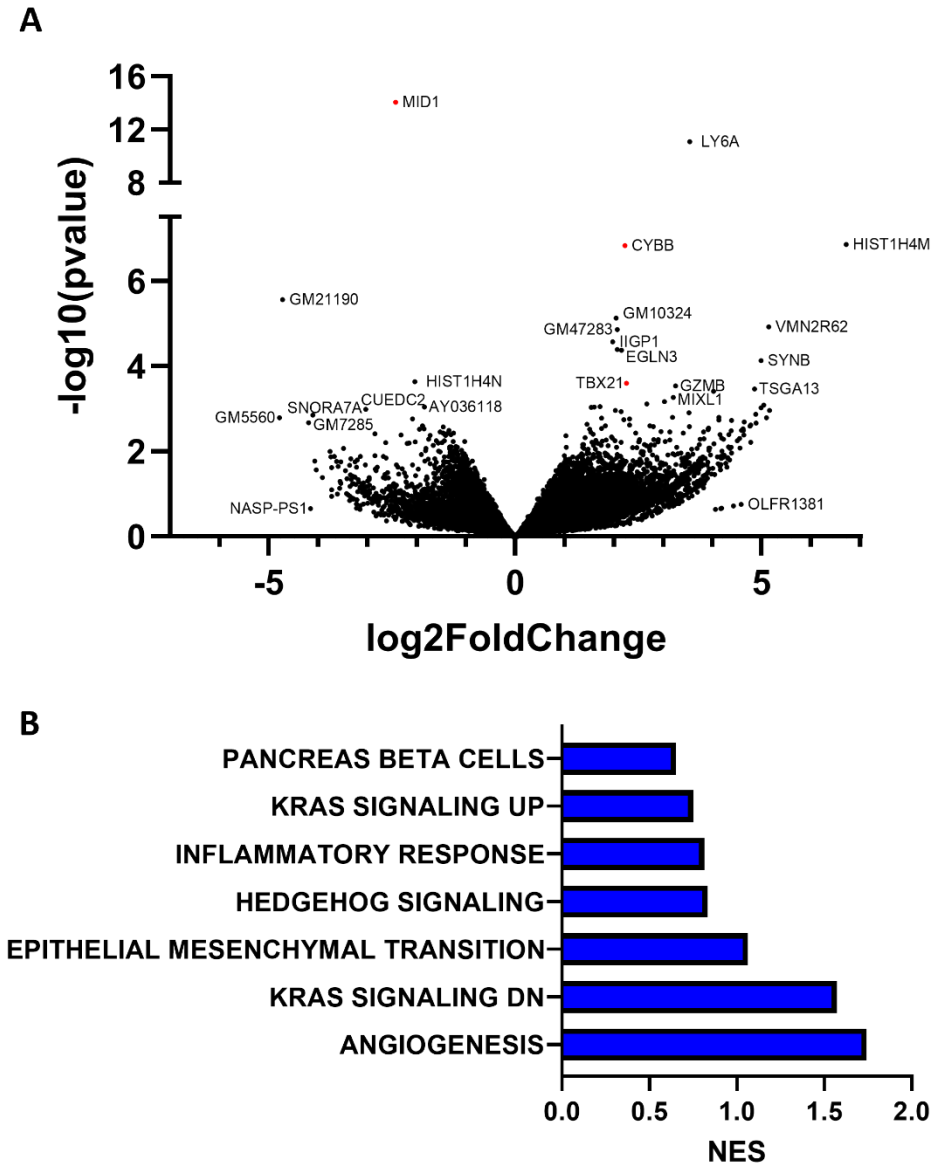

Figure 4.10: Tbet is upregulated in gp91*phox*-/- CD4+ T cells

Naïve CD4+ T cells from WT and gp91*phox*-/- mice were polyclonally stimulated with 10ug/ml immobilised anti-CD3 and 2ug/ml soluble anti-CD28 for 24-48 hours and RNA was isolated for RNAseq analysis. (A) Volcano plot showing differentially expressed genes at 48 hours. Genes of interest shown as red dots. (B) Gene Set Enrichment Analysis of the RNAseq dataset. RNAseq and analysis performed by Dr Rachel Lai.

Next, the contribution of loss of P2X7 signalling to the excess cytokine secretion by EROS deficient CD4+ T cells was investigated. P2X7 knockout mice were unavailable at this time so commercially available P2X7 inhibitors, A438079 and A740003, were used instead. These have previously been described as highly selective and high affinity P2X7 antagonists [198]. First, a titration of both inhibitors was performed to determine the optimal inhibitory concentration. Whole CD4+ T cells were positively selected from WT splenocytes and stimulated with polyclonal anti-CD3/anti-CD28 plus the inhibitors for 48-72 hours. As the concentration of both of the inhibitors increased, secretion of IL-4 and IFNγ also increased (figure 4.11A-B). 5-10μM were the optimal inhibitor concentrations that induced IL-4 and IFNγ secretion, therefore these concentrations were used in further experiments.

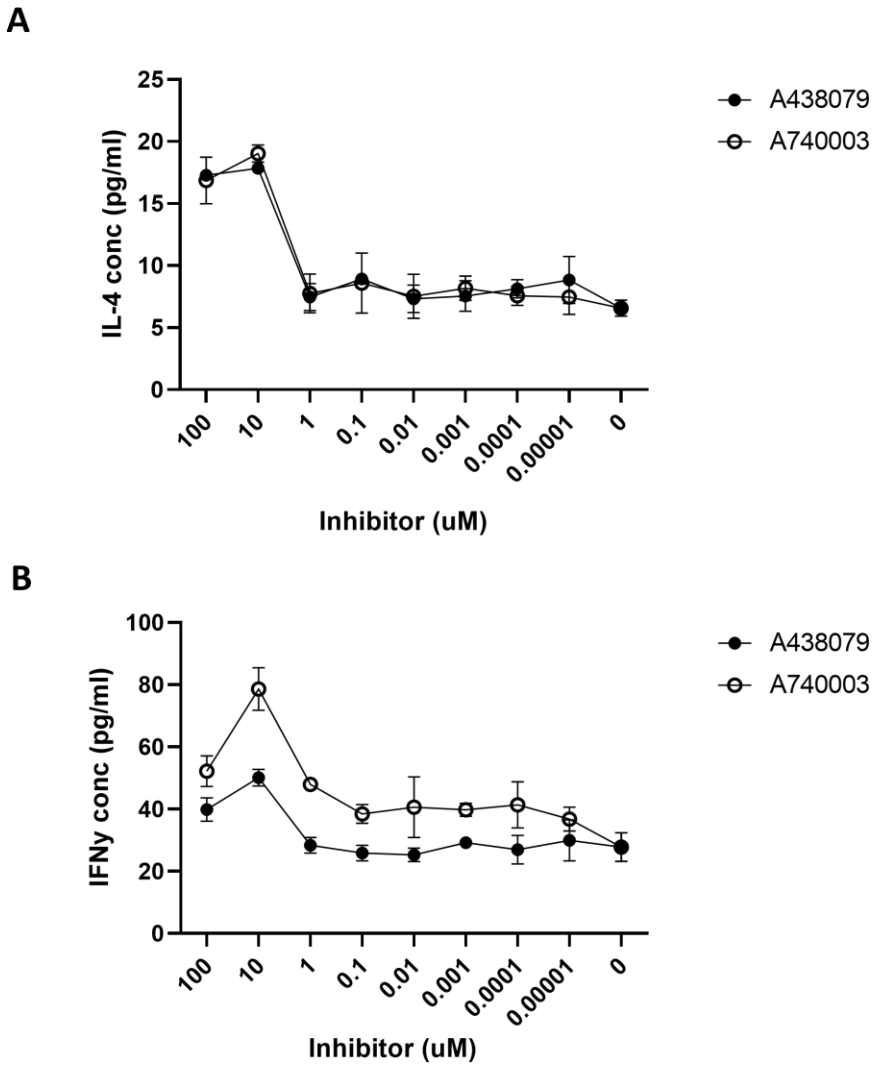

Figure 4.11: Dose response curve following P2X7 inhibition

Whole CD4+ T cells from WT mice were polyclonally stimulated with 10ug/ml immobilised anti-CD3 and 2ug/ml soluble anti-CD28 for 48-72 hours plus the P2X7 inhibitors A438079 and A740003 at the indicated concentrations, and supernatants harvested for (A) IL-4 and (B) IFNγ ELISA analysis. n=2 mice per group. Representative of n=2 experiments. Data represented as mean ± SEM.

Following on from the P2X7 inhibitor titration dose response curves (figure 4.10A-B), 2 inhibitor concentrations were selected for further experiments. Whole CD4+ T cells were positively selected from WT splenocytes and stimulated with polyclonal anti-CD3/anti-CD28 plus 5-10μM P2X7 inhibitors for 48-72 hours, and the supernatants were harvested for ELISA analysis. Treatment with 5μM and 10μM A438079 significantly increased IL-4 secretion (figure 4.12A) but there was no difference in IFNγ secretion (figure 4.12C). Treatment with 10μM A740003 increased IL-4 secretion, but not significantly ($p=0.051$; figure 4.12B), and there was no difference in IFNγ secretion (figure 4.12D). This suggests the excess IL-4 secretion from EROS deficient CD4+ T cells is due to loss of P2X7 signalling.

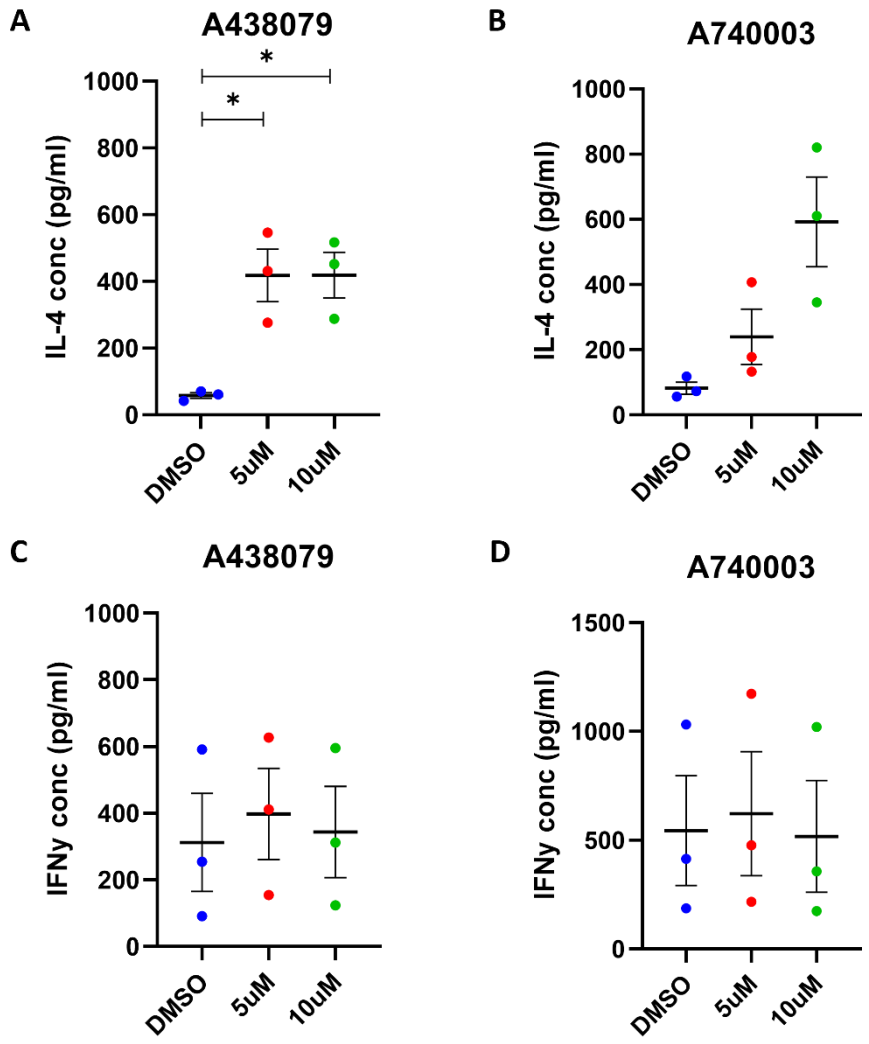

Figure 4.12: P2X7 inhibition causes excess IL-4 secretion from CD4+ T cells

Whole CD4+ T cells from WT mice were polyclonally stimulated with 10ug/ml immobilised anti-CD3 and 2ug/ml soluble anti-CD28 for 48-72 hours plus either DMSO, 5µM or 10µM of (A, C) A438079 or (B, D) A740003. Supernatants were harvested for (A-B) IL-4 and (C-D) IFNγ ELISA analysis. n=3 mice per group. Representative of n=3 experiments. Data represented as mean ± SEM. Statistical significance was calculated using a paired two-tailed Student's *t*-test. * $p<0.05$.

As the excess IL-4 secretion from EROS deficient CD4+ T cells is due to the loss of P2X7 signalling, and EROS deficient CD4+ T cells upregulate *Gata3*, next *Gata3* expression was examined in P2X7 inhibited CD4+ T cells. Whole CD4+ T cells were positively selected from WT splenocytes, stimulated with anti-CD3/anti-CD28 plus 10µM A438079 for 48 hours. The RNA was isolated and qPCR performed, targeting *Gata3*, *Tbx21*/Tbet and *Il4*. Confirming the results of the cytokine data at gene level, *Il4* was upregulated in P2X7 inhibited CD4+ T cells compared to WT control cells (figure 4.13). Also, GATA-3 was upregulated whereas Tbet was downregulated, and the difference between these 2 genes was significant (figure 4.13). This suggests the Th2 skewing in EROS deficiency is due to the loss of P2X7.

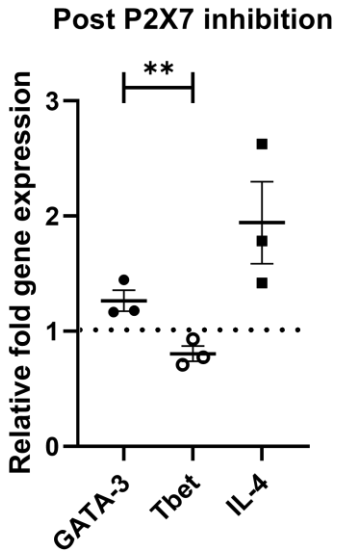

Figure 4.13: GATA-3 and IL-4 are upregulated in P2X7 inhibited CD4+ T cells

Whole CD4+ T cells from WT mice were polyclonally stimulated with 10ug/ml immobilised anti-CD3 and 2ug/ml soluble anti-CD28 plus either 10μM A438079 or DMSO control for 48 hours. Gene expression was determined by qPCR analysis and P2X7 inhibited conditions were compared relative to DMSO controls. HPRT used as housekeeping gene. n=3 mice per group. Data represented as mean ± SEM. Statistical significance was calculated using an unpaired two-tailed Student's *t*-test. ** $p<0.01$.

Recently, P2X7 deficient mice were obtained to confirm the results from the P2X7 inhibitor experiments. Whole CD4+ T cells were positively selected from WT and P2X7-/- splenocytes and subjected to polyclonal anti-CD3/anti-CD28 stimulation for 48-72 hours. There was significantly greater secretion of IL-4 from P2X7 deficient CD4+ T cells compared to WT controls (figure 4.14), supporting the results of the P2X7 inhibitor experiments (figure 4.12A-B).

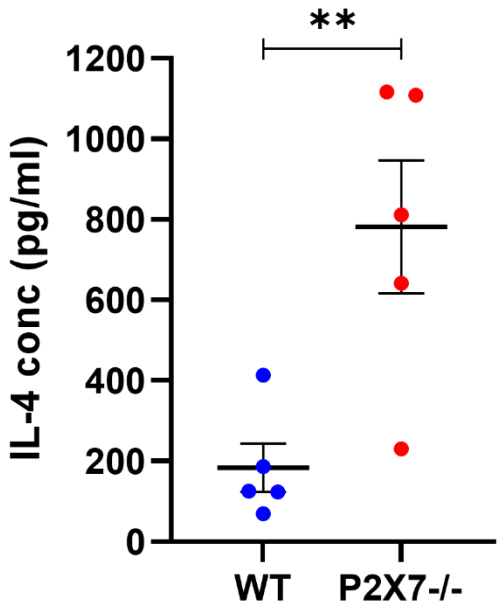

Figure 4.14: P2X7-/- CD4+ T cells secrete excess IL-4

Whole CD4+ T cells from WT or P2X7-/- mice were polyclonally stimulated with 10ug/ml immobilised anti-CD3 and 2ug/ml soluble anti-CD28 for 48-72 hours. Supernatants were harvested for (A) IL-4 ELISA analysis. n=5 mice per group. Data represented as mean ± SEM. Statistical significance was calculated using an unpaired two-tailed Student's *t*-test. ** $p<0.01$.

Then pSTAT6 and pSTAT4 were evaluated in the stimulated P2X7 deficient CD4+ T cells. There was no consistent difference in STAT6 or STAT4 phosphorylation in EROS-/- CD4+ T cells (figure 4.4) so this was a further confirmatory experiment that STAT6 signalling is unchanged despite Th2 skewing. Whole CD4+ T cells were positively selected from WT and P2X7-/- splenocytes and subjected to polyclonal anti-CD3/anti-CD28 stimulation for 72 hours, and levels of STAT4 and STAT6 phosphorylation were measured by intracellular flow cytometry. Confirming the results of the EROS-/- CD4+ T cells, there was no consistent difference in either STAT6 or STAT4 phosphorylation in P2X7-/- CD4+ T cells (figure 4.15A-B).

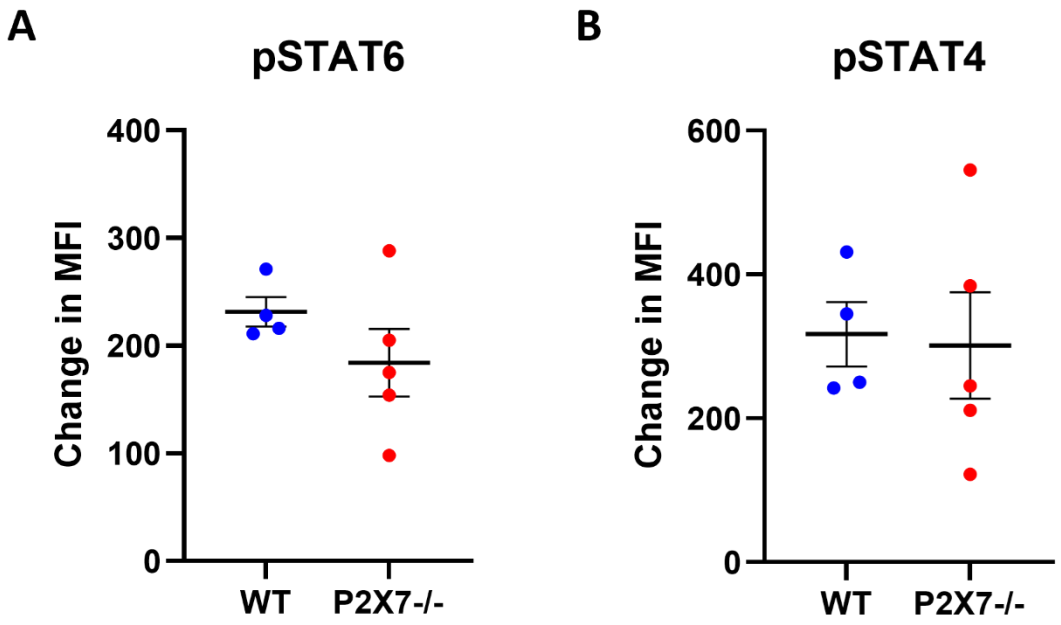

Figure 4.15: No difference in pSTAT6 or pSTAT4 in P2X7-/- CD4+ T cells

Whole CD4+ T cells from WT or P2X7-/- mice were polyclonally stimulated with 10ug/ml immobilised anti-CD3 and 2ug/ml soluble anti-CD28 for 72 hours. Cells were harvested for intracellular flow cytometry and (A) phosphorylated STAT6 and (B) phosphorylated STAT4 levels were measured. n=4 or 5 mice per group. Data represented as mean ± SEM.

Discussion:

EROS deficiency causes Th2 skewing of CD4+ T cells

IL-4, IL-5 and IL-13 were secreted in 10-fold, 4-fold and 9-fold excess respectively from EROS deficient CD4+ T cells, compared to WT CD4+ T cells (figure 4.1A-C). IL-4, IL-5 and IL-13 are the canonical Th2 cytokines [103], demonstrating that loss of EROS causes secretion of a Th2 cytokine profile.

Then RNAseq analysis revealed that *Gata3*, *Rbpj* and *Plexin d1* are highly and significantly upregulated in EROS deficient CD4+ T cells (figure 4.2A). It is well accepted that GATA3 is the Th2 defining transcription factor, and its upregulation is essential for the secretion of IL-4 during a Th2 response [185,199] .

RBPJ can act as a transcriptional activator or repressor [200]. Following ligand binding of the Notch receptor, the intracellular domain of Notch is activated via cleavage, enabling it to translocate to the nucleus where it can target RBPJ and convert it into a transcriptional activator [186,200]. Several binding sites for RBPJ have been identified in the GATA3 promoter [201,202]. Deletion of RBPJ impaired IL-4 production by CD4+ T cells [186], demonstrating its role in promoting Th2 differentiation. This suggests that the upregulation of RBPJ seen in EROS-/- CD4+ T cells may be promoting the expression of GATA-3 and subsequent IL-4 production (figure 4.15).

Plexin D1 is highly expressed on naïve T cells [203]. It has an extracellular signalling domain that binds to the semaphorin family of signalling molecules [204] , including Semaphorin 4a (Sema4A). Neutralisation of Plexin D1 signalling induced the expression of IFNγ and Tbet expression, and reduced the expression of IL-4 and GATA3 expression [187]. This demonstrates that Plexin D1 signalling promotes Th2 differentiation. Additionally, RBPJ binding sites have been identified in the promoter region of Plexin D1 [205], indicating that RBPJ can enhance the transcription of both GATA3 and Plexin D1 to promote Th2 differentiation. This suggests that the Th2 skewing seen in EROS-/- CD4+ T cells is due to the upregulation of RBPJ that promotes the expression of GATA3 and Plexin D1, which can increase the secretion of IL-4 from these cells.

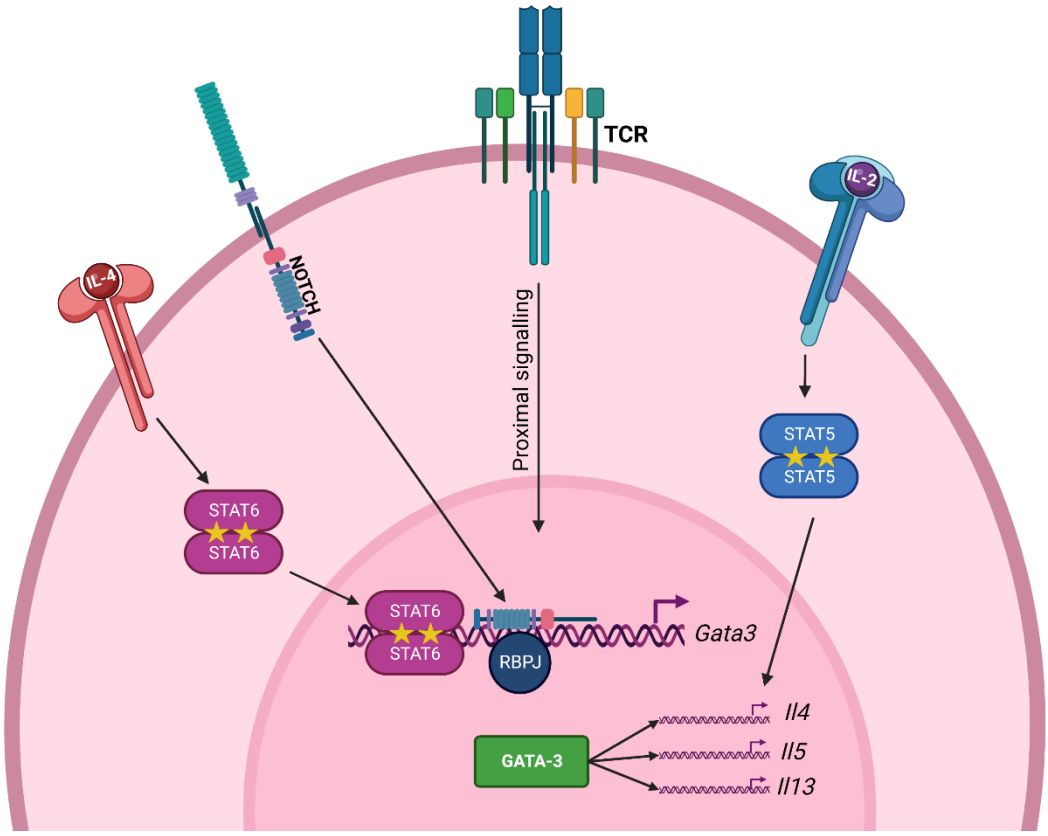

Figure 4.16: Mechanism of Th2 skewing. T cells are activated following engagement of the TCR and co-stimulatory receptors, and signals via proximal and distal TCR signalling molecules. IL-2 binding to the IL-2 receptor triggers the phosphorylation of STAT5, which can upregulate *Il4* transcription. Binding of IL-4 to the IL-4 receptor triggers the phosphorylation of STAT6, which can upregulate *Gata3* transcription. Notch signalling activates RBPJ to upregulate *Gata3* transcription. GATA-3 drives the transcription of *Il4*, *Il5* and *Il13*.

STAT6 signalling is unchanged in EROS deficiency

The first and best described regulator of GATA-3 expression is STAT6. Phosphorylation of STAT6 occurs following the binding of IL-4 to the IL-4 receptor, leading to the upregulation of GATA3 expression during Th2 differentiation [188]. Surprisingly, there is no increase in STAT6 phosphorylation in EROS-/- CD4+ T cells (figure 4.4A, C) despite the upregulation of GATA-3 (figure 4.2A). This may suggest that the GATA-3 upregulation and excess IL-4 secretion seen in EROS-/- CD4+ T cells is occurring via a STAT6-independent pathway. Ouyang *et al*., (2000) found that STAT6 deficient CD4+ T cells are able to sufficiently polarise into GATA-3 expressing, IL-4 secreting Th2 cells [206]. Therefore, it is likely that the preferential

Th2 skewing seen in EROS deficient CD4+ T cells is not a result of increased levels of STAT6 phosphorylation.

STAT5 phosphorylation has also been reported to be involved in Th2 polarisation [192], however it was found to be reduced in EROS deficient CD4+ T cells (figure 4.5B). This conflicts with the GSEA results that identified "IL2 STAT5 Signalling" as an enriched pathway in EROS deficient CD4+ T cells (figure 4.2B). However, IL-2/STAT5 signalling is not exclusively involved in Th2 differentiation, therefore the IL-2/STAT5 signalling pathway may have a different purpose, such as supporting the increased survival of EROS deficient CD4+ T cells.

TCR proximal signalling is unchanged in EROS deficiency

As the Th2 skewing in EROS deficiency CD4+ T cells is not due to changes in STAT6 signalling, other essential signalling pathways were examined. There were no differences in expression of the TCR proximal signalling molecules ZAP70, LCK or LAT at baseline, or any differences in phosphorylation of LCK or ZAP70 (figure 4.6). However, these do not provide a comprehensive panel of TCR signalling molecules and proteins located further downstream in the signalling cascade such as JNK and NF-κB need to be examined.

IL-4Rα expression is abnormal in EROS deficient CD4+ T cells

Signalling cascades are triggered from receptors expressed on the cell surface. IL-4Rα expression was examined as it is involved in an important signalling pathway for propagating Th2 differentiation [194] and has been found to be regulated by DOCK2 [195], an EROS interactor [164]. EROS-/- CD4+ T cells have less downregulation of IL-4Rα expression at 4 hours than WT CD4+ T cells (figure 4.7C). This suggests that EROS deficient CD4+ T cells are downregulating IL-4Rα expression on the membrane at a slower rate. Lengthened IL-4Rα expression may contribute to sustained downstream signalling, such as prolonged STAT6 phosphorylation (rather than increased phosphorylation), ultimately contributing to the Th2 skewing in EROS deficient CD4+ T cells. However, this experiment was only performed once so further repeats would need to be conducted to confirm the results.

EROS regulates purinergic signalling

Another important set of signalling molecules are the ectonucleotidases CD38, CD39 and CD73, that act to degrade NAD and ATP [116,196]. EROS deficient CD4+ T cells express

significantly greater amounts of CD38 and CD73 (figure 4.8A, C), which is in line with findings from a previous study that found greater CD73 expression in gp91*phox* deficient cells [106]. This suggests that ectonucleotidases are ROS controlled genes. However, Emmerson *et al.,* (2018) also found upregulation of CD39, which is not seen in the EROS deficient CD4+ T cells (figure 4.8B). A recent study found that CD39 expression can be inhibited by IL-4 signalling, via STAT6 phosphorylation [207]. Therefore, this suggests that EROS can regulate both the expression of P2X7 and the degradation of its ligands ATP and NAD by increasing the expression of CD38 and CD73. It cannot, however, upregulate CD39 expression due to the increased secretion of IL-4. It also suggests that STAT6 may be playing a role in the abnormal T cell responses seen in EROS deficiency but not via increases in overall phosphorylation levels.

MID1 is a ROS regulated gene

Each RNAseq analysis of the EROS deficient and gp91*phox* deficient CD4+ T cells identified MID1 as the most significantly downregulated gene (figure 4.2A, 4.3, 4.10A). This suggests it may be a previously undescribed ROS controlled gene.

The discovery of MID1 coincided with the finding that mutations in *Mid1* cause Opitz BBB/G syndrome, a severe congenital developmental disorder characterised by malformations along the midline structures [208]. MID1 was first described an E3 ubiquitin ligase for PP2A, catalysing its polyubiquitination and targeting it for proteasomal degradation [209]. It has since been described as an E3 ubiquitin ligase for Interferon Response Factor 3 (IRF3) [210] and type I IFN (IFN-I) receptor IFNAR2 [211]. By targeting 2 integral members of the type I IFN response for degradation, MID1 acts to restrict IFN-I production and thus reduces anti-viral responses. Interestingly, EROS and gp91*phox* deficient mice are more protected from influenza A infections [164,212], which may be due to the downregulation of MID1 resulting in increased IFN-I signalling. MID1 is an ongoing interest in the Thomas lab.

Th2 skewing is not due to loss of ROS

EROS deficient cells lack the expression of gp91*phox* and P2X7, therefore defects in T cell responses may be due to loss of one or both of these signalling pathways. There was no difference in IL-4 or IFNγ secretion between WT or gp91*phox* deficient CD4+ T cells (figure 4.9A-B). However, *Tbet* was upregulated in the transcriptome of gp91*phox* deficient CD4+ T

cells (figure 4.10B), supporting previous studies that found increases in IFNγ production and *Tbet* expression in gp91*phox* deficient CD4+ T cells [96,100,101]. This suggests the loss of gp91*phox* may be causing the 2-fold increase in IFNγ production seen in EROS deficient CD4+ T cells (figure 4.1B), but not responsible for the overall Th2 skewing.

Loss of P2X7 signalling is responsible for Th2 skewing

P2X7 signalling is required to generate Th1 and Th17 responses [146–148]. Inhibition of P2X7 causes an increase in IL-4 secretion (figure 4.12A-B, 4.14) and *Gata3* expression (figure 4.13), whereas IFNγ secretion is more variable (figure 4.12C-D) and *Tbet* expression is reduced (figure 4.13). This suggests that the Th2 skewing seen in EROS deficient CD4+ T cells is due to the loss of P2X7 signalling. In further support, the unchanged phosphorylation of STAT6 and STAT4 in P2X7-/- CD4+ T cells (figure 4.15) mirrors the EROS deficient data (figure 4.4). Therefore, it would be interesting to see in further experiments whether P2X7 deficiency also causes upregulation of *RBPJ* expression and slower turnover of IL-4Rα, as these are the likely mechanisms causing the Th2 skewing.

Together these data suggest that the combined loss of gp91*phox* and P2X7 are contributing to the complex phenotype observed in EROS deficiency. The 2-fold increase in IFNγ secretion and upregulation of *Mid1* expression in EROS deficient CD4+ T cells is due to the loss of gp91*phox* and NADPH oxidase-derived ROS signalling. The overall Th2 skewing in EROS deficient CD4+ T cells, defined by 10-fold increase in IL-4 secretion, 4-fold increase in IL-5 secretion and 9-fold increase in IL-13 secretion and upregulated *Gata3* expression, is due to the loss of P2X7 signalling. This Th2 skewing is likely a result of combined upregulation of alternative pathways such as Notch/RBPJ signalling and prolonged IL-4/STAT6 signalling.

Chapter 5: EROS deficiency has consequences *in vivo*

Introduction

Th2 immunity is critical for coordinating an effective immune response to eradicate extracellular parasitic infections. Secretion of the Th2-associated cytokines IL-4, IL-5 and IL-13 has a multitude of effects on several different immune cells.

- The production of IL-4 can induce immunoglobulin class switching in B cells to become IgG1 and IgE secreting cells [213,214]. IgE can crosslink high affinity FC receptors on the surface of basophils and mast cells, resulting in the degranulation and release of inflammatory mediators that can target parasites [215].
- Activated mast cells can activate Type 2 Innate Lymphoid Cells (ILC2s) [216]. Innate Lymphoid Cells are characterised by their lymphoid morphology but absence of the TCR. ILC2s are analogous to Th2 cells, whereby they depend on GATA-3 for their development and can secrete IL-4, IL-5 and IL-13 [217].
- IL-4 in combination with IL-13 can polarise M2-like macrophages [218] that can act together with neutrophils to directly kill parasites [219]. M2-macrophages can also mediate the inflammatory response [220].
- IL-5 can recruit and activate eosinophils [221] to directly kill the parasites and their larvae [222].

Together, these studies show that induction of Th2 immunity is necessary to form a coordinated immune response against parasitic infections.

As mentioned above, one of the most important functions of a CD4+ T cell is to provide help to B cells during antibody production. Therefore, this chapter will determine whether the Th2 skewing induced by EROS deficient CD4+ T cells (chapter 4), results in functional defects in cell differentiation, antibody production and response to a parasitic infection. Firstly, it will examine the development of T cells and the populations of naïve and memory T cells in EROS deficient mice, as these are essential to form an adequate T cell response. Then it will measure antibody production in T:B cell cocultures and following immunisation of EROS deficient mice. Finally, this chapter will consolidate these concepts by examining a parasitic infection in the context of EROS deficiency.

Hypotheses

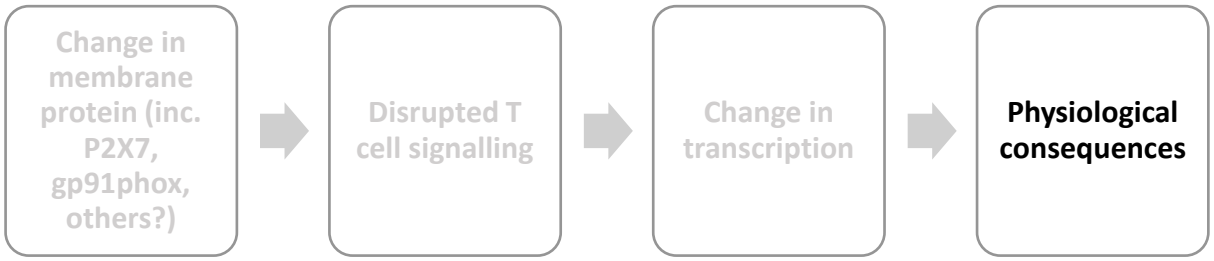

This chapter will address the following parts of my hypothesis:

Loss of EROS affects certain populations of CD4+ T cells

EROS deficiency provides protection against parasitic infections

Results

T cells develop in the thymus through a series of steps according to CD4+ and CD8+ expression, reviewed in [223]. First is the double negative (DN) CD4- CD8- stage, which is further sub-divided into DN1-4 according to CD44 and CD25 expression; DN1 (CD25−CD44+), DN2 (CD25+CD44+), DN3 (CD25+CD44-) and DN4 (CD25−CD44−). Then the double positive (DP) CD4+CD8+ stage occurs, and finally mature single positive (SP) CD4+ or CD8+ expressing CD4+ T cells enter peripheral circulation [223,224]. According to ImmGen, there is medium expression of EROS/*Cybc1* in DN1 and DP thymocytes. There is also evidence that GATA3 is important during thymic development; it is upregulated during DN3 [225] and deletion of GATA3 results fewer downstream DN4, DP and SP cells [226]. Additionally, inactivation of RBPJ also halts development at the DN3 stage [227]. As GATA3 and RBPJ are upregulated in EROS deficient CD4+ T cells, the thymic development of these cells was assessed. The thymus from WT and EROS-/- mice was harvested, macerated and subjected to flow cytometry to examine the developmental stages of T cells. There was no difference in overall DN stages, DN1-4 or DP stages between WT and EROS-/- mice (figure 5.1B-D). This demonstrates that EROS deficiency has no impact on the thymic development of T cells.

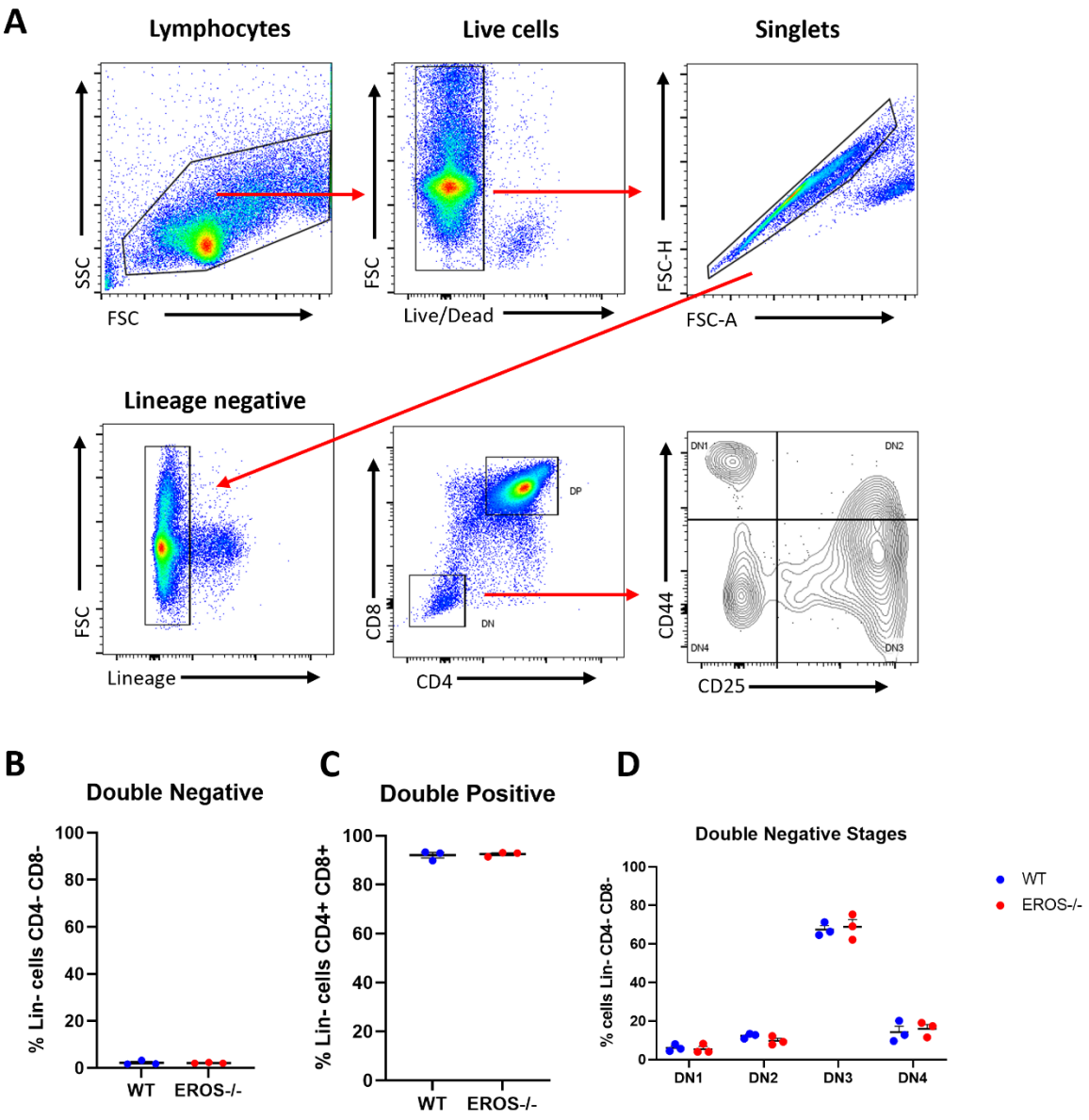

Figure 5.1: EROS-/- CD4+ T cells develop normally in the thymus

Single cell suspensions were prepared from the thymus of WT and EROS-/- mice and stained for flow cytometric analysis. (A) Representative gating strategy. Live cells were gated on lineage negative population. Data shown as percentage of cells (B) negative for CD4+ and CD8+ (C) positive for CD4+ and CD8, or (C) sub-stages during CD4- CD8- double negativity, discriminated by CD25 and CD44 expression. FSC = forward scatter, SSC = side scatter, Lin- = lineage negative, DN = double negative. Each dot represents an individual mouse. n=3 mice per group. Data representative of n=2. Data represented as mean ± SEM.

As the development of EROS deficient T cells appears normal, next the different naïve, effector and memory T cell subsets were examined. During a T cell response, naïve T cells undergo activation and expansion. Following antigen clearance, the pool of activated T cells contract and recirculating T effector memory (TEM) and T central memory (TCM) populations form [228]. Additionally, a further population of TEM that specifically reside in tissues, termed T resident memory (TRM), can also form [229].

Lungs, Peyer's patches and inguinal lymph nodes were harvested from WT and EROS-/- mice and stained for flow cytometry. CD4+ memory T cell populations were determined according to the following marker expression; naïve (CD44low CD62L high), TEM (CD44high CD62Llow), TCM (CD44high CD62Lhigh), TRM (CD44high CD62Llow CD69+) (figure 5.2A). There was no difference in the CD4+ naïve, TEM or TCM populations in the lungs of EROS-/- mice, compared to WT lungs (figure 5.2B-D). There were, however, significantly more TRM cells in EROS-/- lungs than WT lungs in all 3 repeats (figure 5.2B-D). There was no consistent difference in CD4+ naïve, TEM, TCM or TRM populations in either Peyer's patches or inguinal lymph nodes between WT and EROS-/- mice (figure 5.2E-H). This demonstrates that EROS deficiency impacts CD4+ T resident memory populations in peripheral tissues, but other CD4+ T memory/effector subsets are unaffected.

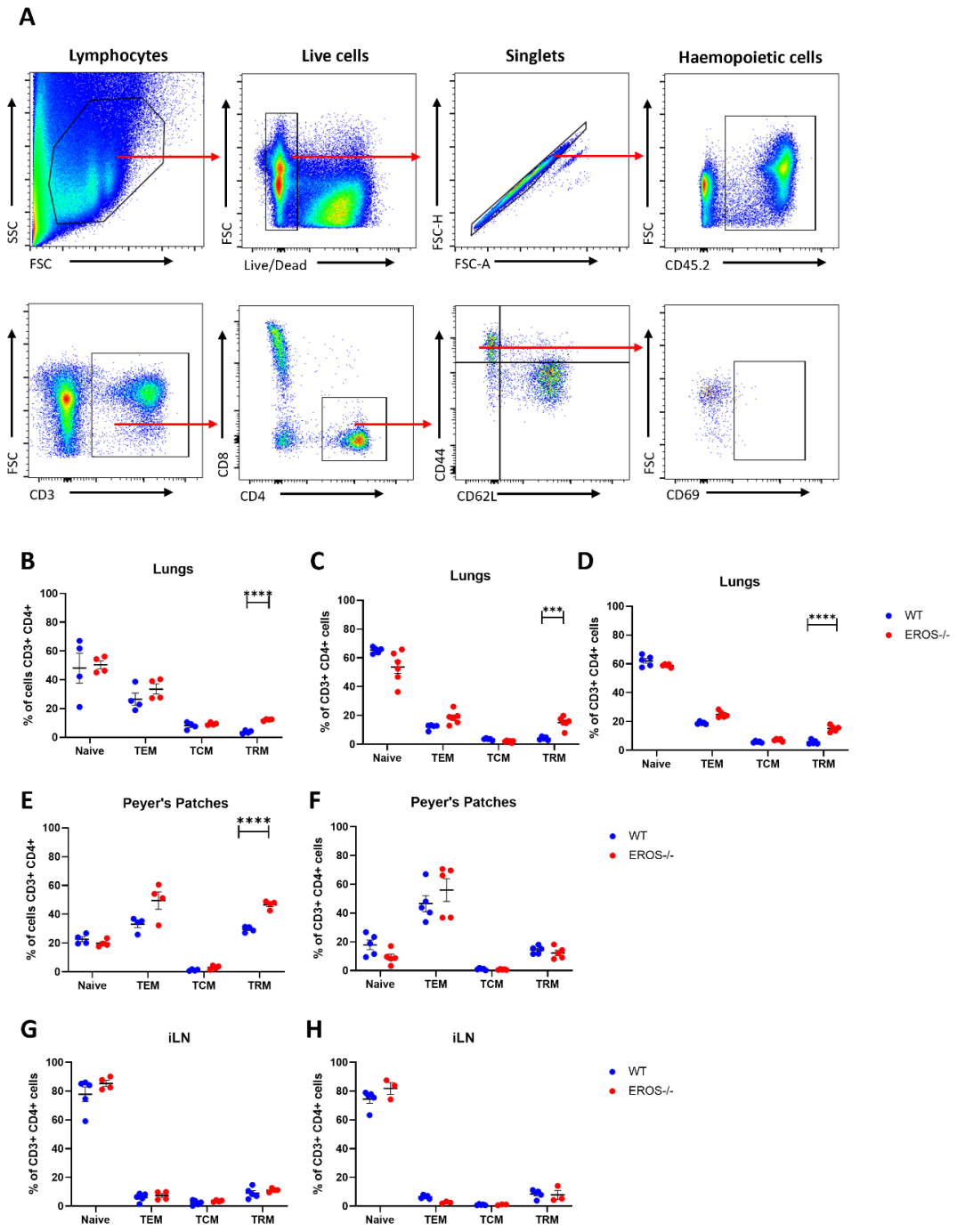

Figure 5.2: EROS deficiency increases CD4+ T Resident Memory (TRM) cells in the lung

Single cell suspensions were prepared from WT and EROS-/- mice and stained for flow cytometric analysis. (A) Representative gating strategy. Live cells were gated on CD3+ CD4+. Naïve, TEM, TCM and TRM were measured in the (B-D) lungs (E-F) Peyer's patches and (G-H) inguinal lymph nodes. Each experimental repeat is shown. Each dot represents an individual mouse. n=4-6 mice per group. Data represented as mean ± SEM. Statistical significance was calculated using an unpaired two-tailed Student's *t*-test. *** p<0.001, **** p<0.0001.

CD8+ effector and memory T cell populations were also examined. Lungs, Peyer's patches and inguinal lymph nodes were harvested from WT and EROS-/- mice and stained for flow cytometry. CD8+ memory T cell populations were determined either by CD8+ expression or CD3+ CD4- expression. Naïve, TEM, TCM and TRM populations were distinguished as described above (figure 5.3A). There was no difference in the CD8+ naïve, TEM or TCM populations in the lungs of EROS-/- mice, compared to WT lungs (figure 5.3B-D). Similar to the CD4+, there were significantly more TRM cells in EROS-/- lungs than WT lungs in 2/3 repeats (figure 5.3B,D). The outlier experiment was not significant, but the trend was the same (figure 5.3C). There was no consistent difference in CD8+ naïve, TEM, TCM or TRM populations in either Peyer's patches or inguinal lymph nodes between WT and EROS-/- mice (figure 5.3E-H). This demonstrates that EROS deficiency also impacts CD8+ T resident memory populations in peripheral tissues.

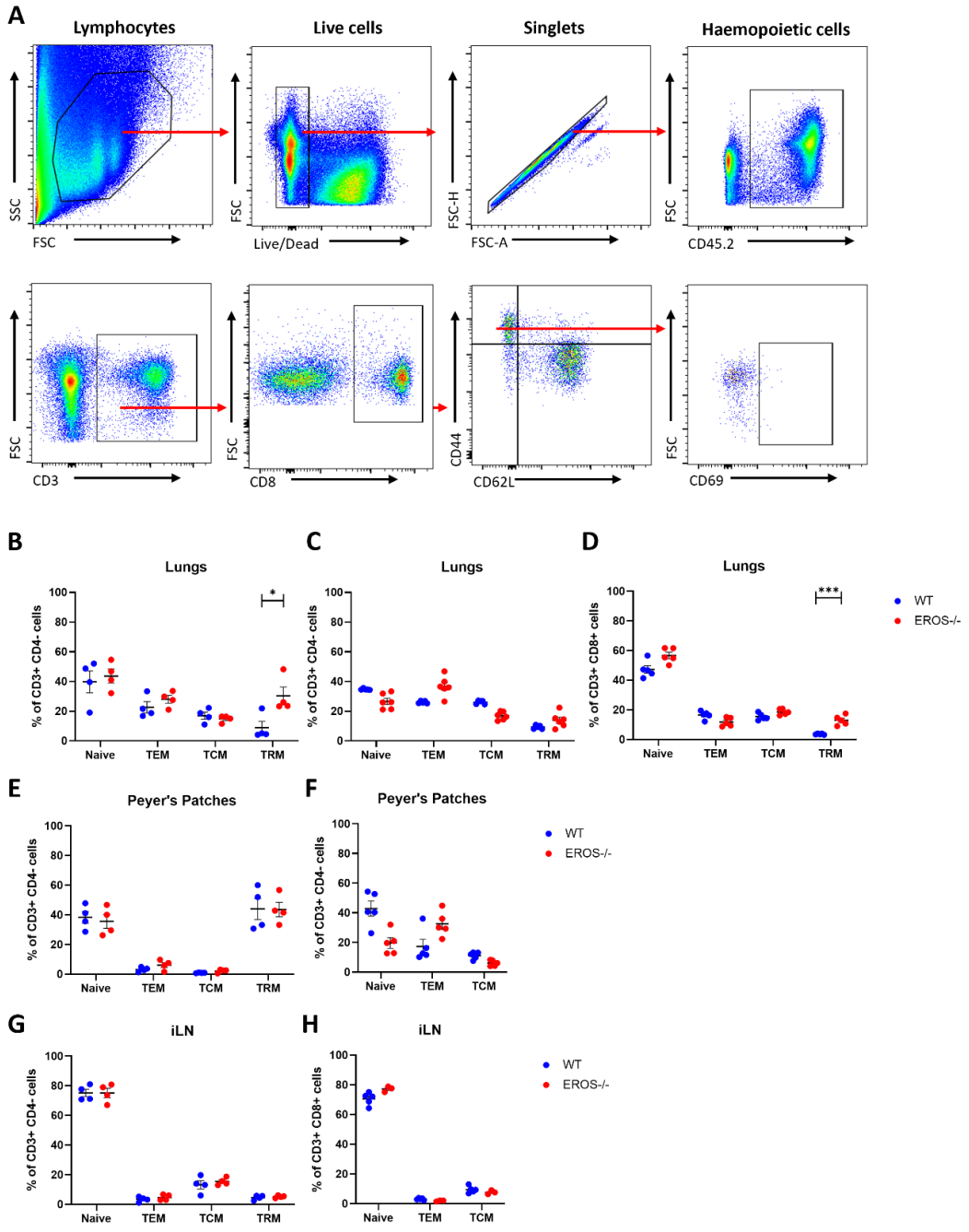

Figure 5.3: EROS deficiency increases CD8+ T Resident Memory (TRM) cells in the lung

Single cell suspensions were prepared from WT and EROS-/- mice and stained for flow cytometric analysis. (A) Representative gating strategy. Live cells were gated on CD3+ CD4-/CD8+. Naïve, TEM, TCM and TRM were measured in the (B-D) lungs (E-F) Peyer's patches and (G-H) inguinal lymph nodes. Each experimental repeat is shown. Each dot represents an individual mouse. n=4-6 mice per group. Data represented as mean ± SEM. Statistical significance was calculated using an unpaired two-tailed Student's *t*-test. * $p<0.05$, *** $p<0.001$.

Next, the naïve, effector and memory subsets were examined in gp91*phox* and P2X7 deficient mice to determine whether the increases in TRM seen in EROS deficient lung (figure 5.2B-D, 5.3B-D) are due to loss of ROS or P2X7 signalling. Lungs, Peyer's patches and inguinal lymph nodes were harvested from WT, gp91*phox*-/- and P2X7-/- mice and stained for flow cytometry. CD4+ Naïve, TEM, TCM and TRM populations were distinguished as described (figure 5.4A). There was no difference in the CD4+ naïve, TEM, TCM or TRM populations in the lungs, Peyer's patches or inguinal lymph nodes of gp91*phox*-/- mice, compared to WT control tissues (figure 5.4B-D). There was, however, significantly more TRM in the lungs of P2X7-/- mice (figure 5.4E). This demonstrates that the increased CD4+ TRM population found in EROS deficiency is not driven by loss of ROS, but by the loss of P2X7.

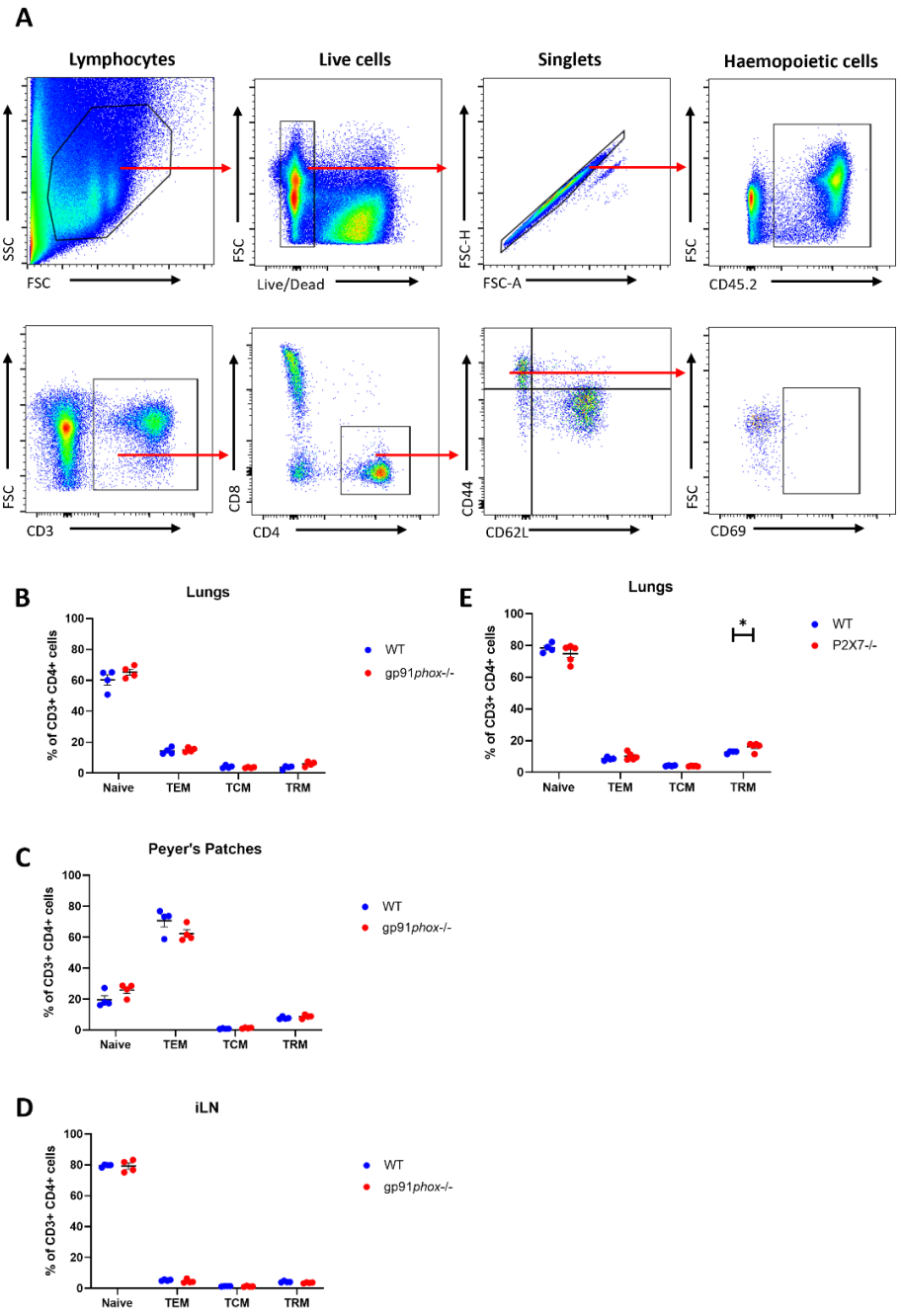

Figure 5.4: More TRM in P2X7-/-, but not gp91*phox*-/- mice

Single cell suspensions were prepared from WT, gp91*phox*-/- and P2X7-/- mice and stained for flow cytometric analysis. (A) Representative gating strategy. Live cells were gated on CD3+ CD4+. Naïve, TEM, TCM and TRM were measured in the (B) lungs (C) Peyer's patches and (D) inguinal lymph nodes of gp91*phox*-/- mice. n=4 mice per group. Naïve, TEM, TCM and TRM were measured in the (E) lungs of P2X7-/- mice. n=5 mice per group. Each dot represents an individual mouse. Data represented as mean ± SEM. Statistical significance was calculated using an unpaired two-tailed Student's *t*-test. * $p<0.05$.

Again, CD8+ effector and memory T cell populations were also examined in gp91*phox* and P2X7 deficient mice. Lungs, Peyer's patches and inguinal lymph nodes were harvested from WT, gp91*phox*-/- and P2X7-/- mice and stained for flow cytometry. CD8+ naïve, TEM, TCM and TRM populations were distinguished as described above (figure 5.5A). Similar to the CD4+ data, there was no difference in the CD8+ naïve, TEM or TCM populations in the lungs, Peyer's patches or inguinal lymph nodes of gp1*phox*-/- mice, compared to WT controls (figure 5.5B-D). However, there was also no difference in CD8+ TRM in the lungs of P2X7-/- mice (figure 5.5E). This demonstrates that the increased CD8+ TRM population found in EROS deficiency is not driven by loss of ROS or P2X7.

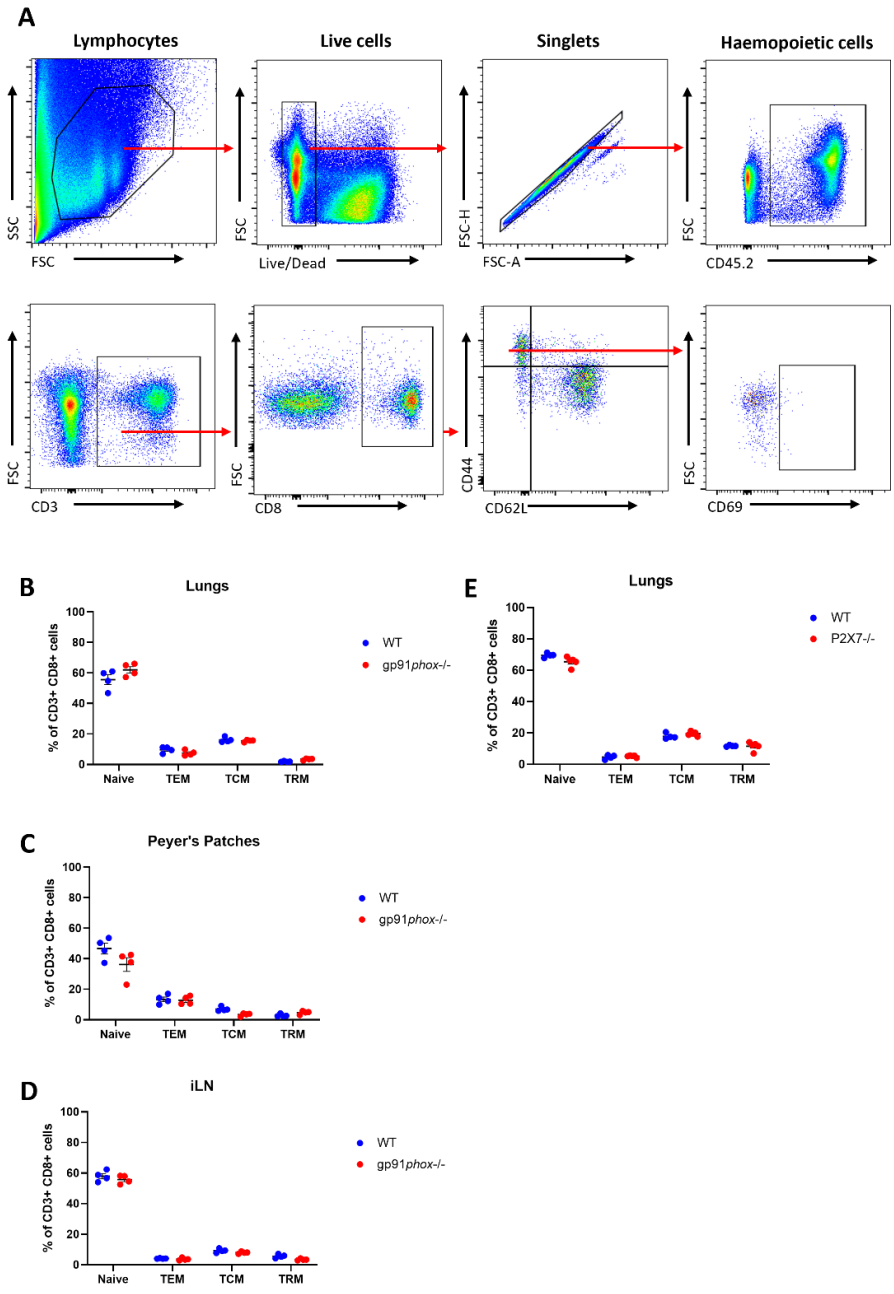

Figure 5.5: No differences in CD8+ naïve, effector or memory populations in gp91*phox*-/- or P2X7-/- mice

Single cell suspensions were prepared from WT, gp91*phox*-/- and P2X7-/- mice and stained for flow cytometric analysis. (A) Representative gating strategy. Live cells were gated on CD3+ CD8+. Naïve, TEM, TCM and TRM were measured in the (B) lungs (C) Peyer's patches and (D) inguinal lymph nodes of gp91*phox*-/- mice. n=4 mice per group. Naïve, TEM, TCM and TRM were measured in the (E) lungs of P2X7-/- mice. n=5 mice per group. Each dot represents an individual mouse. Data represented as mean ± SEM.

Another cell type of interest is Type 2 Innate Lymphoid Cells (ILC2). They have many similarities to Th2 cells including a dependence on GATA3 for their development [230,231], and ability to secrete IL-5 and IL-13 [232]. IL-4 and IL-13 have also been found to promote the proliferation and expansion of ILC2s [233]. Therefore, as IL-4 IL-5 and IL-13 are secreted in excess and GATA3 is upregulated in EROS deficient CD4+ T cells (chapter 4), ILC2s were examined by flow cytometry in the lungs of EROS and gp91*phox* deficient mice (figure 5.6A). There were significantly more ILC2 in EROS-/- mouse lungs, compared to WT lungs (figure 5.6B), whereas there was no significant difference in ILC2s between gp91*phox* deficient and WT mice (figure 5.6C). This suggests that the increased ILC2 population in EROS deficiency is not driven by loss of ROS signalling.

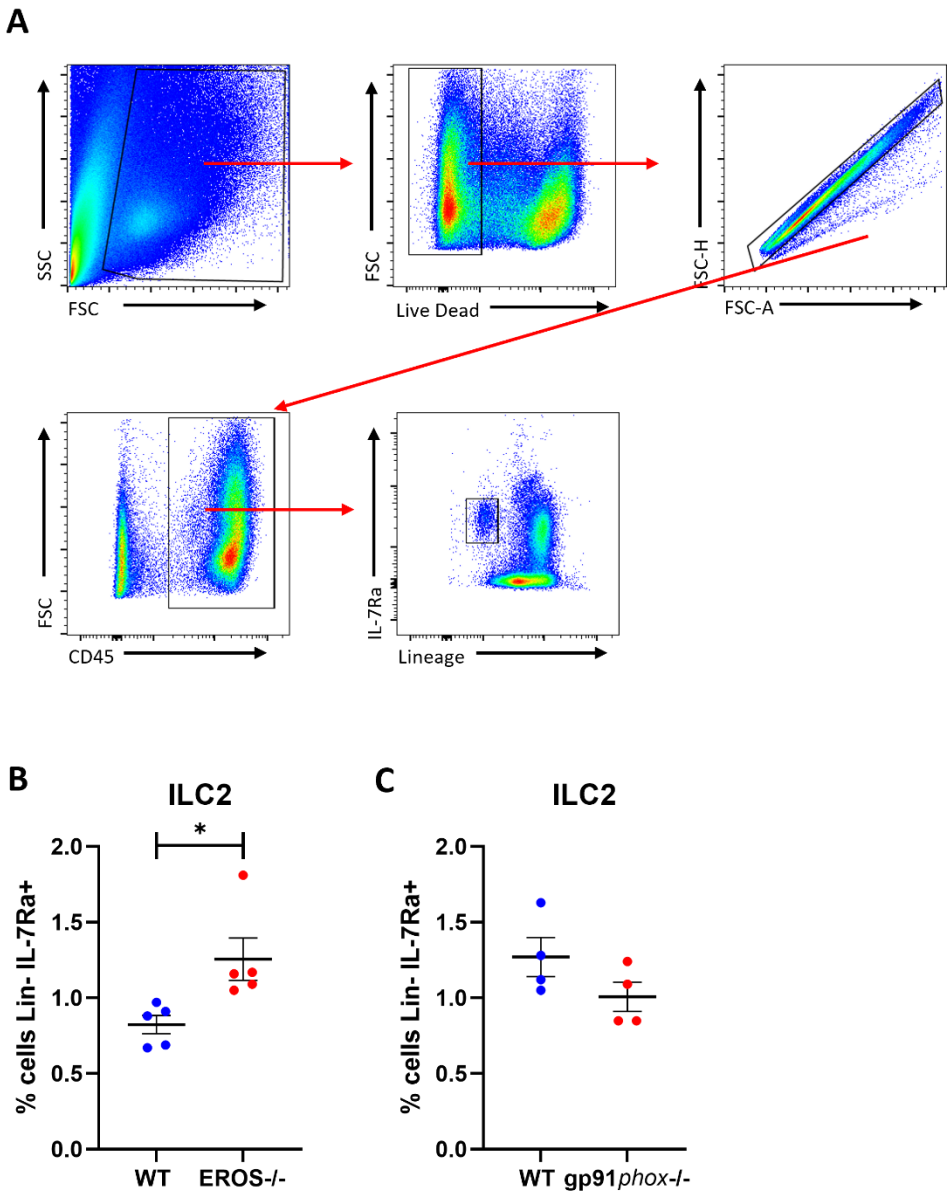

Figure 5.6: There are more ILC2s in EROS-/- mice, but not gp91*phox*-/- mice

Single cell suspensions were prepared from mouse lungs and subjected to flow cytometric analysis. (A) Representative gating strategy. ILC2s were gated according to Lin- IL-7Ra+. ILC2s were examined in (B) EROS-/- or (C) gp91*phox*-/- mice. Each dot represents an individual mouse. n=2 technical repeats for EROS-/-, n=1 repeat for gp91*phox*-/-. Data represented as mean ± SEM. Statistical significance was calculated using an unpaired two-tailed Student's *t*-test. * $p<0.05$.

The ability to provide help to B cells is arguably one of the most important functions of a CD4+ helper T cell. As there is increased cytokine production (chapter 4) and expanded TRM and ILC2 compartments, next antibody production by EROS deficient mice was assessed. *In vitro* co-cultures were set up with combinations of wildtype T or B cells and either EROS-/- or gp91*phox*-/- T or B cells, in the presence of the superantigen Staphylococcal Enterotoxin B (SEB) to induce antibody production. Supernatants were harvested and analysed by ELISA for immunoglobin production by Dr Neelam Panchal (UCL).

When WT T cells and WT B cells are co-cultured, high levels (<1 Optical Density ((OD)) of all isotypes of immunoglobulin were produced (figure 5.7A & E). However, when EROS-/- T and B cells were co-cultured, all levels of immunoglobulin isotypes produced were severely reduced to approximately 0.25 OD (figure 5.7B), indicating there is an issue with antibody production in EROS deficiency. When EROS-/- T cells were co-cultured with WT B cells, levels of all immunoglobulins produced were severely reduced (figure 5.7C) similar to that of the EROS-/- T and B cell condition. This demonstrates that it is the involvement of the EROS-/- T cells that is impacting antibody production. When WT T cells were co-cultured with EROS-/- B cells, levels of immunoglobulins produced were slightly reduced (figure 5.7D) but not to the level of the conditions with the EROS-/- T cells.

In comparison, there was no difference in immunoglobulin production when gp91*phox*-/- T cells were cocultured with WT (figure 5.7G) or gp91*phox*-/- B cells (figure 5.7F), demonstrating that the abnormalities in the EROS-/- conditions are not due to a loss of ROS signalling.

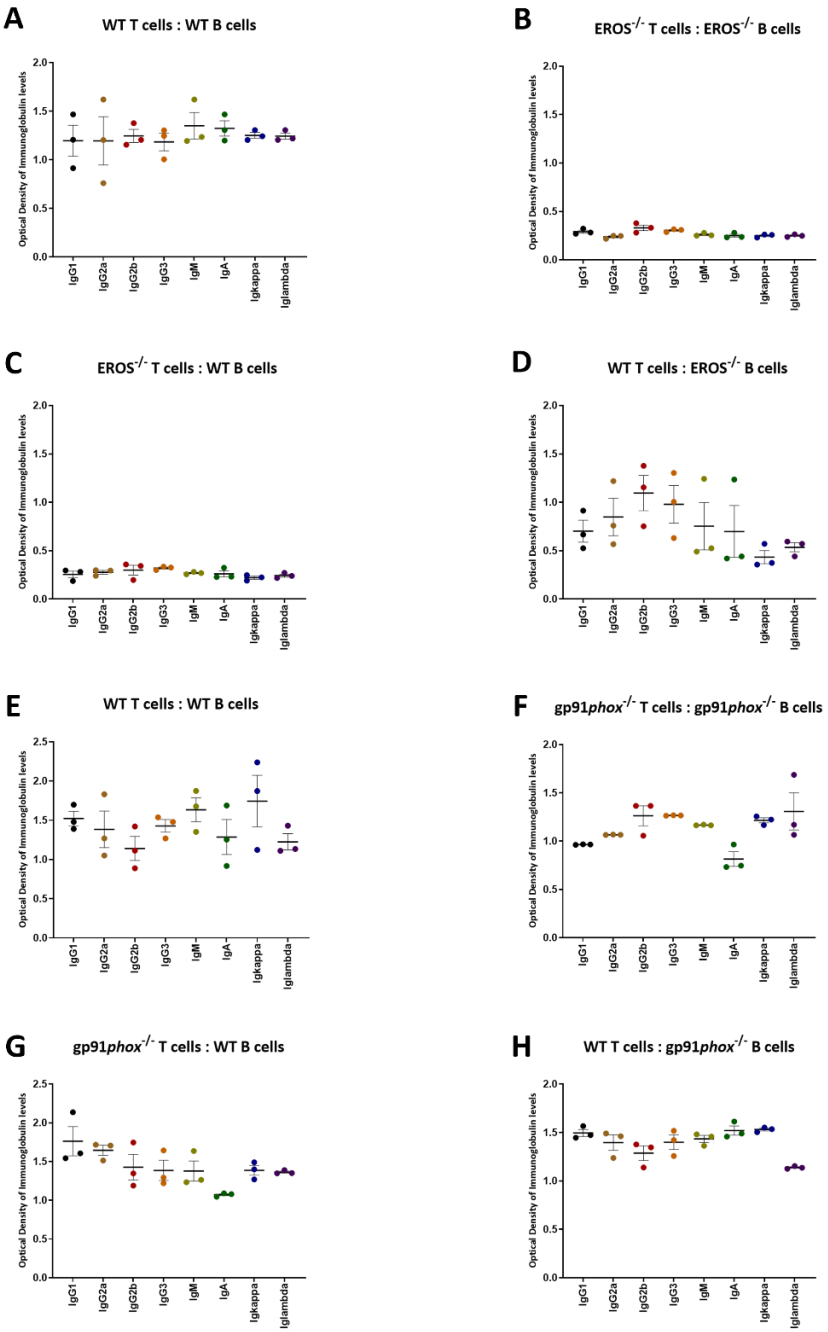

Figure 5.7: Less antibodies are produced in co-cultures with EROS-/- T cells

Naïve CD4+ T cells were isolated from WT or (A-D) EROS-/- or (E-H) gp91*phox*-/- mice and were activated with 10ug/ml immobilised anti-CD3 and 2ug/ml soluble CD28 and 100IU/ml IL-2 for 24 hours. B cells were isolated in parallel and activated with 10ug/ml anti-IgM F'ab fragments for 24 hours. T and B cells were co-cultured at a 1:1 ratio with 150ng/ml Staphylococcal Enterotoxin B (SEB) for 9 days. ELISA assays to measure immunoglobulin

isotypes were performed on supernatants. Each dot represents an individual mouse. n=3 mice per group.

Following on from the abnormalities in antibody production seen in the EROS deficient *in vitro* cocultures, next an *in vivo* immunisation experiment was performed. WT and EROS-/- mice were injected with 4-Hydroxy-3-nitrophenylacetyl (NP) conjugated to Chicken Gamma Globulin (CGG). The NP is a hapten, which is a small chemical that when conjugated to the CGG protein carrier can induce a T cell dependent antigen response [234]. Serum was collected on day 10 and NP-specific IgG1 was measured by Dr Neelam Panchal (UCL). EROS-/- mice produced significantly less NP-specific IgG1 than WT mice (figure 5.8), supporting the *in vitro* data (figure 5.7B) that EROS-/- CD4+ T cells provide inadequate help for B cell antibody production.

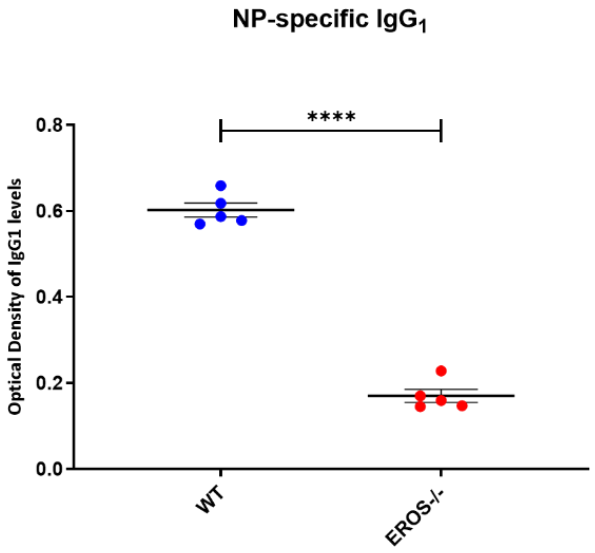

Figure 5.8: EROS-/- mice produce less NP-specific IgG1

WT and EROS-/- mice were immunised with 150mg/kg NP-CGG. NP-specific IgG1 levels in serum were measured by ELISA on day 10. n=5 mice per group. Statistical significance was calculated using an unpaired two-tailed Student's *t*-test. **** p<0.0001.

As EROS deficient mice experience Th2 skewing defined by excess IL-4 secretion and GATA3 upregulation (chapter 4), increased numbers of ILC2s (figure 5.6B) but poorer IgG1 responses (figure 5.8), next *in vivo Heligmosomoides polygyrus* infections were performed to examine anti-parasitic responses in EROS deficiency. WT and EROS-/- mice were infected with *H. polygyrus* larvae by Dr Kara Filbey (University of Manchester). Faecal egg counts were performed on day 14, 21 and 28, and adult worm counts on day 28 post-infection. In EROS-/- mice there were slightly more eggs in the faeces at all time points (figure 5.9A) and worms in the intestines (figure 5.9B) compared to WT mice, but this was not significant.

Peritoneal lavage was collected on day 28 post-infection for IL-4 analysis by ELISA. There was slightly more IL-4 in the peritoneal lavage of both infection-naïve and *H. polygyrus* infected EROS-/- mice, but again this was not significant (figure 5.9C).

CD4+ T cells were isolated from the mediastinal lymph nodes of infection-naïve and *H. polygyrus* infected mice on day 28 post-infection, and either restimulated with *H. polygyrus* Excretory/ Secretory (HES) products or media *in vitro*, then IL-4 secretion was measured by ELISA. There was more IL-4 secretion from the EROS-/- *H. polygrus*-infected CD4+ T cells, in both media treated and HES restimulated conditions, compared to the WT *H. polygyrus*-infected controls, but again this was not significant (figure 5.9D). There was significantly greater IL-4 secretion from EROS-/- *H.polygyrus*-infected CD4+ T cells when restimulated with HES, compared to media treated controls (figure 5.9D). This suggests that EROS deficiency resulted in greater Th2 skewing against *H. polygyrus* infectious products, but overall this was not protective as egg and worm counts are comparable between WT and EROS deficiency.

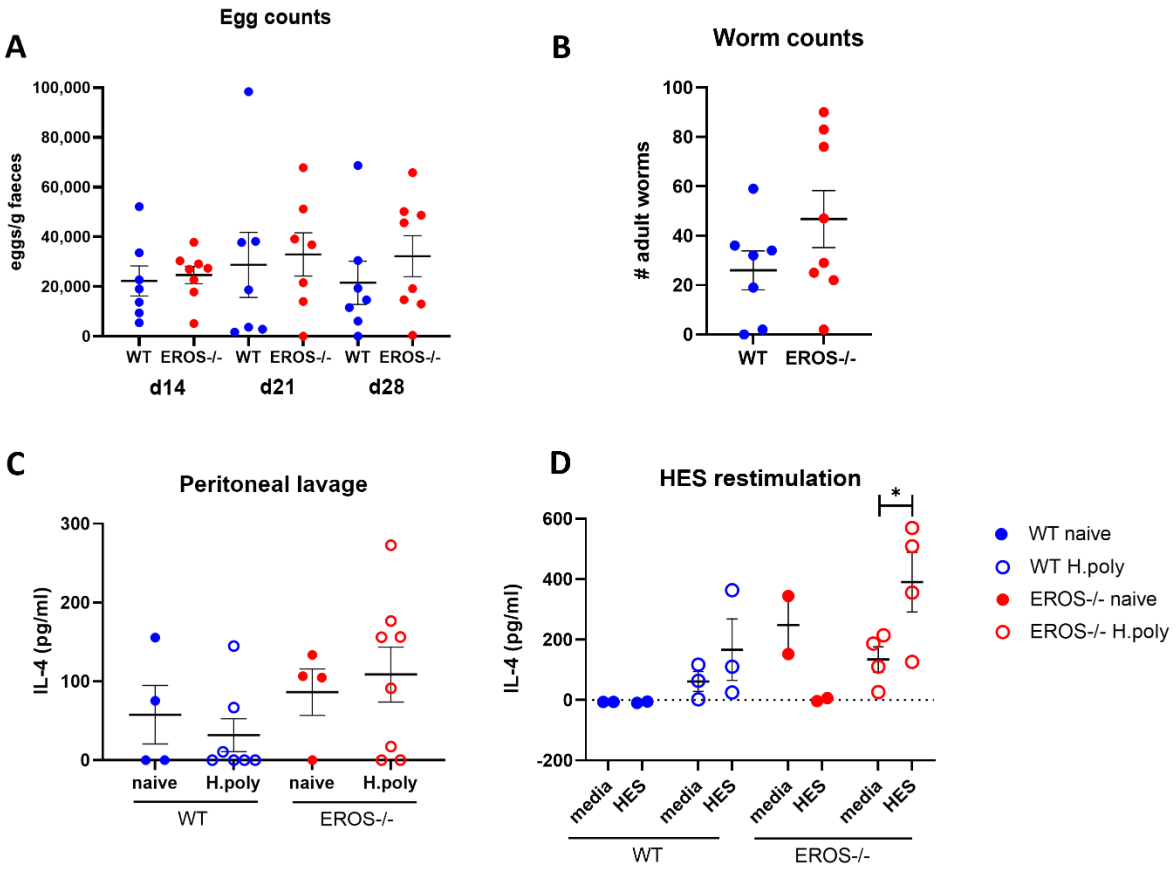

Figure 5.9: EROS deficiency does not provide protection against *H. polygyrus* infection

WT and EROS-/- mice were orally gavaged with approximately 150 L3 *H. polygyrus* larvae. (A) Faecal egg counts were performed on day 14, 21 and 28 post-infection. (B) Adult worm counts on day 28 post-infection. (C) Peritoneal lavage was collected on day 28 post-infection and IL-4 was measured by ELISA. (D) CD4+ T cells were isolated from the mediastinal lymph nodes of infection-naïve and *H. polygyrus* infected WT and EROS-/- mice, restimulated with media or *H. polygyrus* Excretory Secretory (HES) products, and IL-4 secretion was measured by ELISA. Each dot represents an individual mouse. Filled circles indicate infection-naïve and hollow circles indicate *H. polygyrus* infected mice. Statistical significance was calculated using an unpaired two-tailed Student's *t*-test. * $p<0.05$.

Discussion

EROS deficient CD4+ T cells are developmentally normal

EROS deficiency T cells develop comparably to WT T cells (Figure 5.1B-D). Previous studies found that GATA3 and RBPJ, both of which are upregulated in EROS-/- CD4+ T cells, to be involved in the DN3 stage of T cell development [225–227]. However, these studies focused on the deletion or inactivation of these proteins, rather than upregulation, like is seen in EROS deficiency. Also, GATA3 and RBPJ may be upregulated in EROS-/- CD4+ T cells during activation but not during development, therefore may not exert any effects during the developmental stages. Therefore, any differences in the T cell response in EROS deficiency is not due to abnormal T cell development.

Naïve, TEM and TCM populations are unaffected by EROS deficiency

There was no difference in CD4+ or CD8+ naïve, TEM or TCM populations in the lungs, Peyer's patches or lymph nodes of EROS deficient mice (figure 5.2, figure 5.3). This result was somewhat surprising, given that EROS deficient mice have defects in their ability to shed CD62L (chapter 3). However, studies have found that CD62L expression can be regulated by both proteolytic cleavage of the cell surface marker and at the transcriptional level [235]. Therefore, EROS deficiency may only disrupt the proteolytic cleavage of CD62L, but not its transcriptional expression, meaning the expression of CD62L on naïve and memory cells is unaffected by EROS deficiency. Ultimately, EROS deficiency does not impair memory differentiation of CD4+ or CD8+ T cells.

CD4+ and CD8+ T resident memory compartment is enlarged in EROS deficiency

There were significantly more CD4+ and CD8+ TRM in EROS deficient lungs, compared to WT deficient lungs (figure 5.2B-D, 5.3B-D). Stark *et al.,* (2018) found that P2X7 is highly expressed on TRM cells, but not circulating T cells, and can rapidly induce cell death in TRM cells upon ligand binding [160]. This highlights that P2X7 signalling is required to regulate TRM populations in tissues. Therefore, this could account for the greater numbers of TRM in EROS deficiency, as P2X7 is downregulated in EROS deficient mice, so less cell death is triggered in TRM populations.

There was no consistent difference in TRM cell populations in Peyer's patches. There were significantly more CD4+ TRM in EROS-/- Peyer's patches in one experiment (figure 5.2E), but not the other (figure 5.2F). Additionally, there was no difference in CD8+ TRM in EROS-/- Peyer's patches (figure 5.3E). However, it is difficult to draw conclusions from these data as CD8+ TRM could only be examined once due to low cell numbers obtained from the Peyer's patches. To confirm these inconsistent results more experimental repeats would need to be performed.

CD4+ and CD8+ TRM cell populations in the lymph nodes appear comparable between WT and EROS deficiency (figure 5.2G-H, figure 5.3G), however again, these data could be critiqued for lack of experimental repeats.

It is unsurprising that there is a difference in TRM in the lung, but not the Peyer's patches or lymph node of EROS deficient mice, as the lungs are a 'true' peripheral tissue whereas the Peyer's patches and lymph nodes are secondary lymphoid organs and less likely to have TRM.

Increased TRM compartment in EROS deficiency is not due to loss of ROS signalling but loss of P2X7 signalling

As EROS regulates the expression of gp91*phox* and P2X7, TRM cells were examined in gp91*phox*-/- and P2X7-/- mice. There was no difference in CD4+ or CD8+ TRM populations in gp91*phox*-/- lungs (figure 5.4B, 5.5B), but there were significantly more CD4+ TRM in P2X7-/- lungs (figure 5.4E). This suggests that the difference in EROS deficiency is not due to the loss of NADPH oxidase derived ROS signalling, but loss of P2X7 signalling. Intriguingly, there was no difference in CD8+ TRM in P2X7-/- lungs (figure 5.5E), in contrast with previous findings by Stark *et al.,* (2018) [160]. However, Borges da Silva, *et al.,* (2018) found that P2X7 signalling is required for the establishment and maintenance of CD8+ TRM [236]. Although, these studies focused on tissue injury and LCMV infection respectively, whereas the TRM phenotyping in this chapter has been performed at homeostasis, which may account for some differences.

ILC2s are increased in EROS deficiency

There were significantly more ILC2s in EROS deficient mice compared to WT (figure 5.6B), whereas there was no difference in ILC2s in gp91*phox* deficient mice (figure 5.6C). Zheng *et al*., (2020) also found no difference in ILC2s in the lungs of gp91*phox* deficient mice [237]. This is likely due to the fact that ILC2s depend on IL-4, IL-13 [233] and GATA3 [230,231] for their development and expansion, which is upregulated by EROS-/- CD4+ T cells but not gp91*phox*-/- CD4+ T cells (chapter 4). Therefore, the increased secretion of IL-4 and IL-13 and increased expression of GATA3 in EROS deficiency induces both Th2 skewing and increased development of ILC2 cells. A future experiment could examine the transcriptional profile of EROS-/- ILC2s.

EROS deficient T cells provide inadequate help to B cells

The EROS-/- CD4+ T cell response is not as simple as producing excess cytokines (chapter 4) but translates into defects in driving the B cell antibody response. Less antibodies were produced by EROS deficient B cells both in *in vitro* and *in vivo* (figure 5.7B, 5.8), suggesting EROS deficient CD4+ T cells are unable to provide the necessary help to B cells during T dependent antigen immune responses. This is not due to loss of ROS signalling as immunoglobulin levels were normal in gp91*phox* deficient cocultures (figure 5.7E-H). However, a limitation of the *in vivo* experiment is that it is difficult to delineate whether the abnormal IgG1 production is solely due to loss of EROS in the CD4+ T cells, as the *in vitro* co-culture experiment suggests the EROS-/- B cells may also be contributing to the reduced immunoglobulin production (figure 5.7D). The *in vivo* immunisation experiment could be improved by using EROS CD4-Cre mice, in which EROS is only deleted in CD4+ T cells, thus determining to what degree the abnormal immunoglobulin production is due to loss of EROS in the CD4+ T cell. It would also be interesting to phenotype the germinal centres of EROS deficient mice to evaluate T follicular helper (Tfh) and T follicular regulatory (Tfr) cells, and other cell types involved in the germinal centre reaction such as follicular dendritic cells and stromal cells.

EROS deficiency does not protect against *H. polygyrus* infections

As Th2 skewing is required for parasitic immunity, it was hypothesised that EROS deficiency may have conferred some protection against *H. polygyrus* infections. However, egg counts,

worm counts and IL-4 levels in the peritoneal lavage of EROS deficient mice were similar to WT control mice (figure 5.9A-C). There was greater secretion of IL-4 by EROS-/- CD4+ T cells from *H. polygyrus* infected mice in response to HES (figure 5.9D), indicating a stronger Th2 response can be induced in EROS-/- infected mice, however this did not improve clearance of the parasite. HES contains TGF-β-like activity that can induce Tregs. There are more Tregs in EROS-/- mice (data not shown) likely due to the reduced P2X7 expression, which has previously been shown to promote Treg differentiation [120,147]. Therefore, these excess Tregs may be dampening the surplus Th2 response [238]. Additionally, P2X7 signalling has been found to drive IL-33 production from mast cells during *H. polygyrus* infection [216]. Inhibition of P2X7 signalling resulted in reduced IL-33 production and enhanced worm burdens [216]. Although there is an exaggerated Th2 response in EROS deficiency, the complex effects of P2X7 signalling on other cell types may offset any hypothesised protection provided by loss of EROS expression.

Furthermore, an effective anti-Helminth immune response requires the production of specific IgG1 antibodies [239], but EROS-/- mice failed to induce adequate IgG1 responses (figure 5.8). This may explain why there was no additional protection from *H. polygyrus* infection, despite the excess Th2 responses in EROS-/- mice. There may, however, be additional protection against infections with other helminths such as *Schistosoma mansoni,* but this would need to be investigated further.

Overall, EROS deficient mice have normal T cell thymic development, and greater numbers of TRM and ILC2 cells. Despite exaggerated Th2 responses, EROS deficient CD4+ T cells are unable to drive adequate B cell antibody responses, resulting in poor immunity against *H. polygyrus* infections.

Chapter 6: The role of EROS is conserved in human CD4+ T cells

Introduction

Patient cells and cells that have undergone gene editing can provide a useful insight into protein functions and disease pathology. Thomas *et al.* (2018) performed CRISPR-mediated deletion of EROS in the PLB985 cell line. By targeting exon 3, they produced a clone with an 8bp deletion in the EROS gene. The EROS-deficient clone did not express EROS, subsequently had low expression of gp91*phox* and p22*phox,* and consequently had a severely impaired respiratory burst. The authors were able to reconstitute gp91*phox* expression in the EROS-deficient clone by re-introducing EROS using lentiviral transduction methods, demonstrating and consolidating the function of EROS in a human cell. Whilst this EROS-deficient PLB985 clone provides a good model of EROS deficiency, ultimately it still has the disadvantages of a transformed cell line.

The first EROS deficient patient was later found and diagnosed with CGD5 in 2018 [165]. Whole exome sequencing identified a homozygous c.127 A to G substitution mutation in *CYBC1*, the human EROS gene. Predictive software analysis found that this mutation causes an intron that contains 4 stop codons to be retained during splicing, disrupting translation of the EROS protein downstream of exon 4. Western blot analysis of the patient's cells did not detect any EROS protein compared to healthy control cells. This patient underwent a bone marrow transplant and unfortunately died shortly after of graft versus host disease (Talal Chatila, personal communication). A further 8 CGD5 patients were identified in Iceland, with a homozygous c.6 C to G substitution mutation in *CYBC1* [166]*.* This mutation introduces a premature stop codon in the second amino acid, preventing translation of the EROS protein. Subsequently, there was reduced gp91*phox* expression in the macrophages and neutrophils of these patients and their ROS burst was severely impaired. Uncommon opportunistic infections were prevalent in these patients, including *Burkholderia cepacia, Streptococcus pneumoniae, Legionella and Mycobacterium tuberculosis.* The majority of these patients had received early onset Inflammatory Bowel Disease (IBD) diagnoses, a common manifestation of CGD [166,240]. The severe course of disease highlighted here and detailed in section 1.4.3 highlights the importance of EROS in immunity.

Later in 2021 another EROS deficient patient was identified. The patient had experienced multiple episodes of severe infection including, *Mycobacterium tuberculosis*, Staphylococci and *Salmonella* infections. They also had unexplained inflammatory phenomena, including an episode of uveitis and a general positive response to prophylactic steroid treatment. Whole exome sequencing revealed a homozygous c.327 T duplication mutation in exon 7 of *CYBC1*. This mutation results in the insertion of a nucleotide that causes a valine to be replaced with a cysteine at position 110, inducing a sequence frameshift and resulting in a premature stop codon. gnomAD predicts this mutation to be a loss-of-function allele [241], and reports 2 heterozygotes in the South Asian population, meaning incidence of this mutation is likely to rise over time. This patient was then formally diagnosed with CGD5 and is currently awaiting a stem cell transplant.

The unusual course of disease of patients with CGD5, including the unusual plethora of infections including *Legionella* and *Mycobacterium Tuberculosis* and abnormal autoinflammation such as uveitis, demonstrate that CGD5 is somewhat different to CGD1-4. It is important to understand to what extent CGD5 is different from CGD1-4 as this may inform future treatment options and potentially patient outcomes.

This chapter will focus on the role of EROS in human CD4+ cells. First it will focus on describing and validating the newly identified pathogenic EROS mutation. It will then describe the development of a CRISPR-mediated protocol to delete EROS from human CD4+ T cells and subsequent characterisation and functional assessment of the EROS-deficient human CD4+ T cells.

Hypotheses

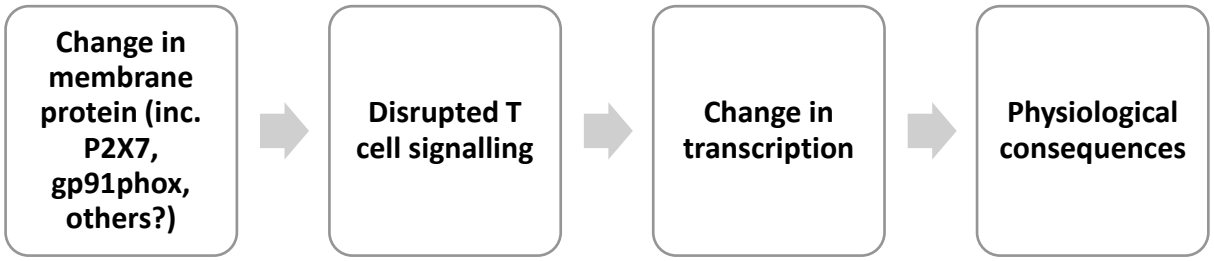

This chapter will address the following parts of my hypothesis:

-The role of EROS is conserved between human and mouse cells

-Loss of EROS causes the downregulation of gp91*phox* and P2X7 in human CD4+ T cells

-Loss of EROS affects gene transcription in human CD4+ T cells

-Loss of EROS disrupts P2X7-driven physiological processes in human CD4+ T cells

Results

To confirm the suspected causative mutation in the EROS gene of the patient, Sanger sequencing was performed. DNA from both the patient and an unrelated healthy control was extracted from whole blood, subjected to PCR to amplify the region of interest and submitted for sequencing. Alignment analysis revealed an additional T base pair inserted into the EROS gene of the patient, but not the healthy control (figure 6.1), which causes a frameshift mutation.

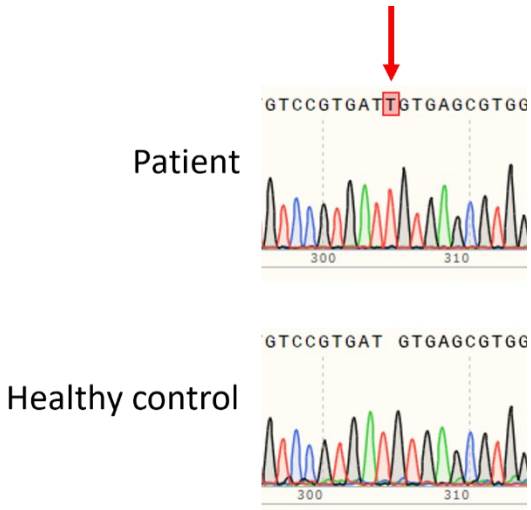

Figure 6.1: EROS patient causative mutation due to additional inserted T in exon 7

DNA was extracted from whole blood from the patient and an unrelated healthy control and subjected to Sanger sequencing. Red arrow indicates additional base pair. Alignments performed using Snapgene.

However, due to the limited amount of patient material, further experiments to characterise the mutation had to be performed *in vitro*. Once the causative patient mutation was confirmed, Dr Talat Malik (Imperial College London) kindly performed site directed mutagenesis to insert the additional T base pair into EROS cDNA, to produce a mutant EROS cDNA with the patient's specific EROS c.327Tdup mutation (referred to as mutant EROS hereafter). This mutant EROS cDNA was transfected into the HEK293 cell line at varying concentrations, with normal EROS as a positive control. Western blots showed that high concentrations of mutant EROS cDNA failed to produce EROS protein upon transfection, unlike normal EROS (figure 6.2A). However, qPCR analysis showed that gene expression of EROS at multiple exon junctions was equivalent between mutant and normal EROS transfections (figure 6.2B). This demonstrates that the mutant allele was efficiently transfected into the HEK293 cells. Ultimately, this suggests that the patient's mutation affects the stability of the EROS protein rather than transcription of the EROS gene.

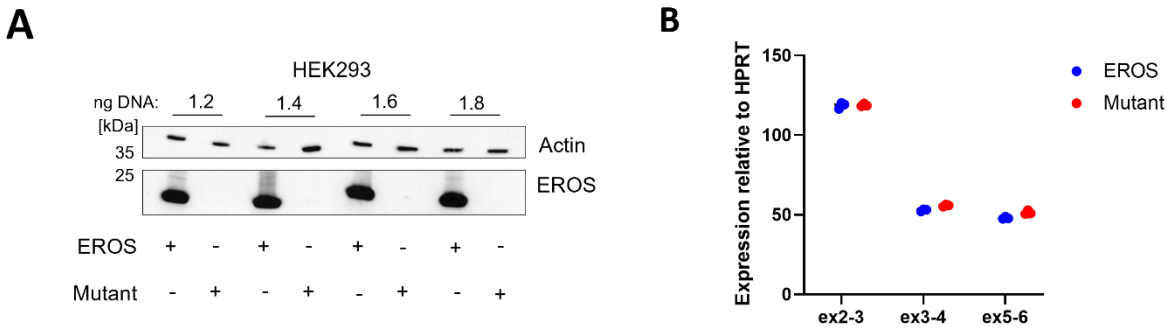

Figure 6.2: Patient mutation affects the stability of the EROS protein but not its transcription

HEK293 cell lines were transfected with varying concentrations of normal EROS cDNA and EROS cDNA containing the patient c.327Tdup mutation. EROS expression was measured by (A) western blot to determine protein expression and (B) qPCR to determine EROS gene expression at several exon junctions. HPRT used as housekeeping gene. Each point represents a technical repeat. Actin used as loading control. Representative of n=3 independent experiments.

Randzavola, Mortimer *et al.,* (2021) performed co-transfection experiments and showed that EROS can increase the abundance of gp91*phox.* Therefore, co-transfection experiments were performed to determine whether the mutant EROS can increase gp91*phox* expression. Normal or mutant EROS cDNA was transfected with gp91*phox* cDNA into HEK293 cells and gp91*phox* and EROS protein expression was measured by western blot. As expected, normal EROS co-transfected with gp91*phox* increased the expression of the 58kDa precursor gp91*phox* compared to when it was transfected alone (figure 6.3). However, when mutant EROS was co-transfected with gp91*phox* there was little gp91*phox* expression, demonstrating the inability of the mutant EROS to stabilise gp91*phox* expression.

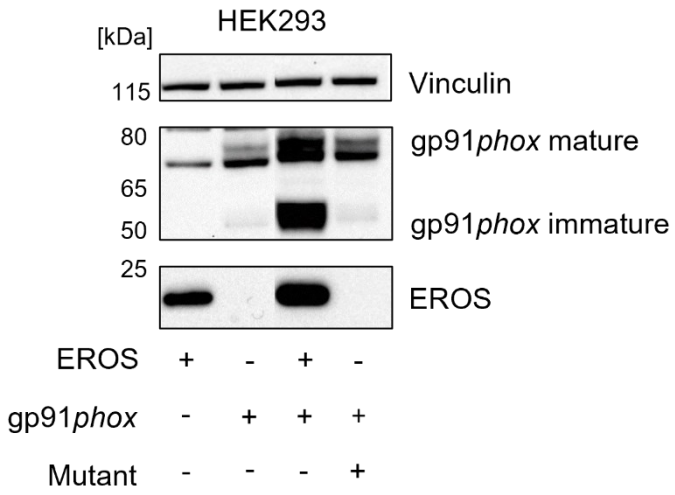

Figure 6.3: Mutant EROS is unable to stabilise gp91*phox* protein expression

HEK293 cells were transfected with gp91*phox* and either normal or mutant c.327Tdup EROS cDNA, and protein expression was measured by western blot. Actin used as loading control. Representative of n=3 experiments.

The EROS antibody used in the western blot in figure 6.3 recognises the C terminus of the EROS protein [242]. As the EROS mRNA is still produced (figure 6.2B), the resultant truncated protein is likely to be misfolded. This means that the EROS protein may still be present, in a mutated form, but the antibody binding epitope may be inaccessible or destroyed. Therefore, to avoid any issues with antibody binding, a GFP-tagged mutant EROS cDNA was developed to prevent complete dependence on antibody detection methods such as western blotting. Using a GFP-tagged EROS construct, Eve Coomber (WTSI) kindly inserted the patient mutation by site directed mutagenesis. This GFP-tagged mutant EROS and GFP-tagged normal EROS was transfected into HEK293 cells and GFP was measured by flow cytometry. As expected, normal EROS had high GFP expression whereas mutant EROS had very little GFP expression (figure 6.4). This confirms the results from the earlier western blots that the patient mutation fails to express a stable EROS protein.

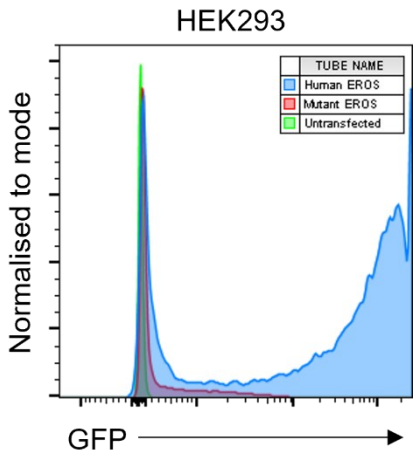

Figure 6.4: Mutant EROS fails to produce a stable EROS protein

HEK293 cells were transfected with either normal GFP-tagged EROS or mutant c.327Tdup GFP-tagged EROS cDNA, and GFP expression was measured by flow cytometry. Representative of n=3 experiments.

Next, the EROS deficient PLB985 cell line [165] was utilised to determine whether the mutant EROS could reconstitute EROS or subsequent gp91*phox* expression in a haematopoietic cell line that has complete absence of both. Nucleofection methods were used as they provide superior transfection efficiency above the lipofectamine transfection methods used previously [243]. GFP-tagged mutant and normal EROS were nucleofected into the EROS deficient PLB985 cells and GFP expression was measured by flow cytometry. There was less GFP expression in the mutant EROS nucleofected condition compared to the normal EROS nucleofected condition (figure 6.5). However, even the normal EROS positive control failed to reconstitute EROS expression to a high level in the EROS deficient PLB985 cells, shown by the low GFP expression (figure 6.5). This suggests that nucleofection is not an effective method for editing PLB985 cells.

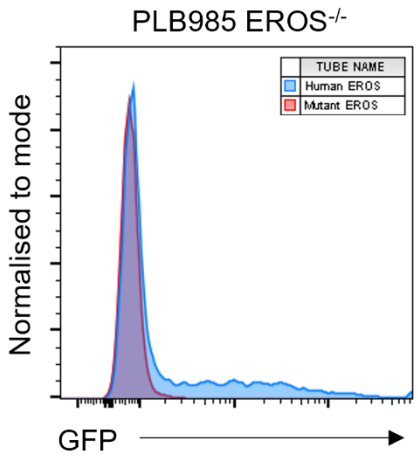

Figure 6.5: Nucleofection methods fail to reconstitute EROS expression in EROS deficient PLB985 cells

GFP-tagged normal EROS and mutant c.327Tdup EROS were nucleofected into an EROS deficient PLB985 cell line and GFP expression was measured by flow cytometry. Representative of n=3 experiments.

As nucleofection methods were unsuccessful in reconstituting EROS expression in PLB985 cells, next lentiviral transduction methods were used as an alternative method of gene transfer. Lentiviral transduction has previously been found to have higher efficiency than nucleofection methods, and better cell viability [244]. Eve Coomber (WTSI) kindly cloned the GFP-tagged mutant EROS into a lentiviral backbone vector. Then the HEK293T cell line was transfected with the lentiviral constructs, virus was harvested and concentrated, then used to transduce EROS deficient PLB985 cells. Figure 6.6A illustrates the ideal reconstitution of EROS and gp91*phox* expression following normal EROS transduction. HEK293T cells transfected with normal EROS had high GFP expression (figure 6.6B), whereas mutant EROS produced little to no GFP expression, similar to figure 6.4. EROS deficient PLB985 cells transduced with normal EROS resulted in high GFP expression, whereas mutant EROS did not have any GFP expression (figure 6.6C). As expected, EROS deficient PLB985 cells transduced with normal EROS resulted in the reconstitution of gp91*phox* expression, whereas mutant EROS failed to reconstitute gp91*phox* expression (figure 6.6D).

In conclusion, these data prove that the c.327Tdup homozygous mutation in EROS is pathogenic. Cells transfected or transduced with this mutated form of EROS fail to express EROS or gp91*phox* protein, suggesting that this loss-of-function mutation is the causative factor of the EROS patient's CGD5 diagnosis.

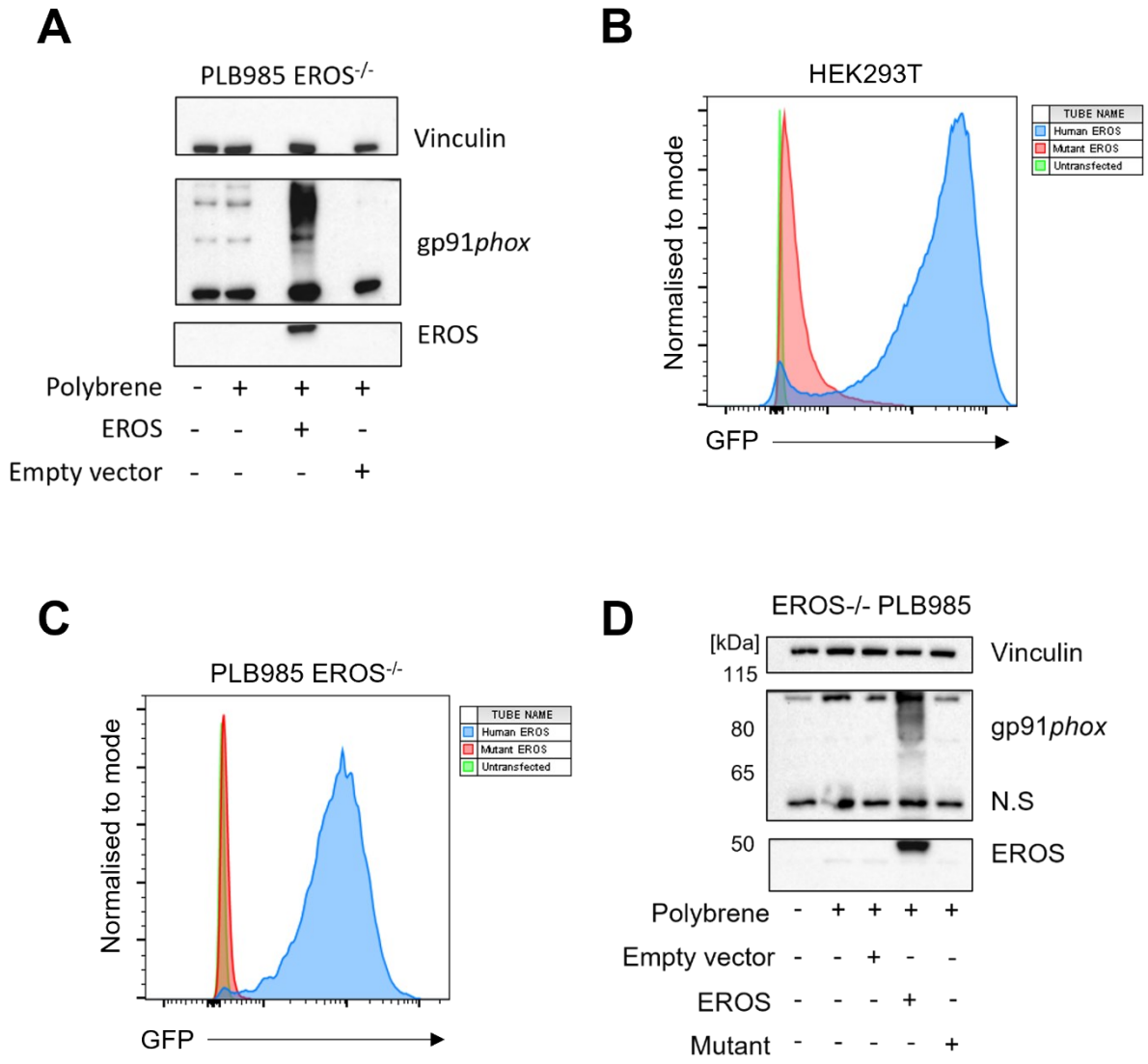

Figure 6.6: Normal EROS but not mutant EROS expression can be reconstituted in EROS deficient PLB985 cells

Western blot showing EROS deficient PLB985 cells were transduced with lentivirus containing normal EROS cDNA (A). GFP-tagged empty vector was used as a control. HEK293T cells were transfected with normal or mutant EROS GFP-tagged cDNA and GFP expression was measured by flow cytometry (B). Resulting virus was used to transduce EROS deficient PLB985 cells. GFP expression was measured by flow cytometry (C) and western blots were performed to assess EROS and gp91*phox* expression (D). Vinculin used as loading control. Data representative of n=3 experiments. Lentiviral experiments were performed by Esme Nichols.

Although the EROS patient mutation described above provides a new understanding of the stability of EROS and confirms its role in regulating gp91*phox* expression, using patient cells has many disadvantages (table 6.1). For example, there have only been 10 confirmed EROS patients, all of whom were very ill with a multitude of opportunistic infections and inflammatory diseases and receiving a variety of medications and immunosuppressants. For these reasons, it is difficult to ascertain what is intrinsic to the lack of EROS and what is secondary to the wider effects of illness or medication when evaluating the patient's T cells. This is especially true of CGD where immunosuppression is a mainstay of therapy, although it is a primary immunodeficiency. Additionally, stem cell transplants are a common treatment for CGD meaning the patient samples are available for a limited period of time. However, T cells in which EROS has been deleted by CRISPR provide an infinite amount of experimental material, with the added bonus that as they have been derived from healthy donors, so there are no complications from illnesses or abnormal TCR repertoires.

Table 6.1: Advantages of using cells with EROS deleted by CRISPR compared to patient cells.

Advantages of CRISPR-edited cells	Disadvantages of patient cells
Infinite resource	Few patients
Normal TCR repertoire	Medication
No illness complications	Illnesses

Therefore, as CRISPR methods provide a potentially unlimited source of human EROS deficient CD4+ T cells without additional complications, a CRISPR method to delete EROS from CD4+ T cells was developed (figure 6.7). PBMC were isolated from leucocyte cones from healthy donors. CD4+ T cells were isolated from PBMC by negative selection and stimulated with anti-CD3/anti-CD28 magnetic beads for 72 hours. Then the activated cells were subjected to nucleofection using single guide RNAs kindly designed by Alasdair Russell's team (CRUK; see table 2.13 for details), and Cas9. Nucleofected cells were rested, then expanded with IL-2 for 7-14 days, depending on number of cells required. EROS deletion was confirmed by DNA sequencing and western blot.

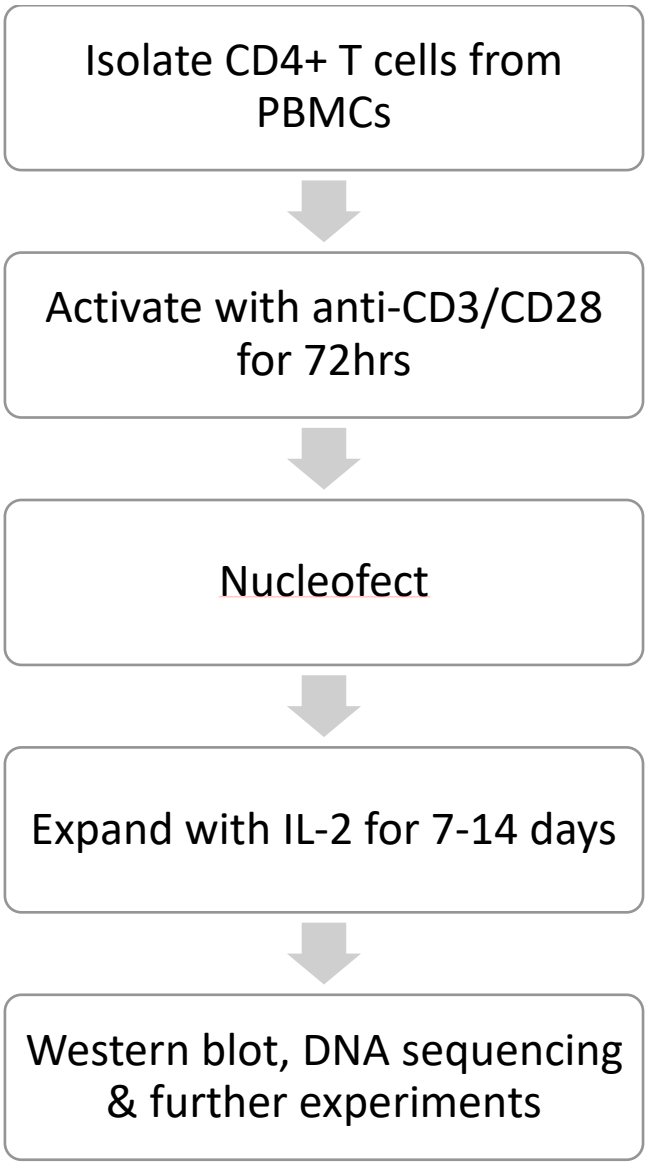

Figure 6.7: Overview of CRISPR protocol to delete EROS from CD4+ T cells

Whole human CD4+ T cells were isolated from PBMCs, and stimulated with anti-CD3/anti-CD28 Dynabeads for 72 hours. Activated cells were nucleofected with Cas9 and single guide RNA in a 1:3 ratio. Nucleofected cells were expanded with IL-2 for 7-14 days. EROS deletion was confirmed by DNA sequencing and western blot, and cells were used in further experiments.

The first stage of CRISPR optimisation consisted of experiments to test which single guide RNA (sgRNA) provided the best deletion of EROS. Three sgRNA were designed and tested, either alone or in combinations, and then subjected to western blot (figure 6.8A) and Sanger sequencing. sgRNA targeting exon 2 provided the best knockout efficiency by protein and DNA, according to Inference for CRISPR Edits (ICE) analysis (figure 6.8A-B). ICE analysis is a software tool provided by Synthego to determine knockout efficiency using the Sanger sequencing results. ICE analysis of sgRNA targeting exon 2 gave an 80% knockout efficiency (figure 6.8B). However, combining sgRNA targeting exon 2 with sgRNA targeting other exons did not further improve knockout efficiency, therefore only sgRNA targeting exon 2 was used in further experiments to minimise the chance of off-target effects. sgRNA targeting exon 3 failed to induce any EROS deletion and EROS protein expression remained high (figure 6.8A).

The next stage of optimisation involved testing different cell numbers per reaction and increasing the molar ratio of Cas9:sgRNA in an attempt to further increase knockout efficiency. However, increasing the number of cells in the reaction to $5x10^5$ decreased knockout efficiency and an EROS band was visible by western blot (figure 6.8C). Additionally, increasing the molar ratio of Cas9:sgRNA to 1:4 also did not further improve knockout efficiency (figure 6.8C). Therefore, in future experiments sgRNA targeting exon 2 using a 1:3 molar ratio of Cas9:sgRNA in a reaction of $2x10^5$ cells was used. Even when a high concentration of protein is loaded on the western blot, there is no EROS band (figure 6.8D), demonstrating the high level of EROS deletion in the human CD4+ T cells.

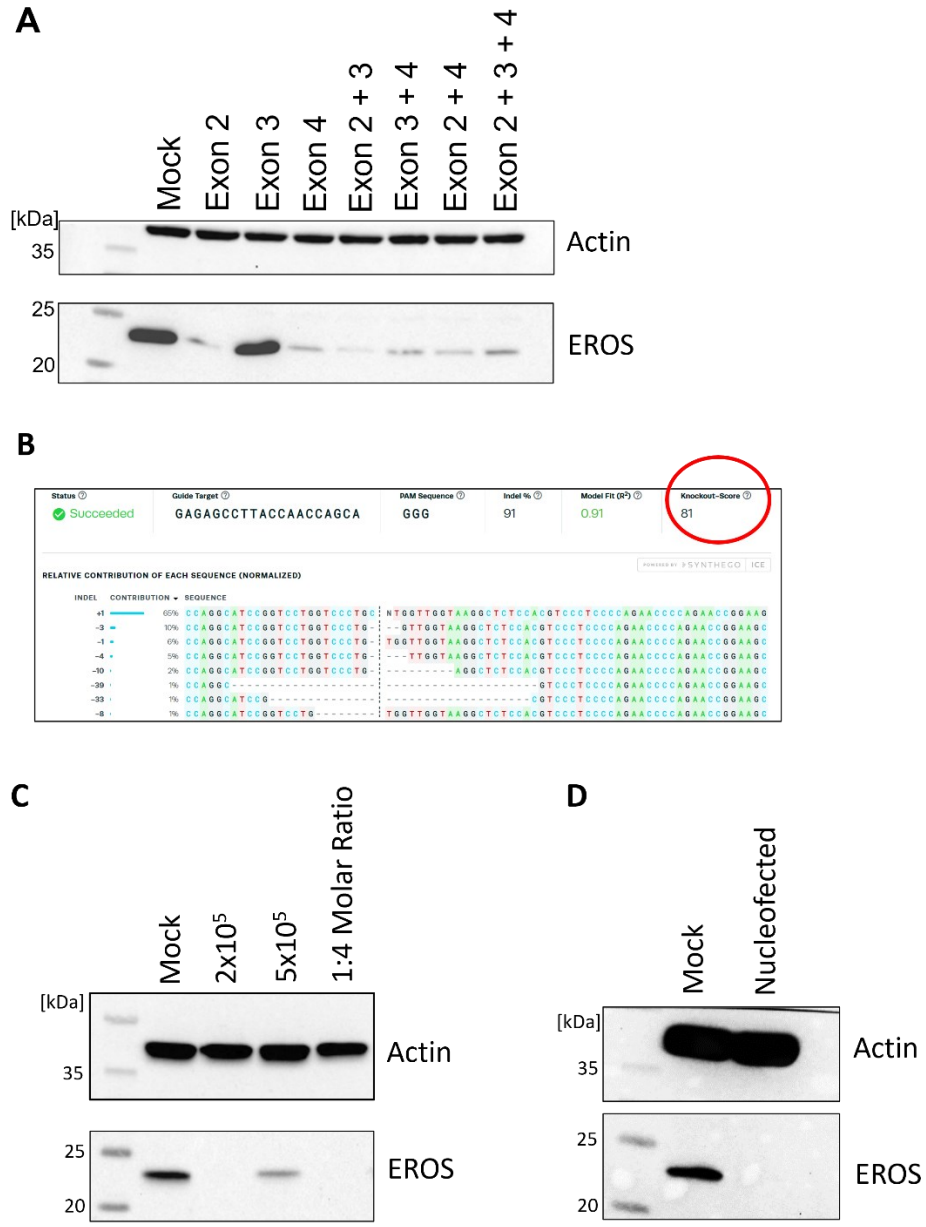

Figure 6.8: Guide RNA targeting exon 2 in a reaction with 2x10^5 cells provides the most efficient EROS deletion

Human CD4+ T cells were nucleofected with single guide RNAs targeting different exons. EROS knockout was determined by (A) western blot and (B) ICE analysis following Sanger sequencing. Knockout score indicated with red circle. Further optimisation consisted of testing 2x10^5-5x10^5 cells per reaction and a 1:4 molar ratio of Cas9:sgRNA, and EROS knockout was determined by western blot (C). sgRNA targeting exon 2 using a 1:3 molar ratio of Cas9:sgRNA in a reaction of 2x10^5 cells was selected and 50µg protein loaded on the western blot (D). Actin used as loading control.

As EROS regulates the expression of gp91*phox* and P2X7 in mouse CD4+ T cells (chapter 3), mouse macrophages and neutrophils [34] and in human EROS deficient cell lines [164], the next step was to evaluate gp91*phox* and P2X7 expression in the nucleofected EROS deleted human CD4+ T cells. Flow cytometry was performed using the gp91*phox*-p22*phox* (clone: 7D5) flow antibody [245]. Analysis found that gp91*phox* expression was reduced in the nucleofected EROS CD4+ T cells compared to mock nucleofected control CD4+ T cells (figure 6.9A). P2X7 expression was measured by western blot, which found that P2X7 was not expressed in the nucleofected CD4+ T cells compared to mock nucleofected CD4+ T cells (figure 6.9B). Together, the loss of gp91*phox* and P2X7 expression confirm the loss of functional EROS expression in the nucleofected CD4+ T cells.

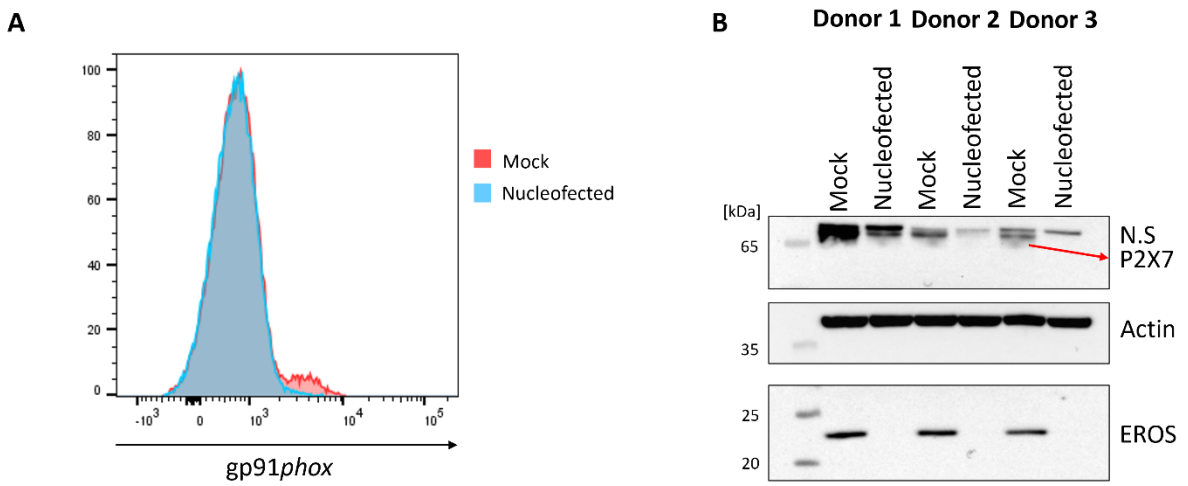

Figure 6.9: Loss of gp91*phox* and P2X7 in nucleofected EROS-deleted human CD4+ T cells

(A) gp91*phox* expression was measured by flow cytometry in nucleofected cells in which EROS has been deleted by CRISPR (blue), compared to mock nucleofected control CD4+ T cells (red). (B) P2X7 expression was measured by western blot in mock and nucleofected cells from 3 different donors. Actin used as loading control. Arrow denotes P2X7 band. N.S = non-specific band.

Next, functional experiments were performed on the EROS-deleted human CD4+ T cells. In section 3.7 it was found that loss of EROS abrogates P2X7 induced surface marker shedding in mouse CD4+ T cells. Typically, activation of P2X7 signalling by its ligand ATP activates the metalloproteinases ADAM10/17 and triggers the shedding of key surface molecules CD62L and CD27 [126,153], but less shedding occurred in EROS-/- mouse CD4+ T cells (section 3.7). Therefore, surface marker shedding was investigated in EROS-deleted human CD4+ T cells. Nucleofected and mock nucleofected control cells were stimulated with ATP and surface marker shedding was measured by flow cytometry. Less shedding of CD27 and CD62L occurred following ATP addition in nucleofected cells compared to mock nucleofected (figure 6.10A). Interestingly, the nucleofected cells expressed significantly higher levels of CD27 at baseline than mock nucleofected cells (figure 6.10B), supporting the results found in section 3.7 and showing further conservation between human and mouse. Overall, the results suggest the role of EROS in regulating P2X7 expression and subsequent signalling is conserved between mouse and human.

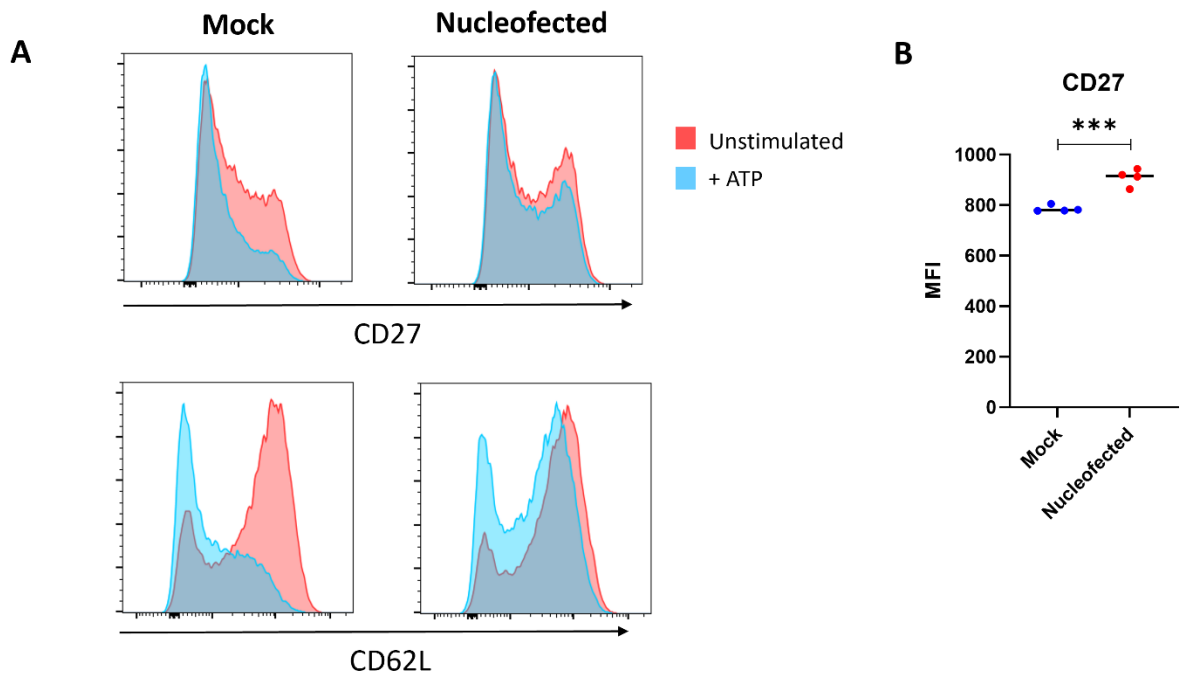

Figure 6.10: Less surface marker shedding occurs in EROS-deleted nucleofected human CD4+ T cells

Mock nucleofected and EROS-deleted nucleofected human CD4+ T cells were stimulated with ATP for 30 minutes. (A) CD27 and CD62L expression were measured by flow cytometry. (B) Graph showing Mean Fluorescence Intensity (MFI) of CD27 expression at baseline in mock nucleofected and EROS-deleted nucleofected CD4+ T cells. Each dot represents a technical repeat. Data representative of n=2. Data represented as mean ± SEM. Statistical significance was calculated using an unpaired two-tailed Student's *t*-test. *** $p<0.001$.

As it appeared the role of EROS is conserved between mouse and human, another striking phenotypic consequence of EROS deficiency in mouse CD4+ T cells is excess secretion of certain cytokines upon stimulation (chapter 4). Therefore, cytokine secretion from the human CRISPR deleted CD4+ T cells was measured. The cells were stimulated with anti-CD3/anti-CD28 for 48-72 hours, and supernatants were harvested for ELISA. In all 3 donors there was greater IL-4 secretion at both timepoints in the EROS-deleted nucleofected cells, compared to the same donors mock nucleofected control cells (Figure 6.11A), supporting the mouse data in chapter 4. In all 3 donors there was less IFNγ secretion at both timepoints in the EROS-deleted nucleofected cells, compared to the same donors mock nucleofected control cells (Figure 6.11B), differing from the mouse data in chapter 4. Overall, these data support the mouse data in chapter 4, that EROS is involved in Th2 skewing.

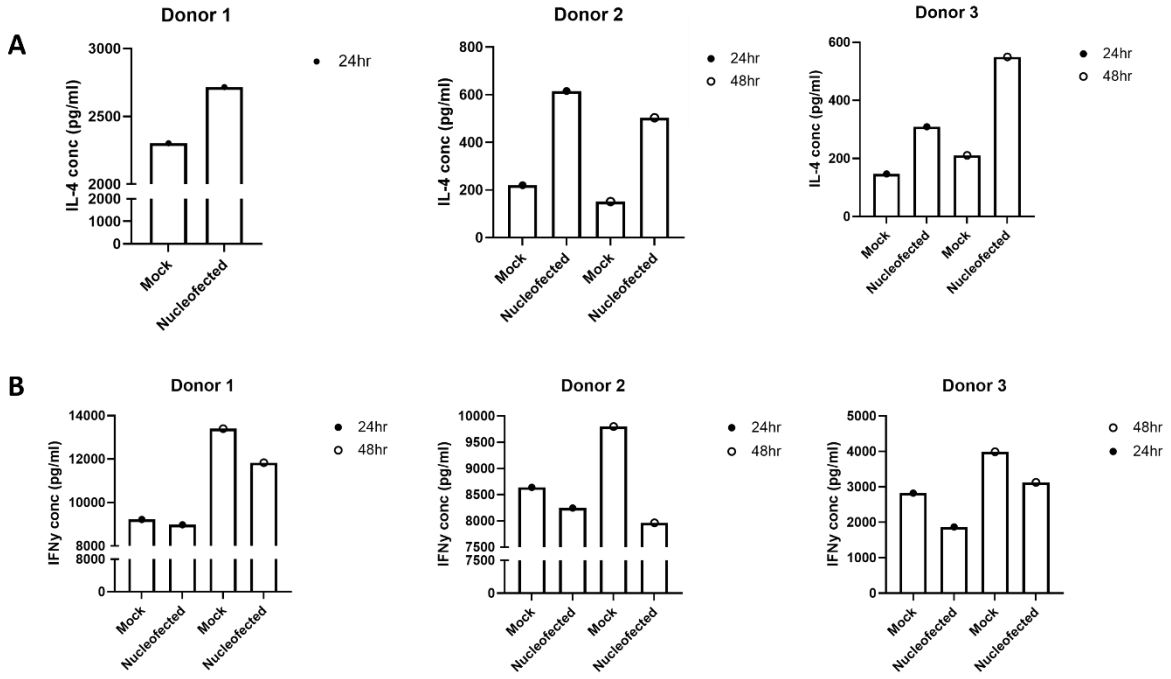

Figure 6.11: More IL-4 is secreted from EROS-deleted human nucleofected CD4+ T cells

EROS-deleted nucleofected and mock nucleofected control cells were stimulated with immobilised anti-CD3 and soluble CD28 for 24-48 hours, and supernatants were harvested for (A) IL-4 and (B) IFNγ ELISA analysis.

Following on from the excess IL-4 secretion by EROS-/- human CD4+ T cells (figure 6.11), next the gene expression of *GATA3* and *Tbet* were examined by qPCR of nucleofected and mock transfected control cells. There was no difference in *GATA3* or *Tbet* expression between mock or nucleofected human CD4+ T cells (figure 6.12A-B). This was surprising as gene expression analysis found that *Gata3* was upregulated in EROS-/- and P2X7 inhibited mouse CD4+ T cells (chapter 4).

MID1 expression was also measured as this was downregulated in EROS-/- mouse CD4+ T cells (chapter 4). However, there was no difference in *MID1* expression between mock and nucleofected human CD4+ T cells (figure 6.12C).

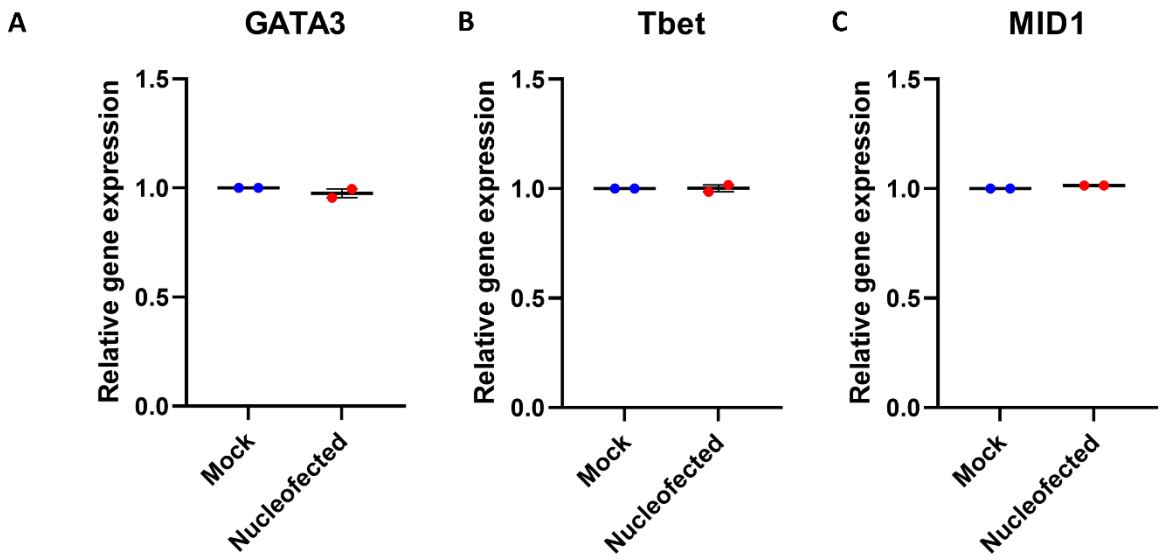

Figure 6.12: No difference in GATA3, Tbet or MID1 in EROS-/- human CD4+ T cells

EROS-deleted nucleofected and mock nucleofected control cells were harvested for qPCR analysis to measure the gene expression of (A) GATA3 (B) Tbet and (C) MID1. HPRT used as housekeeping gene. Each point represents a separate donor. Data represented as mean ± SEM.

Despite the lack of difference in transcription factor gene expression, levels of phosphorylated STAT6 were measured, in a similar manner to the mouse EROS deficient CD4+ T cells (chapter 4). Mock and nucleofected CD4+ T cells were stimulated with anti-CD3/CD28 for 72 hours and phosphorylated STAT6 was measured by intracellular flow cytometry. There was no difference in STAT6 phosphorylation between mock and nucleofected EROS-deficient conditions (figure 6.13B), similar to results seen in mouse experiments (chapter 4).

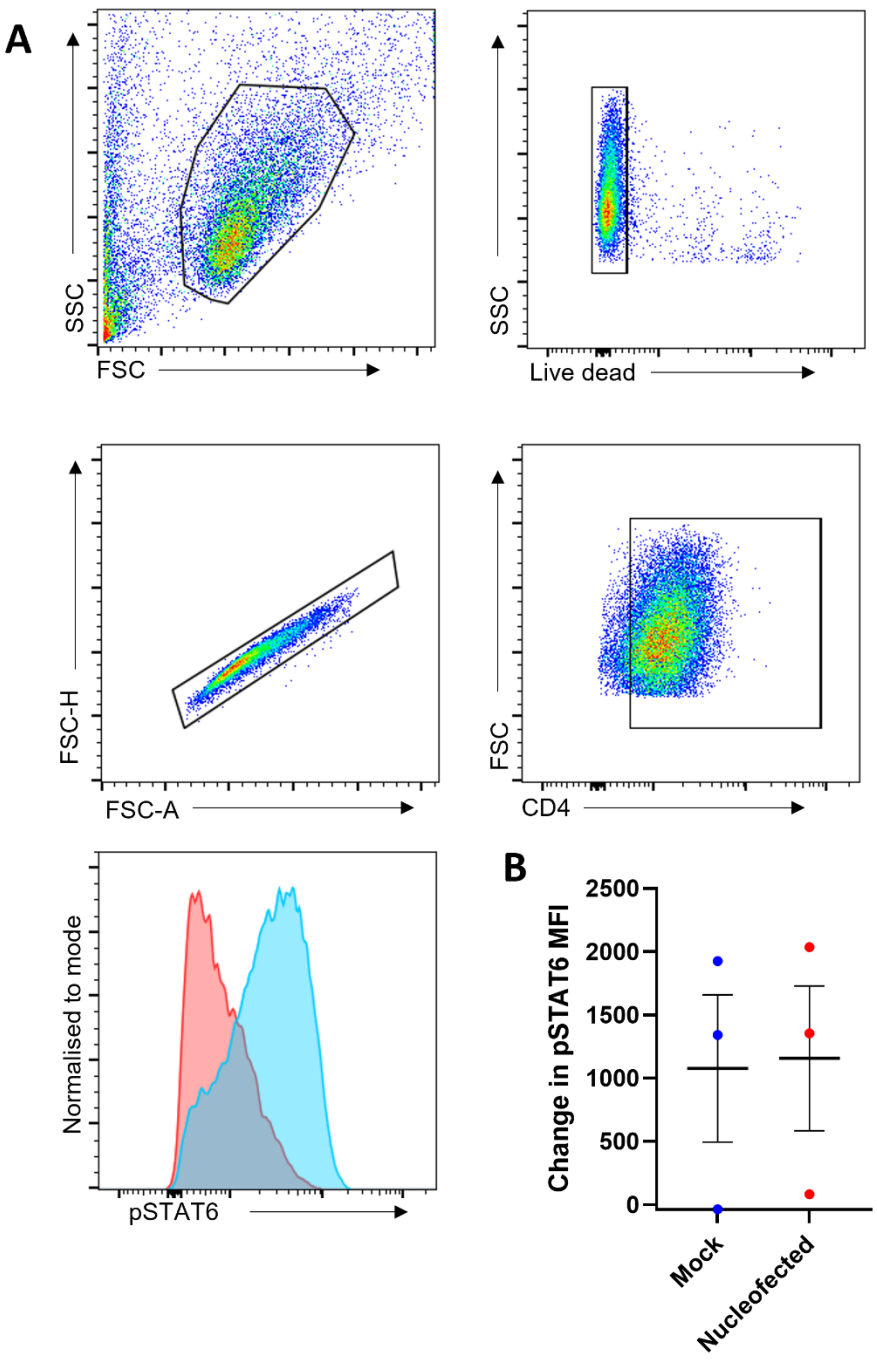

Figure 6.13: No difference in STAT6 phosphorylation in EROS-deleted nucleofected CD4+ T cells

Mock and nucleofected EROS-deleted human CD4+ T cells were polyclonally stimulated with anti-CD3/CD28 for 72 hours and harvested for intracellular flow cytometry. (A) representative gating strategy. (B) Change in phosphorylated STAT6 from baseline. Each dot represents an individual donor. Data represented as mean ± SEM.

Discussion

Mutant EROS fails to upregulate gp91*phox* expression

EROS regulates the expression of gp91*phox* in macrophages, neutrophils [34,164] and CD4+ T cells (chapter 3). However, the latest EROS patient has a mutation consisting of an additional T basepair inserted into exon 7 of the EROS gene (figure 6.1), abrogating the protein expression, but not gene expression, of EROS (figure 6.2A-B). This absence of EROS results in a lack of gp91*phox* expression (figure 6.3), which is ultimately the causative factor for the patient's CGD. This is only the 10th described case of CGD that has arisen as a result of altered stability of gp91*phox.*

Mutant EROS fails to reconstitute EROS expression

It has previously been shown that transduction of normal EROS into an EROS-deficient PLB985 cell line reconstitutes the expression of EROS and subsequently gp91*phox* [165]. However, transduction of the mutant EROS into the EROS-deficient PLB985 cell line is unable to reconstitute EROS or gp91*phox* expression (figure 6.6), confirming that this mutation disrupts the expression of two members of the phagocyte NADPH oxidase complex. Although this patient has a different mutation to the first described EROS patient [165], the lack of EROS and subsequently lack of gp91*phox* expression confirms both the role of EROS in human immune cells, and the importance of EROS as a regulator of gp91*phox*, ensuring proper functioning of the phagocyte NADPH oxidase.

CRISPR deleted cells are advantageous over patient derived cells

The plight of the EROS patients highlights one of the difficulties of using patient derived cells; the patients are often very ill, suffering with recurrent infections as they are more susceptible to opportunistic bacteria, meaning that they are receiving a multitude of medications. This, undoubtedly, has an effect on their immune cells and may affect their T cell receptor repertoire. However, CRISPR edited T cells are derived from healthy donors and can provide an unlimited source of experimental material.

EROS can be deleted from human CD4+ T cells using CRISPR methods

A CRISPR protocol to delete EROS from human CD4+ T cells was developed. This entailed optimising guide RNA choice and concentration, cell numbers (figure 6.8A-C) and

nucleofector pulse (data not shown). A protocol was developed that deleted EROS up to 80% at the gene level, resulting in a complete absence of EROS protein expression (figure 6.8 B&D). EROS deletion was further confirmed by the absence of the 2 proteins it regulates, gp91*phox* and P2X7 (figure 6.9). This shows the EROS can be successfully knocked out from human CD4+ T cells, and confirms that EROS regulates the expression of gp91*phox* and P2X7 in human CD4+ T cells.

Human EROS deficiency is analogous to mouse EROS deficiency

EROS deficient mouse CD4+ T cells secrete excess amounts of IL-4 upon anti-CD3/CD28 polyclonal stimulation and shed less CD27 and CD62L following ATP stimulation (chapter 3). These experiments were replicated using the human EROS deficient CD4+ T cells and found similar results. Less ATP-driven shedding of CD27 and CD62L occurs in human EROS deficient CD4+ T cells compared to control CD4+ T cells (figure 6.10A), just like in mouse EROS deficient CD4+ T cells (chapter 3). Additionally, greater amounts of IL-4 are secreted from human EROS deficient CD4+ T cells (figure 6.11A), comparative to mouse CD4+ T cells (chapter 4).

However, less IFNγ is secreted from human EROS deficient CD4+ T cells upon polyclonal stimulation (figure 6.11B), which is different to mouse EROS deficient CD4+ T cells that secrete greater amounts of IFNγ compared to wildtype control CD4+ T cells (chapter 4). A reason for this difference may be due to the fact that not only do the human CD4+ T cells undergo a stressful nucleofection procedure, they are also stimulated with anti-CD3/CD28 twice, once prior to nucleofection and then restimulated after expansion of the nucleofected cells, at which point the supernatants are collected. Therefore, the human cells may be more exhausted than the mouse cells, which could be confirmed by flow cytometric analysis of exhaustion markers and measuring IL-2 secretion [246]. Another difference between mouse and human EROS deficient CD4+ T cells is that *Gata3* is upregulated in mouse cells (chapter 4), but not human (figure 6.12A). However, an explanation could be that as GATA3 is a crucial transcription factor involved in T cell development [225], it may have developmentally regulated expression and is therefore unaffected by post-developmental gene editing.

Another similarity of note between the mouse and human EROS deficient CD4+ T cells is the lack of difference in STAT6 phosphorylation upon polyclonal stimulation (chapter 4 and figure 6.13B). This further implies that the Th2 polarisation induced by EROS deficiency is STAT6-independent in both mouse and human.

CD27 is upregulated in EROS deficient cells

Another interesting similarity between human and mouse EROS deficient CD4+ T cells is that they both upregulate CD27 expression (chapter 3 and figure 6.10B), likely due to the loss of P2X7 (chapter 5). CD27 is a member of the tumour necrosis factor (TNF) receptor super family. It is expressed on T cells, B cells and NK cells [247] and can be upregulated following TCR stimulation [248]. Binding of CD27 to its ligand CD70 induces the recruitment of TRAF2 and TRAF5, which can activate either the NF-κB or JNK signalling pathways [249]. Early studies found that CD27 signalling was involved in both the primary and memory T cell responses, and CD27-/- mice had impaired CD4+ T cell responses to influenza infection [178]. Interestingly, EROS-/- mice, with upregulated CD27 expression, have better survival rates following influenza infection [164].

CD27 signalling has also been associated with tissue autoimmunity. Remedios *et al.,* (2019) found enhanced skin inflammation and increased numbers of IFNγ secreting T cells in CD27-sufficient mice compared to CD27-deficient mice. They state that the expression of CD27 promotes the survival of autoreactive T cells by suppressing cell-extrinsic apoptosis [250]. This work is supported by other studies that found blockade of CD27 signalling restrains the development of experimental colitis and allergic lung inflammation [251,252]. Therefore, this suggests that the increased CD27 expression may be responsible for the unusual autoimmunity seen in EROS deficient patients.

Overall, pathogenic mutations in EROS can affect the stability of gp91*phox,* and cause CGD5 in humans. EROS can be knocked out of human CD4+ T cells to provide a representative model of human EROS deficiency, that is also analogous to mouse EROS deficiency.

Chapter 7: Discussion

EROS was first described as a regulator of gp91*phox* and P2X7 protein expression in neutrophils and macrophages in 2017 [34]. Shortly after in 2018, the first cases of CGD caused by EROS deficiency (CGD5) were identified in humans [165,166]. The fact that EROS is highly expressed in both mouse and human CD4+ T cells and that EROS deficient CGD5 patients experienced unusual autoimmunity and autoinflammation suggested that EROS deficiency may result in abnormalities in the adaptive immune cells. These points formed the underlying basis for this project.

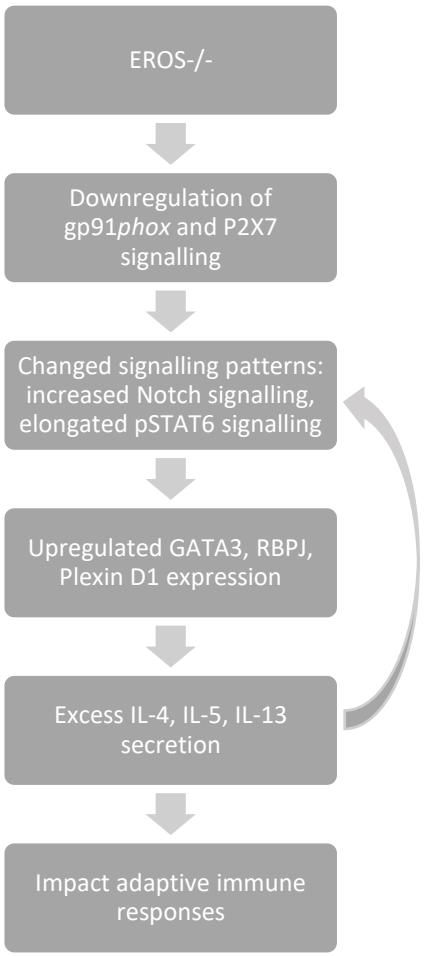

Figure 7.1: The role of EROS in T cell biology. EROS deficiency causes the loss of gp91*phox* and P2X7 signalling. This results in increased Notch signalling and prolonged pSTAT6 signalling causing an upregulation of GATA3, RBPJ and Plexin D1. This causes excess secretion of IL-4, IL-5 and IL-13, which can further propagate T cell signalling and impact adaptive immune responses.

Arguably the most important finding of this project is the impact of EROS deficiency on T cell biology; loss of EROS results in the polarisation of a Th2 response characterised by 10x fold greater IL-4, IL-5 and IL-13 secretion (figure 4.1A-C) and upregulation of *Gata3*, *Rbpj* and *Plexin d1* (figure 4.2A).

This phenotype of EROS deficiency is a combination of loss of P2X7 and gp91*phox* signalling in the CD4+ T cells (figure 3.1-3.3). The loss of gp91*phox* causes upregulation of important signalling molecules CD38 and CD73 (figure 4.8 A,C) and also likely causes the 2x fold increase in IFNγ secretion from EROS deficient CD4+ T cells (figure 4.1D). However, it's the loss of P2X7 that drives the abnormal cytokine secretion from EROS deficient CD4+ T cells. P2X7 deficient or inhibited CD4+ T cells secrete excess amounts of IL-4 (figure 4.12A-B, 4.14), and upregulate *Gata3* (figure 4.13), recapitulating EROS deficiency. Additionally, the increased population of TRM in the lungs of EROS deficient mice (figure 5.2B-D) are due to loss of P2X7 signalling, based on previous literature [160] and that there was increased numbers of TRM in P2X7 deficient mouse lungs (figure 5.5E), but no difference in gp91*phox* deficient mouse lungs (figure 5.5B). The increase in ILC2 cells in EROS deficient mouse lungs (figure 5.6B) is also likely due to the loss of P2X7, owing to their dependence upon GATA3 expression and Th2 cytokines, and lack of difference in gp91*phox* deficient lungs (figure 5.6C). However, this would need to be confirmed in P2X7 deficient mouse lungs. This involvement of P2X7 signalling in Th2 skewing is not previously known, and may have important consequences for adaptive immunity.

The impacts of dysregulated P2X1 and P2X4 expression caused by loss of EROS expression (figure 3.5-3.6) was not further described in relation to T cell biology in this project. Woehrle *et al.,* (2010) found that P2X1 and P2X4 traffic to the immunological synapse to propagate TCR signalling [152], therefore some of the EROS deficient phenotype may be due to changes in P2X1 and P2X4 expression. This could be further explored by using P2X1 or P2X4 deficient CD4+ T cells in the *in vitro* stimulation system and measuring cytokine secretion.

Despite Th2 skewing and increased numbers of ILC2 and TRM cells, EROS deficiency does not confer any protection against *H. polygyrus* infections (figure 5.9). This is likely due to EROS deficient mice having defective IgG1 production (figure 5.8), which is critical for eradicating *H. polygyrus* infections [239]. As IgE is also essential for anti-helminth immunity [253], it may be worthwhile assessing IgE production *in vivo*. It may also be interesting to infect

P2X7 deficient mice with *H. polygyrus*, to determine whether the *in vivo* phenotype aligns with EROS deficiency.

Human EROS deficiency mostly recapitulates mouse EROS deficiency. Human EROS deficient CD4+ T cells have downregulated gp91*phox* and P2X7 expression (figure 6.9), increased IL-4 secretion (figure 6.11A) and abnormal surface marker shedding (figure 6.10A). This demonstrates that the mouse model is a representative model of EROS deficiency for experimental studies. Together, the mouse and human data indicate that CGD5 caused by EROS deficiency is different to CGD1-4 caused purely by loss of NADPH oxidase derived ROS signalling. CGD5 EROS patients have unusual autoinflammatory and autoimmunity (described in section 1.4.3 and chapter 6), likely caused by their dysregulated T cell responses. I have demonstrated that EROS deficient CD4+ T cell responses are extremely different to gp91*phox* deficient CD4+ T cell responses, mostly due to the loss of P2X7 signalling. As there are several heterozygotes with the c.327Tdup mutation in EROS means that CGD5 cases are likely to rise, meaning it will be important to quickly identify and diagnose patients, allowing them to receive treatments faster to reduce morbidity and mortality.

A strength of this thesis is that I have delineated the roles of gp91*phox* and P2X7 in EROS deficiency. By doing this, I have taken what is currently known on the role of EROS, gp91*phox* and P2X7 in T cell biology further. Currently, little is known about the impacts of P2X7 signalling on T cell development. Studies have found that P2X7 signalling induces polarisation into Th1 cells in malaria models [146] and conversion into Th17 cells following ATP stimulation [147], but there is a lack of functional data on the importance of P2X7 in a non-infectious context. There is some conflicting data on the impacts of gp91*phox* signalling on T cell development [96,98–100], however this is the first study to perform RNAseq on gp91*phox* deficient CD4+ T cells.

Another strength is that data from the large scale proteomic and transcriptomic studies support each other. Mass spectrometry analysis has shown that EROS consistently regulates a small number of proteins including; gp91*phox*, p22*phox* (secondary to gp91*phox*), P2X7 and Phactr4 in CD4+ T cells (figure 3.1) and macrophages [164]. RNAseq analysis has shown that *CYBC1* expression is consistently downregulated in EROS-/- analyses and MID1

expression is also downregulated in all 3 RNAseq data sets (figure 4.2A, 4.3, 4.10A). The consistency of these datasets highlights the strength in the conclusions drawn from them.

A further strength of this project is that I successfully developed a CRISPR protocol to produce a human model of EROS deficiency. This human model recapitulates what we find in mouse EROS deficient T cells, validating each model and further characterising EROS deficiency in T cells. This means that the role of EROS in T cell biology can be investigated without the need for patient cells, providing both an unlimited source of experimental material and without the disadvantages of patients cells, as discussed in chapter 6 (table 6.1).

A weakness of this thesis is that the signalling mechanism disrupted by EROS deficiency was not confirmed. It is widely accepted that the classical mechanism of Th2 skewing is induced by IL-4 binding to its receptor, STAT6 is phosphorylated, resulting in the transcription of GATA3. Data in this thesis did not find an increase in STAT6 phosphorylation in mouse or human EROS deficiency (figure 4.4D, F, figure 6.13B). It may be that the phospho-flow experiment was performed 72 hours post stimulation and may have missed a key earlier phosphorylation event. Gene set enrichment analysis indicated that early signalling cascades were disrupted in EROS deficient CD4+ T cells (figure 4.2B). Initial optimisation experiments did not detect any changes in pSTAT6 until 72 hours (figure 4.4B-C), so perhaps using alternative techniques used in the literature such as western blotting could detect pSTAT6 at earlier timepoints [195]. However, it may be that instead of overall increased STAT6 phosphorylation levels, EROS deficiency causes increased duration of STAT6 phosphorylation due to slower IL-4Rα turnover (figure 4.7C), which may be causing the Th2 skewing. Alternatively, it could also be argued that the Th2 skewing seen in EROS deficient CD4+ T cells is STAT6 independent. RNAseq analysis found upregulation of the Notch signalling molecules RBPJ and Plexin D1 (figure 4.2A), and Notch signalling is becoming widely accepted as an alternative method of Th2 skewing [186,202,254,255].

Future work

Confirm disrupted signalling mechanism in EROS deficiency

EROS deficiency results in excess IL-4, IL-5 and IL-13 secretion (figure 4.1A-C) via the upregulation of *Gata3* (figure 4.2A), however the signalling mechanism driving this remains

unclear. Transcriptomics data shows that Notch signalling via increased *Rbpj* gene expression (figure 4.2A) is a likely candidate, as this can induce Th2 skewing [186], however this would require further confirmation. One way to test this could be to overexpress RBPJ in CD4+ T cells using lentiviral methods. If RBPJ and Notch signalling are responsible for the Th2 skewing seen in EROS deficiency then IL-4, IL-5 and IL-13 secretion would be augmented.

This would also contribute to clarifying the role of STAT6 in the Th2 skewing is STAT6-independent or due to prolonged STAT6 signalling. There was no difference in STAT6 phosphorylation (figure 4.4D,F), but there was reduced IL-4Rα turnover in EROS deficiency (figure 4.7C) meaning overall phosphorylation is unchanged but duration of STAT6 signalling may be prolonged. This could be further addressed by performing a highly sensitive phospho-CyTOF mass spectrometry experiment or phospho-proteomics study to measure STAT6 phosphorylation in EROS-/- CD4+ T cells.

Transcriptomic analysis also identified that early signalling pathways are enriched in EROS deficient CD4+ T cells (figure 4.2B). One of the earliest and most important cell signalling pathways is the TCR proximal signalling pathway. There was no difference in baseline expression or phosphorylation of LCK, ZAP70 or LCK (figure 4.6) when measured by western blot. Previous studies have used flow cytometry to measure ZAP70 phosphorylation [256], so perhaps a more sensitive detection method may identify any subtle changes in phosphorylation of the TCR proximal signalling molecules. Additionally, activation of the distal TCR signalling molecules such as AKT, JNK and NF-κB could be examined (reviewed in [257]). These signalling molecules are of interest as they are also located downstream of CD27 [258]. Mouse and human EROS deficient cells express significantly higher levels of CD27 (figure 3.7D-E, figure 6.10B), therefore the signalling pathways that these molecules are involved in may also be upregulated.

Intrinsic vs extrinsic action of EROS

All mouse experiments (chapter 3-5) were performed with global EROS knockout mice. This means that EROS is deficient in every cell type and therefore, it's impossible to delineate whether the phenotypes described in this thesis are due to the intrinsic or extrinsic role of EROS. It is likely that the action of EROS is intrinsic as EROS was knocked out from the CD4+

T cells of an EROS sufficient person in the human CRISPR experiments (chapter 6), yet exhibited similar Th2 skewing seen in the mouse global knockouts. However to confirm this, cytokine secretion could be assessed using cells from EROS CD4-Cre mice. Th2 skewing would suggest that EROS is cell intrinsic, whereas if the cytokine phenotype was different it would suggest that EROS is cell extrinsic.

Asthma/allergy models

Uncontrolled Th2 immunity can result in an allergic response [259]. EROS deficiency causes excess IL-4, IL-5 and IL-13 secretion from CD4+ T cells (figure 4.1A-C) and higher numbers of ILC2 in the lungs (figure 5.6B). Additionally, gp91*phox* deficient mice have been found to have an enhanced allergic asthma phenotype [260]. It would be interesting to see whether EROS deficient mice are more susceptible in models of asthma/allergy such as the house dust mite model. This could potentially lead to the development of therapeutics that target EROS and subsequently Th2 immunity for the treatment of allergic asthma.

Further phenotyping

The phenotype of EROS deficiency is primarily driven by loss of P2X7 signalling in CD4+ T cells. P2X7 is also highly expressed on other T cell subsets including Natural Killer T (NKT) cells [261–263] and gamma-delta T cells [149]. Therefore, it may prove interesting to see whether EROS deficiency, and subsequently P2X7 deficiency, has any impacts on the functions of these two highly important cell types in adaptive immunity.

Final conclusion

EROS negatively regulates Th2 skewing in CD4+ T cells by upregulating the expression of P2X7.

Figures 1.2, 1.4, 1.5, 4.16 were created using Biorender.

References

1. Mortimer, P. M., Mc Intyre, S. A. & Thomas, D. C. Beyond the Extra Respiration of Phagocytosis: NADPH Oxidase 2 in Adaptive Immunity and Inflammation. *Front Immunol* **12**, (2021).

2. Auten, R. L. & Davis, J. M. Oxygen Toxicity and Reactive Oxygen Species: The Devil Is in the Details. *Pediatric Research 2009 66:2* **66**, 121–127 (2009).

3. Tavassolifar, M. J., Vodjgani, M., Salehi, Z. & Izad, M. The Influence of Reactive Oxygen Species in the Immune System and Pathogenesis of Multiple Sclerosis. *Autoimmune Dis* **2020**, (2020).

4. Li, X., Fang, P., Mai, J., Choi, E. T., Wang, H. & Yang, X. Targeting mitochondrial reactive oxygen species as novel therapy for inflammatory diseases and cancers. *Journal of Hematology & Oncology 2013 6:1* **6**, 1–19 (2013).

5. Finkel, T. Signal transduction by mitochondrial oxidants. *J Biol Chem* **287**, 4434–4440 (2012).

6. Kamata, H., Honda, S. I., Maeda, S., Chang, L., Hirata, H. & Karin, M. Reactive oxygen species promote TNFalpha-induced death and sustained JNK activation by inhibiting MAP kinase phosphatases. *Cell* **120**, 649–661 (2005).

7. Scherz-Shouval, R., Shvets, E., Fass, E., Shorer, H., Gil, L. & Elazar, Z. Reactive oxygen species are essential for autophagy and specifically regulate the activity of Atg4. *EMBO J* **26**, 1749–1760 (2007).

8. Vorbach, C., Harrison, R. & Capecchi, M. R. Xanthine oxidoreductase is central to the evolution and function of the innate immune system. *Trends Immunol* **24**, 512–517 (2003).

9. Ives, A., Nomura, J., Martinon, F., Roger, T., LeRoy, D., Miner, J. N., Simon, G., Busso, N. & So, A. Xanthine oxidoreductase regulates macrophage IL1β secretion upon NLRP3 inflammasome activation. *Nature Communications 2015 6:1* **6**, 1–11 (2015).

10. Ty, M. C., Zuniga, M., Götz, A., Kayal, S., Sahu, P. K., Mohanty, A., Mohanty, S., Wassmer, S. C. & Rodriguez, A. Malaria inflammation by xanthine oxidase-produced reactive oxygen species. *EMBO Mol Med* **11**, 9903 (2019).

11. Baron, J. M., Zwadlo-Klarwasser, G., Jugert, F., Hamann, W., Rübben, A., Mukhtar, H. & Merk, H. F. Cytochrome P450 1B1: a major P450 isoenzyme in human blood monocytes and macrophage subsets. *Biochem Pharmacol* **56**, 1105–1110 (1998).

12. Veith, A. & Moorthy, B. ROLE OF CYTOCHROME P450S IN THE GENERATION AND METABOLISM OF REACTIVE OXYGEN SPECIES. *Curr Opin Toxicol* **7**, 44 (2018).

13. Kil, I. S., Lee, S. K., Ryu, K. W., Woo, H. A., Hu, M. C., Bae, S. H. & Rhee, S. G. Feedback Control of Adrenal Steroidogenesis via H2O2-Dependent, Reversible Inactivation of Peroxiredoxin III in Mitochondria. *Mol Cell* **46**, 584–594 (2012).

14. Aitken, A. E. & Morgan, E. T. Gene-Specific Effects of Inflammatory Cytokines on Cytochrome P4502C, 2B6 and 3A4 mRNA Levels in Human Hepatocytes. *Drug Metab Dispos* **35**, 1687 (2007).

15. Lam, G. Y., Huang, J. & Brumell, J. H. The many roles of NOX2 NADPH oxidase-derived ROS in immunity. *Seminars in Immunopathology* vol. 32 415–430 Preprint at https://doi.org/10.1007/s00281-010-0221-0 (2010).

16. Panday, A., Sahoo, M. K., Osorio, D. & Batra, S. NADPH oxidases: An overview from structure to innate immunity-associated pathologies. *Cell Mol Immunol* **12**, 5–23 (2015).

17. Thomas, D. C. The phagocyte respiratory burst: Historical perspectives and recent advances. *Immunol Lett* **192**, 88–96 (2017).

18. El-Benna, J., Dang, P. M. C., Gougerot-Pocidalo, M. A., Marie, J. C. & Braut-Boucher, F. p47phox, the phagocyte NADPH oxidase/NOX2 organizer: structure, phosphorylation and implication in diseases. *Exp Mol Med* **41**, 217 (2009).

19. Yuzawa, S., Ogura, K., Horiuchi, M., Suzuki, N. N., Fujioka, Y., Kataoka, M., Sumimoto, H. & Inagaki, F. Solution Structure of the Tandem Src Homology 3 Domains of p47phox in an Autoinhibited Form *. *Journal of Biological Chemistry* **279**, 29752–29760 (2004).

20. Groemping, Y. & Rittinger, K. Activation and assembly of the NADPH oxidase: a structural perspective. *Biochem J* **386**, 401–416 (2005).

21. Bokoch, G. M. & Diebold, B. A. Current molecular models for NADPH oxidase regulation by Rac GTPase. *Blood* **100**, 2692–2696 (2002).

22. Vermot, A., Petit-Härtlein, I., Smith, S. M. E. & Fieschi, F. NADPH Oxidases (NOX): An Overview from Discovery, Molecular Mechanisms to Physiology and Pathology. *Antioxidants 2021, Vol. 10, Page 890* **10**, 890 (2021).

23. Finkel, T. Signal transduction by reactive oxygen species. *Journal of Cell Biology* vol. 194 7–15 Preprint at https://doi.org/10.1083/jcb.201102095 (2011).

24. Baldridge, C. W. & Gerard, R. W. THE EXTRA RESPIRATION OF PHAGOCYTOSIS. *American Journal of Physiology-Legacy Content* **103**, 235–236 (1932).

25. Sbarra, A. J. & Karnovsky, M. L. The Biochemical Basis of Phagocytosis. *Journal of Biological Chemistry* **234**, 1355–1362 (1959).

26. Rossi, F. & Zatti, M. Biochemical aspects of phagocytosis in poly-morphonuclear leucocytes. NADH and NADPH oxidation by the granules of resting and phagocytizing cells. *Experientia* **20**, 21–23 (1964).

27. Quie, P. G., White, J. G., Holmes, B. & Good, R. A. In Vitro Bactericidal Capacity of Human Polymorphonuclear Leukocytes: Diminished Activity in Chronic Granulomatous Disease of Childhood *. *Journal of Clinical Investigation* **46**, 668–679 (1967).

28. Segal, A. W. & Jones, O. T. G. Novel cytochrome b system in phagocytic vacuoles of human granulocytes [25]. *Nature* **276**, 515–517 (1978).

29. Bromberg, Y. & Pick, E. Unsaturated fatty acids stimulate NADPH-dependent superoxide production by cell-free system derived from macrophages. *Cell Immunol* **88**, 213–221 (1984).

30. Volpp, B. D., Nauseef, W. M. & Clark, R. A. Two cytosolic neutrophil oxidase components absent in autosomal chronic granulomatous disease. *Science (1979)* **242**, 1295–1297 (1988).

31. Abo, A. & Pick, E. Purification and characterization of a third cytosolic component of the superoxide-generating NADPH oxidase of macrophages. *Journal of Biological Chemistry* **266**, 23577–23585 (1991).

32. Knaus, U. G., Heyworth, P. G., Evans, T., Curnutte, J. T. & Bokoch, G. M. Regulation of Phagocyte Oxygen Radical Production by the GTP-Binding Protein Rac 2. *Science (1979)* **254**, 1512–1515 (1991).

33. Wientjes, F. B., Hsuan, J. J., Totty, N. F. & Segal, A. W. p40(phox), a third cytosolic component of the activation complex of the NADPH oxidase to contain src homology 3 domains. *Biochemical Journal* **296**, 557–561 (1993).

34. Thomas, D. C., Clare, S., Sowerby, J. M., Pardo, M., Juss, J. K., Goulding, D. A., van der Weyden, L., Storisteanu, D., Prakash, A., Espéli, M., Flint, S., Lee, J. C., Hoenderdos, K., Kane, L., Harcourt, K., Mukhopadhyay, S., Umrania, Y., Antrobus, R., Nathan, J. A., *et al.* Eros is a novel transmembrane protein that controls the phagocyte respiratory burst and is essential for innate immunity. *Journal of Experimental Medicine* **214**, 1111–1128 (2017).

35. Bridges, R. A., Berendes, H. & Good, R. A. A Fatal Granulomatous Disease of Childhood: The Clinical, Pathological, and Laboratory Features of a New Syndrome. *AMA J Dis Child* **97**, 387–408 (1959).

36. Baehner, R. L. & Nathan, D. G. Leukocyte Oxidase: Defective Activity in Chronic Granulomatous Disease. *Science (1979)* **155**, 835–836 (1967).

37. Dinauer, M. C., Orkin, S. H., Brown, R., Jesaitis, A. J. & Parkos, C. A. The glycoprotein encoded by the X-linked chronic granulomatous disease locus is a component of the neutrophil cytochrome b complex. *Nature* **327**, 717–720 (1987).

38. Segal, A. W., Heyworth, P. G., Cockcroft, S. & Barrowman, M. M. Stimulated neutrophils from patients with autosomal recessive chronic granulomatous disease fail to phosphorylate a Mr-44,000 protein. *Nature* **316**, 547–549 (1985).

39. Clark, R. A., Malech, H. L., Gallin, J. I., Nunoi, H., Volpp, B. D., Pearson, D. W., Nauseef, W. M. & Curnutte, J. T. Genetic Variants of Chronic Granulomatous Disease: Prevalence of Deficiencies of Two Cytosolic Components of the NADPH Oxidase System. *http://dx.doi.org/10.1056/NEJM198909073211005* **321**, 647–652 (2010).

40. Arnold, D. E. & Heimall, J. R. A Review of Chronic Granulomatous Disease. *Advances in Therapy* vol. 34 2543–2557 Preprint at https://doi.org/10.1007/s12325-017-0636-2 (2017).

41. Roxo-Junior, P. & Simão, H. M. L. Chronic granulomatous disease: why an inflammatory disease? *Brazilian Journal of Medical and Biological Research* **47**, 924 (2014).

42. Kuhns, D. B., Alvord, W. G., Heller, T., Feld, J. J., Pike, K. M., Marciano, B. E., Uzel, G., DeRavin, S. S., Priel, D. A. L., Soule, B. P., Zarember, K. A., Malech, H. L., Holland, S. M. & Gallin, J. I. Residual NADPH Oxidase and Survival in Chronic Granulomatous Disease. *N Engl J Med* **363**, 2600 (2010).

43. Roos, D. Chronic granulomatous disease. *Br Med Bull.* **118**, 50–63 (2016).

44. Schäppi, M. G., Jaquet, V., Belli, D. C. & Krause, K. H. Hyperinflammation in chronic granulomatous disease and anti-inflammatory role of the phagocyte NADPH oxidase. *Seminars in Immunopathology 2008 30:3* **30**, 255–271 (2008).

45. Ramanuja, S., Wolf, K. M., Sadat, M. A., Mahoney, S. J., Dinauer, M. C. & Nelson, R. P. Newly diagnosed chronic granulomatous disease in a 53-year-old woman with Crohn disease. *Ann Allergy Asthma Immunol* **95**, 204–209 (2005).

46. Cale, C. M., Morton, L. & Goldblatt, D. Cutaneous and other lupus-like symptoms in carriers of X-linked chronic granulomatous disease: incidence and autoimmune serology. *Clin Exp Immunol* **148**, 79–84 (2007).

47. Rupec, R. A., Petropoulou, T., Belohradsky, B. H., Walchner, M., Liese, J. G., Plewig, G. & Messer, G. Lupus erythematosus tumidus and chronic discoid lupus erythematosus in carriers of X-linked chronic granulomatous disease. *Eur J Dermatol* **10**, 184–189 (2000).

48. Marciano, B. E., Zerbe, C. S., Falcone, E. L., Ding, L., DeRavin, S. S., Daub, J., Kreuzburg, S., Yockey, L., Hunsberger, S., Foruraghi, L., Barnhart, L. A., Matharu, K., Anderson, V., Darnell, D. N., Frein, C., Fink, D. L., Lau, K. P., Long Priel, D. A., Gallin, J. I., *et al.* X-linked carriers of chronic granulomatous disease: Illness, lyonization, and stability. *Journal of Allergy and Clinical Immunology* **141**, 365–371 (2018).

49. Magnani, A., Brosselin, P., Beauté, J., de Vergnes, N., Mouy, R., Debré, M., Suarez, F., Hermine, O., Lortholary, O., Blanche, S., Fischer, A. & Mahlaoui, N. Inflammatory manifestations in a single-center cohort of patients with chronic granulomatous disease. *J Allergy Clin Immunol* **134**, 655-662.e8 (2014).

50. Marciano, B. E., Rosenzweig, S. D., Kleiner, D. E., Anderson, V. L., Darnell, D. N., Anaya-O'Brien, S., Hilligoss, D. M., Malech, H. L., Gallin, J. I. & Holland, S. M. Gastrointestinal involvement in chronic granulomatous disease. *Pediatrics* **114**, 462–468 (2004).

51. Röhm, M., Grimm, M. J., D'Auria, A. C., Almyroudis, N. G., Segal, B. H. & Urban, C. F. NADPH oxidase promotes neutrophil extracellular trap formation in pulmonary aspergillosis. *Infect Immun* **82**, 1766–1777 (2014).

52. Fuchs, T. A., Abed, U., Goosmann, C., Hurwitz, R., Schulze, I., Wahn, V., Weinrauch, Y., Brinkmann, V. & Zychlinsky, A. Novel cell death program leads to neutrophil extracellular traps. *Journal of Cell Biology* **176**, 231–241 (2007).

53. Petersen, J. E., Hiran, T. S., Goebel, W. S., Johnson, C., Murphy, R. C., Azmi, F. H., Hood, A. F., Travers, J. B. & Dinauer, M. C. Enhanced cutaneous inflammatory reactions to Aspergillus fumigatus in a murine model of chronic granulomatous disease. *J Invest Dermatol* **118**, 424–429 (2002).

54. Goebel, W. S., Mark, L. A., Billings, S. D., Meyers, J. L., Pech, N., Travers, J. B. & Dinauer, M. C. Gene correction reduces cutaneous inflammation and granuloma formation in murine X-linked chronic granulomatous disease. *J Invest Dermatol* **125**, 705–710 (2005).

55. Segal, B. H., Han, W., Bushey, J. J., Joo, M., Bhatti, Z., Feminella, J., Dennis, C. G., Vethanayagam, R. R., Yull, F. E., Capitano, M., Wallace, P. K., Minderman, H., Christman, J. W., Sporn, M. B., Chan, J., Vinh, D. C., Holland, S. M., Romani, L. R., Gaffen, S. L., *et al.* NADPH oxidase limits innate immune responses in the lungs in mice. *PLoS One* **5**, (2010).

56. Deffert, C., Carnesecchi, S., Yuan, H., Rougemont, A. L., Kelkka, T., Holmdahl, R., Krause, K. H. & Schäppi, M. G. Hyperinflammation of chronic granulomatous disease is abolished by NOX2 reconstitution in macrophages and dendritic cells. *J Pathol* **228**, 341–350 (2012).

57. Olofsson, P., Holmberg, J., Tordsson, J., Lu, S., Åkerström, B. & Holmdahl, R. Positional identification of Ncf1 as a gene that regulates arthritis severity in rats. *Nat Genet* **33**, 25–32 (2003).

58. Gelderman, K. A., Hultqvist, M., Pizzolla, A., Zhao, M., Nandakumar, K. S., Mattsson, R. & Holmdahl, R. Macrophages suppress T cell responses and arthritis development in mice by producing reactive oxygen species. *Journal of Clinical Investigation* **117**, 3020–3028 (2007).

59. Toledano, M. B. & Leonard, W. J. Modulation of transcription factor NF-kappa B binding activity by oxidation-reduction in vitro. *Proceedings of the National Academy of Sciences* **88**, 4328–4332 (1991).

60. Brar, S. S., Kennedy, T. P., Sturrock, A. B., Huecksteadt, T. P., Quinn, M. T., Murphy, T. M., Chitano, P. & Hoidal, J. R. NADPH oxidase promotes NF-κB activation and

proliferation in human airway smooth muscle. *Am J Physiol Lung Cell Mol Physiol* **282**, 782–795 (2002).

61. Clark, R. A. & Valente, A. J. Nuclear factor kappa B activation by NADPH oxidases. *Mech Ageing Dev* **125**, 799–810 (2004).

62. Fan, J., Frey, R. S., Rahman, A. & Malik, A. B. Role of Neutrophil NADPH Oxidase in the Mechanism of Tumor Necrosis Factor-α-induced NF-κB Activation and Intercellular Adhesion Molecule-1 Expression in Endothelial Cells *. *Journal of Biological Chemistry* **277**, 3404–3411 (2002).

63. Trevelin, S. C., Dos Santos, C. X., Ferreira, R. G., De Sá Lima, L., Silva, R. L., Scavone, C., Curi, R., Alves-Filho, J. C., Cunha, T. M., Roxo-Júnior, P., Cervi, M. C., Laurindo, F. R. M., Hothersall, J. S., Cobb, A. M., Zhang, M., Ivetic, A., Shah, A. M., Lopes, L. R. & Cunha, F. Q. Apocynin and Nox2 regulate NF-κ B by modifying thioredoxin-1 redox-state. *Sci Rep* **6**, 1–12 (2016).

64. Han, W., Li, H., Cai, J., Gleaves, L. A., Polosukhin, V. v., Segal, B. H., Yull, F. E. & Blackwell, T. S. NADPH Oxidase Limits Lipopolysaccharide-Induced Lung Inflammation and Injury in Mice through Reduction-Oxidation Regulation of NF-κB Activity. *The Journal of Immunology* **190**, 4786–4794 (2013).

65. Warnatsch, A., Tsourouktsoglou, T. D., Branzk, N., Wang, Q., Reincke, S., Herbst, S., Gutierrez, M. & Papayannopoulos, V. Reactive Oxygen Species Localization Programs Inflammation to Clear Microbes of Different Size. *Immunity* **46**, 421 (2017).

66. Anrather, J., Racchumi, G. & Iadecola, C. NF-κB regulates phagocytic NADPH oxidase by inducing the expression of gp91phox. *Journal of Biological Chemistry* **281**, 5657–5667 (2006).

67. Gauss, K. A., Nelson-Overton, L. K., Siemsen, D. W., Gao, Y., DeLeo, F. R. & Quinn, M. T. Role of NF-κB in transcriptional regulation of the phagocyte NADPH oxidase by tumor necrosis factor-α. *J Leukoc Biol* **82**, 729–741 (2007).

68. Olofsson, P., Holmberg, J., Tordsson, J., Lu, S., Åkerström, B. & Holmdahl, R. Positional identification of Ncf1 as a gene that regulates arthritis severity in rats. *Nature Genetics 2002 33:1* **33**, 25–32 (2002).

69. Kelkka, T., Kienhöfer, D., Hoffmann, M., Linja, M., Wing, K., Sareila, O., Hultqvist, M., Laajala, E., Chen, Z., Vasconcelos, J., Neves, E., Guedes, M., Marques, L., Krönke, G., Helminen, M., Kainulainen, L., Olofsson, P., Jalkanen, S., Lahesmaa, R., *et al.* Reactive oxygen species deficiency induces autoimmunity with type 1 interferon signature. *Antioxid Redox Signal* **21**, 2231–2245 (2014).

70. Sareila, O., Hagert, C., Kelkka, T., Linja, M., Xu, B., Kihlberg, J. & Holmdahl, R. Reactive Oxygen Species Regulate Both Priming and Established Arthritis, but with Different Mechanisms. *Antioxid Redox Signal* **27**, 1473–1490 (2017).

71. Thayer, T. C., Delano, M., Liu, C., Chen, J., Padgett, L. E., Tse, H. M., Annamali, M., Piganelli, J. D., Moldawer, L. L. & Mathews, C. E. Superoxide Production by Macrophages and T Cells Is Critical for the Induction of Autoreactivity and Type 1 Diabetes. *Diabetes* **60**, 2144–2151 (2011).

72. Padgett, L. E., Burg, A. R., Lei, W. & Tse, H. M. Loss of NADPH Oxidase–Derived Superoxide Skews Macrophage Phenotypes to Delay Type 1 Diabetes. *Diabetes* **64**, 937–946 (2015).

73. Cruz, C. M., Rinna, A., Forman, H. J., Ventura, A. L. M., Persechini, P. M. & Ojcius, D. M. ATP activates a reactive oxygen species-dependent oxidative stress response and secretion of proinflammatory cytokines in macrophages. *J Biol Chem* **282**, 2871–2879 (2007).

74. Noguchi, T., Ishii, K., Fukutomi, H., Naguro, I., Matsuzawa, A., Takeda, K. & Ichijo, H. Requirement of Reactive Oxygen Species-dependent Activation of ASK1-p38 MAPK Pathway for Extracellular ATP-induced Apoptosis in Macrophage *. *Journal of Biological Chemistry* **283**, 7657–7665 (2008).

75. Dostert, C., Pétrilli, V., van Bruggen, R., Steele, C., Mossman, B. T. & Tschopp, J. Innate immune activation through Nalp3 inflammasome sensing of asbestos and silica. *Science* **320**, 674–677 (2008).

76. Ma, M. W., Wang, J., Dhandapani, K. M. & Brann, D. W. NADPH Oxidase 2 Regulates NLRP3 Inflammasome Activation in the Brain after Traumatic Brain Injury. *Oxid Med Cell Longev* **2017**, (2017).

77. Meissner, F., Seger, R. A., Moshous, D., Fischer, A., Reichenbach, J. & Zychlinsky, A. Inflammasome activation in NADPH oxidase defective mononuclear phagocytes from patients with chronic granulomatous disease. *Blood* **116**, 1570–1573 (2010).

78. Pfeiffer, Z. A., Guerra, A. N., Hill, L. M., Gavala, M. L., Prabhu, U., Aga, M., Hall, D. J. & Bertics, P. J. Nucleotide receptor signaling in murine macrophages is linked to reactive oxygen species generation. *Free Radic Biol Med* **42**, 1506–1516 (2007).

79. Sokolovska, A., Becker, C. E., Ip, W. K. E., Rathinam, V. A. K., Brudner, M., Paquette, N., Tanne, A., Vanaja, S. K., Moore, K. J., Fitzgerald, K. A., Lacy-Hulbert, A. & Stuart, L. M. Activation of caspase-1 by the NLRP3 inflammasome regulates the NADPH oxidase NOX2 to control phagosome function. *Nature Immunology 2013 14:6* **14**, 543–553 (2013).

80. Emmendörffer, A., Roesler, J., Eisner, J., Raeder, E., Lohmann-Matthes, M.-L. & Meier, B. Production of oxygen radicals by fibroblasts and neutrophils from a patient with x-linked chronic granulomatous disease. *Eur J Haematol* **51**, 223–227 (2009).

81. Bedard, K. & Krause, K. H. The NOX family of ROS-generating NADPH oxidases: Physiology and pathophysiology. *Physiol Rev* **87**, 245–313 (2007).

82. Suh, Y. A., Arnold, R. S., Lassegue, B., Shi, J., Xu, X., Sorescu, D., Chung, A. B., Griendling, K. K. & Lambeth, J. D. Cell transformation by the superoxide-generating oxidase Mox1. *Nature* **401**, 79–82 (1999).

83. Alvarez, L. A., Kovačič, L., Rodríguez, J., Gosemann, J. H., Kubica, M., Pircalabioru, G. G., Friedmacher, F., Cean, A., Ghişe, A., SĂrĂndan, M. B., Puri, P., Daff, S., Plettner, E., Von Kriegsheim, A., Bourke, B. & Knaus, U. G. NADPH oxidase-derived H2O 2 subverts pathogen signaling by oxidative phosphotyrosine conversion to PB-DOPA. *Proc Natl Acad Sci U S A* **113**, 10406–10411 (2016).

84. Paffenholz, R., Bergstrom, R. A., Pasutto, F., Wabnitz, P., Munroe, R. J., Jagla, W., Heinzmann, U., Marquardt, A., Bareiss, A., Laufs, J., Russ, A., Stumm, G., Schimenti, J. C. & Bergstrom, D. E. Vestibular defects in head-tilt mice result from mutations in Nox3, encoding an NADPH oxidase. *Genes Dev* **18**, 486–491 (2004).

85. Shiose, A., Kuroda, J., Tsuruya, K., Hirai, M., Hirakata, H., Naitoi, S., Hattori, M., Sakaki, Y. & Sumimoto, H. A novel superoxide-producing NAD(P)H oxidase in kidney. *Journal of Biological Chemistry* **276**, 1417–1423 (2001).

86. Van Buul, J. D., Fernandez-Borja, M., Anthony, E. C. & Hordijk, P. L. Expression and localization of NOX2 and NOX4 in primary human endothelial cells. *Antioxid Redox Signal* **7**, 308–317 (2005).

87. Yang, S., Zhang, Y., Ries, W. & Key, L. Expression of Nox4 in osteoclasts. *J Cell Biochem* **92**, 238–248 (2004).

88. Schürmann, C., Rezende, F., Kruse, C., Yasar, Y., Löwe, O., Fork, C., van de Sluis, B., Bremer, R., Weissmann, N., Shah, A. M., Jo, H., Brandes, R. P., & Schröder, K. The NADPH oxidase Nox4 has anti-atherosclerotic functions. *Eur Heart J* **36**, 3447–3456 (2015).

89. Goettsch, C., Babelova, A., Trummer, O., Erben, R. G., Rauner, M., Rammelt, S., Weissmann, N., Weinberger, V., Benkhoff, S., Kampschulte, M., Obermayer-Pietsch, B., Hofbauer, L. C., Brandes, R. P. & Schröder, K. NADPH oxidase 4 limits bone mass by promoting osteoclastogenesis. *Journal of Clinical Investigation* **123**, 4731–4738 (2013).

90. Bánfi, B., Molnár, G., Maturana, A., Steger, K., Hegedûs, B., Demaurex, N. & Krause, K. H. A Ca(2+)-activated NADPH oxidase in testis, spleen, and lymph nodes. *J Biol Chem* **276**, 37594–37601 (2001).

91. Bedard, K., Jaquet, V. & Krause, K. H. NOX5: From basic biology to signaling and disease. *Free Radical Biology and Medicine* vol. 52 725–734 Preprint at https://doi.org/10.1016/j.freeradbiomed.2011.11.023 (2012).

92. Forteza, R., Salathe, M., Miot, F., Forteza, R. & Conner, G. E. Regulated hydrogen peroxide production by duox in human airway epithelial cells. *Am J Respir Cell Mol Biol* **32**, 462–469 (2005).

93. Ameziane-El-Hassani, R., Morand, S., Boucher, J. L., Frapart, Y. M., Apostolou, D., Agnandji, D., Gnidehou, S., Ohayon, R., Noël-Hudson, M. S., Francon, J., Lalaoui, K., Virion, A. & Dupuy, C. Dual oxidase-2 has an intrinsic Ca2+-dependent H 2O2-generating activity. *Journal of Biological Chemistry* **280**, 30046–30054 (2005).

94. Aycan, Z., Cangul, H., Muzza, M., Bas, V. N., Fugazzola, L., Chatterjee, V. K., Persani, L. & Schoenmakers, N. Digenic DUOX1 and DUOX2 Mutations in Cases With Congenital Hypothyroidism. *J Clin Endocrinol Metab* **102**, 3085–3090 (2017).

95. Grasberger, H., Gao, J., Nagao-Kitamoto, H., Kitamoto, S., Zhang, M., Kamada, N., Eaton, K. A., El-Zaatari, M., Shreiner, A. B., Merchant, J. L., Owyang, C. & Kao, J. Y. Increased Expression of DUOX2 is an Epithelial Response to Mucosal Dysbiosis Required for Immune Homeostasis in Mouse Intestine. *Gastroenterology* **149**, 1849 (2015).

96. Jackson, S. H., Devadas, S., Kwon, J., Pinto, L. A. & Williams, M. S. T cells express a phagocyte-type NADPH oxidase that is activated after T cell receptor stimulation. *Nat Immunol* **5**, 818–827 (2004).

97. Harrington, L. E., Hatton, R. D., Mangan, P. R., Turner, H., Murphy, T. L., Murphy, K. M. & Weaver, C. T. Interleukin 17-producing CD4+ effector T cells develop via a lineage distinct from the T helper type 1 and 2 lineages. *Nat Immunol* **6**, 1123–1132 (2005).

98. Kwon, B. I., Kim, T. W., Shin, K., Kim, Y. H., Yuk, C. M., Yuk, J. M., Shin, D. M., Jo, E. K., Lee, C. H. & Lee, S. H. Enhanced Th2 cell differentiation and function in the absence of Nox2. *Allergy: European Journal of Allergy and Clinical Immunology* **72**, 252–265 (2017).

99. Tse, H. M., Thayer, T. C., Steele, C., Cuda, C. M., Morel, L., Piganelli, J. D. & Mathews, C. E. NADPH Oxidase Deficiency Regulates Th Lineage Commitment and Modulates Autoimmunity. *The Journal of Immunology* **185**, 5247–5258 (2010).

100. Shatynski, K. E., Chen, H., Kwon, J. & Williams, M. S. Decreased STAT5 phosphorylation and GATA-3 expression in NOX2-deficient T cells: Role in T helper development. *Eur J Immunol* **42**, 3202–3211 (2012).

101. Lee, K., Won, H. Y., Bae, M. A., Hong, J. H. & Hwang, E. S. Spontaneous and aging-dependent development of arthritis in NADPH oxidase 2 deficiency through altered differentiation of CD11b+ and Th/Treg cells. *Proc Natl Acad Sci U S A* **108**, 9548–9553 (2011).

102. Won, H. Y., Jang, E. J., Min, H. J. & Hwang, E. S. Enhancement of Allergen-induced Airway Inflammation by NOX2 Deficiency. *Immune Netw* **11**, 169 (2011).

103. Saravia, J., Chapman, N. M. & Chi, H. Helper T cell differentiation. *Cellular & Molecular Immunology 2019 16:7* **16**, 634–643 (2019).

104. van de Geer, A., Cuadrado, E., Slot, M. C., van Bruggen, R., Amsen, D. & Kuijpers, T. W. Regulatory T cell features in chronic granulomatous disease. *Clin Exp Immunol* **197**, 222–229 (2019).

105. Devadas, S., Zaritskaya, L., Rhee, S. G., Oberley, L. & Williams, M. S. Discrete Generation of Superoxide and Hydrogen Peroxide by T Cell Receptor Stimulation: Selective Regulation of Mitogen-Activated Protein Kinase Activation and Fas Ligand Expression. *J Exp Med* **195**, 59 (2002).

106. Emmerson, A., Trevelin, S. C., Mongue-Din, H., Becker, P. D., Ortiz, C., Smyth, L. A., Peng, Q., Elgueta, R., Sawyer, G., Ivetic, A., Lechler, R. I., Lombardi, G. & Shah, A. M. Nox2 in regulatory T cells promotes angiotensin II–induced cardiovascular remodeling. *Journal of Clinical Investigation* **128**, 3088–3101 (2018).

107. Efimova, O., Szankasi, P. & Kelley, T. W. Ncf1 (p47phox) is essential for direct regulatory T cell mediated suppression of CD4+ effector T cells. *PLoS One* **6**, e16013 (2011).

108. Chose, O., Sansilvestri-Morel, P., Badier-Commander, C., Bernhardt, F., Fabiani, J.-N., Rupin, A. & Verbeuren, T. J. Distinct Role of nox1, nox2, and p47phox in Unstimulated Versus Angiotensin II-Induced NADPH Oxidase Activity in Human Venous Smooth Muscle Cells. *J Cardiovasc Pharmacol* **51**, 131–139 (2008).

109. Li, J. M., Wheatcroft, S., Fan, L. M., Kearney, M. T. & Shah, A. M. Opposing Roles of p47phox in Basal Versus Angiotensin II-Stimulated Alterations in Vascular O2- Production, Vascular Tone, and Mitogen-Activated Protein Kinase Activation. *Circulation* **109**, 1307–1313 (2004).

110. Purushothaman, D. & Sarin, A. Cytokine-dependent regulation of NADPH oxidase activity and the consequences for activated T cell homeostasis. *Journal of Experimental Medicine* **206**, 1515–1523 (2009).

111. Kopp, R., Krautloher, A., Ramírez-Fernández, A. & Nicke, A. P2X7 Interactions and Signaling – Making Head or Tail of It. *Frontiers in Molecular Neuroscience* vol. 12 183 Preprint at https://doi.org/10.3389/fnmol.2019.00183 (2019).

112. North, R. A. & Surprenant, A. Pharmacology of cloned P2X receptors. *Annu Rev Pharmacol Toxicol* **40**, 563–580 (2000).

113. Li, L.-H., Lin, J.-S., Chiu, H.-W., Lin, W.-Y., Ju, T.-C., Chen, F.-H., Chernikov, O. V., Liu, M.-L., Chang, J.-C., Hsu, C.-H., Chen, A., Ka, S.-M., Gao, H.-W. & Hua, K.-F. Mechanistic Insight Into the Activation of the NLRP3 Inflammasome by Neisseria gonorrhoeae in Macrophages. *Front Immunol* **10**, 1815 (2019).

114. De Torre-Minguela, C., Barberà-Cremades, M., Gómez, A. I., Martín-Sánchez, F. & Pelegrín, P. Macrophage activation and polarization modify P2X7 receptor secretome influencing the inflammatory process. *Sci Rep* **6**, 1–11 (2016).

115. Ghiringhelli, F., Apetoh, L., Tesniere, A., Aymeric, L., Ma, Y., Ortiz, C., Vermaelen, K., Panaretakis, T., Mignot, G., Ullrich, E., Perfettini, J. L., Schlemmer, F., Tasdemir, E., Uhl, M., Génin, P., Civas, A., Ryffel, B., Kanellopoulos, J., Tschopp, J., *et al.* Activation of the NLRP3 inflammasome in dendritic cells induces IL-1B-dependent adaptive immunity against tumors. *Nat Med* **15**, 1170–1178 (2009).

116. Junger, W. G. Immune cell regulation by autocrine purinergic signalling. *Nature Reviews Immunology* vol. 11 201–212 Preprint at https://doi.org/10.1038/nri2938 (2011).

117. Adinolfi, E., Cirillo, M., Woltersdorf, R., Falzoni, S., Chiozzi, P., Pellegatti, P., Callegari, M. G., Sandonà, D., Markwardt, F., Schmalzing, G., Virgilio, F. di, Schmalzing, F. & Virgilio, D. Trophic activity of a naturally occurring truncated isoform of the P2X7 receptor. *The FASEB Journal* **24**, 3393–3404 (2010).

118. Shemon, A. N., Sluyter, R., Fernando, S. L., Clarke, A. L., Dao-Ung, L. P., Skarratt, K. K., Saunders, B. M., Khai, S. T., Gu, B. J., Fuller, S. J., Britton, W. J., Petrou, S. & Wiley, J. S. A Thr357 to Ser polymorphism in homozygous and compound heterozygous subjects causes absent or reduced P2X7 function and impairs ATP-induced mycobacterial killing by macrophages. *J Biol Chem* **281**, 2079–2086 (2006).

119. Adriouch, S., Dox, C., Welge, V., Seman, M., Koch-Nolte, F. & Haag, F. Cutting Edge: A Natural P451L Mutation in the Cytoplasmic Domain Impairs the Function of the Mouse P2X7 Receptor. *The Journal of Immunology* **169**, 4108–4112 (2002).

120. Hubert, S., Rissiek, B., Klages, K., Huehn, J., Sparwasser, T., Haag, F., Koch-Nolte, F., Boyer, O., Seman, M. & Adriouch, S. Extracellular NAD+ shapes the Foxp3+ regulatory T cell compartment through the ART2–P2X7 pathway. *Journal of Experimental Medicine* **207**, 2561–2568 (2010).

121. Nicke, A., Kuan, Y. H., Masin, M., Rettinger, J., Marquez-Klaka, B., Bender, O., Górecki, D. C., Murrell-Lagnado, R. D. & Soto, F. A Functional P2X7 Splice Variant with an Alternative Transmembrane Domain 1 Escapes Gene Inactivation in P2X7 Knock-out Mice. *J Biol Chem* **284**, 25813 (2009).

122. Schwarz, N., Drouot, L., Nicke, A., Fliegert, R., Boyer, O., Guse, A. H., Haag, F., Adriouch, S. & Koch-Nolte, F. Alternative Splicing of the N-Terminal Cytosolic and Transmembrane Domains of P2X7 Controls Gating of the Ion Channel by ADP-Ribosylation. *PLoS One* **7**, e41269 (2012).

123. Xu, X. J., Boumechache, M., Robinson, L. E., Marschall, V., Gorecki, D. C., Masin, M. & Murrell-Lagnado, R. D. Splice variants of the P2X7 receptor reveal differential agonist dependence and functional coupling with pannexin-1. *J Cell Sci* **125**, 3776–3789 (2012).

124. Seman, M., Adriouch, S., Scheuplein, F., Krebs, C., Freese, D., Glowacki, G., Deterre, P., Haag, F. & Koch-Nolte, F. NAD-Induced T Cell Death: ADP-Ribosylation of Cell

Surface Proteins by ART2 Activates the Cytolytic P2X7 Purinoceptor. *Immunity* **19**, 571–582 (2003).

125. Hong, S., Schwarz, N., Brass, A., Seman, M., Haag, F., Koch-Nolte, F., Schilling, W. P. & Dubyak, G. R. Differential regulation of P2X7 receptor activation by extracellular NAD and ecto-ARTs in murine macrophages and T cells. *J Immunol* **183**, 578 (2009).

126. Scheuplein, F., Schwarz, N., Adriouch, S., Krebs, C., Bannas, P., Rissiek, B., Seman, M., Haag, F. & Koch-Nolte, F. NAD + and ATP Released from Injured Cells Induce P2X 7 - Dependent Shedding of CD62L and Externalization of Phosphatidylserine by Murine T Cells . *The Journal of Immunology* **182**, 2898–2908 (2009).

127. Chessell, I. P., Hatcher, J. P., Bountra, C., Michel, A. D., Hughes, J. P., Green, P., Egerton, J., Murfin, M., Richardson, J., Peck, W. L., Grahames, C. B. A., Casula, M. A., Yiangou, Y., Birch, R., Anand, P. & Buell, G. N. Disruption of the P2X7 purinoceptor gene abolishes chronic inflammatory and neuropathic pain. *Pain* **114**, 386–396 (2005).

128. Solle, M., Labasi, J., Perregaux, D. G., Stam, E., Petrushova, N., Koller, B. H., Griffiths, R. J. & Gabel, C. A. Altered cytokine production in mice lacking P2X(7) receptors. *J Biol Chem* **276**, 125–132 (2001).

129. Nicke, A., Kuan, Y. H., Masin, M., Rettinger, J., Marquez-Klaka, B., Bender, O., Górecki, D. C., Murrell-Lagnado, R. D. & Soto, F. A Functional P2X7 Splice Variant with an Alternative Transmembrane Domain 1 Escapes Gene Inactivation in P2X7 Knock-out Mice. *J Biol Chem* **284**, 25813 (2009).

130. Taylor, S. R. J., Gonzalez-Begne, M., Sojka, D. K., Richardson, J. C., Sheardown, S. A., Harrison, S. M., Pusey, C. D., Tam, F. W. K. & Elliott, J. I. Lymphocytes from P2X7-deficient mice exhibit enhanced P2X7 responses. *J Leukoc Biol* **85**, 978–986 (2009).

131. Chen, L. & Brosnan, C. F. Exacerbation of Experimental Autoimmune Encephalomyelitis in P2X7R−/− Mice: Evidence for Loss of Apoptotic Activity in Lymphocytes. *The Journal of Immunology* **176**, 3115–3126 (2006).

132. Sharp, A. J., Polak, P. E., Simonini, V., Lin, S. X., Richardson, J. C., Bongarzone, E. R. & Feinstein, D. L. P2x7 deficiency suppresses development of experimental autoimmune encephalomyelitis. *J Neuroinflammation* **5**, 1–13 (2008).

133. Craigie, E., Birch, R. E., Unwin, R. J. & Wildman, S. S. The relationship between P2X4 and P2X7: A physiologically important interaction? *Front Physiol* **4 AUG**, 216 (2013).

134. Burnstock, G. & Knight, G. E. Cellular Distribution and Functions of P2 Receptor Subtypes in Different Systems. (2004).

135. Di Virgilio, F., Dal Ben, D., Sarti, A. C., Giuliani, A. L. & Falzoni, S. The P2X7 Receptor in Infection and Inflammation. *Immunity* vol. 47 15–31 Preprint at https://doi.org/10.1016/j.immuni.2017.06.020 (2017).

136. Torres, G. E., Egan, T. M. & Voigt, M. M. Hetero-oligomeric assembly of P2X receptor subunits. Specificities exist with regard to possible partners. *J Biol Chem* **274**, 6653–6659 (1999).

137. Guo, C., Masin, M., Qureshi, O. S. & Murrell-Lagnado, R. D. Evidence for functional P2X4/P2X7 heteromeric receptors. *Mol Pharmacol* **72**, 1447–1456 (2007).

138. Nicke, A. Homotrimeric complexes are the dominant assembly state of native P2X7 subunits. *Biochem Biophys Res Commun* **377**, 803–808 (2008).

139. Antonio, L. S., Stewart, A. P., Xu, X. J., Varanda, W. A., Murrell-Lagnado, R. D. & Edwardson, J. M. P2X4 receptors interact with both P2X2 and P2X7 receptors in the form of homotrimers. *Br J Pharmacol* **163**, 1069–1077 (2011).

140. Weinhold, K., Krause-Buchholz, U., Rödel, G., Kasper, M. & Barth, K. Interaction and interrelation of P2X7 and P2X4 receptor complexes in mouse lung epithelial cells. *Cell Mol Life Sci* **67**, 2631–2642 (2010).

141. Sakaki, H., Fujiwaki, T., Tsukimoto, M., Kawano, A., Harada, H. & Kojima, S. P2X4 receptor regulates P2X7 receptor-dependent IL-1β and IL-18 release in mouse bone marrow-derived dendritic cells. *Biochem Biophys Res Commun* **432**, 406–411 (2013).

142. JG, M., JK, R., DG, W. & HB, C. Upregulated expression of purinergic P2X(7) receptor in Alzheimer disease and amyloid-beta peptide-treated microglia and in peptide-injected rat hippocampus. *J Neuropathol Exp Neurol* **65**, 1090–1097 (2006).

143. E, M., M, A., C, D., I, Y., C, B., C, L. D., M, B., A, P., V, S., A, H., JM, K., B, F., B, D. & C, D. New role of P2X7 receptor in an Alzheimer's disease mouse model. *Mol Psychiatry* **24**, 108–125 (2019).

144. JM, S., P, C., D, F., M, C., M, I., S, F., R, F., L, T. & F, D. V. Activation of microglia by amyloid {beta} requires P2X7 receptor expression. *J Immunol* **182**, 4378–4385 (2009).

145. Jiang, T., Hoekstra, J., Heng, X., Kang, W., Ding, J., Liu, J., Chen, S. & Zhang, J. P2X7 receptor is critical in α-synuclein–mediated microglial NADPH oxidase activation. *Neurobiol Aging* **36**, 2304–2318 (2015).

146. Salles, É. M. de, Menezes, M. N. de, Siqueira, R., Silva, H. B. da, Amaral, E. P., Castillo-Méndez, S. I., Cunha, I., Cassado, A. dos A., Vieira, F. S., Olivieri, D. N., Tadokoro, C. E., Alvarez, J. M., Coutinho-Silva, R. & D'Império-Lima, M. R. P2X7 receptor drives Th1 cell differentiation and controls the follicular helper T cell population to protect against Plasmodium chabaudi malaria. *PLoS Pathog* **13**, (2017).

147. Schenk, U., Frascoli, M., Proietti, M., Geffers, R., Traggiai, E., Buer, J., Ricordi, C., Westendorf, A. M. & Grassi, F. ATP inhibits the generation and function of regulatory T cells through the activation of purinergic P2X receptors. *Sci Signal* **4**, ra12–ra12 (2011).

148. Vergani, A., Tezza, S., D'Addio, F., Fotino, C., Liu, K., Niewczas, M., Bassi, R., Molano, R. D., Kleffel, S., Petrelli, A., Soleti, A., Ammirati, E., Frigerio, M., Visner, G., Grassi, F.,

Ferrero, M. E., Corradi, D., Abdi, R., Ricordi, C., *et al.* Long-term heart transplant survival by targeting the ionotropic purinergic receptor P2X7. *Circulation* **127**, 463–475 (2013).

149. Frascoli, M., Marcandalli, J., Schenk, U. & Grassi, F. Purinergic P2X7 Receptor Drives T Cell Lineage Choice and Shapes Peripheral γδ Cells. *The Journal of Immunology* **189**, 174–180 (2012).

150. Yip, L., Woehrle, T., Corriden, R., Hirsh, M., Chen, Y., Inoue, Y., Ferrari, V., Insel, P. A. & Junger, W. G. Autocrine regulation of T-cell activation by ATP release and P2X 7 receptors . *The FASEB Journal* **23**, 1685–1693 (2009).

151. Schenk, U., Westendorf, A. M., Radaelli, E., Casati, A., Ferro, M., Fumagalli, M., Verderio, C., Buer, J., Scanziani, E. & Grassi, F. Purinergic control of T cell activation by ATP released through pannexin-1 hemichannels. *Sci Signal* **1**, (2008).

152. Woehrle, T., Yip, L., Elkhal, A., Sumi, Y., Chen, Y., Yao, Y., Insel, P. A. & Junger, W. G. Pannexin-1 hemichannel-mediated ATP release together with P2X1 and P2X4 receptors regulate T-cell activation at the immune synapse. *Blood* **116**, 3475–3484 (2010).

153. Moon, H., Na, H. Y., Chong, K. H. & Kim, T. J. P2X7 receptor-dependent ATP-induced shedding of CD27 in mouse lymphocytes. *Immunol Lett* **102**, 98–105 (2006).

154. Garbers, C., Jänner, N., Chalaris, A., Moss, M. L., Floss, D. M., Meyer, D., Koch-Nolte, F., Rose-John, S. & Scheller, J. Species specificity of ADAM10 and ADAM17 proteins in interleukin-6 (IL-6) trans-signaling and novel role of ADAM10 in inducible IL-6 receptor shedding. *Journal of Biological Chemistry* **286**, 14804–14811 (2011).

155. Nolte, M. A., van Olffen, R. W., van Gisbergen, K. P. J. M. & van Lier, R. A. W. Timing and tuning of CD27-CD70 interactions: the impact of signal strength in setting the balance between adaptive responses and immunopathology. *Immunol Rev* **229**, 216–231 (2009).

156. Taylor, S. R. J., Gonzalez-Begne, M., Dewhurst, S., Chimini, G., Higgins, C. F., Melvin, J. E. & Elliott, J. I. Sequential Shrinkage and Swelling Underlie P2X 7 -Stimulated Lymphocyte Phosphatidylserine Exposure and Death. *The Journal of Immunology* **180**, 300–308 (2008).

157. Shapiro, V. S., Philips, R. L., Mccue, S. A. & Rajcula, M. J. Induced Cell Death − Receptor Double-Positive Thymocytes from P2X7 Cutting Edge: HDAC3 Protects. (2019) doi:10.4049/jimmunol.1801438.

158. Proietti, M., Cornacchione, V., RezzonicoJost, T., Romagnani, A., Faliti, C. E., Perruzza, L., Rigoni, R., Radaelli, E., Caprioli, F., Preziuso, S., Brannetti, B., Thelen, M., McCoy, K. D., Slack, E., Traggiai, E. & Grassi, F. ATP-gated ionotropic P2X7 receptor controls follicular T helper cell numbers in peyer's patches to promote host-microbiota mutualism. *Immunity* **41**, 789–801 (2014).

159. Faliti, C. E., Gualtierotti, R., Rottoli, E., Gerosa, M., Perruzza, L., Romagnani, A., Pellegrini, G., De Ponte Conti, B., Rossi, R. L., Idzko, M., Mazza, E. M. C., Bicciato, S., Traggiai, E., Meroni, P. L. & Grassi, F. P2X7 receptor restrains pathogenic Tfh cell generation in systemic lupus erythematosus. *Journal of Experimental Medicine* **216**, 317–336 (2019).

160. Stark, R., Wesselink, T. H., Behr, F. M., Kragten, N. A. M., Arens, R., Koch-Nolte, F., van Gisbergen, K. P. J. M. & van Lier, R. A. W. TRM maintenance is regulated by tissue damage via P2RX7. *Sci Immunol* **3**, (2018).

161. White, J. K., Gerdin, A. K., Karp, N. A., Ryder, E., Buljan, M., Bussell, J. N., Salisbury, J., Clare, S., Ingham, N. J., Podrini, C., Houghton, R., Estabel, J., Bottomley, J. R., Melvin, D. G., Sunter, D., Adams, N. C., Tannahill, D., Logan, D. W., Macarthur, D. G., *et al.* XGenome-wide generation and systematic phenotyping of knockout mice reveals new roles for many genes. *Cell* **154**, 452 (2013).

162. Ryoden, Y., Fujii, T., Segawa, K. & Nagata, S. Functional Expression of the P2X7 ATP Receptor Requires Eros. *The Journal of Immunology* **204**, 559–568 (2020).

163. Gemmer, M. & Förster, F. A clearer picture of the ER translocon complex. *J Cell Sci* **133**, (2020).

164. Randzavola, L. O., Mortimer, P. M., Garside, E., Dufficy, E. R., Schejtman, A., Roumelioti, G., Yu, L., Pardo, M., Tolley, C., Brandt, C., Harcourt, K., Nahorski, M., Woods, G., Williamson, J. C., Suresh, S., Sowerby, J. M., Rae, W. M., Lehner, P. J., Choudhary, J., *et al.* EROS-mediated control of NOX2 and P2X7 biosynthesis. (2021) doi:10.1101/2021.09.14.460103.

165. Thomas, D. C., Charbonnier, L.-M., Schejtman, A., Aldhekri, H., Coomber, E. L., Dufficy, E. R., Beenken, A. E., Lee, J. C., Clare, S., Speak, A. O., Thrasher, A. J., Santilli, G., Al-Mousa, H., Alkuraya, F. S., Chatila, T. A. & Smith, K. G. C. EROS/CYBC1 mutations: Decreased NADPH oxidase function and chronic granulomatous disease. *Journal of Allergy and Clinical Immunology* **143**, 782-785.e1 (2019).

166. Arnadottir, G. A., Norddahl, G. L., Gudmundsdottir, S., Agustsdottir, A. B., Sigurdsson, S., Jensson, B. O., Bjarnadottir, K., Theodors, F., Benonisdottir, S., Ivarsdottir, E. v., Oddsson, A., Kristjansson, R. P., Sulem, G., Alexandersson, K. F., Juliusdottir, T., Gudmundsson, K. R., Saemundsdottir, J., Jonasdottir, A., Jonasdottir, A., *et al.* A homozygous loss-of-function mutation leading to CYBC1 deficiency causes chronic granulomatous disease. *Nat Commun* **9**, (2018).

167. Skarnes, W. C., Rosen, B., West, A. P., Koutsourakis, M., Bushell, W., Iyer, V., Mujica, A. O., Thomas, M., Harrow, J., Cox, T., Jackson, D., Severin, J., Biggs, P., Fu, J., Nefedov, M., de Jong, P. J., Stewart, A. F. & Bradley, A. A conditional knockout resource for the genome–wide study of mouse gene function. *Nature* **474**, 337 (2011).

168. Johnston, C. J. C., Robertson, E., Harcus, Y., Grainger, J. R., Coakley, G., Smyth, D. J., McSorley, H. J. & Maizels, R. Cultivation of Heligmosomoides Polygyrus: An Immunomodulatory Nematode Parasite and its Secreted Products. *J Vis Exp* **2015**, 52412 (2015).

169. Hsu, P. D., Scott, D. A., Weinstein, J. A., Ran, F. A., Konermann, S., Agarwala, V., Li, Y., Fine, E. J., Wu, X., Shalem, O., Cradick, T. J., Marraffini, L. A., Bao, G. & Zhang, F. DNA targeting specificity of RNA-guided Cas9 nucleases. *Nature Biotechnology 2013 31:9* **31**, 827–832 (2013).

170. Tang, C., Fang, M., Tan, G., Zhang, S., Yang, B., Li, Y., Zhang, T., Saxena, R., Mohan, C. & Wu, T. Discovery of Novel Circulating Immune Complexes in Lupus Nephritis Using Immunoproteomics. *Front Immunol* **13**, 1 (2022).

171. Kim, T. H., Goodman, J., Anderson, K. v. & Niswander, L. Phactr4 regulates neural tube and optic fissure closure by controlling PP1-, Rb-, and E2F1-regulated cell-cycle progression. *Dev Cell* **13**, 87–102 (2007).

172. Zhang, Y., Kim, T. H. & Niswander, L. Phactr4 regulates directional migration of enteric neural crest through PP1, integrin signaling, and cofilin activity. *Genes Dev* **26**, 69 (2012).

173. Allen, P. B., Greenfield, A. T., Svenningsson, P., Haspeslagh, D. C. & Greengard, P. Phactrs 1–4: A family of protein phosphatase 1 and actin regulatory proteins. *Proc Natl Acad Sci U S A* **101**, 7187 (2004).

174. Solimini, N. L., Liang, A. C., Xu, C., Pavlova, N. N., Xu, Q., Davoli, T., Li, M. Z., Wong, K. K. & Elledge, S. J. STOP gene Phactr4 is a tumor suppressor. *Proc Natl Acad Sci U S A* **110**, (2013).

175. Cao, F., Liu, M., Zhang, Q.-Z. & Hao, R. PHACTR4 regulates proliferation, migration and invasion of human hepatocellular carcinoma by inhibiting IL-6/Stat3 pathway. *Eur Rev Med Pharmacol Sci* https://www.europeanreview.org/article/11295 (2016).

176. Luck, K., Kim, D. K., Lambourne, L., Spirohn, K., Begg, B. E., Bian, W., Brignall, R., Cafarelli, T., Campos-Laborie, F. J., Charloteaux, B., Choi, D., Coté, A. G., Daley, M., Deimling, S., Desbuleux, A., Dricot, A., Gebbia, M., Hardy, M. F., Kishore, N., *et al.* A reference map of the human binary protein interactome. *Nature 2020 580:7803* **580**, 402–408 (2020).

177. Hengel, R. L., Thaker, V., Pavlick, M. v., Metcalf, J. A., Dennis, G., Yang, J., Lempicki, R. A., Sereti, I. & Lane, H. C. Cutting Edge: L-Selectin (CD62L) Expression Distinguishes Small Resting Memory CD4 + T Cells That Preferentially Respond to Recall Antigen . *The Journal of Immunology* **170**, 28–32 (2003).

178. Hendriks, J., Gravestein, L. A., Tesselaar, K., van Lier, R. A. W., Schumacher, T. N. M. & Borst, J. CD27 is required for generation and long-term maintenance of T cell immunity. *Nature Immunology 2000 1:5* **1**, 433–440 (2000).

179. Rabe, B., Chalaris, A., May, U., Waetzig, G. H., Seegert, D., Williams, A. S., Jones, S. A., Rose-John, S. & Scheller, J. Transgenic blockade of interleukin 6 transsignaling abrogates inflammation. *Blood* **111**, 1021–1028 (2008).

180. Hintzen, R. Q., de Jong, R., Lens, S. M., Brouwer, M., Baars, P. & van Lier, R. A. Regulation of CD27 expression on subsets of mature T-lymphocytes. *The Journal of Immunology* **151**, (1993).

181. van Oosterwijk, M. F., Juwana, H., Arens, R., Tesselaar, K., van Oers, M. H. J., Eldering, E. & van Lier, R. A. W. CD27–CD70 interactions sensitise naive CD4+ T cells for IL-12-induced Th1 cell development. *Int Immunol* **19**, 713–718 (2007).

182. Libregts, S., van Olffen, R. W., van der Sluijs, K. F., van Lier, R. A. W. & Nolte, M. A. Function of CD27 in helper T cell differentiation. *Immunol Lett* **136**, 177–186 (2011).

183. Vázquez-Villoldo, N., Domercq, M., Martín, A., Llop, J., Gómez-Vallejo, V. & Matute, C. P2X4 receptors control the fate and survival of activated microglia. *Glia* **62**, 171–184 (2014).

184. He, W., Wang, Q., Sha, W., Wang, L., Li, D. & Chen, G. P2X4 Inhibition reduces microglia inflammation and apoptosis by NLRP3 and improves nervous system defects in rat brain trauma model. *Journal of Clinical Neuroscience* **99**, 224–232 (2022).

185. Zheng, W. P. & Flavell, R. A. The transcription factor GATA-3 is necessary and sufficient for Th2 cytokine gene expression in CD4 T cells. *Cell* **89**, 587–596 (1997).

186. Amsen, D., Blander, J. M., Lee, G. R., Tanigaki, K., Honjo, T. & Flavell, R. A. Instruction of Distinct CD4 T Helper Cell Fates by Different Notch Ligands on Antigen-Presenting Cells. *Cell* **117**, 515–526 (2004).

187. Carvalheiro, T., Rafael-Vidal, C., Malvar-Fernandez, B., Lopes, A. P., Pego-Reigosa, J. M., Radstake, T. R. D. J. & Garcia, S. Semaphorin4A-Plexin D1 Axis Induces Th2 and Th17 While Represses Th1 Skewing in an Autocrine Manner. *Int J Mol Sci* **21**, 1–11 (2020).

188. Kaplan, M. H., Schindler, U., Smiley, S. T. & Grusby, M. J. Stat6 is required for mediating responses to IL-4 and for development of Th2 cells. *Immunity* **4**, 313–319 (1996).

189. Kaplan, M. H., Sun, Y. L., Hoey, T. & Grusby, M. J. Impaired IL-12 responses and enhanced development of Th2 cells in Stat4-deficient mice. *Nature* **382**, 174–177 (1996).

190. Thierfelder, W. E., van Deursen, J. M., Yamamoto, K., Tripp, R. A., Sarawar, S. R., Carson, R. T., Sangster, M. Y., Vignali, D. A. A., Doherty, P. C., Grosveld, G. C. & Ihle, J. N. Requirement for Stat4 in interleukin-12-mediated responses of natural killer and T cells. *Nature* **382**, 171–174 (1996).

191. Kagami, S. I., Nakajima, H., Suto, A., Hirose, K., Suzuki, K., Morita, S., Kato, I., Saito, Y., Kitamura, T. & Iwamoto, I. Stat5a regulates T helper cell differentiation by several distinct mechanisms. *Blood* **97**, 2358–2365 (2001).

192. Cote-Sierra, J., Foucras, G., Guo, L., Chiodetti, L., Young, H. A., Hu-Li, J., Zhu, J. & Paul, W. E. Interleukin 2 plays a central role in Th2 differentiation. *Proc Natl Acad Sci U S A* **101**, 3880 (2004).

193. Hwang, J. R., Byeon, Y., Kim, D. & Park, S. G. Recent insights of T cell receptor-mediated signaling pathways for T cell activation and development. *Experimental & Molecular Medicine 2020 52:5* **52**, 750–761 (2020).

194. Swain, S. L., Weinberg, A. D., English, M. & Huston, G. IL-4 directs the development of Th2-like helper effectors. *The Journal of Immunology* **145**, (1990).

195. Tanaka, Y., Hamano, S., Gotoh, K., Murata, Y., Kunisaki, Y., Nishikimi, A., Takii, R., Kawaguchi, M., Inayoshi, A., Masuko, S., Himeno, K., Sasazuki, T. & Fukui, Y. T helper type 2 differentiation and intracellular trafficking of the interleukin 4 receptor-α subunit controlled by the Rac activator Dock2. *Nature Immunology 2007 8:10* **8**, 1067–1075 (2007).

196. Pfister, M., Ogilvie, A., da Silva, C. P., Grahnert, A., Guse, A. H. & Hauschildt, S. NAD degradation and regulation of CD38 expression by human monocytes/macrophages. *Eur J Biochem* **268**, 5601–5608 (2001).

197. Göllner, M., Ihrig-Biedert, I., Petermann, V., Saurin, S., Oelze, M., Kröller-Schön, S., Vujacic-Mirski, K., Kuntic, M., Pautz, A., Daiber, A. & Kleinert, H. NOX2ko Mice Show Largely Increased Expression of a Mutated NOX2 mRNA Encoding an Inactive NOX2 Protein. *Antioxidants* **9**, 1–19 (2020).

198. Donnelly-Roberts, D. L., Namovic, M. T., Han, P. & Jarvis, M. F. Mammalian P2X7 receptor pharmacology: comparison of recombinant mouse, rat and human P2X7 receptors. *Br J Pharmacol* **157**, 1203 (2009).

199. Ting, C.-N., Olson, M. C., Barton, K. P. & Leiden, J. M. Transcription factor GATA-3 is required for development of the T-cell lineage. *Nature* **384**, 474–478 (1996).

200. Maillard, I. & Adler, S. H. Review Notch and the Immune System Notch1-2 but not Notch3-4 contain a C-terminal tran. *Immunity* **19**, 781–791 (2003).

201. Fang, T. C., Yashiro-Ohtani, Y., del Bianco, C., Knoblock, D. M., Blacklow, S. C. & Pear, W. S. Notch directly regulates Gata3 expression during T helper 2 cell differentiation. *Immunity* **27**, 100–110 (2007).

202. Amsen, D., Antov, A., Jankovic, D., Sher, A., Radtke, F., Souabni, A., Busslinger, M., McCright, B., Gridley, T. & Flavell, R. A. Direct regulation of Gata3 expression determines the T helper differentiation potential of Notch. *Immunity* **27**, 89–99 (2007).

203. Carvalheiro, T., Affandi, A. J., Malvar-Fernández, B., Dullemond, I., Cossu, M., Ottria, A., Mertens, J. S., Giovannone, B., Bonte-Mineur, F., Kok, M. R., Marut, W., Reedquist, K. A., Radstake, T. R. & García, S. Induction of Inflammation and Fibrosis by Semaphorin 4A in Systemic Sclerosis. *Arthritis and Rheumatology* **71**, 1711–1722 (2019).

204. Zhang, Y. F., Zhang, Y., Jia, D. D., Yang, H. Y., Cheng, M. D., Zhu, W. X., Xin, H., Li, P. F. & Zhang, Y. F. Insights into the regulatory role of Plexin D1 signalling in cardiovascular development and diseases. *J Cell Mol Med* **25**, 4183 (2021).

205. Rehman, M., Gurrapu, S., Cagnoni, G., Capparuccia, L. & Tamagnone, L. PlexinD1 Is a Novel Transcriptional Target and Effector of Notch Signaling in Cancer Cells. *PLoS One* **11**, e0164660 (2016).

206. Ouyang, W., Löhning, M., Gao, Z., Assenmacher, M., Ranganath, S., Radbruch, A. & Murphy, K. M. Stat6-Independent GATA-3 Autoactivation Directs IL-4-Independent Th2 Development and Commitment. *Immunity* **12**, 27–37 (2000).

207. Fang, F., Cao, W., Mu, Y., Okuyama, H., Li, L., Qiu, J., Weyand, C. M. & Goronzy, J. J. IL-4 prevents adenosine-mediated immunoregulation by inhibiting CD39 expression. *JCI Insight* **7**, (2022).

208. Quaderi, N. A., Schweiger, S., Gaudenz, K., Franco, B., Rugarli, E. I., Berger, W., Feldman, G. J., Volta, M., Andolfi, G., Gilgenkrantz, S., Marion, R. W., Hennekam, R. C. M., Opitz, J. M., Muenke, M., Ropers, H. H. & Ballabio, A. Opitz G/BBB syndrome, a defect of midline development, is due to mutations in a new RING finger gene on Xp22. *Nature Genetics 1997 17:3* **17**, 285–291 (1997).

209. Trockenbacher, A., Suckow, V., Foerster, J., Winter, J., Krauß, S., Ropers, H. H., Schneider, R. & Schweiger, S. MID1, mutated in Opitz syndrome, encodes an ubiquitin ligase that targets phosphatase 2A for degradation. *Nature Genetics 2001 29:3* **29**, 287–294 (2001).

210. Chen, X., Xu, Y., Tu, W., Huang, F., Zuo, Y., Zhang, H. G., Jin, L., Feng, Q., Ren, T., He, J., Miao, Y., Yuan, Y., Zhao, Q., Liu, J., Zhang, R., Zhu, L., Qian, F., Zhu, C., Zheng, H., *et al.* Ubiquitin E3 ligase MID1 inhibits the innate immune response by ubiquitinating IRF3. *Immunology* **163**, 278 (2021).

211. Chen, X., Zhao, Q., Xu, Y., Wu, Q., Zhang, R., Du, Q., Miao, Y., Zuo, Y., Zhang, H., Huang, F., Ren, T., He, J., Qiao, C., Li, Y., Li, S., Xu, Y., Wu, D., Yu, Z., Lv, H., *et al.* E3 ubiquitin ligase MID1 ubiquitinates and degrades type-I interferon receptor 2. *Immunology* (2022) doi:10.1111/IMM.13544.

212. Snelgrove, R. J., Edwards, L., Rae, A. J. & Hussell, T. An absence of reactive oxygen species improves the resolution of lung influenza infection. *Eur J Immunol* **36**, 1364–1373 (2006).

213. Lebman, D. A. & Coffman, R. L. Interleukin 4 causes isotype switching to IgE in T cell-stimulated clonal B cell cultures. *J Exp Med* **168**, 853 (1988).

214. Coffman, R. L. & Carty, J. A T cell activity that enhances polyclonal IgE production and its inhibition by interferon-gamma. *The Journal of Immunology* **136**, (1986).

215. Harris, N. & Gause, W. C. B cell function in the immune response to helminths. *Trends Immunol* **32**, 80 (2011).

216. Shimokawa, C., Kanaya, T., Hachisuka, M., Ishiwata, K., Hisaeda, H., Kurashima, Y., Kiyono, H., Yoshimoto, T., Kaisho, T. & Ohno, H. Mast Cells Are Crucial for Induction of Group 2 Innate Lymphoid Cells and Clearance of Helminth Infections. *Immunity* **46**, 863-874.e4 (2017).

217. Spits, H., Artis, D., Colonna, M., Diefenbach, A., di Santo, J. P., Eberl, G., Koyasu, S., Locksley, R. M., McKenzie, A. N. J., Mebius, R. E., Powrie, F. & Vivier, E. Innate lymphoid cells — a proposal for uniform nomenclature. *Nature Reviews Immunology 2013 13:2* **13**, 145–149 (2013).

218. Stein, M., Keshav, S., Harris, N. & Gordon, S. Interleukin 4 potently enhances murine macrophage mannose receptor activity: a marker of alternative immunologic macrophage activation. *J Exp Med* **176**, 287 (1992).

219. Bonne-Année, S., Kerepesi, L. A., Hess, J. A., O'Connell, A. E., Lok, J. B., Nolan, T. J. & Abraham, D. Human and Mouse Macrophages Collaborate with Neutrophils To Kill Larval Strongyloides stercoralis. *Infect Immun* **81**, 3346 (2013).

220. Herbert, D. R., Hölscher, C., Mohrs, M., Arendse, B., Schwegmann, A., Radwanska, M., Leeto, M., Kirsch, R., Hall, P., Mossmann, H., Claussen, B., Förster, I. & Brombacher, F. Alternative macrophage activation is essential for survival during schistosomiasis and downmodulates T helper 1 responses and immunopathology. *Immunity* **20**, 623–635 (2004).

221. Lilly, C. M., Chapman, R. W., Sehring, S. J., Mauser, P. J., Egan, R. W. & Drazen, J. M. Effects of interleukin 5-induced pulmonary eosinophilia on airway reactivity in the guinea pig. *Am J Physiol Lung Cell Mol Physiol* **270**, (1996).

222. Shin, E. H., Osada, Y., Sagara, H., Takatsu, K. & Kojima, S. Involvement of complement and fibronectin in eosinophil-mediated damage to Nippostrongylus brasiliensis larvae. *Parasite Immunol* **23**, 27–37 (2001).

223. Petrie, H. T. Cell migration and the control of post-natal T-cell lymphopoiesis in the thymus. *Nature Reviews Immunology 2003 3:11* **3**, 859–866 (2003).

224. Misslitz, A., Pabst, O., Hintzen, G., Ohl, L., Kremmer, E., Petrie, H. T. & Förster, R. Thymic T Cell Development and Progenitor Localization Depend on CCR7. *J Exp Med* **200**, 481 (2004).

225. Hendriks, R. W., Nawijn, M. C., Engel, J. D., van Doorninck, H., Grosveld, F. & Karis, A. Expression of the transcription factor GATA-3 is required for the development of the earliest T cell progenitors and correlates with stages of cellular proliferation in the thymus. doi:10.1002/(SICI)1521-4141(199906)29:06.

226. Pai, S. Y., Truitt, M. L., Ting, C. N., Leiden, J. M., Glimcher, L. H. & Ho, I. C. Critical Roles for Transcription Factor GATA-3 in Thymocyte Development. *Immunity* **19**, 863–875 (2003).

227. Tanigaki, K., Tsuji, M., Yamamoto, N., Han, H., Tsukada, J., Inoue, H., Kubo, M. & Honjo, T. Regulation of αβ/γδ T Cell Lineage Commitment and Peripheral T Cell Responses by Notch/RBP-J Signaling. *Immunity* **20**, 611–622 (2004).

228. Kaech, S. M., Wherry, E. J. & Ahmed, R. Effector and memory T-cell differentiation: implications for vaccine development. *Nature Reviews Immunology 2002 2:4* **2**, 251–262 (2002).

229. Szabo, P. A., Miron, M. & Farber, D. L. Location, location, location: Tissue resident memory T cells in mice and humans. *Sci Immunol* **4**, (2019).

230. Hoyler, T., Klose, C. S. N., Souabni, A., Turqueti-Neves, A., Pfeifer, D., Rawlins, E. L., Voehringer, D., Busslinger, M. & Diefenbach, A. The transcription factor GATA3 controls cell fate and maintenance of type 2 innate lymphoid cells. *Immunity* **37**, 634 (2012).

231. Mjösberg, J., Bernink, J., Golebski, K., Karrich, J. J., Peters, C. P., Blom, B., te Velde, A. A., Fokkens, W. J., van Drunen, C. M. & Spits, H. The Transcription Factor GATA3 Is Essential for the Function of Human Type 2 Innate Lymphoid Cells. *Immunity* **37**, 649–659 (2012).

232. Moro, K., Yamada, T., Tanabe, M., Takeuchi, T., Ikawa, T., Kawamoto, H., Furusawa, J. I., Ohtani, M., Fujii, H. & Koyasu, S. Innate production of TH2 cytokines by adipose tissue-associated c-Kit+Sca-1+ lymphoid cells. *Nature 2009 463:7280* **463**, 540–544 (2009).

233. Symowski, C. & Voehringer, D. Th2 cell-derived IL-4/IL-13 promote ILC2 accumulation in the lung by ILC2-intrinsic STAT6 signaling in mice. *Eur J Immunol* **49**, 1421–1432 (2019).

234. Shimizu, T., Osaka, Y., Banri-Koike, C., Yoshida, M., Endo, K., Furukawa, K., Oda, M., Murakami, A., Ogawa, S., Abe, R. & Azuma, T. T cells specific to hapten–carrier but not to carrier alone assist in the production of anti-hapten and anti-carrier antibodies. *Int Immunol* **19**, 1157–1164 (2007).

235. Chao, C. C., Jensen, R. & Dailey, M. O. Mechanisms of L-selectin regulation by activated T cells. *The Journal of Immunology* **159**, (1997).

236. Borges Da Silva, H., Beura, L. K., Wang, H., Hanse, E. A., Gore, R., Scott, M. C., Walsh, D. A., Block, K. E., Fonseca, R., Yan, Y., Hippen, K. L., Blazar, B. R., Masopust, D., Kelekar, A., Vulchanova, L., Hogquist, K. A. & Jameson, S. C. The purinergic receptor P2RX7 directs metabolic fitness of long-lived memory CD8+ T cells. *Nature* **559**, 264–268 (2018).

237. Zheng, C., Wu, H., Lu, Z., Bi, J. & Wan, X. IL-33-induced reactive oxygen species are required for optimal metabolic programming in group 2 innate lymphoid cells. *Cell Mol Immunol* **17**, 1266 (2020).

238. Grainger, J. R., Smith, K. A., Hewitson, J. P., McSorley, H. J., Harcus, Y., Filbey, K. J., Finney, C. A. M., Greenwood, E. J. D., Knox, D. P., Wilson, M. S., Belkaid, Y., Rudensky, A. Y. & Maizels, R. M. Helminth secretions induce de novo T cell Foxp3 expression and regulatory function through the TGF-β pathway. *Journal of Experimental Medicine* **207**, 2331–2341 (2010).

239. Hewitson, J. P., Filbey, K. J., Bieren, J. E., Camberis, M., Schwartz, C., Murray, J., Reynolds, L. A., Blair, N., Robertson, E., Harcus, Y., Boon, L., Huang, S. C.-C., Yang, L., Tu, Y., Miller, M. J., Voehringer, D., Gros, G. le, Harris, N. & Maizels, R. M. Concerted Activity of IgG1 Antibodies and IL-4/IL-25-Dependent Effector Cells Trap Helminth Larvae in the Tissues following Vaccination with Defined Secreted Antigens, Providing Sterile Immunity to Challenge Infection. *PLoS Pathog* **11**, e1004676 (2015).

240. Uhlig, H. H., Schwerd, T., Koletzko, S., Shah, N., Kammermeier, J., Elkadri, A., Ouahed, J., Wilson, D. C., Travis, S. P., Turner, D., Klein, C., Snapper, S. B. & Muise, A. M. The Diagnostic Approach to Monogenic Very Early Onset Inflammatory Bowel Disease. *Gastroenterology* **147**, 990 (2014).

241. Karczewski, K. J., Francioli, L. C., Tiao, G., Cummings, B. B., Alföldi, J., Wang, Q., Collins, R. L., Laricchia, K. M., Ganna, A., Birnbaum, D. P., Gauthier, L. D., Brand, H., Solomonson, M., Watts, N. A., Rhodes, D., Singer-Berk, M., England, E. M., Seaby, E. G., Kosmicki, J. A., *et al.* The mutational constraint spectrum quantified from variation in 141,456 humans. *Nature 2020 581:7809* **581**, 434–443 (2020).

242. Rabbit Polyclonal Anti-C17orf62 Antibody. https://www.atlasantibodies.com/products/antibodies/primary-antibodies/triple-a-polyclonals/c17orf62-antibody-hpa045696/.

243. Maurisse, R., de Semir, D., Emamekhoo, H., Bedayat, B., Abdolmohammadi, A., Parsi, H. & Gruenert, D. C. Comparative transfection of DNA into primary and transformed mammalian cells from different lineages. *BMC Biotechnol* **10**, 1–9 (2010).

244. Cao, F., Xie, X., Gollan, T., Zhao, L., Narsinh, K., Lee, R. J. & Wu, J. C. Comparison of Gene-Transfer Efficiency in Human Embryonic Stem Cells. *Mol Imaging Biol* **12**, 15 (2010).

245. Yu, L., DeLeo, F. R., Biberstine-Kinkade, K. J., Renee, J., Nauseef, W. M. & Dinauer, M. C. Biosynthesis of Flavocytochrome b 558: gp91phox IS SYNTHESIZED AS A 65-kDa PRECURSOR (p65) IN THE ENDOPLASMIC RETICULUM. *Journal of Biological Chemistry* **274**, 4364–4369 (1999).

246. Jiang, Y., Li, Y. & Zhu, B. T-cell exhaustion in the tumor microenvironment. *Cell Death & Disease 2015 6:6* **6**, e1792–e1792 (2015).

247. Lens, S. M. A., Tesselaar, K., van Oers, M. H. J. & van Lier, R. A. W. Control of lymphocyte function through CD27–CD70 interactions. *Semin Immunol* **10**, 491–499 (1998).

248. Hintzen, R. Q., de Jong, R., Lens, S. M., Brouwer, M., Baars, P. & van Lier, R. A. Regulation of CD27 expression on subsets of mature T-lymphocytes. *The Journal of Immunology* **151**, (1993).

249. Akiba, H., Nakano, H., Nishinaka, S., Shindo, M., Kobata, T., Atsuta, M., Morimoto, C., Ware, C. F., Malinin, N. L., Wallach, D., Yagital, H. & Okumura, K. CD27, a Member of the Tumor Necrosis Factor Receptor Superfamily, Activates NF-κB and Stress-activated Protein Kinase/c-Jun N-terminal Kinase via TRAF2, TRAF5, and NF-κB-inducing Kinase *. *Journal of Biological Chemistry* **273**, 13353–13358 (1998).

250. Remedios, K. A., Meyer, L., Zirak, B., Pauli, M. L., Truong, H.-A., Boda, D. & Rosenblum, M. D. CD27 Promotes CD4 + Effector T Cell Survival in Response to Tissue Self-Antigen . *The Journal of Immunology* **203**, 639–646 (2019).

251. Manocha, M., Svend, R., Laouar, A., Liao, G., Bhan, A., Borst, J., Terhorst, C. & Manjunath, N. Blocking CD27-CD70 Costimulatory Pathway Suppresses Experimental Colitis. *The Journal of Immunology* **183**, 270–276 (2009).

252. Makino, F., Ito, J., Abe, Y., Harada, N., Kamachi, F., Yagita, H., Takahashi, K., Okumura, K. & Akiba, H. Blockade of CD70–CD27 Interaction Inhibits Induction of Allergic Lung Inflammation in Mice. *https://doi.org/10.1165/rcmb.2011-0354OC* **47**, 298–305 (2012).

253. Cooper, P. J., Ayre, G., Martin, C., Rizzo, J. A., Ponte, E. v. & Cruz, A. A. Geohelminth infections: a review of the role of IgE and assessment of potential risks of anti-IgE treatment. *Allergy* **63**, 409–417 (2008).

254. Fang, T. C., Yashiro-Ohtani, Y., Bianco, C. del, Knoblock, D. M., Blacklow, S. C. & Pear, W. S. Notch Directly Regulates Gata3 Expression during T Helper 2 Cell Differentiation. *Immunity* **27**, 100 (2007).

255. Amsen, D., Antov, A. & Flavell, R. A. The different faces of Notch in T-helper-cell differentiation. *Nature Reviews Immunology 2009 9:2* **9**, 116–124 (2009).

256. Wen, Z., Shimojima, Y., Shirai, T., Li, Y., Ju, J., Yang, Z., Tian, L., Goronzy, J. J. & Weyand, C. M. NADPH oxidase deficiency underlies dysfunction of aged CD8+ Tregs. *Journal of Clinical Investigation* **126**, 1953–1967 (2016).

257. Shah, K., Al-Haidari, A., Sun, J. & Kazi, J. U. T cell receptor (TCR) signaling in health and disease. *Signal Transduction and Targeted Therapy 2021 6:1* **6**, 1–26 (2021).

258. Borst, J., Hendriks, J. & Xiao, Y. CD27 and CD70 in T cell and B cell activation. *Curr Opin Immunol* **17**, 275–281 (2005).

259. Akdis, C. A., Arkwright, P. D., Brüggen, M. C., Busse, W., Gadina, M., Guttman-Yassky, E., Kabashima, K., Mitamura, Y., Vian, L., Wu, J. & Palomares, O. Type 2 immunity in the skin and lungs. *Allergy* **75**, 1582–1605 (2020).

260. Yuk, C. M., Kwon, B.-I. & Lee, S.-H. Effect of NADPH oxidase 2 (Nox2) deficiency on the function of Th2 cells (HYP4P.415). *The Journal of Immunology* **192**, (2014).

261. Kawamura, H., Aswad, F., Minagawa, M., Govindarajan, S. & Dennert, G. P2X7 Receptors Regulate NKT Cells in Autoimmune Hepatitis. *The Journal of Immunology* **176**, 2152–2160 (2006).

262. Rissiek, B., Danquah, W., Haag, F. & Koch-Nolte, F. Technical Advance: a new cell preparation strategy that greatly improves the yield of vital and functional Tregs and NKT cells. *J Leukoc Biol* **95**, 543–549 (2014).

263. Liu, Q. & Kim, C. H. Control of Tissue-Resident Invariant NKT Cells by Vitamin A Metabolites and P2X7-Mediated Cell Death. *The Journal of Immunology* **203**, 1189–1197 (2019).